# PERFORMANCE PREDICTION MODEL FOR POSITIVE DISPLACEMENT HELICAL SCREW FLOWMETERS

**Volker Bernd Klügl**

A thesis submitted in partial fulfilment of
the requirements of the University of Glamorgan
for the degree of Doctor of Philosophy

May 1998

The University of Glamorgan in collaboration with
Leistritz Aktiengesellschaft, Nürnberg, Germany

Last Revision: 14.06.03

## Declaration

This thesis has not been nor is currently submitted for the award of any other degree or similar qualifications.

.....

V.B. Klügl

to my parents

## Acknowledgements

I would like to acknowledge with gratitude the guidance and encouragement and patience offered by my Director of studies, Dr. W. T. Evans.

I would also like to thank my second supervisor, Dr. M. Wincek for his guidance and receptiveness for numerous discussions on various theories, Dr. H.-J. Fricke for his critical assessment, Dr. J. Zech for his encouragement and support.

Further thanks to J. Klein, D. Butler, S. Correia, A. Schmitz, S. Silva and T. Wong for helping me with testing and the layout of graphics.

Special thanks to all my friends, but especially to Gernot Meyer, Stefan Mänzel and Martin Remiger who had given me all the support I needed, and kept the spirit alive for a life after submission.

The financial support provided by the Leistritz Aktiengesellschaft and the appreciation of my work by the chairman H. Schaak and Dr. W. Moser is also greatly acknowledged as well as the grant given by the DAAD.

## Abstract

A general model is developed describing the performance of positive displacement flowmeters. This model allows to predict the performance of any positive displacement meter if 8 coefficients describing the meter design are known. The logic is that a flowmeter performs at a defined pressure loss for a given speed. This pressure loss times flowrate is then energy balanced against all internal losses. Pressure loss and speed are the reasons for leakage. Rotational speed times the theoretical swept volume is the theoretical flowrate and this flowrate, when combined with leakage flow can be used to calculate the effective or true flowrate. The 8 coefficients describe the influence of the design of a meter on laminar leakage flow, turbulent leakage flow, speed related leakage flow, viscous friction, mechanical friction, constant friction, impulse energy losses and ball bearing friction, respectively.

This model was applied to a twin-screw type displacement flowmeter which uses two helical rotors which form separate pockets and allow the flow-rate of the fluid to be measured. Based on the general prediction model it was found that for this type of flowmeter mainly two coefficients are the reasons for deviation from linearity. These are the constant friction power losses $\kappa_C$ produced by mechanical sliding and the turbulent leakage flow losses $\kappa_{tur}$. When the values of $\kappa_C$ and $\kappa_{tur}$ are zero then the error against flowrate is constant.

A complete model of an actual twin-screw type displacement flowmeter was realised, determining all 8 loss coefficients. In order to do so, tests with a twin-screw type displacement flowmeter have been carried out on the overall meter performance, leakage flow losses and bearing friction. The theoretical work includes the determination of all 8 coefficients based on a study of the rotor geometry of the meter and a calculation of the fluid forces and torques acting on the rotors.

The theoretical results of the final performance prediction model were compared with experimental results and show a good accordance. It was found that one optimal circumference clearance value can be determined for every different fluid property and flowrate. The flowmeter performance may be increased by minimising mechanical sliding and turbulent leakage flow losses.

# Table of content

## List of figures

# List of tables

# Notation

## Symbols

| | | |
|---|---|---|
| $A$ | [mm²] | Cross sectional area of a clearance |
| $A_I$ | [mm²] | Area of the cross section of rotor$_I$ normal to the axis |
| $A_{II}$ | [mm²] | Area of the cross section of rotor$_{II}$ normal to the axis |
| $A_b$ | [mm²] | Area of the cross section of the bore |
| $A_{bI}$ | [mm²] | Circular area of the bore of rotor$_I$ |
| $A_{bII}$ | [mm²] | Circular area of the bore of rotor$_{II}$ |
| $A_{overlap}$ | [mm²] | Lens shaped area of the overlap of the two bores |
| $A_c$ | [mm²] | Section carved out by the cycloid |
| $A_k$ | [mm²] | Section carved out by the radius $d_{ch}/2$ |
| $A_{fl}$ | [mm²] | Area of the cross section filled with fluid |
| $A_{1;2;3}$ | [mm²] | Different areas of the cross section of the rotor normal to the axis |
| $A_i$ | [mm²] | Pressure loaded area through axis of rotation |
| $A_X$ | [mm²] | Projected profile area in X - direction |
| $A_Y$ | [mm²] | Projected profile area in Y - direction |
| $a$ | [mm] | Centre distance of the axis or the rotors of the flowmeter |
| $b$ | [mm] | Breadth of the clearance (length of the clearance edge) |
| $b_{\overline{C}}$ | [mm] | Breadth of the circumference clearance parallel to axis of rotation |
| $C_0$ | [kN] | Basic static bearing load rating |
| $c$ | [m/s] | Velocity of fluid flow in the clearance |
| $d_m$ | [mm] | Mean bearing diameter |
| $d$ | [mm] | Inner diameter of the bearing |
| $d_{bI}$ | [mm] | Bore diameter of housing$_I$ |
| $d_{bII}$ | [mm] | Bore diameter of housing$_{II}$ |
| $d_{ch}$ | [mm] | Diameter of chamfer circle |

| | | |
|---|---|---|
| $d_H$ | [mm] | Hydraulic diameter |
| $d_{iI}$ | [mm] | Root diameter of $rotor_I$ |
| $d_{iII}$ | [mm] | Root diameter of $rotor_{II}$ |
| $d_o$ | [mm] | Outer diameter of the bearing |
| $d_{oI}$ | [mm] | Outer diameter of $rotor_I$ |
| $d_{oII}$ | [mm] | Outer diameter of $rotor_{II}$ |
| $d_{rI}$ | [mm] | Rolling diameter of $rotor_I$ |
| $d_{rII}$ | [mm] | Rolling diameter of $rotor_{II}$ |
| $d_{xII}$ | [mm] | Distance of resulting force in X-direction to the centre of rotation |
| $d_{yII}$ | [mm] | Distance of resulting force in Y-direction to the centre of rotation |
| $E$ | [%] | Error in flowrate, deviation from true value |
| $F$ | [N] | Resulting bearing load |
| $F_a$ | [N] | Axial load on the bearing |
| $F_r$ | [N] | Radial load on the bearing |
| $F_{ch}$ | [N] | Load created by the fluid pressure in one complete chamber |
| $f_a$ | [mm²] | Fluid pressure axial load area |
| $f_{aI}$ | [mm²] | Fluid pressure axial load area of $rotor_I$ |
| $f_{aII}$ | [mm²] | Fluid pressure axial load area of $rotor_{II}$ |
| $f_r$ | [mm²] | Fluid pressure radial load area |
| $f_x$ | [mm²] | Fluid pressure load area in X-direction |
| $f_x$ | [mm²] | Fluid pressure load area in Y-direction |
| $f$ | [-] | Correction factor for the roll-off diameter |
| $f_0$ | [-] | Bearing friction coefficient for lubrication method |
| $f_1$ | [-] | Bearing friction coefficient for load application |
| $f_{sl}$ | [N] | Bearing sliding friction coefficient |
| $h$ | [mm] | Height of the leakage clearance |

| | | |
|---|---|---|
| $h_{rs}$ | [mm] | Variable height of the leakage clearance |
| $J$ | [kgm²] | Inertia |
| $K_{SC}$ | [mm³] | Circumference clearance static leakage coefficient |
| $K_{DC}$ | [mm³] | Circumference clearance rotational leakage coefficient |
| $K_{UC}$ | [mm³] | Circumference clearance rotational friction coefficient |
| $K_{SR}$ | [mm³] | Root clearance static leakage coefficient |
| $K_{DC}$ | [mm³] | Root clearance rotational leakage coefficient |
| $K_{SF}$ | [mm³] | Flank clearance static leakage coefficient |
| $K_{DF}$ | [mm³] | Flank clearance rotational leakage coefficient |
| $K_{dp}$ | [mm³] | Pressure related loss coefficient |
| $\ell_{poc}$ | [mm] | Length of a pocket |
| $\ell$ | [mm] | Length of the clearance |
| $\ell_r$ | [mm] | Total (minimum) length of rotors |
| $\ell_X$ | [mm] | Projected length of profile area in X - direction |
| $\ell_Y$ | [mm] | Projected length of profile area in Y - direction |
| $M_I$ | | Centre point of rotor$_{\mathrm{I}}$ |
| $M_{II}$ | | Centre point of rotor$_{\mathrm{II}}$ |
| $M$ | [Nmm] | Total bearing friction torque |
| $M_0$ | [Nmm] | Lubricant friction torque |
| $M_1$ | [Nmm] | Rolling friction torque |
| $M_{sl}$ | [Nmm] | Sliding friction torque |
| $m_I$ | [-] | Number of starts of rotor$_{\mathrm{I}}$ |
| $m_{II}$ | [-] | Number of starts of rotor$_{\mathrm{II}}$ |
| $n$ | [rpm] | Rotor or bearing rotational speed |
| $P$ | [N] | Resulting bearing load |
| $P$ | [Nmm/s] | Total power |
| $P_B$ | [Nmm/s] | Roller bearing power losses |
| $P_C$ | [Nmm/s] | Constant independent power losses |

| | | |
|---|---|---|
| $P_D$ | [Nmm/s] | Rotational viscous friction power losses |
| $P_{D(CFRT)}$ | [Nmm/s] | Rotational viscous friction power losses in CFRT clearance |
| $P_S$ | [Nmm/s] | Power loss due to leakage flow |
| $P_T$ | [Nmm/s] | Impulse power loss |
| $P_U$ | [Nmm/s] | Mechanical friction power losses |
| $P_{U(CFRT)}$ | [Nmm/s] | Mechanical friction power losses in CFRT clearance |
| $P_{UB}$ | [Nmm/s] | Mechanical friction power loss in the bearings |
| $p_{in}$ | [N/m²] | Pressure at the inflow side of the flowmeter |
| $p_{out}$ | [N/m²] | Pressure at the outflow side of the flowmeter |
| $p_{poc}$ | [N/m²] | Pressure in a specified pocket |
| $\Delta p$ | [N/m²] | Pressure drop |
| $p_I$ | [mm] | Pitch of $rotor_I$ |
| $p_{II}$ | [mm] | Pitch of $rotor_{II}$ |
| Re | [-] | Reynolds number |
| $r$ | [-] | Ratio of outer diameters ($d_{oI}/d_{oII}$) |
| $r_i$ | [mm] | Distance from area $A_i$ to axis of rotation |
| $r_v$ | [mm] | Radius coordinate at the intersection point from the cycloid to the chamber circle |
| $r_I$ | [mm] | The radius coordinate of a point of the cycloid profile of $rotor_I$ |
| $r_{II}$ | [mm] | The radius coordinate of a point of the cycloid profile of $rotor_{II}$ |
| $T$ | [Nmm] | Torque |
| $T_I$ | [Nmm] | Fluid pressure torque acting on $rotor_I$ |
| $T_{II}$ | [Nmm] | Fluid pressure torque acting on $rotor_{II}$ |
| $T_{ch}$ | [Nmm] | Torque created by the fluid pressure in one complete chamber |
| $T_B$ | [Nmm] | Roller bearing friction torque |
| $T_C$ | [Nmm] | Constant independent friction torque |
| $T_D$ | [Nmm] | Rotational viscous friction torque |
| $T_{D(CFRT)}$ | [Nmm] | Rotational viscous friction torque in CFRT clearance |

| | | |
|---|---|---|
| $T_{(b;a;o;i;f)}$ | [mm] | Deviations from nominal values |
| $T_T$ | [Nmm] | Impulse loss torque |
| $T_U$ | [Nmm] | Mechanical friction torque |
| $T_{U(CFRT)}$ | [Nmm] | Mechanical friction torque in CFRT clearance |
| $\overline{T}$ | [Nmm] | Mean friction torque |
| $T_I$ | [Nmm] | Hydraulic torque acting on $rotor_I$ |
| $T_{II}$ | [Nmm] | Hydraulic torque acting on $rotor_{II}$ |
| $T_{red}$ | [Nmm] | Combined torque on both rotor related to $rotor_I$ |
| $t$ | [s] | Time |
| $t_M$ | [radian] | Rolling angle of $M_I$ around $M_{II}$ |
| $t_I$ | [mm³] | Fluid pressure torque volume acting on $rotor_I$ |
| $t_{II}$ | [mm³] | Fluid pressure torque volume acting on $rotor_{II}$ |
| $u$ | [m/s] | Relative velocity in a leakage area; peripheral velocity |
| $u_I$ | [m/s] | Relative velocity at related to $rotor_I$ |
| $u_{II}$ | [m/s] | Relative velocity at related to $rotor_{II}$ |
| $V_{th}$ | [mm³] | Theoretical swept volume |
| $V_D$ | [mm³] | Rotational leakage volume |
| $\dot{V}$ | [l/min] | Flowrate through the flowmeter |
| $\dot{V}_D$ | [l/min] | Leakage flow due to rotation |
| $\dot{V}_{D(CFRT)}$ | [l/min] | Rotational leakage flow through CFRT clearance |
| $\dot{V}_e$ | [l/min] | Effective flowrate through the flowmeter |
| $\dot{V}_L$ | [l/min] | Total leakage flowrate through the flowmeter |
| $\dot{V}_S$ | [l/min] | Total static leakage flow due to the pressure drop |
| $\dot{V}_{S(CFRT)}$ | [l/min] | Static leakage flow through CFRT clearance |
| $\dot{V}_{SD}$ | [l/min] | Static leakage flow related to the density |
| $\dot{V}_{SV}$ | [l/min] | Static leakage flow related to the viscosity |
| $\dot{V}_{th}$ | [l/min] | Theoretical flowrate |
| $W$ | [N/mm] | Kinetic energy |

| | | |
|---|---|---|
| $w$ | [m/s] | Axial velocity of the fluid in the flowmeter |
| $x(t_M)$ | [mm] | X coordinate |
| $y(t_M)$ | [mm] | Y coordinate |
| $Y$ | [-] | Characteristic bearing parameter |
| $\alpha$ | [radian] | Angular coordinate of the cycloid |
| $\alpha_D$ | [-] | Orifice coefficient |
| $\beta_I$ | [radian] | Profile angle of rotor$_I$ |
| $\beta_{II}$ | [radian] | Profile angle of rotor$_{II}$ |
| $\gamma$ | [radian] | Centre angle of the profile |
| $\gamma_I$ | [radian] | Centre angle of the profile related to the rotor |
| $\gamma_I^*$ | [radian] | Centre angle of the profile related to the bore |
| $\gamma_{II}$ | [radian] | Centre angle of the profile related to the rotor |
| $\gamma_{II}^*$ | [radian] | Centre angle of the profile related to the bore |
| $\varepsilon$ | [-] | Ratio of the number of starts ($m_I/m_{II}$) |
| $\zeta$ | [-] | Factor for the rolling diameter for the applied profile |
| $\eta_{fl}$ | [mPas] | Dynamic viscosity of the fluid |
| $\eta_v$ | [-] | Volumetric efficiency |
| $\eta_m$ | [-] | Mechanic efficiency |
| $\kappa$ | [radian] | Head angle of the profile |
| $\kappa_I$ | [radian] | Head angle of rotor$_I$ |
| $\kappa_{II}$ | [radian] | Head angle of rotor$_{II}$ |
| $\kappa_B$ | [$Ns^{7/3}m^{-1/3}$] | Ball bearing viscous friction power loss coefficient |
| $\kappa_C$ | [Nmm] | Constant torque power loss coefficient |
| $\kappa_D$ | [mm³] | Viscous friction power loss coefficient |
| $\kappa_U$ | [mm³] | Mechanical friction power loss coefficient |
| $\kappa_T$ | [$mm^5$] | Impulse power loss coefficient |
| $\kappa_{lam}$ | [mm³] | Laminar slip coefficient |
| $\kappa_{rot}$ | [mm³] | Rotational slip coefficient |

| | | |
|---|---|---|
| $\kappa_{tur}$ | [mm²] | Turbulent slip coefficient |
| $\lambda_I$ | [radian] | Gap angle of rotor$_I$ |
| $\lambda_{II}$ | [radian] | Gap angle of rotor$_{II}$ |
| $\mu_I$ | [-] | Bearing friction coefficient depending on load and design |
| $\nu_{fl}$ | [mm²/s] | Kinematic viscosity of the fluid |
| $\rho_{fl}$ | [kg/m³] | Density of the fluid |
| $\rho_I$ | [radian] | Angle for the rotation of rotor$_I$ |
| $\rho_{II}$ | [radian] | Angle for the rotation of rotor$_{II}$ |
| $\sigma_I$ | [radian] | Ground angle of rotor$_I$ |
| $\sigma_{II}$ | [radian] | Ground angle of rotor$_{II}$ |
| $\phi_P$ | [radian] | Pitch angle of the thread |
| $\phi_I$ | [radian] | Angular position of rotor$_I$ |
| $\phi_{II}$ | [radian] | Angular position of rotor$_{II}$ |
| $\psi$ | [radian] | Angle for dimensionless length value |
| $\psi_r$ | [radian] | Angle for dimensionless total rotor length |
| $\omega$ | [1/s] | Angular velocity |
| $\omega_I$ | [1/s] | Angular velocity of rotor$_I$ |
| $\omega_{II}$ | [1/s] | Angular velocity of rotor$_{II}$ |
| $\xi$ | [radian] | Angle describing the limits of the displacement chamber |

## Indices

| | |
|---|---|
| *a* | Axial direction |
| *a* | Related to the centre distance of the rotors |
| *b* | Related to the bore of the housing |
| *C* | Related to circumference clearance |
| *ch* | Related to chamfer circle |
| *D* | Flow related to rotational motion |
| *d* | Related to driven flank of the rotor |
| *DC* | Related to rotational motion of circumference clearance |
| *DF* | Related to rotational motion of flank clearance |
| *DR* | Related to rotational motion of root clearance |
| *DT* | Related to rotational motion of triangular clearance |
| *e* | Related to effective flowrate |
| *F* | Related to flank clearance |
| *f* | Related to the flanks of the rotor |
| *fl* | Related to fluid properties |
| *H* | Related to hydraulic diameter |
| *I* | Related to $\text{rotor}_{\text{I}}$ |
| *i* | Related to the inner diameter of the rotor |
| *II* | Related to $\text{rotor}_{\text{II}}$ |
| *in* | Related to inflow side of the flowmeter |
| *L* | Related to total leakage flowrate through the flowmeter |
| *lam* | Related to laminar flow pattern |
| *m* | Related to mean bearing diameter (mean value) |
| *o* | Related to the outer diameter of the rotor |
| *out* | Related to outflow side of the flowmeter |
| *P* | Related to the thread |
| *r* | Radial direction |

| | |
|---|---|
| *r* | Related to rolling diameter |
| *R* | Related to root clearance |
| *S* | Flow related to pressure drop |
| *SC* | Related to static leakage flow through the circumference clearance |
| *SD* | Related to static leakage flow related to the density |
| *SF* | Related to static leakage flow through the flank clearance |
| *sl* | Related to sliding friction |
| *SR* | Related to static leakage flow through the root clearance |
| *ST* | Related to static leakage flow through the triangular clearance |
| *SV* | Related to static leakage flow related to the viscosity |
| *t* | Related to idling flank of the rotor |
| *T* | Related to triangular clearance |
| *TM* | Trade mark |
| *th* | Related to a theoretical value |
| *tur* | Related to turbulent flow pattern |

## Common terms in flowmetering according to BS7405 /1/

**Flow rate** The quantity of fluid passing through the cross-section of a conduit in a short period of time, divided by that time.

**Accuracy** The qualitative expression for the closeness of a measured value to the true value.

**Uncertainty** An estimate characterizing the range of values within which the true value of a measurement lies.

**Error** The difference between true and indicated value.

**Meter factor** The number of pulses generated per unit volume of fluid metered. Throughout this thesis error will always be systematic.

**Linearity** The deviation (within preset limits) of a flowmeter's performance from the ideal straight line relationship between meter output and flow rate.

**Turndown** The ratio of the specified maximum to minimum flow rates.

**Repeatability ( of a measurement)**

The quantitative expression of the closeness of agreement between successive measurements of the same value of the same quality carried out by the same method with the same measuring instrument at the same location at appropriately short intervals of time.

**Repeatability ( of a measuring instrument)**

The quantity which characterizes the ability of a measuring instrument to give identical indications or responses for repeated applications of the same value of the quantity measured under stated conditions of use.

# 1 Introduction

The measurement of fluid flow is important for such varied applications as the measurement of blood-flow-rates in a human artery to the measurement of the flow of liquid oxygen in a rocket. In some cases extreme precision is called for, while in other instances only crude measurements are necessary. The selection of the proper instrument for a particular application is governed by many variables, including cost. This is especially important because for many industrial operations the accuracy of a fluid flow measurement is directly related to the profit. A simple example is the flowmeter in the petrol pump at the neighbourhood service station and it is especially this field of application we are concerned with for the current design of screw-type flowmeters. In this application, screw-type flowmeters are aimed to replace the commonly used four-piston design because they are smaller in overall size and perform at a reduced pressure drop. The overall performance and application of helical screw flowmeters is discussed in relation to flowmeters in general with an emphasis on positive displacement flowmeters in chapter 3. The performance of the Leistritz flowmeter is reviewed in detail, discussing fluid, performance and installation considerations in chapter 4. The screw profile used to form the displacement chambers is described in chapter 6 and the governing parameters for the screw profile are presented together with their theoretical and practical limitations. Literature on screw pump profiles is reviewed and the geometry of screw type flowmeters is described.

The main focus however of the current study is to find a logic and a mathematical model to predict the accuracy and performance of a screw type flowmeter in relation to the geometric design variations. Most types of flowmeters, including the positive displacement and hence screw type flowmeter, to the authors knowledge, have not been modelled completely, and all the fluid to flowmeter interaction effects are not yet understood.

It is claimed common knowledge that slippage is the principal cause of error in displacement flowmeters. Hence if all the seals in the flowmeter were perfect, the only errors in flow measurement that these meters would exhibit, would be those due to the inaccuracies of the measurement of the flowmeter displacement volume, the fluid properties, and to the accuracy capabilities of the calibration facility. Obviously, the seals cannot be perfect, clearances must exist for the flowmeter to operate, and these clearances allow a leakage error flow which is not registered by the rotating motion of the flowmeter. In order to describe a model for the performance prediction of the positive displacement flowmeter, which is often simply called a PD meter, it is most suitable to find an accurate description of all power losses occurring in the meter. Once these are known the overall pressure drop can be calculated. The input power is the

flowrate times pressure drop over the meter. Pressure drop causes leakage flow or slip through various clearances which, when combined with rotational leakage, provides the reason for inaccurate metering. The sources of frictional power losses are the friction in the bearings, mechanical friction and fluid friction in the profile. The mechanical friction is influenced by the hydraulic forces of the fluid on the rotors and the pressure drop. This was taken as a basis to subdivide the problem and built a model of the flowmeter using smaller models concerning separate problems. For a screw type flowmeter these are:

(a) the relation between pressure drop and the creation of driving torque and forces on the rotor (chapter 7).

(b) the relation between bearing friction, load and speed (chapter 8).

(c) the calculation of fluid friction in the flowmeter (chapter 9).

(d) the calculation of leakage caused by the pressure drop (chapter 9).

(e) the calculation of leakage caused by the rotational motion (chapter 9).

(f) the determination of the load on the bearings related to the hydraulic load, the frictional forces and the forces within the rotors (chapter 11).

For a helical screw flowmeter these influences on the performance of the flowmeter are complex and difficult to visualise. This includes the understanding of the displacement chamber itself, shape and size of clearances, load distribution on the bearings, mechanical and hydraulical interaction of the rotors and the generation of the driving torque. Hence in the current study the primary aim was first to find a general model for PD flowmeter describing the performance of a flowmeter related to 8 constant loss coefficients as described in detail in chapter 5, and then determine the loss coefficients themselves. It is important to note that the general prediction model is valid for all types of positive displacement flowmeters.

The verification of the performance prediction model relies on the verification of all 8 single coefficients occurring in the logic. The results of the prediction model have been compared with the experimental results and as a consequence some coefficients have been modified to adapt the model to the experimental results. The prediction model was then used to determine the performance of the existing design, regarding different clearance and operating conditions. Information on an improvement of the current flowmeter was gained, omitting costly experiments. Recommendations to achieve an improvement of the performance of the current flowmeter are given and the theoretical performance of different sizes is discussed.

# 2 Fluid properties considerations

All flowmeters are affected to some degree by one or more fluid properties, which therefore have an influence on the performance and performance prediction of the flowmeter. Reference texts and physical property data handbooks list viscosity, specific gravity, vapour pressure and other parameters for the fluids to be measured with the current application. Parameters which influence the fluid properties are operating pressure and temperature effecting density, viscosity, specific gravity, lubricity and compressibility. In the current work aspects, of fluid property considerations are restricted as follows:

(a) Regarding the flowmeter no temperature and/or pressure compensation is applied

(b) The change in fluid condition, especially compressibility effects according to the 50 kPa maximum pressure drop, are neglected

(c) The influence of chemical properties is not taken into account

(d) Effects of lubricity and surface tension will not be discussed

Fluids intended to be used with the current flowmetering device are petrol, diesel oil, fuel oil and lubricating oils. The temperature range of interest is from -10 °C to +50 °C. Relevant fluids properties are according to DIN 51601, 51603, 51607, test-fluid data sheets, and taken from Adler /2/ and Dubbel /3/ and Menke /4/ and listed in heavy type in Table 1. These values are not complete and sometimes the DIN standards provide only the upper and lower limit of a specified range. The fuel companies do not provide any fluid property values for their fuels. Because of very inconsistent results according to the low viscosity, no viscosity values could be obtained from measurements with readily available standard instrumentation. Hence the unknown density and viscosity values for all fluids in the temperate range between -10°C and +50°C had to be approximated. In order to do so, the values for the variations in the fluid density have been determined according to the PTB (Physikalische Technische Bundesanstalt Germany) guideline presented by Menke /4/. The viscosity variations for this temperature range were estimated by comparison to similar fluids with know properties as listed in Adler /2/ or Dubbel /3/ respectively. All approximated values are printed in light italic type in Table 1. Throughout this thesis the units used are $mm^2/s$ for the kinematic viscosity, mPas for the dynamic viscosity and $kg/m^3$ for the density. Values in literature, which have been originally in different units were transformed to meet the standard units of this thesis. A table with the different units used can be found in Appendix A "Units of viscosity".

| temperature | density | kinematic viscosity | dynamic viscosity | density | kinematic viscosity | dynamic viscosity |
|---|---|---|---|---|---|---|
| °C | kg/m³ | mm²/s | mPas | kg/m³ | mm²/s | mPas |
| | Testfluid Hebrosol® | | | Testfluid Shellsol | | |
| T min = -10 °C | **0.80** | *2.00* | *1.60* | **0.80** | *3.50* | *2.80* |
| T = 15 °C | **0.76** | *1.05* | *0.80* | **0.76** | *1.85* | *1.40* |
| T = 20 °C | **0.74** | **1.05** | **0.78** | **0.74** | **1.85** | **1.37** |
| T max = 50 °C | **0.71** | *0.60* | *0.43* | **0.71** | *0.90* | *0.64* |
| | Unleaded low density & viscosity | | | Unleaded high density & viscosity | | |
| T min = -10 °C | **0.76** | *2.00* | *1.52* | **0.89** | *4.00* | *3.56* |
| T = 15 °C | **0.72** | *1.00* | *0.72* | **0.85** | *2.00* | *1.70* |
| T = 20 °C | **0.70** | **1.00** | **0.70** | **0.83** | **2.00** | **1.66** |
| T max = 50 °C | **0.67** | *0.60* | *0.40* | **0.80** | *1.00* | *0.80* |
| | Diesel Oil low density & viscosity | | | Diesel Oil high density & viscosity | | |
| T min = -10 °C | **0.80** | *4.00* | *3.20* | **0.84** | *28.00* | *23.52* |
| T = 15 °C | **0.82** | *2.00* | *1.64* | **0.86** | *9.00* | *7.74* |
| T = 20 °C | **0.81** | **2.00** | **1.62** | **0.85** | **8.00** | **6.80** |
| T max = 50 °C | **0.79** | *1.00* | *0.79* | **0.83** | *3.50* | *2.91* |
| | Fuel Oil EL DIN 51603 T1 | | | Water | | |
| T min = -10 °C | **0.84** | *17.00* | *14.28* | - | - | - |
| T = 15 °C | **0.86** | *7.00* | *6.02* | **1.00** | **1.79** | **1.79** |
| T = 20 °C | **0.85** | **6.00** | **5.10** | **1.00** | **1.16** | **1.15** |
| T max = 50 °C | **0.83** | *3.50* | *2.91* | **0.98** | **0.55** | **0.54** |

*Table 1 Relevant fluid properties; values in light italic type approximated*

# 3 General classification

Screw type flowmeters are discussed in relation to flowmeters in general with an emphasis on PD flowmeters. The overall performance and application of helical screw flowmeters is presented together with a discussion of the main designs: The BiRotor$^{TM}$ meter of Brooks, the helical gear flowmeter of Fluidyne, the helical screw flowmeter of Litre Meter and Kral and screw flowmeter of Leistritz. All helical flowmeters show a high accuracy and are suitable for measuring highly viscous fluids.

Screw type flowmeters are rotary PD fluid flowmeters using helical sealing elements. PD flowmeters are briefly differentiated in respect to all other flowmeters. The characteristics of rotational motion PD fluid flowmeters are stated, and PD fluid flowmeters using helical sealing elements are described together with examples of different manufacturers design solutions. A brief review of screw pump applications provides additional understanding in the positive displacement principle of engaged helical screw elements, as helical flowmeters can be seen as screw pump devices in reverse action. Additionally the use of screw type metering pumps and screw type servo controlled meters is presented.

There are many different types of flowmeters available commercially and described in literature. No one flowmeter type is ideal for all applications and skill and knowledge is required to select the appropriate flowmeter for a particular application. Flowmeters considered in BS 7405 /1/ are arranged in ten major closed conduit groups, as given below.

(a) Orifices, venturis and nozzles

(b) Other differential pressure types

(c) Positive displacement types

(d) Rotary turbine types

(e) Fluid oscillatory types

(f) Electromagnetic types

(g) Ultrasonic types

(h) Direct and indirect mass types

(i) Thermal types

(j) Miscellaneous types

The general application of flowmeters, often combined with a guide to the selection of the proper flowmeter is discussed in a variety of publications and fluid measurement text books. In publications, a general approach to flow metering is presented by Eade

/5/, Franklin /6/, Furness /7/, Gerrard /8;9/, Hendrix /10;11/, Kinghorn /12/, Medlock /13/ and Stevens /14/.

Some publications such as Lomas /15/, Mannion /16/, and Reeve /17;18/ focus on the selection criteria and discuss the evaluation of different meters for various applications. Reeve /17/ proposes his idea of a perfect flowmeter consisting of the following:

(a) 100:1 turndown

(b) negligible head loss

(c) 10 msec response time

(d) 0.05% full scale accuracy

(e) suitable for all fluids and gases

(f) universal connections

(g) immunity to corrosive or external conditions

(h) suitable for ambients from -40°C to 80°C

(i) insensitive to flow parameters

(j) all at an economic price with minimum maintenance

These requirements are exaggerated, but give a good picture of the conflicting performance criteria aspects expected to be delivered by a flow metering device.

The general techniques and methods of flow metering are comprehensively covered by several books: Cheremisinoff /19/ and Furness /20/ review fluid behaviour and characteristics, fundamentals of fluid flow, flow measurement by PD flowmeters and other techniques. A full bibliography on fluid flow measurement is available for the years up to 1971 by Dowden /21/, and from the year 1971 onwards to date on the Internet's FLUIDEX /22/ index which is regularly updated.

## 3.1 Positive displacement flowmeters

This family of flowmeters is available in a wide variety of designs, some of which are synonymous with high performance and reliability, the common feature of each being that the liquid is carried through in isolated compartments. PD flowmeters operate by the successive mechanical division of the metered fluid into separate pockets. The number of pockets of known size which are passed indicate total volume, and the frequency at which they pass gives flow rate. The PD flowmeter therefore indicates both quantity and rate of flow. According to BS 7405 /1/ the group can be subdivided into four main classes as follows:

(a) reciprocating motion ( single and multiple piston)

(b) rotating motion ( vane and gear types)

(c) oscillating motion ( semi-rotary flowmeters)

(d) nutating motion (disc flowmeters)

The main types are described by Baker and Morris /23;24/, together with a comprehensive discussion of relevant literature. Advantages and disadvantages are listed by Hayward /25/. Spitzer /26/ provides detailed notes of the design performance and operating constraints of a wide range of PD flowmeters.

Benard /27/ underlines the insensitivity of PD flowmeters to flow profile alterations, swirl or eddies. It is therefore not necessary to have long straight lengths of pipe upstream or downstream of the flowmeter. The liquid metered should be free from entrained gas and a de-aerator is advisable in some applications. PD flowmeters are simple and accurate. They are largely used for the measurement of bulk deliveries of liquids from road tankers and, because of their good repeatability, they are used as secondary standards in flowrate measurement. If used for this purpose they are normally provided with a digital shaft encoder.

The most common design in measuring petrol is the piston meter, a design in which four pistons trap liquid as it passes through (Figure 1). The crankshaft rotates with a rotational speed proportional to the flow through the meter. Flowmeters of this type have claims to high accuracy, but may also have a large pressure drop and be bulky in size.

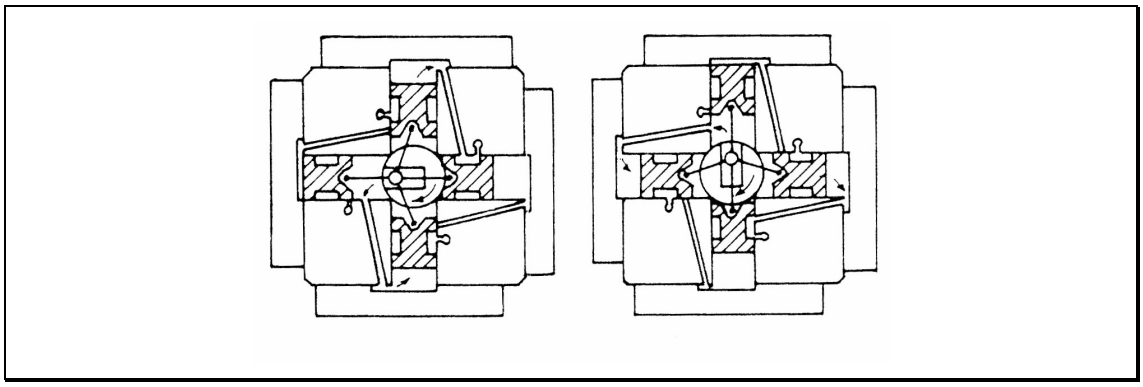

*Figure 1 Reciprocating piston flowmeter; Baker, Morris /23/*

The performance of all PD flowmeters follows the same pattern. At low fluid flows the meter has to overcome frictional resistance before motion commences and leakage could be significant. As the flow increases, less slip occurs and performance improves until at high flows viscous friction causes a large head loss and hence increased wear. Baker and Morris /23/ suggest that at both lower and higher flows, increased slippage

occurs and causes the flowmeter to under register. Hendrix /10/ states that PD flowmeters can provide high accuracy and fast response in applications involving precise flow control or transfer of valuable fluids liable to taxation.

Significant contributions are made by the following scientists: Hayward /25/ comments that the turndown of PD meter is about 20:1, linearity ±0.0 5%, and accuracy when newly calibrated ±0.2 % of volume over the range. Spitzer /26/ notes the general feature of increase in pressure drop across the meter with increasing viscosity. This imposes limits on the maximum viscous flow which can be metered. Hendrix /11/ suggests that viscosity changes due to variations in temperature will introduce relatively little errors into readings. For a typical meter, calibrated at 1 mPas, error increases gradually to 1.2 % at 100 mPas; above this viscosity no further shift is evident. In this statement Hendrix /11/ does not refer to any specific meter, operating or turndown range. Lomas /15/ states that the basic limitations of a PD meter are moving parts having close clearances, effectively limiting its use to clean liquids and necessitating regular maintenance on the meter. Also the choice of suitable materials is limited, restricting the flowmeters corrosion resistant properties. High temperatures and pressures also can result in distortion problems due to different expansions of moving parts and housing.

## 3.2 Rotating motion, vane and gear type flowmeters

There are several designs of flowmeters with multiple rotors including the helical screw flow presented by Baker and Morris /23/. The helical screw meter is the focus of the current work and is discussed later. Figure 2 shows a two rotor meter, where the main rotor consists of four vanes which form the metering compartments. The second rotor is a sealing rotor which returns the vanes to the inlet side of the meter. The rotor may be two or three lobed and its rotation will be linked precisely to that of the main rotor. It transmits a net fluid flow across the meter equal to the volume of the vane which it returns to the inlet. Figure 3 shows a multirotor flowmeter with a large sealing rotor and smaller rotors which transmit the fluid. Other gear type flowmeters work with two engaged gears, the reverse principle of the common gear pump. Some designs, for example the oval gear flowmeters, use ellipsoidal or oval gears to form the displacement chamber.

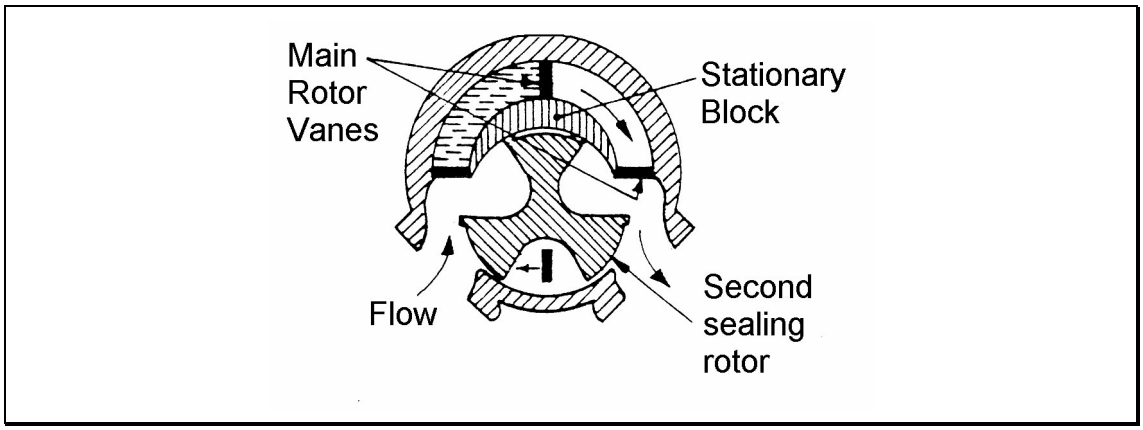


*Figure 2 Two rotor flowmeter, main rotor has four vanes; Baker and Morris /23/*

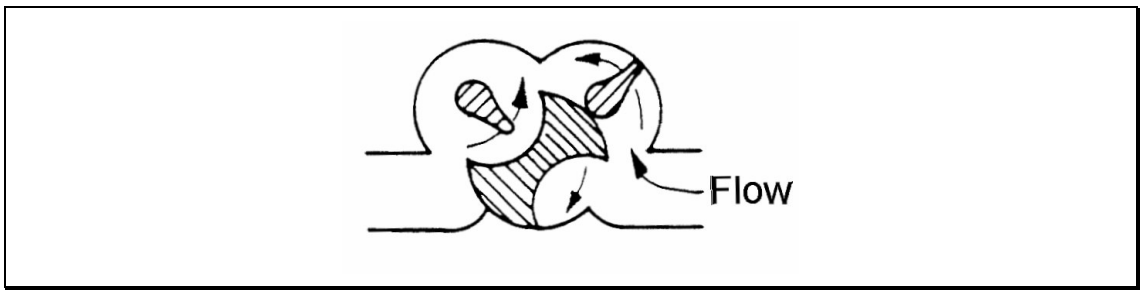


*Figure 3 Multirotor flowmeter, large sealing rotor with smaller rotors which transmit the fluid; Baker and Morris /23/*

## 3.3 Helical rotor PD flowmeter general characteristics

Basic characteristics and operation of the helical rotor PD flowmeters are reviewed. Advantages and limitations of the different types of helical rotor flowmeters are discussed and typical applications described.

### 3.3.1 Operating principle

Helical rotor flowmeters are positive-displacement flowmeters which use the mechanical action of two helical rotors. They can be regarded as a helical screw pump acting in reverse. The inter-meshing, fluted rotors trap discrete volumes of fluid against the measuring chamber wall, hence these parts must be manufactured to a high degree of precision. As the fluid enters the intake of the measuring chamber, the rotors momentarily divide the product into precise segments of volume and then pass these segments to the outlet chamber (Figure 5). During this liquid movement the speed of rotation of the two rotors is directly proportional to liquid throughput. The two helical fluted rotors within the measuring chamber are hydraulically unbalanced, so that the rotors are set into motion by the fluid pressure drop.

For some designs the rotors are controlled by timing gears to prevent metal to metal contact. Because there are no reciprocating or sliding parts, Konopka /28/ claims that these flowmeters provide long trouble-free service.

### 3.3.2 Wetted parts

Wetted parts of helical rotor flowmeters include the body, O-rings, rotors, and bearings. Bodies are available in stainless and carbon steel. Rotors are typically constructed of stainless steel or aluminium in the smaller sizes, and either carbon steel or aluminium in the larger sizes. Standard bearings are typically made of stainless steel, the grade of which may be unsuitable for some common applications such as water, aqueous solutions, bases, or salts. Helical rotor flowmeters are often limited by the bearing materials of construction. Spitzer /26/ underlines the importance, as with all flowmeters, of compatibility of the materials of construction of each component. The effects of wear and corrosion on the performance of the flowmeter are significant when slippage becomes excessive, the bearings fail or the seals leak.

### 3.3.3 Sensing system

Helical rotor flowmeters are often used in conjunction with suitable associated electronics to produce an output signal used in the exact measurement of a liquid product. Magnetic, optical and inductive sensing systems are prevalent in helical rotor flowmeter designs. The magnetic sensing system employs a magnetic gear, the teeth of which are sensed by a magnetic pickup and amplified. The optical sensing system utilises a magnetically driven optically encoded disc, the rotation of which is sensed by an optical pickup in order to sense a pulse each revolution.

### 3.3.4 Application

Helical rotor flowmeters are generally applicable to nonabrasive lubricating liquids with dynamic viscosities from approximately 1 mPas to 30,000 mPas. Slippage can pose a problem in low viscosity applications, especially if there is any wear of machined parts, so most applications are for monitoring high viscosity liquids. The low pressure drop introduced into the piping system makes this flowmeter design attractive for high viscosity applications. The field of application, as well as the range of suitable viscosities, varies for each manufacturer respectively and is discussed in detail later.

### 3.3.5 Installation condition

Like all PD flowmeters, the helical rotor flowmeter is not sensitive to flow profile alterations, swirl or eddies.

### 3.3.6 General performance

Baker and Morris /23/ state that as the sealing surfaces are in the longitudinal plane, the forces required to operate the flowmeter are relatively small and the pressure drop through the flowmeter is relatively low. Use with high viscosity liquids is possible without establishing undue constraints on the piping system. Spitzer /26/ remarks that volumetric flows can be measured with an accuracy that ranges from approximately ±0.2 to ±0.4 % rate, depending on the application and the flowmeter design. He also states that flows with low viscosity fluids are generally measured less accurately than viscous flows due to errors caused by increased slippage through the flowmeter.

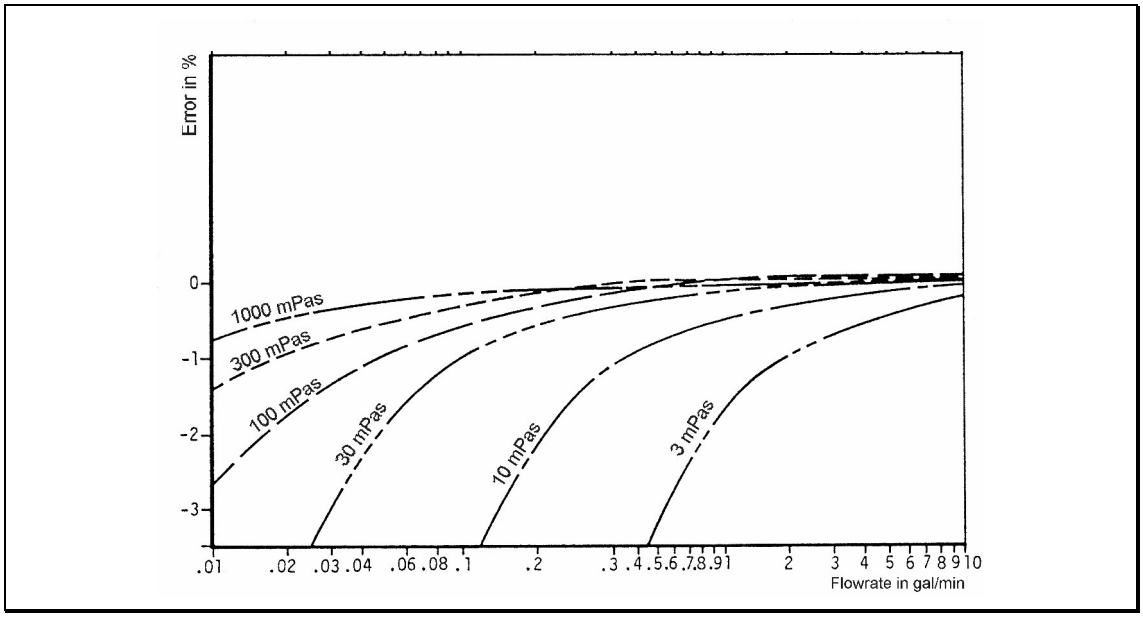


*Figure 4* *Calibration curves for a 2 ½ inch (63.5mm) Helix meter: the curves continue to converge up a flowrate of 150 gal/min (570 l/min); Gerrard /29/*

Figure 4 illustrates how accuracy is affected by viscosity changes for a turndown range of 1000:1. Spitzer /26/ states that viscous liquids can exhibit relatively large variations in viscosity over a relatively small temperature range. This causes inaccuracies due to viscosity changes, which may be larger than the stated accuracy of the flowmeter. Spitzer /26/ does not present any specific values to underline his statement. Low liquid lubricity can adversely affect bearing and rotor tolerances, which must be maintained in order to maintain accuracy. Spitzer /26/ also states that turndown can be as high as 100:1 in certain applications, although lower turndowns are typical of actual applications.

### 3.3.7 Operation constraints

Helical rotor flowmeters are usually pressure and temperature limited by the flange ratings and the temperature ratings of the sensor, which can be up to approximately 300°C in certain applications. The pressure drop across these flowmeters should typically be kept below approximately 2 bar in order to prevent excessive bearing wear and premature bearing failure. The pressure drop and flowrate limitations vary for each flowmeter manufacturer.

## 3.4 Helical rotor meter design variations

The author found four major manufactures of helical rotor flowmeters, i.e. Brooks, Fluidyne, Kral and Leistritz, using different meter designs, which are described in the following.

### 3.4.1 BiRotor™ meter (Brooks)

The axial flow BiRotor™ positive-displacement flowmeter by Brooks Instrument, Division of Emerson Electric /30/ uses two rotors with a 3-4 start arrangement. The two rotors of the flowmeter shown in Figure 5 are designed with different outer diameters. The relative angular position between the two rotors is controlled by two gears which are mounted on the rotor shafts and engage with one another, so that synchronised rotation is obtained. There is a very small clearance between the surfaces of the rotors, which never make contact with one another. The meter is particularly suitable for handling non-lubricating fluids.

The axial design BiRotor™ measuring unit is mounted parallel to flow. This orientation results in compact installation, improved accuracy and low pressure loss. It is claimed to be ideal for high capacity pipeline, refinery, barge and tanker loading and other bulk transfer applications. The operation of the flowmeter is made clear from the sequence of operations shown in Figure 5.

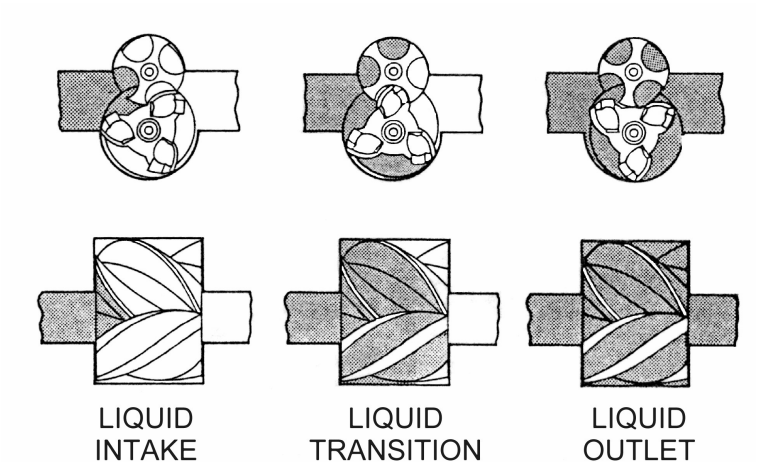


*Figure 5 Operating principle of a Brooks BiRotor™ positive-displacement flowmeter; Brooks Instruments, Division of Emerson Electric /30/*

### 3.4.2 Helical gear meter (Fluidyne)

The helical gear flowmeter by Fluidyne Instrumentation, Oakland California uses two rotors with a 1-1 start arrangement (Figure 6). Timing gears allow no contact between the metering elements themselves, eliminating friction and wear in the profile. Gerrad /29/ underlines the limiting factors in the accuracy and turndown of a PD meter. These are slip and pressure drop, which are minimised by designing the helical measuring elements to produce an optimum ratio of longitudinal to lateral sealing surface. Designed for food and beverage applications requiring a cleanable pocketless design, the large dimensions of the progressive cavities of this meter allow the passage of gels, undissolved solids, and other agglomerates, which cause blockage in other PD flowmeters. Spitzer /26/ states that the helical gear flowmeters are typically used on highly viscous liquids where it is often difficult to apply other flowmeters. This design is tolerant of dirt, as there are few passages that are easily plugged, but is susceptible to overspeed and bearing damage. The performance of the meter is essentially independent of viscosity. An overall accuracy of ±0.5 % over a 150:1 turndown range and better than ±0.2 % over a 20:1 turndown range is claimed by the manufacturer. The repeatability is at least ±0.1 % and more a function of counting pulses than fluid dynamics. The meter design can handle flow rate capacities from 1.9 litres to 15100 litres per minute. All flowmeters are geometrically scaled in proportion so that the surface to sealing ratio remains constant.

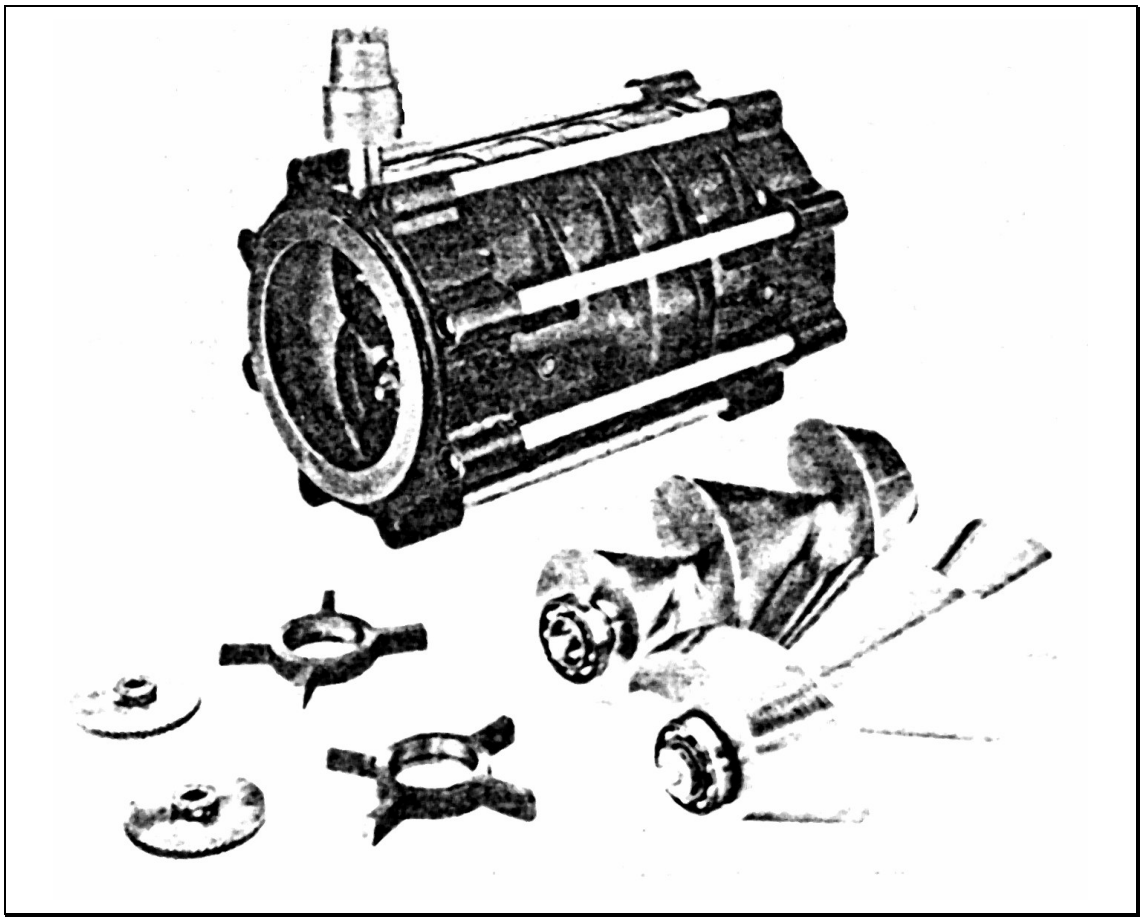

*Figure 6 Disassembled 10 inch (25.4 cm) helix-type flow transducer using radially pitched helical measuring elements; Considine /31/*

### 3.4.3 Helical screw meter (Litre Meter and Kral)

The helical screw meter by Kral /32/ and Litre Meter Ltd /33/ uses two rotors of different diameters with a 2-3 start arrangement (Figure 7). The rotors show a cycloidical profile and mesh with direct metal to metal contact, rolling on each other (Figure 8). Kral /32/ claims the design to provide the "perfect" solution for the measurement of higher viscosity liquids, i.e. bitumen, synthetic oils, waste oil, printing inks, resins, glues and food products such as honey, jams, fats, oils and chocolate for a viscosity range from 1.2 mm²/s to 5000 mm²/s The basic meter is derived from a range of screw pumps. The helical screw flowmeters are available in a flow range from 0.015 l/min to 7500 l/min with a claimed accuracy of 0.1 % of measured value with 0.01 % repeatability for a 1:70 turndown range. Roller and needle bearings are used in combination. For installation, any orientation may be used and most flowmeters accept bi-directional flow.

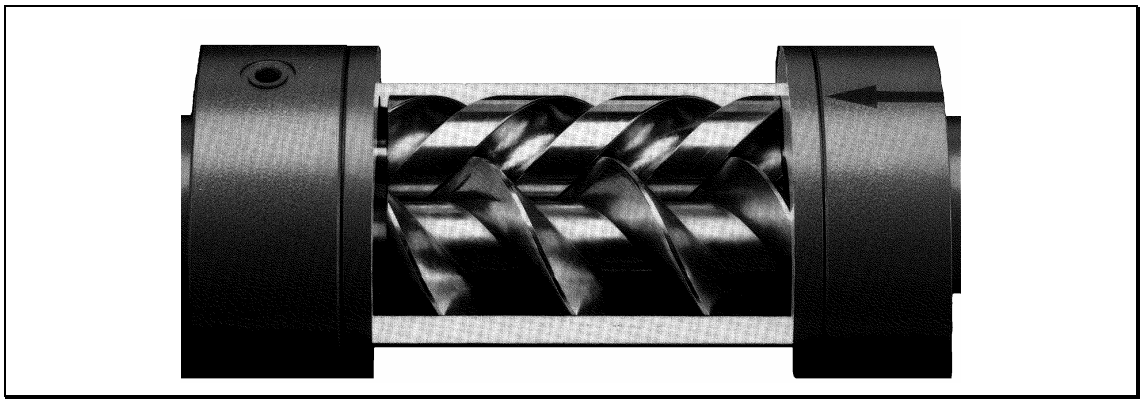

*Figure 7 Helical meter assembly; Litre Meter /33/*

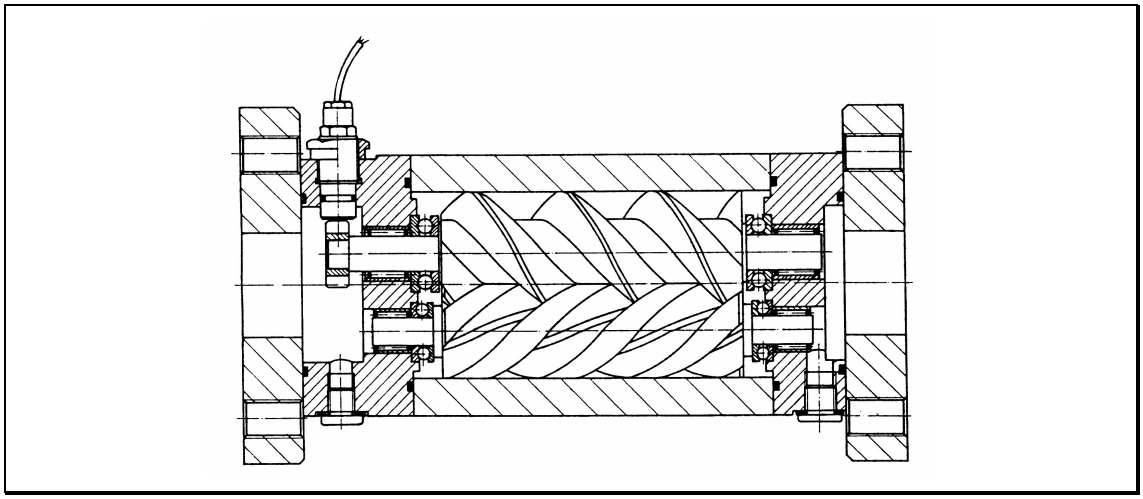

*Figure 8 Screw-Volumeter; Kral /32/*

### 3.4.4 Screw flowmeter (Leistritz)

The screw flowmeter by the Leistritz Aktiengesellschaft /34/ uses 2 rotors of different diameters with a 2-3 start arrangement similar to the Kral /32/ solution and is build in one size only allowing flowrates from 2 l/min to 80 l/min (Figure 9). The rotors have a cycloidical profile and mesh with direct metal to metal contact, rolling on each other. The Leistritz screw flowmeter was developed for the measurement of low viscosity fluids (1 mPas) with maximum accuracy. The rotational motion is transferred by a disk and two inductive pick-ups to an impulse signal proportional to the fluid flow. A staggered positioning of the two pick-ups can be used for a recognition of the flow direction.

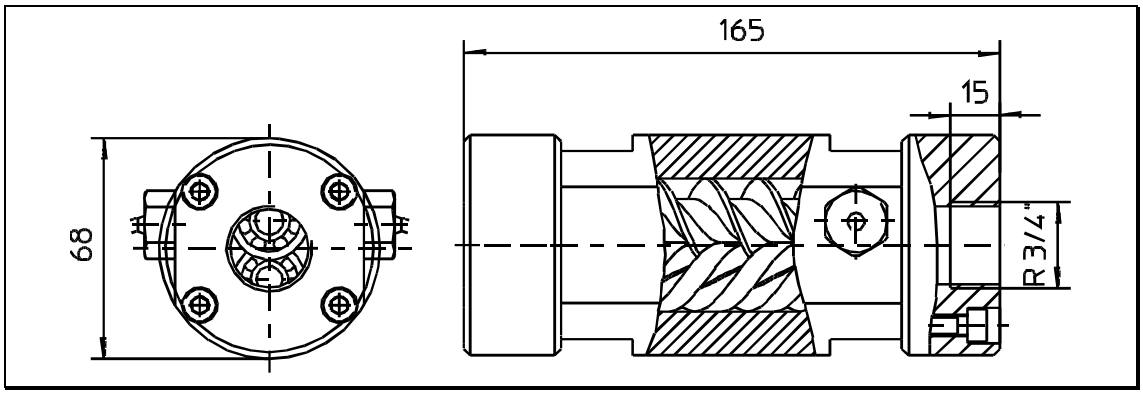


*Figure 9* *Section through a screw flowmeter assembly with a ¾ inch hose connector; Leistritz /34/*

The screw flowmeter can be used for low lubricating and non lubricating fluids such as petrol, fuel oil, kerosene, lubricating oils and other oils of different viscosities. The various viscosity values for those fluids are listed in Table 1 in chapter 2 "Fluid properties considerations". The range of flow measurement is claimed to be from 2-80 l/min. The meter is approved for fiscal measurement of hydrocarbon products by the Physikalische Technische Bundesanstalt Germany (PTB) for an accuracy of ±0.3 % of measured value with a repeatability ±0.05 % (Figure 10). For a dynamic viscosity of $\eta < 1$ mPas (kinematic viscosity of 0.8 mm²/s) the approved range is within 2 to 50 l/min. For a dynamic viscosity of $\eta < 22$ mPas (kinematic viscosity of 17.6 mm²/s) the approved range is within 2 to 80 l/min. The operating pressure can be up to 350 bar in a temperature range from -10 °C to +50 °C.

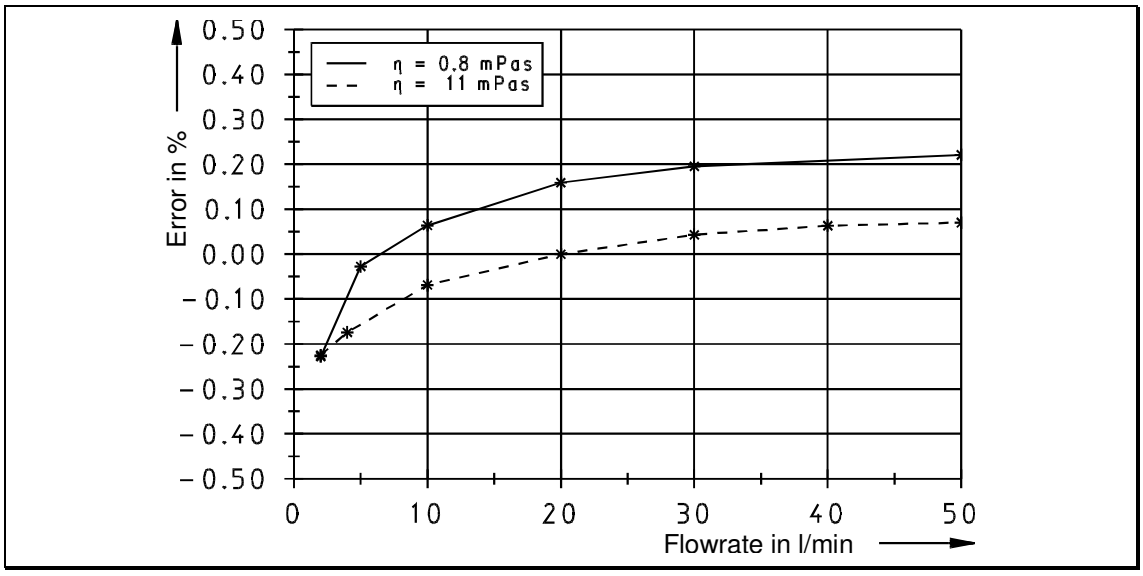


*Figure 10* *Systematic error against flowrate of the Leistritz screw flowmeter; Leistritz /34/*

## 3.5 Screw type servo controlled flowmeters

One problem with PD flowmeters is the pressure drop across the meter which is required to drive the rotor, and which causes fluid to leak past the blades of the rotor.

Benard /27/ mentions a screw type PD flowmeter which was developed at the Technical University of Denmark to overcome this problem. In this flowmeter, the rotor movement is servo assisted so that it will always rotate at such a speed that the pressure drop across the flowmeter is a minimum. The flowmeter was shown to have a turndown of 500:1.

Conrad and Trostman /35/ describe a servo controlled PD screw flowmeter for a flow range from 1.2 l/min to 40 l/min controlled by a microprocessor. Due to the servo control the flowmeter does not introduce any pressure drop in the fluid line. Hence it is claimed to perform with a low sensitivity to variations in viscosity of the fluid. At flowrates above 30 l/min the difference in plots of error against flowrate obtained using 5 and 35 mm²/s oils was insignificant. At 2 l/min the difference between 5 mm²/s and 35 mm²/s curves was about 0.3 %. Further the flowmeter is said to possess a high degree of accuracy and repeatability in measurement. In their paper they discuss the calibration and the results obtained. However the accuracy values obtained are not significantly different to those claimed by Leistritz /34/ .

## 3.6 Screw pumps

A brief review of screw pump applications provides additional understanding in the positive displacement principle of engaged helical screw elements, as helical flowmeters can be seen as screw pump devices in reverse action. Karassik /36/ describes screw pumps as a special type of rotary positive displacement pump in which the flow through the pumping elements is truly axial. The liquid is carried between screw threads on one or more rotors and is displaced axially as the helical rotors rotate and mesh. In all other types of rotary pumps the liquid is forced to travel circumferentially. In applications where liquid agitation or churning is objectionable, thus Karassik /36/ claims that the screw pump, because of its unique axial flow pattern and low internal velocities, has a number of advantages over other rotary pumps and is able to operate at 10,000 rpm and even higher. Screw pumps are classified into single- or multiple-rotor types. The latter are further divided into timed and untimed categories. Multiple-screw pumps are available in a variety of configurations and designs. All use one driven rotor in mesh with one or more sealing or idling rotors.

Screw pumps use the same principle as helical screw flowmeters. The intermeshing of the threads on the rotors and the close fit of the surrounding housing creates one or

more sets of moving seals in series between pump inlet and outlet. These sets of seals form fully enclosed cavities which move continuously from inlet to outlet. Two main types of screw rotors can be classified, the timed and the untimed version.

Timed rotors rely on external means for phasing the mesh of the threads and for supporting the forces acting on the rotors. In this concept, theoretically, the threads do not come into contact with each other or with the housing bores in which they rotate.

Untimed rotors rely on the precision and accuracy of the screw forms for proper mesh and transmission of rotation. The rotors can be compared directly with precision-made helical gears with a high helix angle. This design usually employs three rotor screws with the center, or driven, rotor in mesh with two close-fitting sealing, or idler, rotors symmetrically positioned about the central axis (Figure 11). A close-fitting housing provides the only transverse bearing support for both driven and idler rotors.

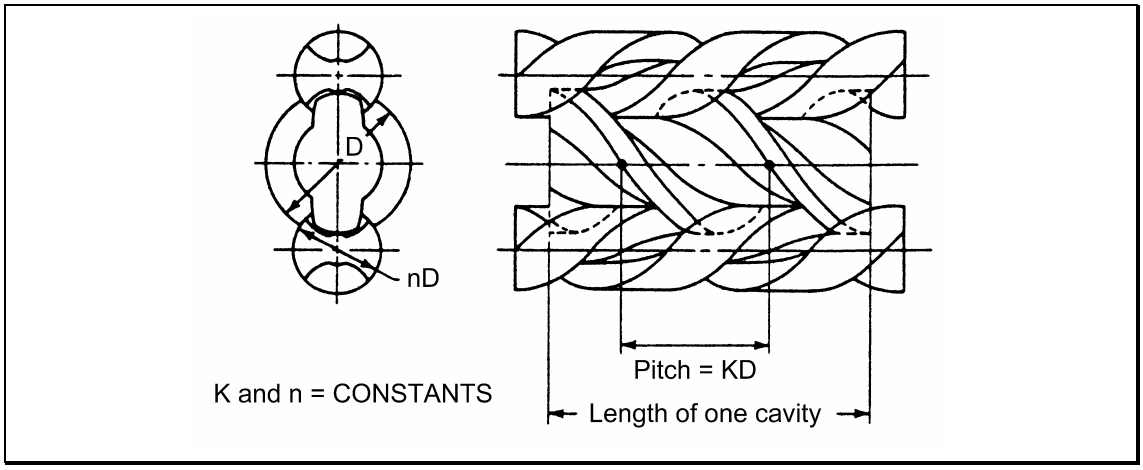


*Figure 11 Thread proportions of a triple screw pump, showing pitch and diameter; Karassik /36/*

Screw pumps can be used for pumping viscous liquids such as fuel and lubricating oils, coolants and emulsions. They are used in a number of processes, on ships, on off-shore platforms, in power utilities, in oil refining and transfer and in the chemical industry. The screw pump is capable of handling oil viscosities ranging from 50 mm²/s to 50,000 mm²/s at a delivery rate up to 1200 m³/h (20,000 l/min); Leistritz /37/.

# 4 Performance of the Leistritz flowmeter

To evaluate a performance prediction model a good knowledge of the performance of the current design of meter is necessary. The performance of the Leistritz flowmeter is reviewed in detail, discussing fluid, performance and installation considerations. Measurements on accuracy, installation conditions, batch accuracy, endurance and manufacturing quality have been performed. The results are presented according to performance criteria stated in BS 7405 /1/. According to the tests performed, the meter was proved to have an overall performance within the high levels of accuracy claimed by the manufacturer and the PTB (Physikalische Technische Bundesanstalt Germany). The uncertainty of the meter is affected by the fluid parameters, temperature, density and viscosity. Higher bearing friction and a poor manufacturing quality are the main reasons for a decrease in the linearity of the meter.

## 4.1 Measurements

Experimental measurements were made on a specially designed test rig, to determine the performance of the current meter for the range of flowrates from 2 to 50 l/min. The maximum throughput rate was chosen according to the desired application in the field. Although desirable, a larger flowrate up to 300 l/min could not be realised within the available budget. The rig consisted of a pump with an over pressure valve, one sump tank and a tank mounted 3 m above ground level, to provide a non pulsating flow for low flow-rates. The type of meter used was the Leistritz screw flowmeter with the specified assembly conditions and clearance parameters which existed in May 1995.

### 4.1.1 Reference meter calibration

Initially a screw type reference flowmeter was calibrated using a 20 litre volumetric cylinder gauge. Several repetitions were made in order to assure reproducible results. For flow-rates from 5 to 50 l/min the rig was used with the pump and the bypass valve (Figure 12), and for the lower flow-rates from 2 to 5 l/min with the constant level tank (Figure 13). After initial tests, the best meter available was selected as the designated reference meter. Requirements described by Mankin /38/ were followed. These are; to start with a wetted tank, to test the meter at its maximum and minimum flowrates and to repeat tests as many as four times to eliminate random error. The meter was calibrated in two different installations: with fluid flow through the meter from bottom to top and vice versa. Temperature conditions were from 17 °C to 27 °C, Hebrosol® was used as a petrol substitute for safety and health reasons and cutting oil with a viscosity of 10 mm²/s was used as an example for a fluid with a higher viscosity. The accuracy achieved for the reference meter was ±0.15 % of the actual reading (Figure 16). After

the systematic error related to flowrate was eliminated, an accuracy of ±0.05 % of the actual reading could be obtained (Figure 17). This linearised plot of the reference meter was used as a calibration standard for all other measurements. The measurement was found to be independent of flow direction.

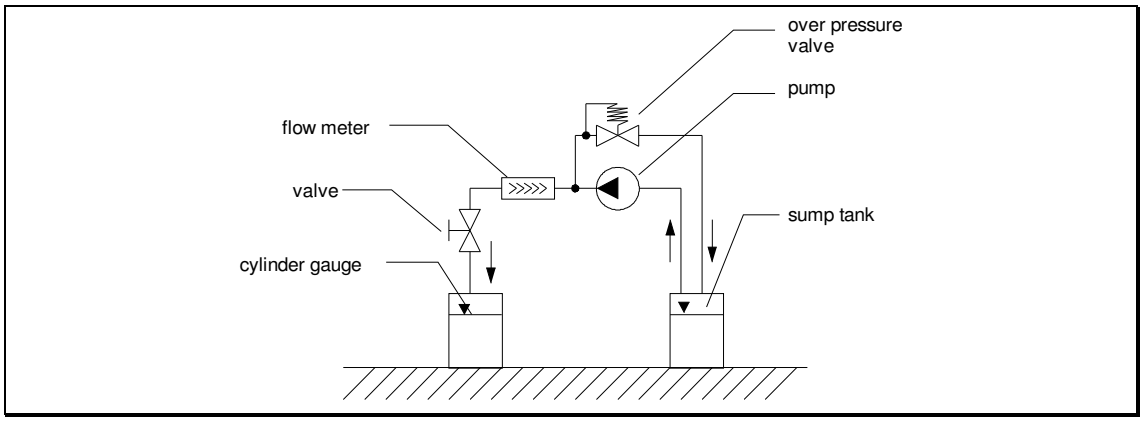


*Figure 12 Test rig for the calibration of a screw type flowmeter for 5-50 l/min*

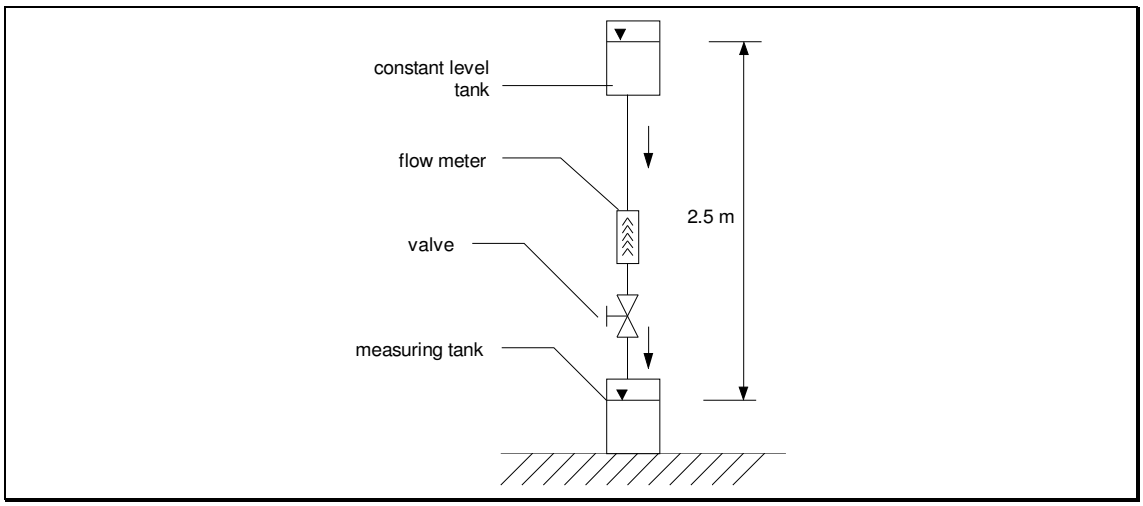


*Figure 13 Test rig for the calibration of a screw type flowmeter for 2-5 l/min*

### 4.1.2 Design variation tests

For a series of different flowmeters of the same type, the meter error was determined using the reference meter instead of the volumetric gauge. Other accessories, such as a bypass with valves, were built into the rig to control the flow through the tested meter. In a method similar to the calibration of the reference meter, for flow-rates from 5 to 50 l/min the rig was used with the pump and the bypass valve (Figure 14), and for the lower flow-rates from 2 to 5 l/min with the constant level tank (Figure 15).

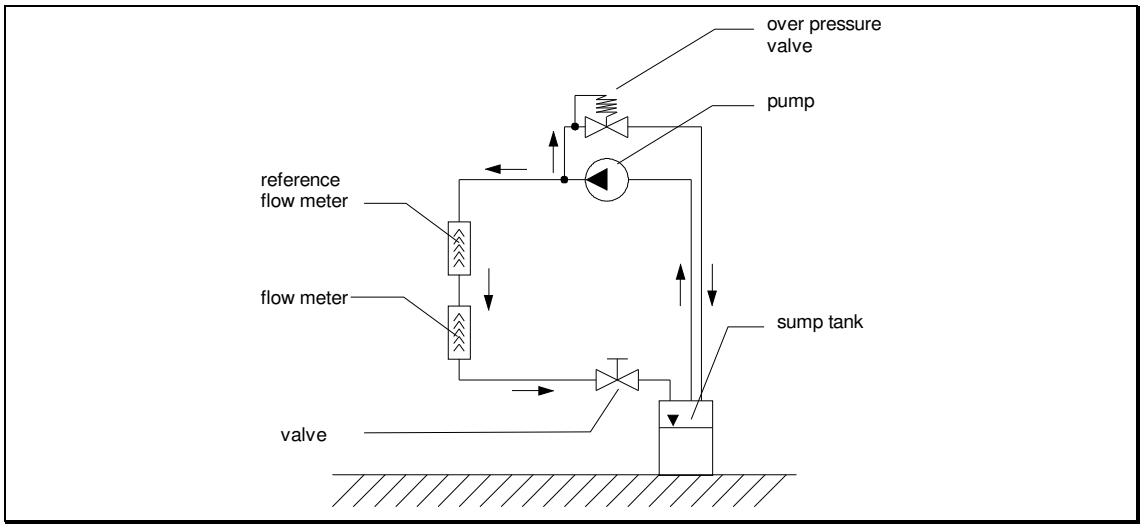


*Figure 14 Test rig for the calibration of a screw type flowmeter with a reference meter for 5-50 l/min*

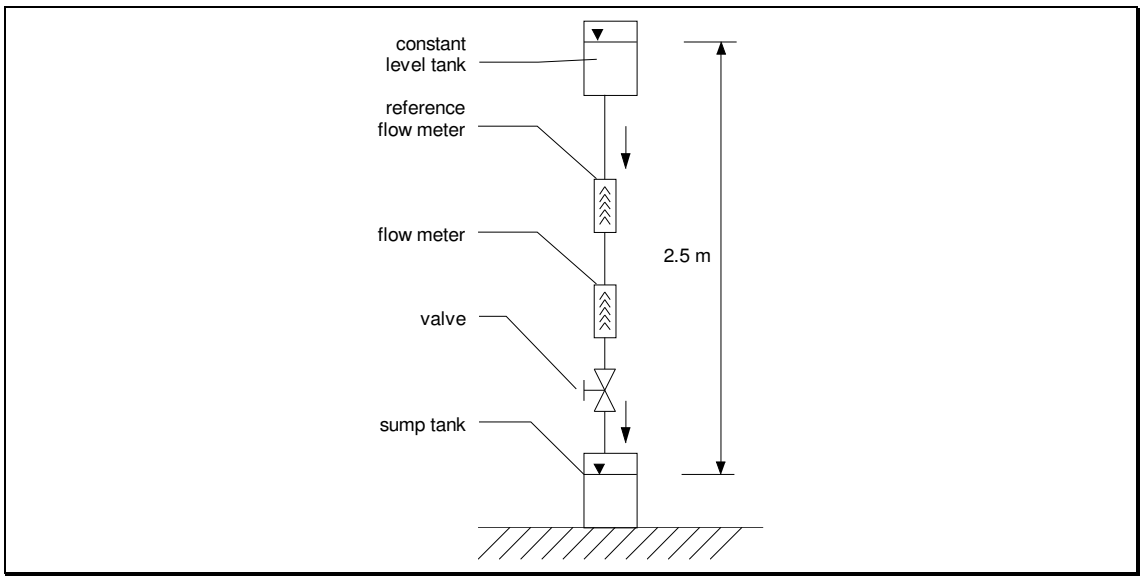


*Figure 15 Test rig for the calibration of a screw type flowmeter with a reference meter 2-5 l/min*

Tests were performed using flowmeters with different clearance dimensions within the required tolerances, and with flowmeters of different manufacturing quality and bearing quality as defined in the following. In order to compare manufacturing quality, a pair of rotors within the design specifications of pitch accuracy was tested against a pair of rotors, which were known to be outside the specified requirements. In order to compare bearing quality two different sets of bearings were used, one of which produced significantly more friction than the other set.

### 4.1.3 Endurance tests

A flow of 50 l/min was continuously supplied to five flowmeters assembled in line. After every 2000m³, which equals an operating time of 27 days, the test was stopped and the meter error and the head loss of the five flowmeters was measured. Additionally the flowmeters were disassembled and the condition of rotors and bearings were checked. The test ended after one year of operating time when 20000m³ of total volume had been reached. The bearings were send to the manufacturer for a wear analysis of runways and balls.

### 4.1.4 Limitations

The experimental results have limitations as listed in the following. These limitations are the reason for the necessity of the current work:

(a) No clearance variation:

Variations of clearance dimensions always results in a change of the complete rotor and bearing assembly, which itself is influencing the flowmeter performance significantly. Hence the clearance influence can not be measured as a stand alone value.

(b) No design variations:

Major design changes of the flowmeter could not be realised within the available budget, especially because all components have to be machined to a very high and uniform degree of accuracy to achieve comparable results.

(c) Little fluid variation:

Only a limited number of tests has been performed with a higher viscosity fluid (lubricating cutting oil with kinematic viscosity $\nu \approx 10$ mm²/s). No tests have been performed using shellsol, petrol, diesel oil or water.

(d) No turndown variations:

The only tested turndown range was from 2 to 50 l/min. No flowrates above 50 l/min were tested, although a flowrate of up to 300 l/min was of interest.

(e) No combined test:

According to the limitations above, no test have been performed with any combination of the variations listed above. This would include for example a combination of higher viscosity and higher clearances.

## 4.2 Performance discussion

The performance of flowmeters can vary significantly depending on both the design and the fluid parameters. Flowmeter performance is judged from accuracy and repeatability figures. If a meter is consistently accurate then it is also repeatable. However, repeatability by itself does not guarantee accuracy. Performance criteria related to BS 7405 /1/ are presented together with the results of the measurements performed as described above.

### 4.2.1 Accuracy

This is a qualitative expression for the closeness of a measured value to the true value. Throughout this work all values of accuracy are related to the actual reading. For the reference meter and Hebrosol®, the error was determined to ±0.15 % of the actual reading for the non-linearised value (Figure 16). An improvement of accuracy can be achieved by eliminating the systematic error as described in the following.

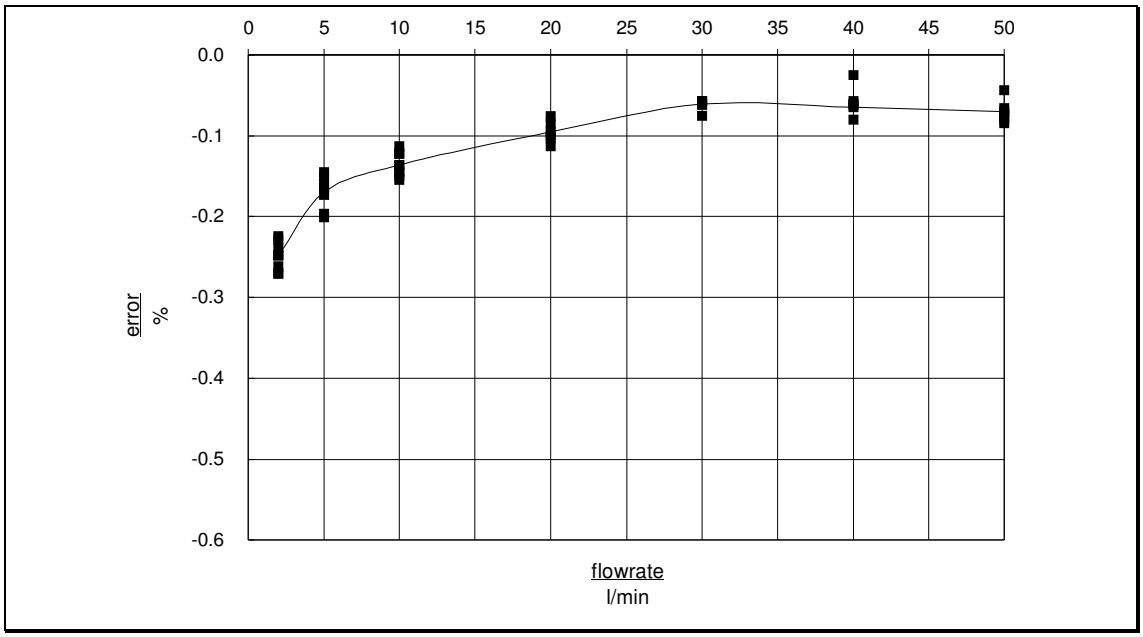


*Figure 16 Calibration of a screw type flowmeter; error vs. flow-rate*

### 4.2.2 Repeatability

Repeatability is the quantitative expression of the closeness of agreement between successive measurements. It can be affected by variations in temperature, pressure, viscosity and other fluid properties as well as external environmental influences. The variations in output may deviate from a mean value in accordance with established statistical laws.

Both the results of the calibration of the reference meter with the volumetric gauge as described in 4.1.1, and the repeated determination of the meter error of flowmeters against the reference meter as described in 4.1.2 show a high repeatability. It is interesting to note that the comparative method, as described in 4.1.2, gives better results than the actual volumetric calibration. The random variation is below ±0.05 % of reading, which is within the best classification of measurement devices (Figure 17).

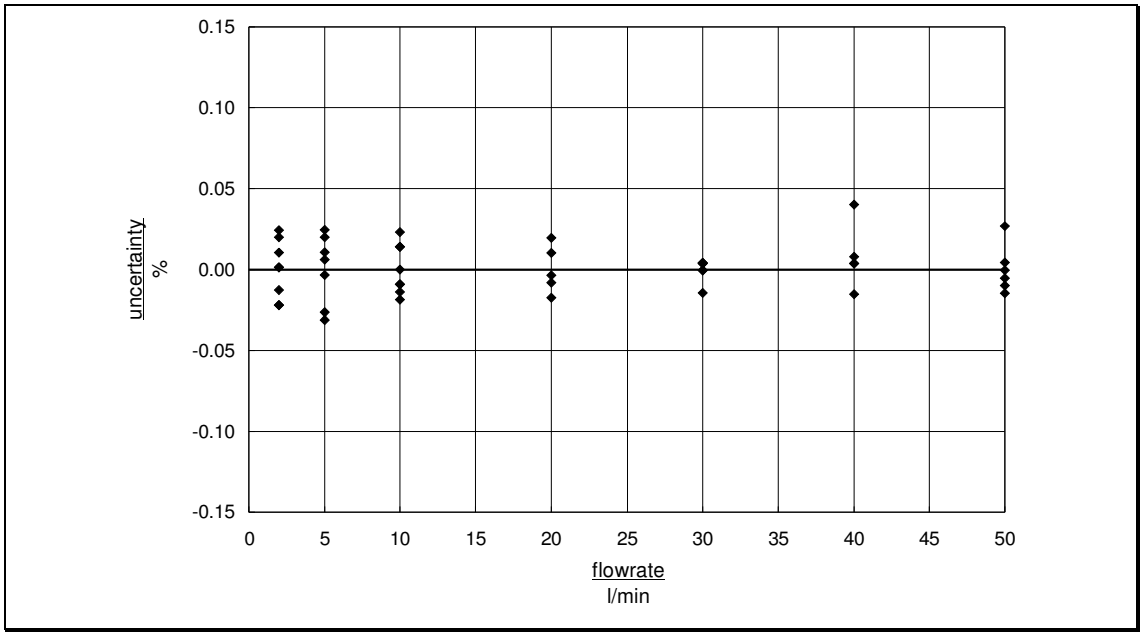


*Figure 17 Random error of calibration of a screw type flowmeter; uncertainty vs. flow-rate*

### 4.2.3 Linearity

This is the deviation of a flowmeter's performance from the ideal straight line relationship between meter output and flow rate, hence the difference between maximum and minimum error value. Linearity is often an important parameter in determining the selection of a flowmeter but it should not be confused with uncertainty. The results of the calibration show a significant systematic deviation related to flow-rate, the characteristic linearity curve of the flowmeter. Tests using a fluid of higher viscosity than petrol, such as diesel oil, show a significant lower deviation from linearity (Figure 18). Low manufacturing quality (Figure 19) and increased bearing friction (Figure 20), as described in 4.1.2, produced a decrease in the linearity of the meter.

It was impossible to prove a relation between the clearances dimensions caused by the production tolerances and the linearity of the flowmeter. The reason for this is that the rotors could not changed without changing the bearing assembly. The influence of

the bearing assembly on the performance of the flowmeter exceeds the influence of the clearances. Clearances exceeding the allowed tolerances have not been tested, because the manufacturing process of grinding with a shaped tools does not allow any modifications in the profile. A change would result in the need for new tools. Additional trail and error time to adjust the machining process would be required and exceed the available budget.

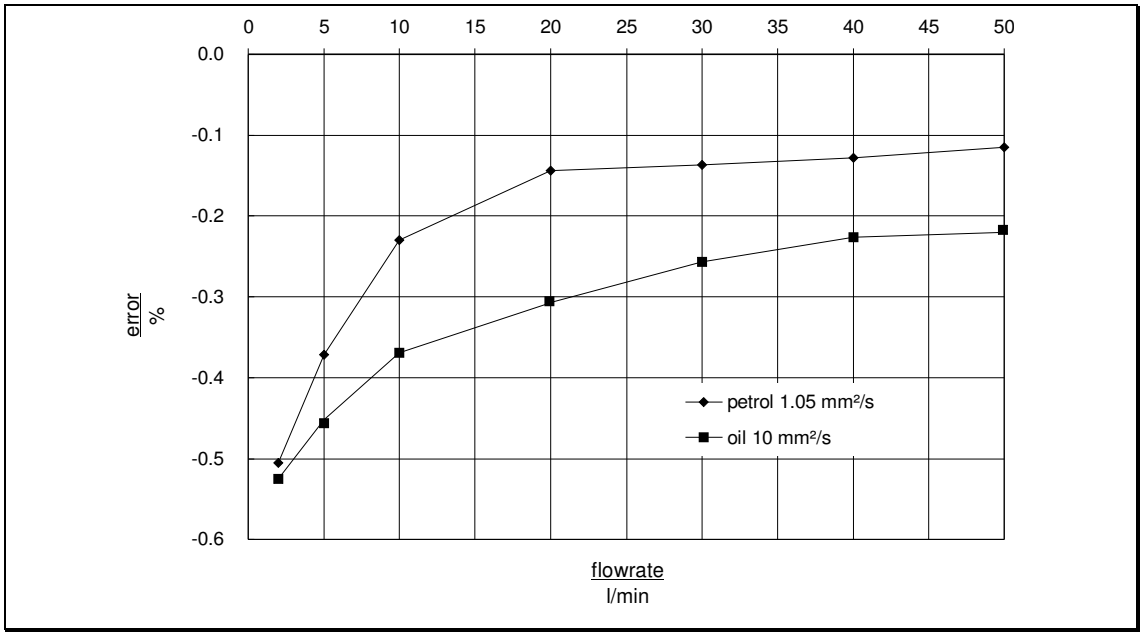


*Figure 18 Measurement of fluids with different viscosity; error vs. flow-rate*

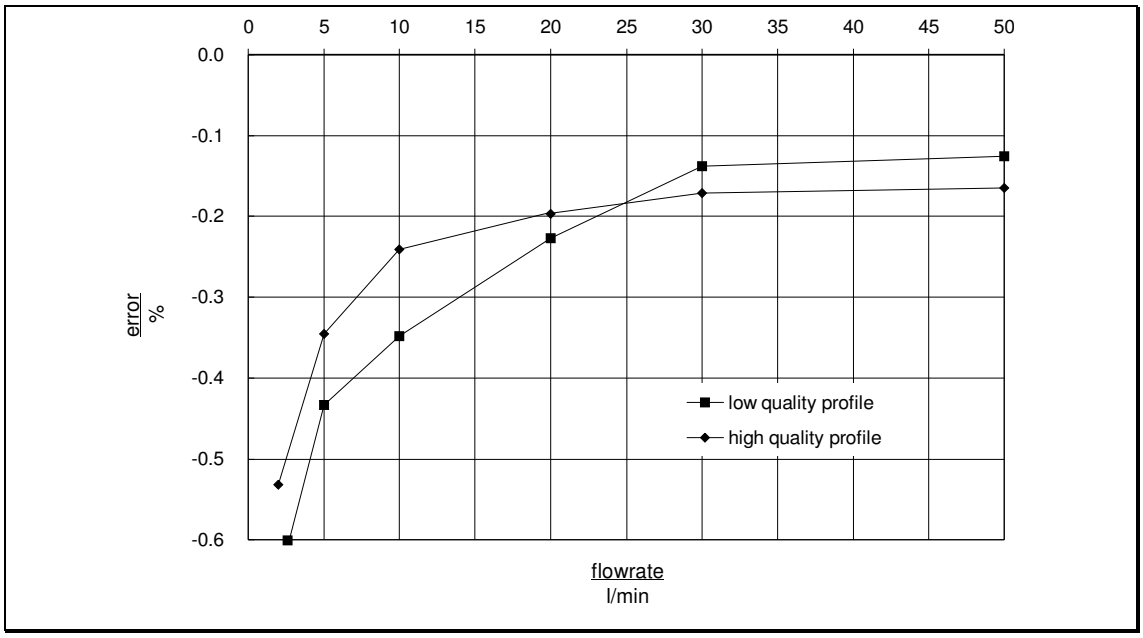


*Figure 19 Influence of the manufacturing quality on the flowmeter performance; error vs. flow-rate*

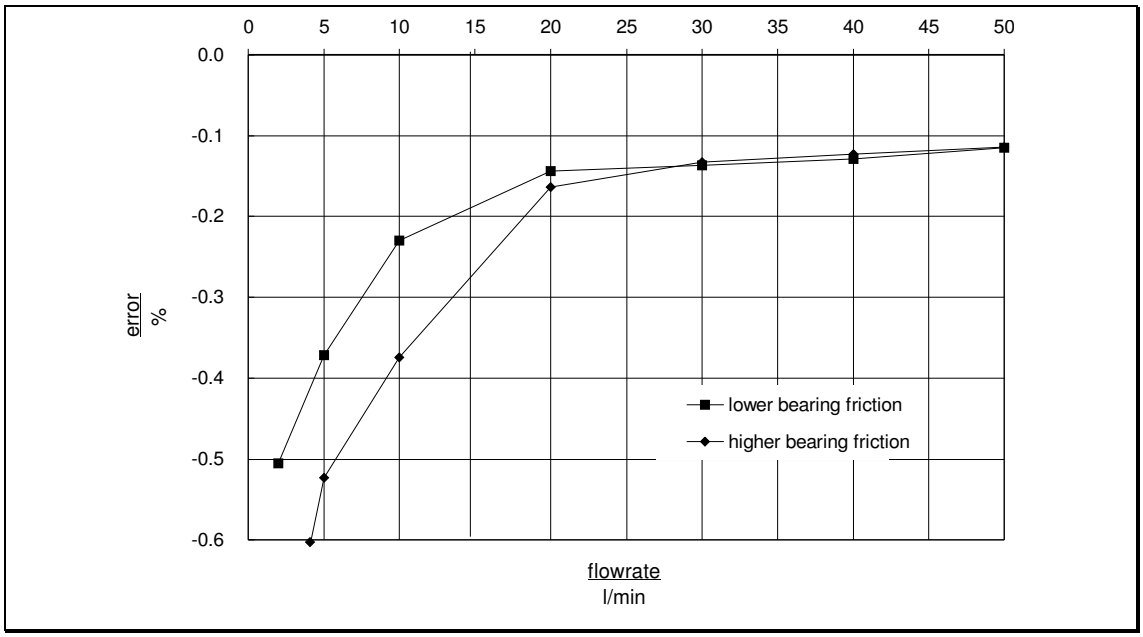


*Figure 20 Influence of the bearing quality (bearing friction) on the flowmeter performance; error vs. flow-rate*

### 4.2.4 Turndown

Turndown is the ratio of the specified maximum to minimum flow rates. If a meter is highly repeatable but not necessarily linear, the output can be conditioned to increase the useful flow range. Fluid property effects, particularly density and viscosity are also

important since these may alter the linear operating range of the meter significantly. For low flows the range is limited by slippage. The Leistritz screw flowmeter has a 25:1 turndown for a dynamic viscosity of 1 mPas. For low flows, below a flowrate of 2 l/min, linearity is decreasing approximately expressible by an exponential equation. For high flows the limiting factors are an increasing head loss and resulting bearing load and wear. For the current application according to the results of the endurance tests, a bearing failure has not occurred for a constant flowrate of 50 l/min with one year of continuous operation. Hence a statement regarding the maximum operating flowrate can not be made.

### 4.2.5 Pressure drop

The main application of the meter is a diesel/petrol filling station, the limited pumping capacity of which may be adversely affected by a high head loss generated by the meter. In addition with hydrocarbon liquid applications having a high vapour pressure, excessive pressure drop may result in cavitation or vaporisation of the liquid with the consequent loss of metering accuracy. The pressure drop of the complete meter is limited to 0.5 bar = 50000 Pa for petrol at 50 l/min. The maximum measured pressure drop of the meter without valves was below 0.3 bar (Figure 21). The pressure drop over the rotors, as mentioned in Figure 21, is the pressure drop over the flowmeter minus the pressure drop of the flow through the empty housing.

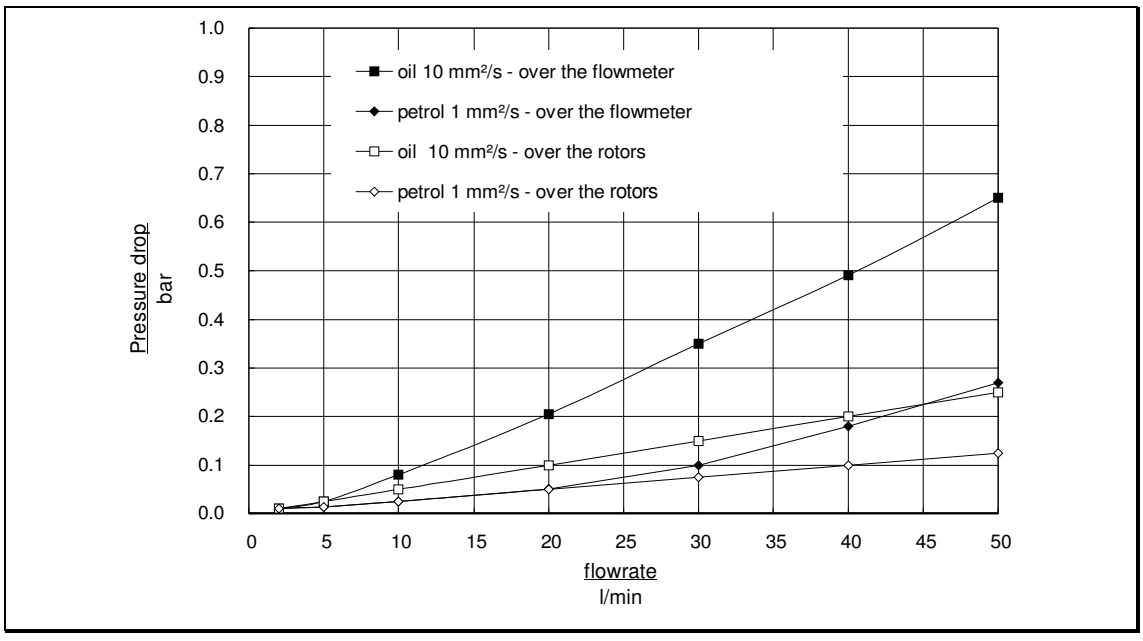


*Figure 21 Measurement results of the Leistritz screw flowmeter; pressure drop against flowrate*

### 4.2.6 Installation requirements

The tested flowmeters were not influenced by inlet pipework, which gives rise to inlet swirl conditions. The performance of the flowmeter does not vary between horizontal and vertical installations. With bi-directional operation, performance does not vary significantly between forward and reverse directions. The screw flowmeters were not found to be affected by the inlet flow conditions.

### 4.2.7 Durability

During the complete test of one year of continuous operation, the accuracy of the tested flowmeters did not change significantly. The rotors showed slight marks at the engaging surfaces, but no wear. All bearings showed an increased axial internal bearing clearance and some bearing balls and runways showed marks. To summarise, after the endurance test, all parts were fully functional and their use could have been continued.

## 4.3 Conclusion

The Leistritz flowmeter was proved to have an excellent overall performance within the high accuracy claimed by the manufacturer and the PTB (Physikalische Technische Bundesanstalt; Germany). For a range within 2 to 50 l/min, the approved accuracy is ±0.3 % of the measured value with a repeatability ±0.05 % for a dynamic viscosity of $\eta < 1$ mPas.

Two aspects are important for the performance prediction of the flowmeter, the determination of linearity and uncertainty. Changes of temperature, density and viscosity in the fluid, effect the uncertainty of the flowmeter. Higher bearing friction and a low manufacturing quality are the main reasons for a decrease in the linearity of the flowmeter. A flowmeter with a poor linearity is affected more by fluid property changes than a screw flowmeter showing a good linearity. Hence the bearing assembly and profile accuracy and quality as described in 4.1.2 have to be controlled carefully.

# 5 General performance prediction

The model as described below is the original work of the author, as the result of a thorough study of the different ideas of flowmeter modelling. This model is considered a central feature of this thesis. One main idea which the author regards as being especially new is the direct relation of the energy loss in the fluid to the internal losses in the flowmeter. Hence the calculation of the torque on the rotor by the fluid pressure is not necessary and the error of a flowmeter can be calculated directly as a mathematical function of the given operating speed. The logic is that a flowmeter performs at a defined pressure loss for a given speed. This pressure loss times flowrate is then energy balanced against all internal losses. Pressure loss and speed are the causes of leakage. Rotational speed times the theoretical swept volume, describe the theoretical flowrate. This flowrate, when combined the leakage flow can be used to calculate the effective or true flowrate. The flowmeter performance is then related to 8 geometric coefficients influenced by the design of a flowmeter. These represent different frictional and volumetric losses in the flowmeter.

## 5.1 Literature review

Not much literature is available on the performance prediction of PD flowmeters. Baker /24/ and Morris /23/ use the geometry of a sliding vane flowmeter to set down two main equations of the flow through a PD flowmeter. However, the model of Baker and Morris /23/ does not include all relevant volumetric and mechanical losses to successfully model a PD flowmeter performance.

Additional influences proposed by Bavendiek /39/, Schlösser /40-44/ and Wilson /45-49/ allow a more accurate description of the governing equation. They present a theory, describing the performance of rotary positive-displacement pumps and fluid motors in terms of torque and delivery. All authors mentioned basically claim that the performance of a motor can be outlined in terms of two simple equations, a volumetric and a torque equation. Firstly these authors developed a volumetric equation, making use of the equation for ideal bulk flow and an equation which gives leakage flow. They differentiate between 3 types of leakage flows:

(a) leakage flow related to pressure drop and viscosity (laminar flow),

(b) leakage flow related to pressure drop and density (turbulent flow) and

(c) leakage flow related to speed.

The different leakage flows are supposed parallel and summarised over the motor or pump. Secondly all the authors mentioned above propose that the turning force due to

pressure drop which acts on the rotors, will precisely balance the frictional torques due to viscous friction in clearance spaces, mechanical friction, constant friction, internal acceleration losses and ball bearing friction. Schlösser /40- 44/ proposes that the driving torque of a pump can calculated from differential pressure and displacement volume.

## 5.2 Meter performance prediction theory

The logic is that a flowmeter performs at a defined pressure loss for a given speed. This pressure loss times flowrate is then balanced against all internal losses. Pressure loss and speed are the sources of leakage. Rotational speed times the theoretical swept volume, or the frequency of pulses of the counting device, describe the theoretical flowrate $\dot{V}_{th}$ which, knowing the leakage flow can be used to calculate the effective or true flowrate $\dot{V}_e$. Using these two flowrates, the characteristic of a flowmeter can be obtained:

$$E = \frac{\dot{V}_{th} - \dot{V}_e}{\dot{V}_e} \qquad (1)$$

The sum of all internal losses consists of five components, considering all influences discussed in literature, Baker and Morris /23/, Schlösser /43/, Wilson /49/, Bavendiek /39/:

$$\sum P_i = P_D + P_U + P_C + P_T + P_B \qquad (2)$$

These are:

$P_D$ Viscous friction power loss
$P_U$ Mechanical friction power loss
$P_C$ Constant torque power loss
$P_T$ Impulse power loss
$P_B$ Ball bearing viscous friction power loss

If each of these losses is now further investigated in turn, each power loss is then a function of a loss coefficient. The viscous friction power loss $P_D$ or viscous friction torque $T_D$ is caused by the shear stress in the fluid in the narrow clearances between the rotors and the housing, the magnitude of which is represented by the viscous friction power loss coefficient $\kappa_D$. The torque will be directly proportional to the viscosity of the liquid, directly proportional to the speed and inversely proportional to the clearances.

$$T_D \sim \eta_{fl} n \qquad (3a)$$

$$P_D = \kappa_D \eta_{fl} \omega^2 \qquad \text{units of } \kappa_D = mm^3 \qquad (3b)$$

The mechanical friction power loss $P_U$ is caused by sliding friction. The mechanical friction torque $T_U$ is independent of the fluid and of speed and directly proportional to

the pressure drop. This friction arises in the bearings and in areas of close contact between rotor and housing and its magnitude is represented by the mechanical friction power loss coefficient $\kappa_U$. The variation with the head loss is caused by physical deflections within the flowmeter which are proportional to pressure.

$$T_U \sim \Delta p \tag{4a}$$

$$P_U = \kappa_U \Delta p \omega \qquad \text{units of } \kappa_U = mm^3 \tag{4b}$$

The constant torque power loss $P_C$ is caused by a constant retarding torque which is independent of speed, pressure and viscosity and therefore constant. The constant retarding torque can then be replaced by constant torque power loss coefficient $\kappa_C$ and is caused by friction in seals or at other points of close contact where clearances do not change with pressure.

$$T_C = const \tag{5a}$$

$$P_C = \kappa_C \omega \qquad \text{units of } \kappa_C = Nmm \tag{5b}$$

The impulse power loss $P_T$ was introduced by Schlösser /40-44/ as an additional loss to the three types listed above, which already have been presented by Wilson /45/. This impulse and acceleration loss torque $T_T$, which is generated by an internal acceleration of the fluid in the flowmeter, is related to the density of the fluid and the speed squared. $\kappa_T$ is the impulse power loss coefficient representing the magnitude of internal acceleration in the flowmeter.

$$T_T \sim \rho_{fl} n^2 \tag{6a}$$

$$P_T = \kappa_T \rho_{fl} \omega^3 \qquad \text{units of } \kappa_T = mm^5 \tag{6b}$$

The ball bearing speed dependent friction power loss $P_B$ was presented by Bavendiek /39/ as a bearing friction torque $T_B$. It is deduced from the common ball bearing speed dependent torque and can be represented by the ball bearing viscous friction power loss coefficient $\kappa_B$.

$$T_B \sim \left( \frac{\eta_{fl}}{\rho_{fl}} \right)^{2/3} n^{2/3} \tag{7a}$$

$$P_B = \kappa_B \left( \frac{\eta_{fl}}{\rho_{fl}} \right)^{2/3} \omega^{5/3} \qquad \text{units of } \kappa_B = Ns^{7/3} m^{-1/3} \tag{7b}$$

Using the constant coefficients $\kappa_{D,}$ $\kappa_{U,}$ $\kappa_{C,}$ $\kappa_{T,}$ and $\kappa_B$ instead of the proportional equations, the sum of power losses can be written as:

$$\sum P_i = \kappa_D \eta_{fl} \omega^2 + \kappa_U \Delta p \omega + \kappa_C \omega + \kappa_T \rho_{fl} \omega^3 + \kappa_B \nu_{fl}^{\frac{2}{3}} \omega^{\frac{5}{3}} \qquad (8)$$

The volumetric governing equation for flowmeters, applying the model of Schlösser /40- 44/, has to consider viscosity related slip $\dot{V}_{SV}$, density related slip $\dot{V}_{SD}$, and slippage due to viscous drag $\dot{V}_D$.

$$\dot{V}_e = \dot{V}_{th} + \dot{V}_{SV} + \dot{V}_{SD} - \dot{V}_D \qquad (9)$$

The viscosity related slip $\dot{V}_{SV}$ is proportional to pressure, inversely proportional to viscosity and related to the constant laminar slip coefficient $\kappa_{lam}$, which represents the sum of all clearances which show a laminar leakage flow pattern.

$$\dot{V}_{SV} = \kappa_{lam} \frac{\Delta p}{\eta_{fl}} \qquad \text{units of } \kappa_{lam} = mm^3 \qquad (10)$$

The density related slip $\dot{V}_{SD}$ is proportional to the square root of pressure, inversely proportional to the square root of the fluid density and related to the constant turbulent slip coefficient $\kappa_{tur}$, which represents the sum of all clearances which show a turbulent leakage flow pattern.

$$\dot{V}_{SD} = \kappa_{tur} \sqrt{\frac{\Delta p}{\rho_{fl}}} \qquad \text{units of } \kappa_{rot} = mm^2 \qquad (11)$$

The rotational leakage flow $\dot{V}_D$ is proportional to speed, and related to the constant rotational slip coefficient $\kappa_{rot}$, which represents a rotational leakage volume.

$$\dot{V}_D = \kappa_{rot} \frac{\omega}{2\pi} \qquad \text{units of } \kappa_{rot} = mm^3 \qquad (12)$$

According to the law of energy conservation, the power loss in the fluid which actually passes the flowmeter, which is the effective flowrate, has to equal the sum of all losses in the flowmeter. This are frictional losses and the pressure losses in the leakage flow.

$$\dot{V}_e \Delta p = \sum P_i + \Delta p \left( \dot{V}_{SV} + \dot{V}_{SD} - \dot{V}_D \right) \qquad (13)$$

The effective flowrate is not known at this point, hence using equation 9, the sum of internal power losses is related to the theoretical flowrate:

$$\dot{V}_{th} \Delta p = \sum P_i \qquad (14)$$

Therefore the pressure drop can be expressed as follows:

$$\Delta p = \frac{\kappa_D \eta_{fl} \omega + T_C + \kappa_T \rho_{fl} \omega^2 + \kappa_B \nu_{fl}^{\frac{2}{3}} \omega^{\frac{2}{3}}}{\frac{\dot{V}_{th}}{\omega} - \kappa_U} \tag{15}$$

Introducing the constant coefficients $\kappa_{lam}$ and $\kappa_{tur}$ for the viscosity and density related slip as described by Schlösser /40-44/, and a rotational leakage volume $\kappa_{rot}$, the effective flowrate can be described related to a known pressure drop to:

$$\dot{V}_e = \dot{V}_{th} + \kappa_{lam} \frac{\Delta p}{\eta_{fl}} + \kappa_{tur} \sqrt{\frac{\Delta p}{\rho_{fl}}} - \kappa_{rot} \frac{\omega}{2\pi} \tag{16}$$

with:

$\kappa_B$ Ball bearing viscous friction power loss coefficient
$\kappa_C$ Constant torque power loss coefficient
$\kappa_D$ Viscous friction power loss coefficient
$\kappa_U$ Mechanical friction power loss coefficient
$\kappa_T$ Impulse power loss coefficient
$\kappa_{lam}$ Laminar slip coefficient
$\kappa_{rot}$ Rotational slip coefficient
$\kappa_{tur}$ Turbulent slip coefficient

Now using equation (15) the systematic flowmeter error can be calculated for every operating point directly related to the rotor speed. The design of the flowmeter is described by these 8 constant coefficients as listed above together with the theoretical swept volume $V_{th}$. Once these coefficients are determined the performance of a flowmeter can be accurately modelled.

## 5.3 Discussion

The equations above were used to plot calibration curves of PD flowmeters under varying conditions, using a set of roughly estimated values as mean values for the constant coefficients. It is important to note that the following observations are not related to any specific flowmeter design. A coefficient with its value set to zero means that this type of loss does not refer to a specified flowmeter. A high value for a coefficient means that this type of loss is dominant.

### 5.3.1 Influence of the coefficients

As stated above, there are 8 different coefficients which influence the flowmeter performance. Additionally a variation in density and viscosity is taken into account.

Using a mean value for all coefficients a typical plot of a PD flowmeter calibration curve was created. To determine the influence of each coefficient, the value of all other coefficients was set to zero (Figure 22). Secondly, using mean values for all coefficients, each coefficient was varied in turn over a wide range and the results were plotted (Figure 23 and Figure 24). The following should be noted for the different coefficients:

Only four flowmeter design coefficients have an influence on the shape of the calibration curve, hence produce the deviation from linearity (Figure 22). These 4 reasons for deviation which occur related to the design of the flowmeter are as follows:

(a) The impulse power loss: flowmeters such as the piston flowmeter or the rotary vane flowmeter accelerate the fluid on its path through the flowmeter. If this type of loss is present the flowmeter tends to under register for higher flowrates. (indicated by "only impulse loss" in Figure 22)

(b) The constant torque power loss: the presence of a constant loss independent of speed or viscosity causes the flowmeter to under register for low flow rates. (indicated by "only constant loss" in Figure 22)

(c) The ball bearing viscous friction power loss: the presence of a roller bearing loss causes the flowmeter to under register for low flows. (indicated by "only bearing loss" in Figure 22)

(d) The turbulent slip: the presence of clearances with turbulent density related leakage flow as well causes the flowmeter to under register for low flow rates (indicated by "only turbulent leakage" in Figure 22).

All other losses and leakages have no influence on the shape or linearity of the calibration curve. If all the four listed reasons for deviation from linearity are absent i.e. $\kappa_T = 0$, $\kappa_C = 0$, $\kappa_B = 0$, $\kappa_{tur} = 0$, the error is constant and hence the calibration curve is a horizontal line (indicated by no " all main coefficient set to zero " in Figure 22).

Four influences intensify an existing deviation related to their magnitude. A higher value of coefficient causes the performance of the flowmeter to decrease and the error curve to shift (laminar leakage Figure 23). These coefficients are:

(a) Laminar slip: describing the amount of laminar leakage flow according to the geometry of the flowmeter. More and wider clearances cause a decrease in performance

(b) Viscous friction power loss: describing the power loss by viscous friction in the flowmeter as produced by narrow clearances of parts moving with a high relative velocity.

(c) Variations in density

(d) Variation in viscosity

Two influences are almost neutral. They do not influence the linearity of the flowmeter, but cause the calibration curve of the flowmeter to move in its vertical position. These neutral coefficients are:

(a) Mechanical friction power loss: These are all losses related to dry friction caused by a force which is directly related to pressure (Figure 24). The linearity is hardly influenced even for a maximum applicable friction coefficient. A higher coefficient $\kappa_U$ as selected would prevent the flowmeter from rotating, because the condition $\kappa_U < \dot{V}_{th}/\omega$ in equation (15) must be true.

(b) Rotational slip: This leakage flow has no influence on the linearity at all. A higher rotational leakages can be regarded as an increase in theoretical swept volume.

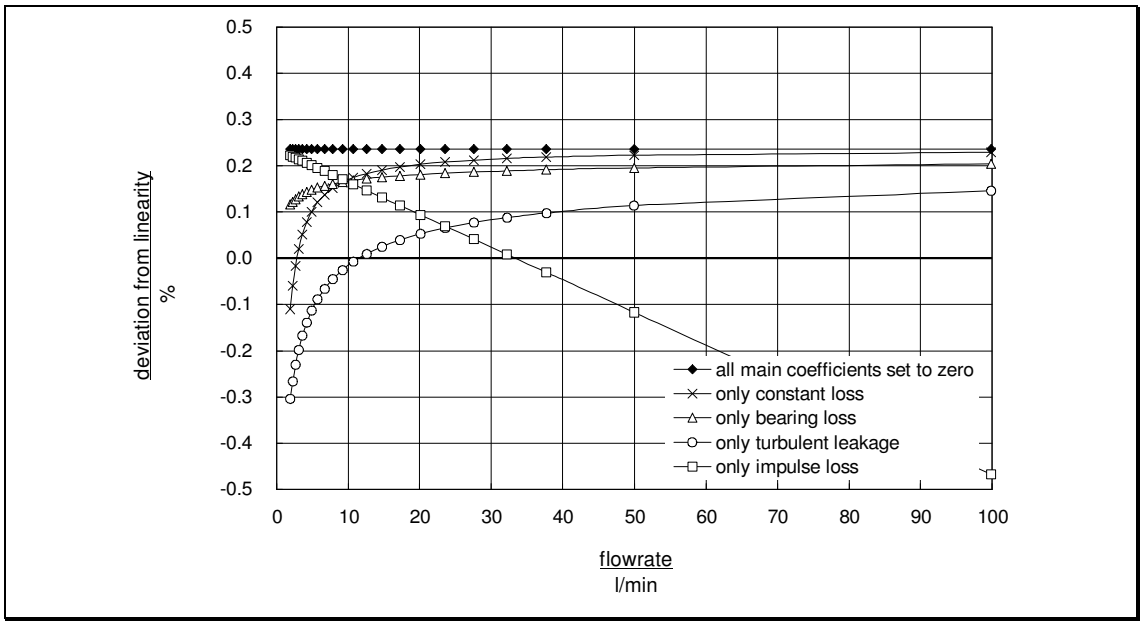


*Figure 22 The influence of different types of losses on the shape of the calibration curve of a PD flowmeter; with $\kappa_T = 0$, $\kappa_C = 0$, $\kappa_B = 0$, $\kappa_{tur} = 0$, there is no deviation from linearity.*

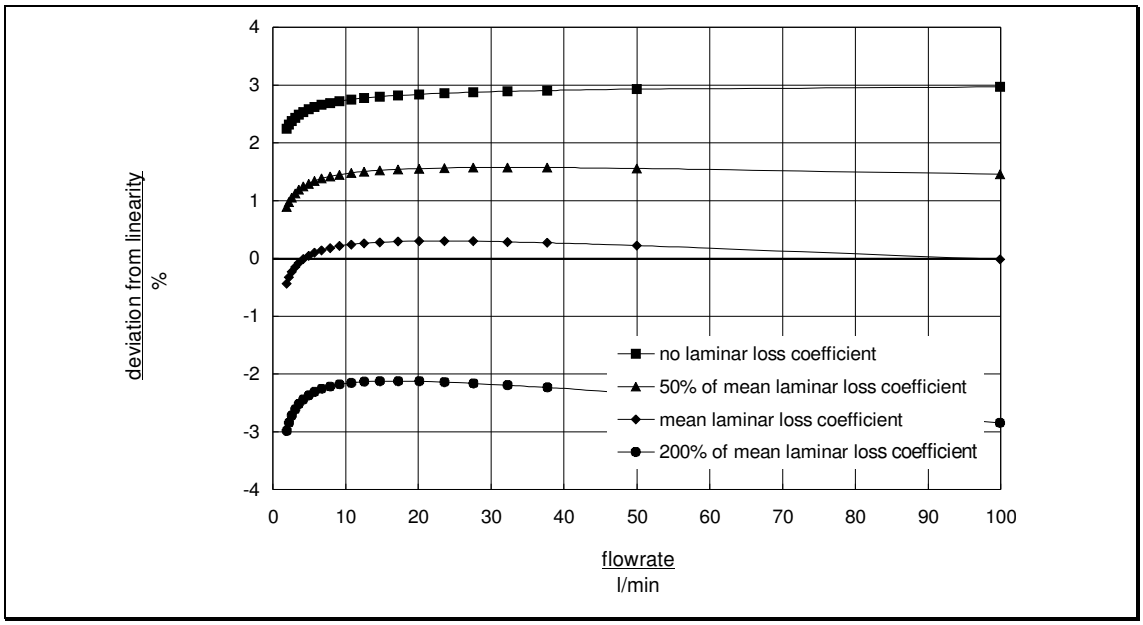


*Figure 23 Amplifying influence of laminar leakage flow on the flowmeter performance*

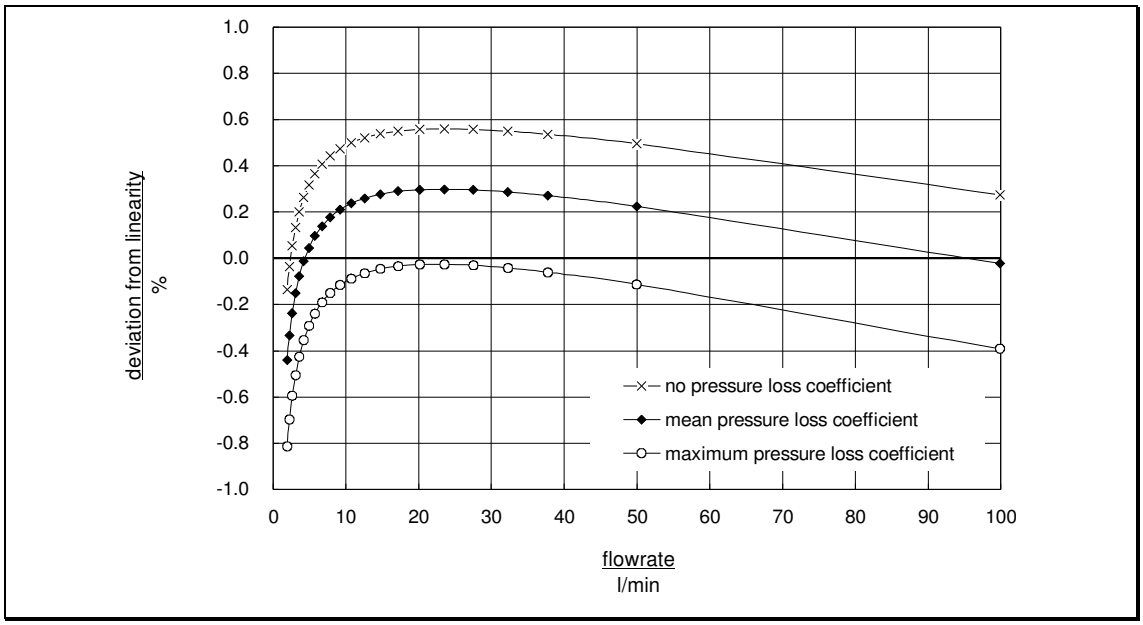


*Figure 24 The influence of the pressure related mechanical friction power losses in the flowmeter on the calibration curve*

### 5.3.2 Sensitivity to temperature changes of a given fluid

Modern PD flowmeters provide an electronic linearisation of the flowmeter characteristic. The question arises, whether the development and effort to obtain a flowmeter with a good mechanical linearity is desirable? A change in temperature of the fluid causes the viscosity and density to change. As mentioned above, the variation of

both amplifies an existing deviation from linearity. Because temperature insensitivity is regarded an important feature of a flowmeter, the influence of viscosity and density variations is described in more detail in the following. A change in temperature from -10 °C to +50 °C is estimated to change the fluid density from 80% to 110% and viscosity from 50% to 200%. For the three reasons of deviation from linearity, namely impulse, bearing and constant loss, these variations in density and viscosity were applied to a high and a low value of each of the loss coefficients. The turbulent leakage flow can not be discussed without the knowledge of the clearance itself, as the turbulent slip coefficient $\kappa_{tur}$ is related to geometry, fluid properties and speed and has to be determined for each operating point separately. The following observations have been made regarding the temperature change as described above:

(a) For the three loss coefficients, the ball bearing viscous friction power loss coefficient $\kappa_B$ (Figure 25), the impulse power loss coefficient $\kappa_T$ (Figure 26) and the constant torque power loss coefficient $\kappa_C$ (Figure 27), a higher value for each loss coefficient causes a higher variation in the plot of flowmeter performance, hence a decrease in accuracy.

(b) Only flowmeters with a good performance can be linearised effectively. Linearised flowmeters with a poor performance will exhibit a poor repeatability if temperature changes occur in the fluid.

It is important to note that with the four reasons of deviation ($\kappa_C$; $\kappa_T$; $\kappa_{tur}$; $\kappa_B$;) absent, a variation in viscosity or density has no affect on the flowmeter characteristic.

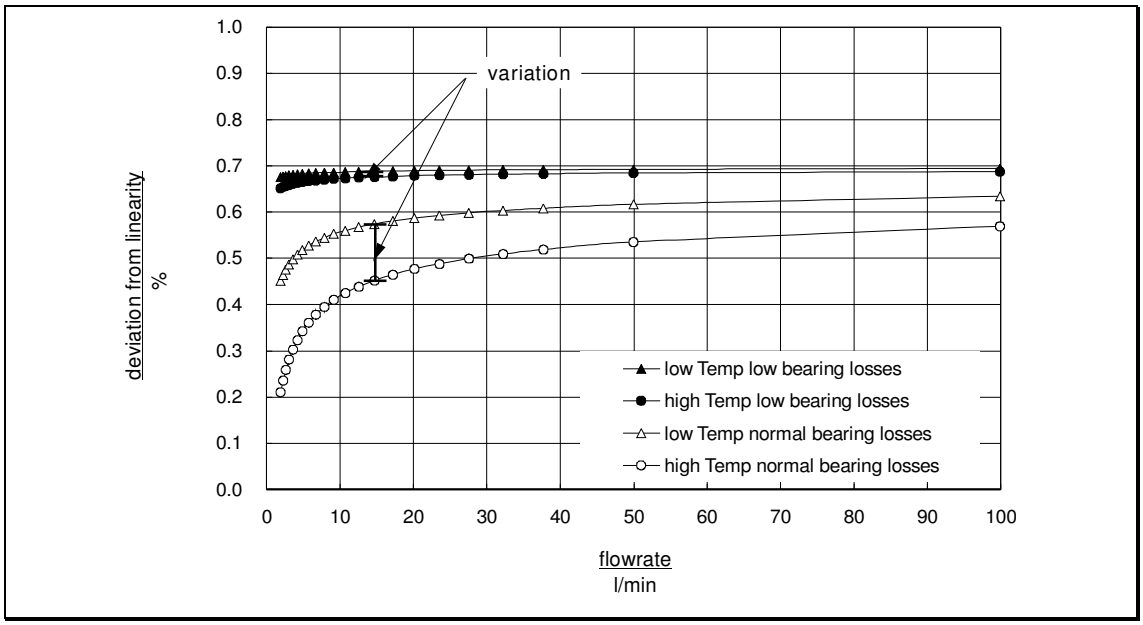


*Figure 25 Temperature related deviations in the flowmeter characteristic for low and normal bearing loss coefficients*

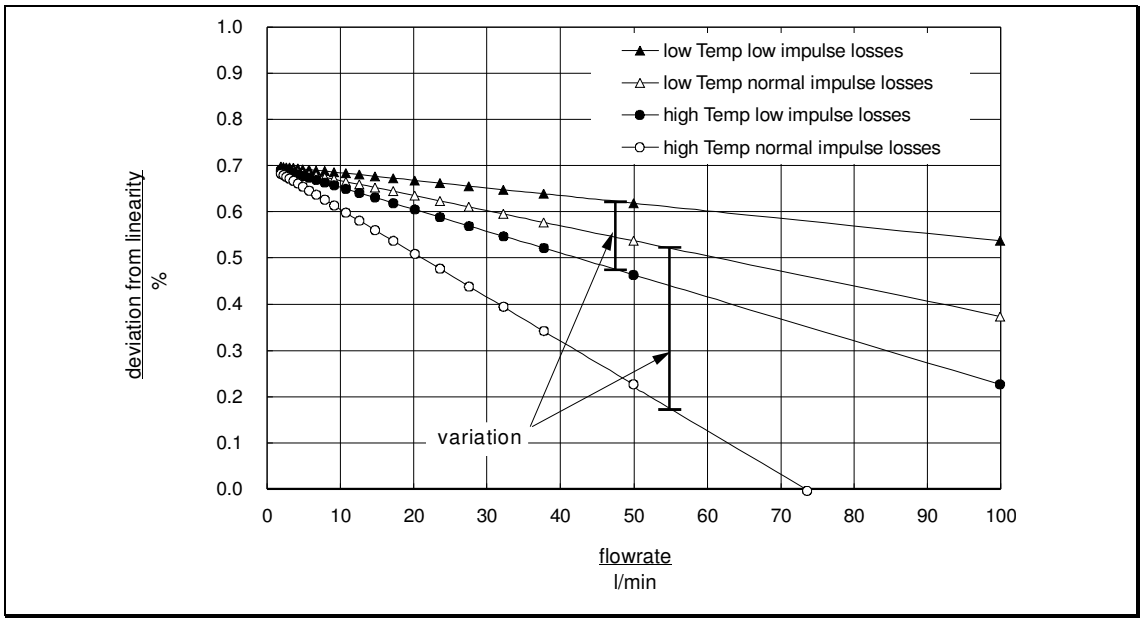


*Figure 26 Temperature related deviations in the flowmeter characteristic for low and normal impulse loss coefficients*

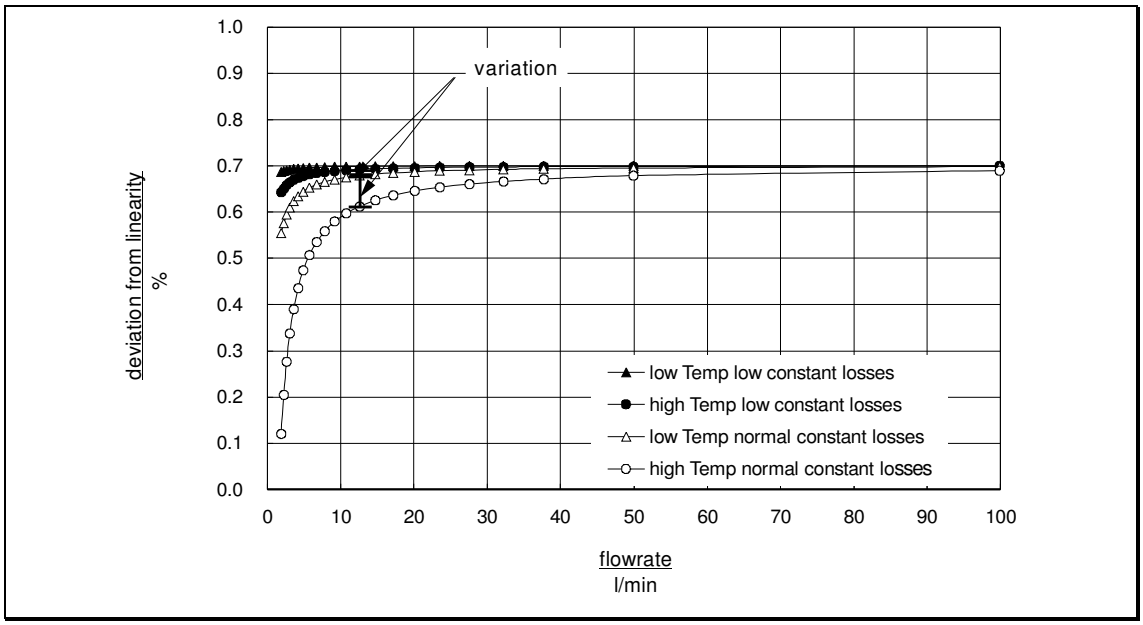


*Figure 27 Temperature related deviations in the flowmeter characteristic for low and normal constant loss coefficients*

### 5.3.3 Influences of the loss coefficients on pressure drop

There are only four loss coefficients which have an influence on the head loss of the flowmeter, the viscous friction coefficient $\kappa_D$, the pressure related friction coefficient $\kappa_U$, the bearing friction $\kappa_B$ and the impulse coefficient $\kappa_T$. As a consequence, viscosity and density of the fluid, which are related to those four coefficients, also influence the pressure drop over the flowmeter. All other coefficients have no effect on the pressure drop.

## 5.4 Conclusion

Of the 8 coefficients which have been introduced, only four loss coefficients can be claimed reasons for deviation from linearity. They give rise to constant friction losses, impulse losses, bearing friction losses and turbulent leakage losses. With those reasons for deviations absent, the plot of error over flowrate is linear and the error is constant. Screw type flowmeters have a low overall pressure drop and show no increased slippage for higher flow rates. Resulting from this, the impulse coefficient has to be almost zero and the three other coefficients involved in the generation of pressure drop relatively small.

The constant friction and the turbulent leakage coefficient affect the plot of accuracy most, and are hence the main reason for flowmeter inaccuracy. Therefore the following is proposed for further modelling of the coefficients.

(a) All sources of constant friction have to be determined and modelled. This is especially difficult as the absolute value of this power loss is expected to be very small and has to be calculated accurately. One of the main possibilities for a constant friction torque is sliding friction in the bearings due to mechanical contact of balls and sealing elements.

(b) All sources of turbulent leakage have to be determined and modelled. For extremely low pressure differences all leakage flows are laminar. The flow in the triangular clearance formed by rotors and housing is expected to change from laminar to turbulent flow before other leakage flows.

(c) Pressure related losses have relatively little influence on the accuracy of the flowmeter. For this coefficient $\kappa_U$, an accurate calculation of the fluid load distribution on rotors is therefore not considered necessary.

Hence for a screw type flowmeter, mainly two coefficients account for deviation from linearity. These are power losses $\kappa_C$ caused by a constant friction torque produced by mechanical sliding and leakage flow losses $\kappa_{tur}$, having a turbulent flow pattern. When the values of $\kappa_C$ and $\kappa_{tur}$ are zero then the error against flowrate is constant.

# 6 Rotor geometry

Screw-meters use helix type rotors to seal inlet and outlet side from each other. There are various different possibilities known to design the helix. Not all of them meet the requirement of total theoretical inlet and outlet separation and a clear definition of the displacement chambers. However, the shape of the profile has a major influence on the flowmeter performance. The profile used is described and the governing parameters presented together with their theoretical and practical limitations. Literature on screw pump profiles is reviewed and the geometry of screw type flowmeters is described. The design of a displacement chamber is presented and characteristic angular positions to describe the chamber are listed separately for the two rotors. The minimum length of a displacement chamber and the theoretical flow-rate are deduced. Of all possible theoretical profiles evaluated for the flowmeter application regarding machinability, sizing and bearing situation, only 12 different designs were found to be realistic from a practical standpoint.

## 6.1 Literature review

### 6.1.1 Montelius screw profiles

There does not appear to be a great deal of information published in the open literature on the Montelius screw pump profiles as used in the current flowmeter applications. The Montelius screw profile is a profile where all rotors use cycloids to describe the profile. A set of rotors of this design will always roll on each other like gears and provide a complete theoretical sealing of inlet and outlet side.

Ryazantsev /50/ states that the profiles developed by Carl Montelius (montelius profiles), are those used most widely in manufacturing triple screw pumps. These rotors have spirals formed by cycloid profiles which in absence of a chamfer on the profile of the idling rotor theoretically provide tight sealing of the rotor channels. This profile satisfies the Montelius condition for tightness of the profile, which is:

$$m_I = m_{II} - 1 \qquad (17)$$

with:

$m_I$ the number of starts of the driven rotor

$m_{II}$ the number of starts of the idling rotor

Five types of rotor profiles for screw-pumps and their properties with regard to working space formation have been analysed by Hamelberg /51/. Characteristic parameters for the flow rate, the specific work, and the power allow the capacities of different rotors to be compared. The performance characteristic, the effect of gap width,

and the working mode of multi-stage rotors are explained. Not all profiles meet the requirement of total theoretical inlet and outlet separation (Montelius condition) and a clear definition of the displacement chambers. The most commonly used profile for a high sealing performance is the Montelius cycloid profile, which can be used in variations for two or three rotor systems. Due to a good balance of the hydraulic forces the three rotor profile is mostly used for pump applications. The equations for the describing cycloids for the two rotor Montelius profile and the dimensionless minimum rotor length are presented in polar coordinates.

Kalishevskii /52/ presents a cycloidical twin screw profile in a 1-2 and a 2-3 version. He compares mechanical and volumetric efficiency of both pump profiles. Ryazantsev /53/ states that the pumps with the theoretical montelius profile are difficult to machine, because the sharp edge at the root of the driven rotor and the corresponding edge at the tool cause a low surface finish and increased cutting tool wear. The pumps show a low service life, and especially on high pressure pumps some sticking is observed. Three different methods of correcting the montelius profile have been developed. The first method consists of increasing the radial chamfer, the second of a special type of superimposing another profile and in the third method the idling rotor chamfer is formed by the arc of a circle of diameter while the profile of the driven rotor is an equidistant simple epicycloid described by the centre of this circle. All three may be recommended; however, from the combination of structural, production and design advantages, Ryazantsev /53/ claims the second method of profile correction to be preferred. Profiles presented by Kalishevskii /52/, other than the profiles described by Ryazantsev /53;50/, have no chamfer correction and the rolling circle of $rotor_I$ is significantly bigger than its outer diameter, hence the rolling diameter of $rotor_{II}$ is smaller than its root diameter. Equations for the calculation of the theoretical swept volume of a 2-3 triple screw pump are presented by Geimer /54/.

The author has found limitations in the usage of all equations describing screw profiles. The existing sets of equations do not apply to any outer diameter and centre distance combination, it is not possible to completely determine a screw profile of the two screws related to each other, without using random methods. In addition the equations to determine the theoretical cross section of the rotor profiles or the theoretical flow-rate are not sufficient.

### 6.1.2 Other screw profiles

Further work on the profiles of screws for large capacity twin screw pumps has been done by Ryazantsev /55/. He claims that the performance of single start twin screw

pumps can be improved using a special designed and tested asymmetrical profile, and draws the conclusion that the investigated profile can be used in the case where a twin screw pump is pumping a low viscosity fluid at high pressure. The profile itself can not be compared with the profile used in the current flowmeter application. Another method to improve the volumetric efficiency of large capacity pumps is presented by Ryazantsev /56/ for a 2-2 profile with cycloidical meshing. The drawback is a lower mechanical efficiency.

## 6.2 Geometry of cycloidical twin screw profiles

The profile of the helical rotors has two main purposes: first, the sealing of inlet and outlet side of the flowmeter and second, to provide a gearing to transmit power from one rotor to the other. The screw profile is a three dimensional helical screw, which is best described in the cross section perpendicular to the axis of rotation by the outer and hub diameters (Figure 28). The exact equations derived and the description of the logic to create the profile of both related rotors are presented in the following.

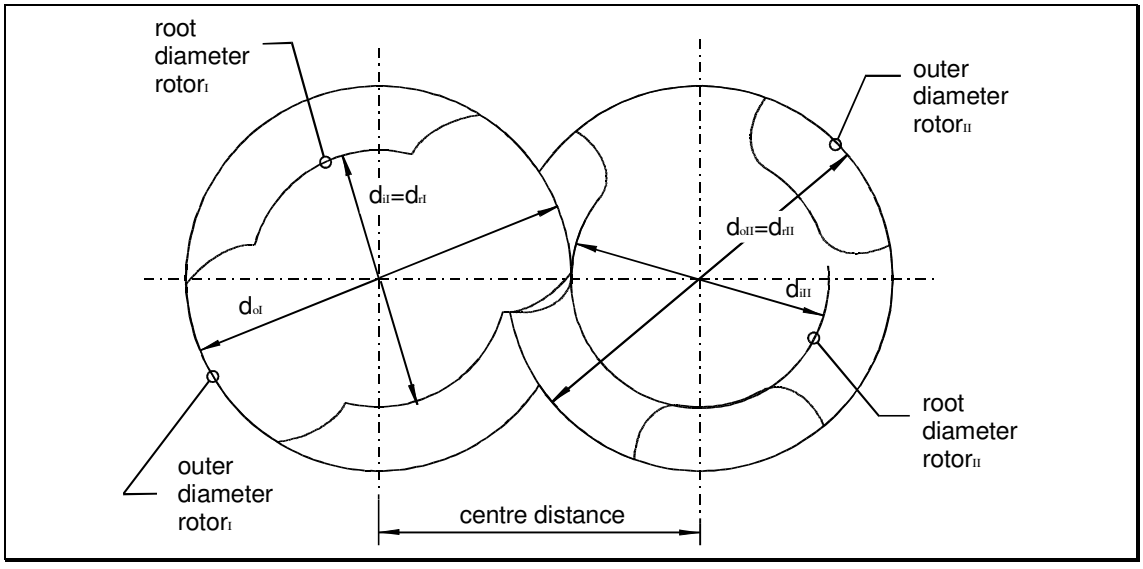


*Figure 28 Cross section of a cycloid screw profile*

Both rotors use cycloids to generate the flanks of the profile, and therefore the characteristics of the profile are very much related to the attributes of the cycloid. A cycloid itself is described by a circle rotating on another circle. The profile of $rotor_I$ is created by the outer diameter of $rotor_{II}$ rolling on the hub diameter of $rotor_I$ and vice versa. Thus the ratio of the rolling diameters, which can be compared with the rolling diameters of a gear combination, has to equal the ratio of the number of starts.

$$\frac{d_{iI}}{d_{oII}} = \frac{m_I}{m_{II}} \tag{18}$$

Hence the sum of both rolling diameters equals the double centre distance and therefore the two missing diameters to describe the profile, which are the outer diameter of $rotor_I$ and the hub diameter of $rotor_{II}$, can be calculated. All other parameters such as the different centre angles to describe the head, flank and hub sections of the profiles can be determined in relation to these diameters.

To summarise, the cross section of similar profiles can be determined from the ratio of the number of starts $\varepsilon$ and the ratio of the outer diameters $r$. The size is related to the outer diameter $d_{oI}$ of $rotor_I$ and the helix is described by the angle of the pitch of the thread.

$$\varepsilon = \frac{m_I}{m_{II}} \tag{19}$$

is the ratio of the number of start with $m_I$ as the number of starts of $rotor_I$ and $m_{II}$ the number of starts of $rotor_{II}$. According to the Montelius condition the starts for a twin-screw profile must differ by one and therefore the possible variations are $\varepsilon = m_I / (m_I + 1)$ which can be $1/2; 2/3; \ldots$. The ratio used in the current application is 2/3.

$$r = \frac{d_{oI}}{d_{oII}} \tag{20}$$

is the ratio of the outer diameters, $d_{oI}$ is the diameter of $rotor_I$ and $d_{oII}$ is the diameter of $rotor_{II}$. The limits for the outer diameter of $rotor_I$ is its own hub diameter on the minimum side and the double centre distance for the maximum. The ratio used in the current application is 1.09.

As stated above, besides the profile formed by exact theoretical cycloids already referred to as montelius profile, in practice a corrected profile is used for certain advantages as described by Ryazantsev /53/. However throughout this work all

deliberations will refer to the theoretical profile, because all significant values can be accurately calculated.

The profile of $rotor_I$ is described by a point on the outside diameter of $rotor_{II}$ rolling on the hub diameter of $rotor_I$. This point can be chosen as the endpoint of the profile of $rotor_{II}$. Therefore the edge of $rotor_{II}$ will always be in contact with the flanks of $rotor_I$. On the other hand, the profile of $rotor_{II}$ is an epicycloid described by a point on the outer diameter of $rotor_I$ which is connected to the roll-off diameter of $rotor_I$ and rolling on the roll-off diameter of $rotor_{II}$. Hence, the edge of $rotor_I$ will always be in touch with the flank of $rotor_{II}$. The description of cycloids can be found in relevant handbooks such as Bartsch /57/ or Dubbel /58/, or related to screw profiles in the work of Hamelberg /51/ and Geimer /54/. Equations for the theoretical profile are explained in Appendix B "Description of cycloids with theoretical profile" and additionally the equations for the corrected profile are explained in Appendix C "Description of cycloids with a corrected profile". A pair of rotors with a profile created by cycloids is shown in Figure 29, including all significant angles and dimensions.

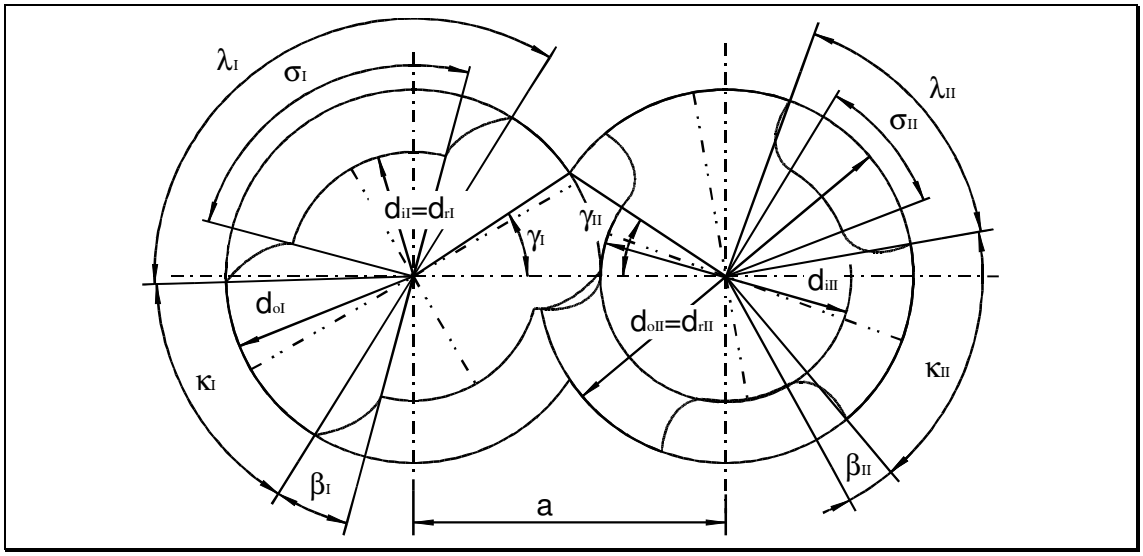


*Figure 29 Section of a cycloid rotor profile with all angles and dimensions*

All equations are related to the outer diameters, the ratios of outer diameters and the ratio of number of starts. The ratio of the number of starts is a significant value and corresponds to various relations between the two rotors, such as the rotational speeds, the pitch, the helix angle and the rolling diameters:

$$\varepsilon = \frac{m_I}{m_{II}} = \frac{\omega_{II}}{\omega_I} = \frac{p_I}{p_{II}} = \frac{d_{iI}}{d_{oII}} = \frac{d_{rI}}{d_{rII}} = \frac{d_{oI}\tan\phi_{PI}}{d_{oII}\tan\phi_{PII}} = \frac{r\tan\phi_{PI}}{\tan\phi_{PII}} \qquad (21)$$

Other parameters are as follows starting with the pitch angle at the outer diameter:

$$\tan\phi_P = \frac{p}{\pi d_o} \tag{22}$$

Root and roll-off diameter of rotor$_I$:

$$d_{iI} = \varepsilon\, d_{oII} = d_{oI}\frac{\varepsilon}{r} \tag{23}$$

The distance of the centres:

$$a = \frac{1}{2}\left(d_{oII} + \varepsilon\, d_{oII}\right) = \frac{1+\varepsilon}{2} d_{oII} = d_{oI}\frac{1+\varepsilon}{2r} \tag{24}$$

Root diameter of rotor$_{II}$:

$$d_{iII} = 2a - d_{oI} = (1+\varepsilon)d_{oII} - d_{oI} = d_{oI}\left(\frac{1+\varepsilon}{r} - 1\right) \tag{25}$$

The centre angles of the different parts of the profile will be used for the description of rotor positions and also corresponds to clearance dimensions: The equations of the angles are as follows starting with the profile interference angle of rotor$_I$:

$$\gamma_I = \arccos\left(\frac{4a^2 + d_{oI}^2 - d_{oII}^2}{4ad_{oI}}\right) = \arccos\left(\frac{(1+\varepsilon)^2 + r^2 - 1}{2(1+\varepsilon)r}\right) \tag{26}$$

Profile interference angle of rotor$_{II}$:

$$\gamma_{II} = \arccos\left(\frac{4a^2 - d_{oI}^2 + d_{oII}^2}{4ad_{oII}}\right) = \arccos\left(\frac{(1+\varepsilon)^2 - r^2 + 1}{2(1+\varepsilon)}\right) \tag{27}$$

Profile angle of rotor$_I$:

$$\beta_I = \frac{\gamma_{II}}{\varepsilon} - \gamma_I \tag{28}$$

Profile angle of rotor$_{II}$:

$$\beta_{II} = \gamma_{II} - \varepsilon\gamma_I = \varepsilon\beta_I \tag{29}$$

The following equations for centre angles are valid for geometries with parameters selected according to the condition for a displacement chamber to be as short as possible. This condition will be described later in this chapter, all calculations throughout the thesis refers to a profile which satisfies this condition. These are the gap angles $\lambda$, the ground angles $\sigma$ and the head angles $\kappa$ as follows:

$$\lambda_I = \frac{2\pi}{m_I} - \gamma_I \qquad\qquad \lambda_{II} = \gamma_{II} + \beta_{II} \tag{30}$$

$$\sigma_I = \frac{2\pi}{m_I} - 2\beta_I - \gamma_I \qquad \sigma_{II} = \gamma_{II} - \beta_{II} = \nu\gamma_I \tag{31}$$

$$\kappa_I = \gamma_I \qquad \kappa_{II} = \frac{2\pi}{m_{II}} - \gamma_{II} - \beta_{II} \tag{32}$$

## 6.3 Development of a displacement chamber

The displacement chamber of a screw type flowmeter is formed by the two rotors and the housing. It describes a totally sealed pocket, but is far more complex than, for example, a piston in a bore. The easiest way to maintain a clear picture is to perform a cold cast of the chamber, while the flowmeter is assembled. A true cast is difficult to obtain; the end portions of the displacement chamber are extremely fine, hence a casting was simulated with a 3D design software (Figure 30).

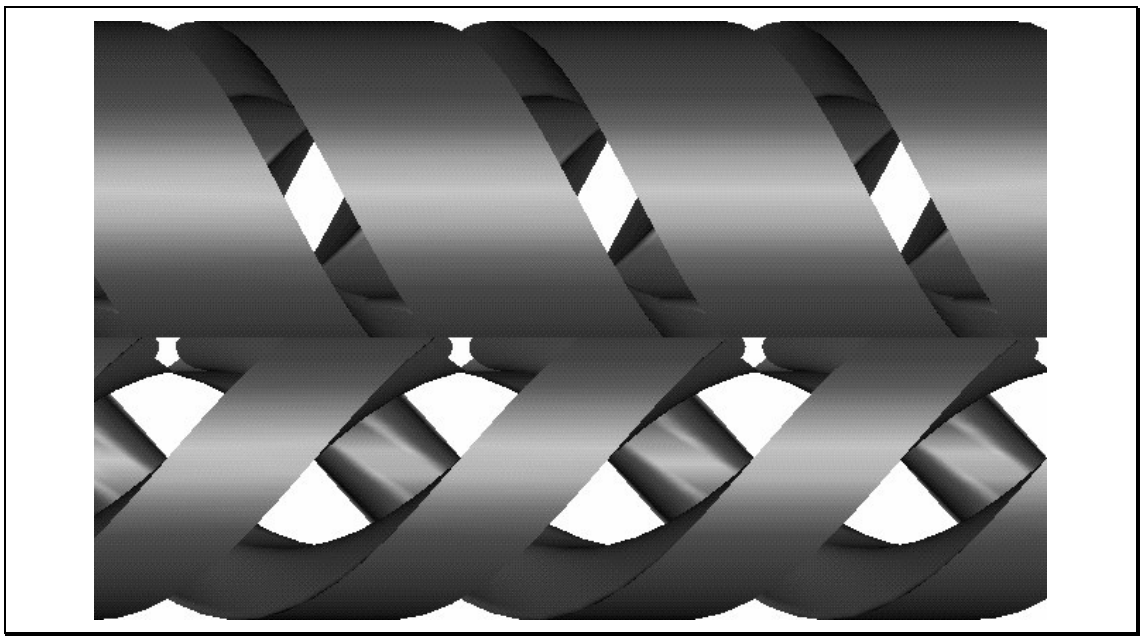

*Figure 30 Cast of the displacement chamber simulated with a 3D design software.*

The pocket is a complex 3D body bordered by various curved surfaces. A better way to describe the displacement chamber mathematically, is to look at the cross section of the profile normal to the axis. In this section, the fluid can be marked and the angles of characteristic positions can be described by using the angles derived.

### 6.3.1 Characteristic angular positions for the separate rotors

The development for the displacement chamber is shown for each rotor separately (Figure 31; Figure 32); the starting positions of $\text{rotor}_{\text{I}}$ and $\text{rotor}_{\text{II}}$ are different. The positions of the rotors are defined by the angle $\phi$ which is the angle between the edges of $\text{rotor}_{\text{II}}$ and the horizontal. Also defined is the angle $\psi$ relative to the starting position of the chamber $\phi_{START}$.

$$\psi = \phi - \phi_{START} \tag{33}$$

The angle $\psi$ is a dimensionless value for the length of the rotors ( $lenght = \psi \times pitch$ ). The cross section for $\psi=0$ equals the inlet side of the flowmeter and the sectional area moves from inlet to outlet side as $\psi$ increases.

The displacement chambers are symmetrical to their own middle and the two parts related to the two rotors start with a difference in the angular position of $\gamma_{II} - \lambda_{II} + \beta_{II}$ (Table 2). Hence, depending on those angles, one part of the chamber is normally longer than the other part of the chamber and the longer part determines the required length of the pair of rotors.

| **position** | **rotor$_I$** | **rotor$_{II}$** |
|---|---|---|
| start | $\phi_{II} = \lambda_{II} - \gamma_{II}$ | $\phi_{II} = \beta_{II}$ |
| maximum | $\phi_{II} = \frac{2\pi}{m_{II}} + \gamma_{II}$ | $\phi_{II} = \lambda_{II} + \gamma_{II}$ |
| decrease | $\phi_{II} = 2\pi \frac{m_I}{m_{II}} + \lambda_{II} - \gamma_{II}$ | $\phi_{II} = 2\pi - \gamma_{II}$ |
| end | $\phi_{II} = 2\pi + \gamma_{II}$ | $\phi_{II} = 2\pi + \lambda_{II} - \beta_{II}$ |
| length | $l = 2\pi + 2\gamma_{II} - \lambda_{II}$ | $l = 2\pi + \lambda_{II} - 2\beta_{II}$ |

*Table 2 Characteristic angular positions for both rotors*

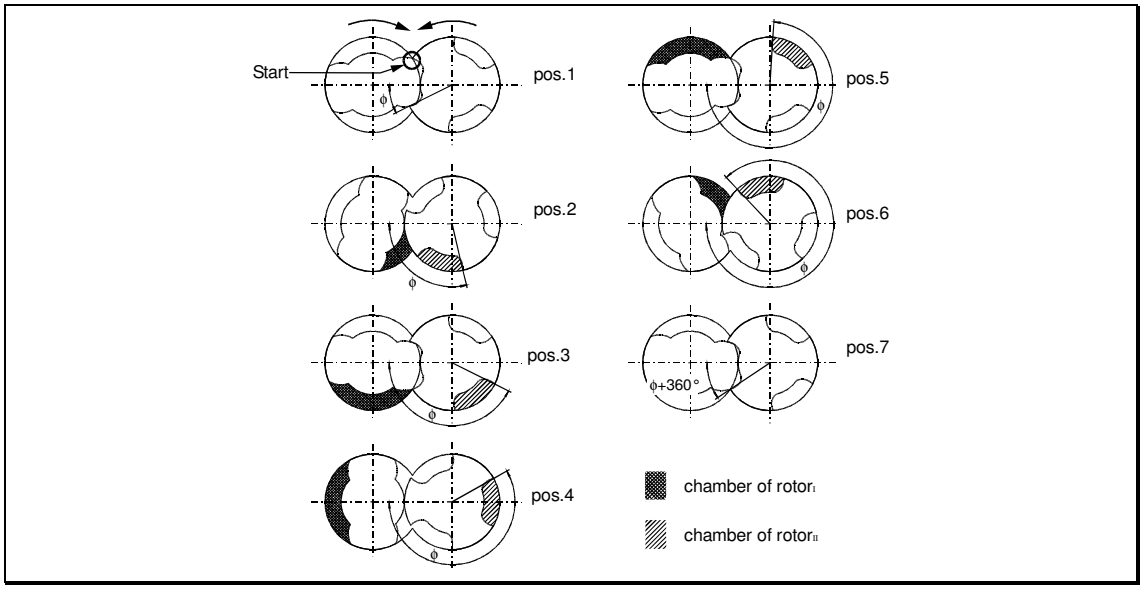


*Figure 31 Characteristic angular positions of rotor$_I$*

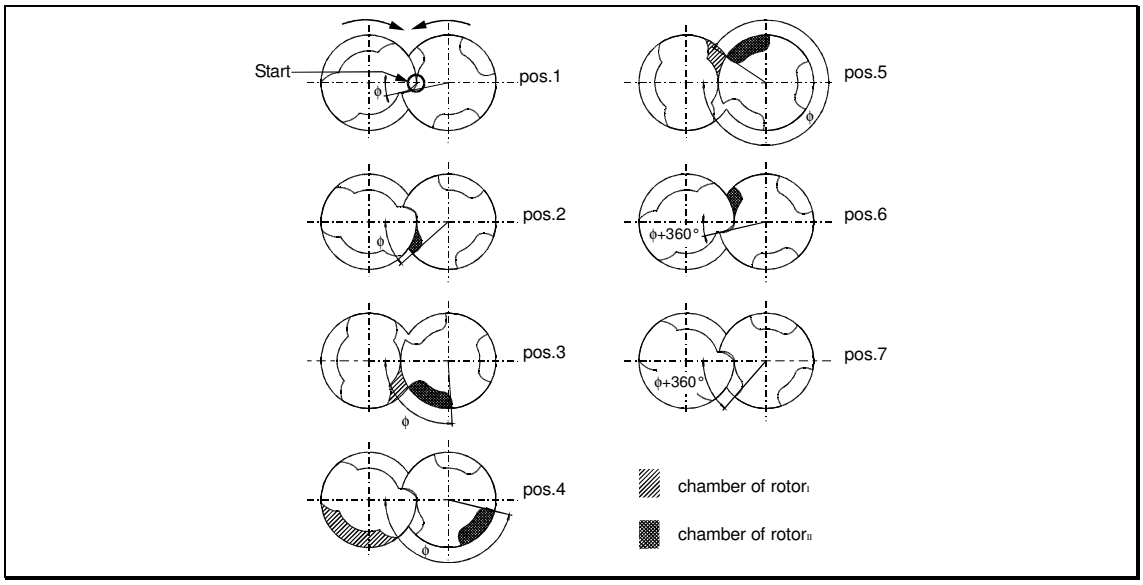


*Figure 32 Characteristic angular positions of rotor$_{II}$*

### 6.3.2 Determination of the minimum length of chamber

The length of the chamber should be kept as short as possible in order to keep the rotor length short. This can be achieved if the parts for both rotors are starting and ending at the same angular position. This will be found for $\gamma_{II} - \lambda_{II} - \beta_{II} = 0$, when the overall length and the starting and ending angle will be the same for both rotors.

| **position** | **rotor$_I$** | **rotor$_{II}$** |
|---|---|---|
| start | $\phi_{II} = \beta_{II}$ | |
| maximum | $\phi_{II} = \frac{2\pi}{m_{II}} + \gamma_{II}$ | $\phi_{II} = 2\gamma_{II} + \beta_{II}$ |
| decrease | $\phi_{II} = 2\pi\frac{m_I}{m_{II}} + \beta_{II}$ | $\phi_{II} = 2\pi - \gamma_{II}$ |
| end | $\phi_{II} = 2\pi + \gamma_{II}$ | |
| length | $l = 2\pi + \gamma_{II} - \beta_{II}$ | |

*Table 3 Characteristic positions for minimal length*

For all further equations this condition will be valid, even if not explicitly mentioned. A pair of rotors which is longer than the minimal length will always provide a total separation of inlet and outlet side. Every $2\pi/m_I$ of a revolution of rotor$_I$ a new displacement chamber starts. Using rotors machined to the minimal length, for most

positions no full displacement chamber is developed and only a sealing line provides the separation of the two sides.

### 6.3.3 Description of the displacement chamber for minimum length

The outline of how a minimum length chamber is created in detail is shown in Figure 33 which shows the end cross section of the profile. The displacement chamber starts when the edge of the ridge of $rotor_I$ reaches the intersection of the two bores of the housing, to engage with the profile of $rotor_{II}$. At the same angular position of the rotors, the edge of the ridge of $rotor_{II}$ turns over the edge of the housing, to engage with the profile of $rotor_I$. The new chamber is thus bordered by the profiles of the two rotors (Figure 33/ pos.1/pos.2). The area of the flow cross section of the chamber increases (Figure 33/ pos.2-4) until the chamber is bordered only by $rotor_I$ and the housing, or $rotor_{II}$ and the housing (Figure 33/ pos.5). It will keep its maximum value (Figure 33/ pos.5-7), until $rotor_{II}$ starts to engage again into the profile of $rotor_I$ (Figure 33/ pos.7). The area of the fluid cross section decreases (Figure 33/ pos.8-9) until its end (Figure 33/ pos.10). The position of rotation of $rotor_{II}$ is described by the angle $\phi$ which is larger than 360° for a completed chamber (Figure 33/pos.10). The angle $\psi$, multiplied with the pitch of the thread, equals the actual length. A rotor shorter than this length will not provide a total separation of inlet and outlet of the flowmeter. Regarding the inlet side of the flowmeter, a rotor with exactly this length will have only one position where the rotors and the housing form a fully developed chamber, which is pos.1 in Figure 33. For all the other positions the rotors and the housing form only one sealing line to provide the separation of inlet and outlet side.

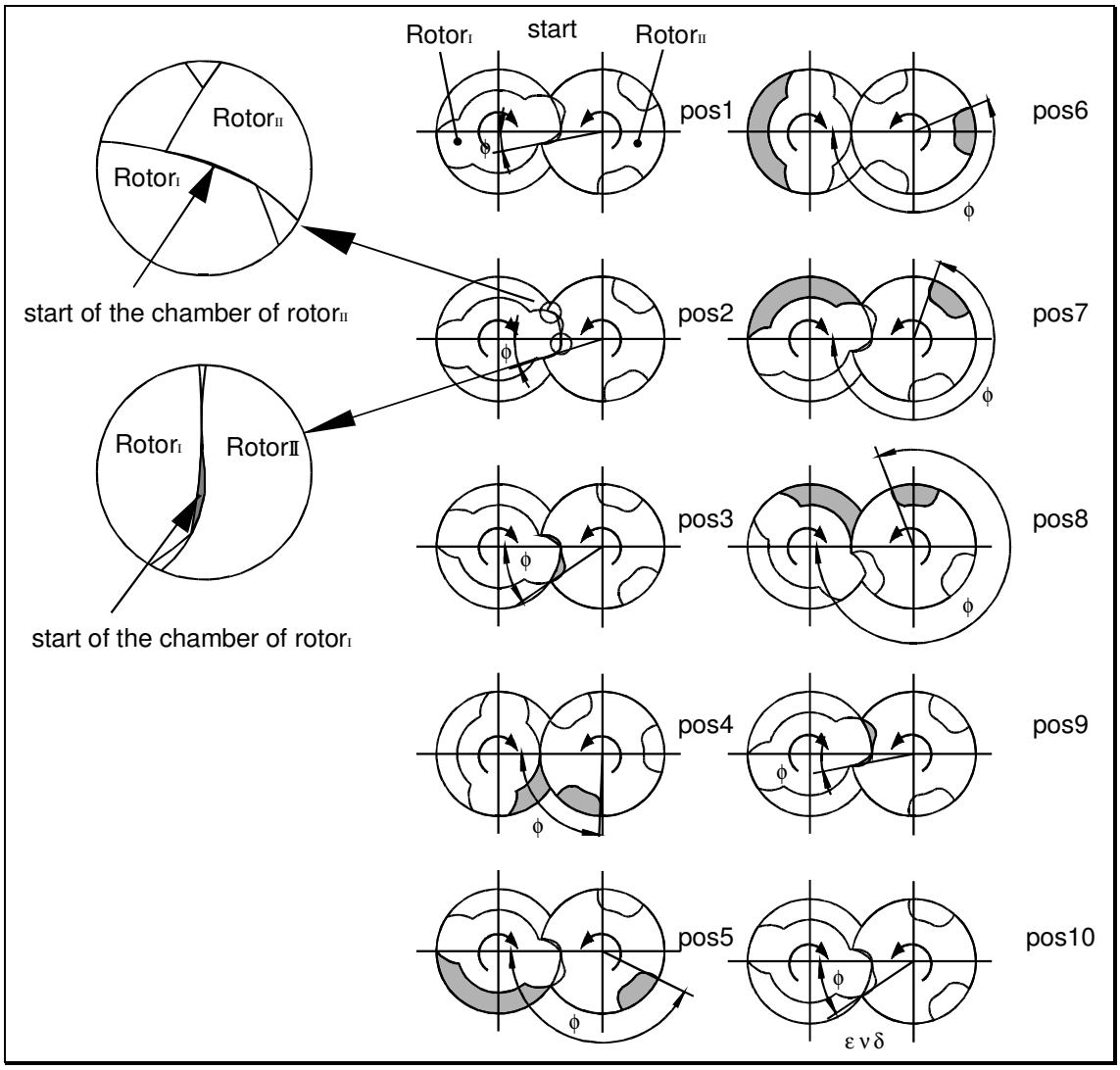


*Figure 33 The different characteristic cross sections of a displacement chamber of a twin-screw profile*

## 6.4 Selection of suitable flowmeter geometries

From a practical standpoint, only certain parameter values can be used in flowmeter design. To refer to a particular rotor design, a grouping of the main variables of outer rotor diameter $d_{oI}$ of rotor$_I$, the ratio $\varepsilon$ of the number of starts and the ratio $r$ of the outer diameters of both rotors. This forms a "$d_{oI};\varepsilon;r$" profile. The profile of the current design is a 24;2-3;1.09 profile, which means rotor$_I$ has 2 starts with a outer diameter of 24 mm and rotor$_{II}$ respectively 3 starts (2+1) and a 22 mm outer diameter (24/1.09). The dimensions of the rotors change by varying the outer diameter ratio $\varepsilon$ and the number of starts $r$ (Figure 34). This affects the profile itself, the centre angles and the flooded section of the profile (Figure 35).

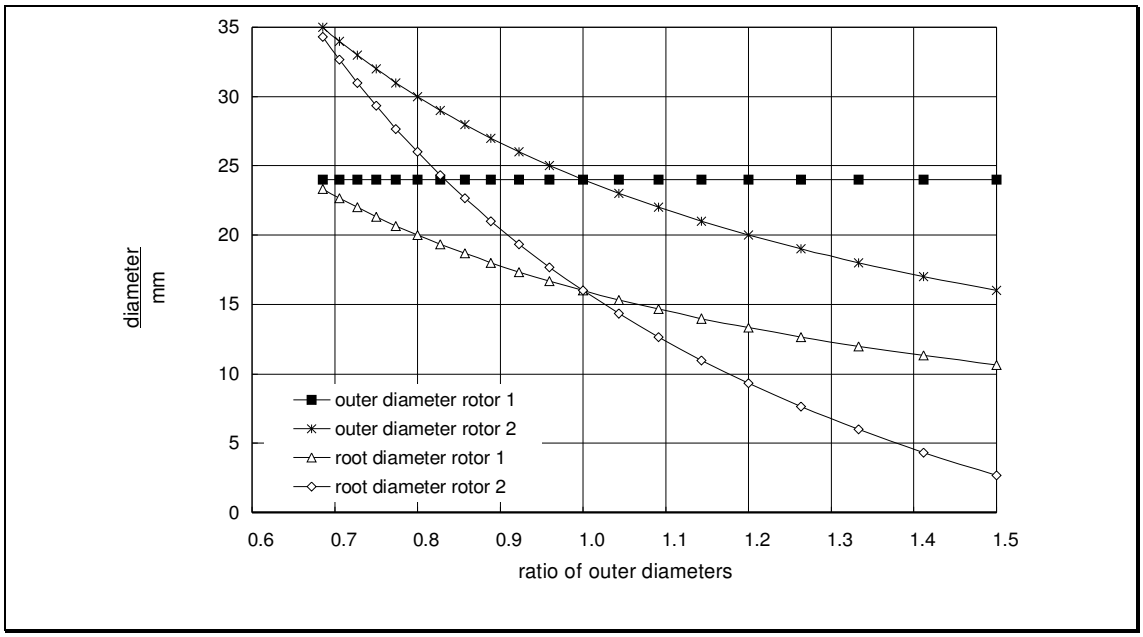


*Figure 34 The diameters of a 24;2/3 profile in relation to the ratio of the outer diameters r*

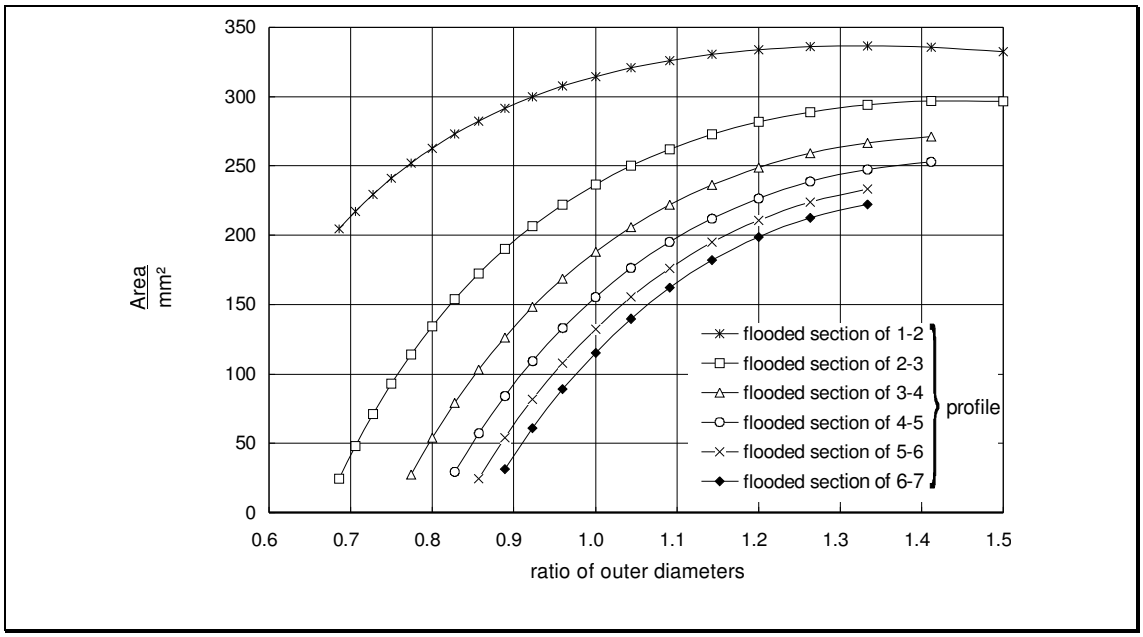


*Figure 35 The flooded section areas of different profiles in relation to the ratio of the outer diameters r*

To find a suitable profile, the data of all geometries was evaluated according to the following rules, related to the geometry, the manufacturing, the size and the available bearings.

(a) The profile has to be realistic. All centre angles have to be positive, the outer diameters have to be bigger than the root diameters and the flooded section has to be positive.

(b) For manufacturing reasons, the root diameter is not allowed to be too small relative to the outer diameter. The machining cut causes the helix angle to vary from outer diameter to the root. The variation is increasing with the depth of the groove and makes it increasingly difficult to machine the profile. Additionally a deep cut weakens the material and may cause vibrations during the machining process. Hence the root diameter was selected to be not smaller than half of outer diameter.

(c) For a reasonable sizing of the flowmeter the limit the ratio of flooded section to bore section was selected to be larger than 0.2

(d) The flowmeter uses ball bearings which are only available in standardised sizes. According to the current design, the outer diameter of the bearing is identical to the outer diameter of the rotor, the inner diameter of the bearing must be smaller than the root diameter of the profile.

Only some profile geometries fulfil all requirements. The remaining profiles will be discussed in the later using the performance prediction model. It may be noted here that the profiles with equal outer diameters provide the best properties for the manufacturing process. With a ratio of number of start of $\varepsilon$=0.8 and higher and for $\varepsilon$=0.5 it is not possible to obtain equal diameters under the stated conditions. The outer diameter of $rotor_I$ was selected to be 24 mm.

| Profile | $d_{oII}$ | $d_{iI}$ | $d_{iII}$ | flooded section |
|---|---|---|---|---|
| 24; 1-2; 0.92 | 26.00 | 13.00 | 15.00 | 299.86 |
| 24; 1-2; 0.86 | 28.00 | 14.00 | 18.00 | 282.52 |
| 24; 1-2; 0.80 | 30.00 | 15.00 | 21.00 | 262.83 |
| 24; 2-3; 1.09 | 22.00 | 14.67 | 12.67 | 262.04 |
| 24; 2-3; 1.00 | 24.00 | 16.00 | 16.00 | 236.65 |
| 24; 2-3; 0.92 | 26.00 | 17.33 | 19.33 | 206.52 |
| 24; 3-4; 1.14 | 21.00 | 15.75 | 12.75 | 236.37 |
| 24; 3-4; 1.09 | 22.00 | 16.50 | 14.50 | 221.94 |
| 24; 3-4; 1.00 | 24.00 | 18.00 | 18.00 | 188.00 |
| 24; 4-5; 1.26 | 19.00 | 15.20 | 10.20 | 238.68 |
| 24; 4-5; 1.14 | 21.00 | 16.80 | 13.80 | 212.10 |
| 24; 4-5; 1.09 | 22.00 | 17.60 | 15.60 | 195.21 |

*Table 4 Suitable rotor geometries for a flowmeter*

## 6.5 Theoretical flow rate

The theoretical flow is defined as the amount of fluid to pass the flowmeter without leakage. This is described by the part of the section which is filled with fluid and the longitudinal movement per revolution, which equals the pitch of the thread. The area filled with fluid is the area of the bore minus the areas of the sections of the two rotors. The sections for the theoretical profile can be calculated as described in Appendix D "Calculation of the fluid area of the theoretical profile". The theoretical swept volume can be related to each of both rotors. Because of the different speeds, the swept volume has a differing values for each rotor. The flow rate and swept volume in this thesis will always be related to the pitch and speed of $rotor_I$.

Flow rate:

$$\dot{V} = p_I A_{fl} n_I \tag{34}$$

with:

$$A_{fl}=A_b - A_I - A_{II} \tag{35}$$

longitudinal velocity of the fluid:

$$c = n_I p_I \tag{36}$$

# 7 Hydraulic forces and torques on the rotors

The fluid pressure creates forces and torques on the rotors. These hydraulic loads on the rotors are transmitted to the bearings, where they cause frictional losses. An original comprehensive study of the author on these forces and torques on the rotors has been performed, evaluating the distribution of the load on the bearings and its change over one revolution. All original equations are included in the program library in Appendix E "Calculation of hydraulic loads". However, as stated in the performance prediction section, the determination of the loads on the bearings is not critical for the performance prediction of the flowmeter. Hence this report will not present any details of the determination of the hydraulic forces on the rotors, but state the general logic used by the author and prove the results obtained. This is considered especially important as methods in literature, which describe the determination of forces on the rotors, are contradictory.

Throughout the current study $rotor_I$ is right-handed and $rotor_{II}$ left-handed. Hence looking at the rotors from the inlet side, $rotor_I$ rotates counter-clockwise and $rotor_{II}$ clockwise. The X-direction is in the plane of the axis, positive in the direction from the center of $rotor_I$ to the center of $rotor_{II}$. The Y-direction is perpendicular to the plane of the axis. Looking at the rotors from the inlet side, with $rotor_I$ on the left, the positive direction is downwards. The Z-direction is in the axis of the rotors and in a positive flow direction. The torque is positive for each rotor in its rotational direction.

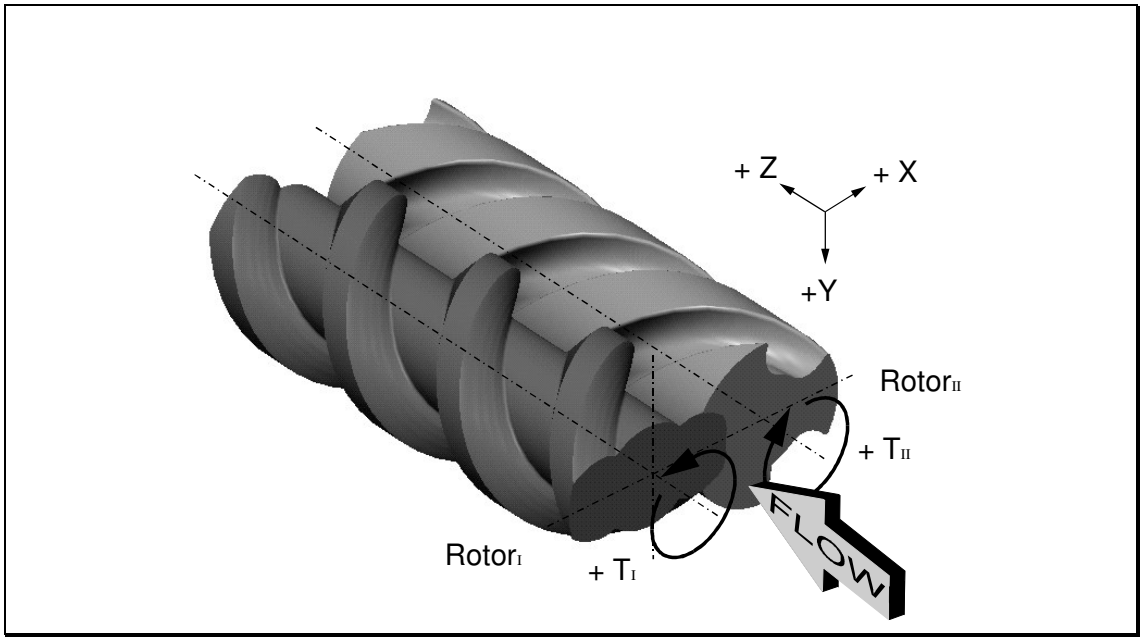


*Figure 36 Definition of the coordinates used for the determination of the forces and torques acting on the rotors*

Loads and torques on screw rotors of the current design can be calculated. The torque created is related to the flooded cross section, the loads are related to the geometry. The torque on $rotor_I$ is positive and the torque on $rotor_{II}$ negative, which means that $rotor_{II}$ is pushed in the counter direction of rotation. $Rotor_I$ has to convey the driving power over the profile to overcome the fluid torque and frictional torque on $rotor_{II}$. In order to calculate the loss coefficient, areas representing the rotor load are presented for all suitable rotor profiles. With the analytical methods available, the logic introduced has been proven to be correct. The results are inconsistent with the theory presented 1995 by Geimer /54/ in his dissertation on screw pumps.

## 7.1 Literature

Hamelberg /51;59/ presents five types of rotor profiles for screw-pumps. Rotor forces and rotor moments resulting from the pressure distribution on the rotor surface which cause elastic rotor deflections are analysed. Detailed equations are presented to calculate torque and forces on the rotors. Therefore the length of the rotor was split into different sections and the load was determined separately for horizontal and vertical components. He states that the sealing line is moving from the inlet to the outlet side of the pump, causing a periodic change in the forces on the rotors. As the fluid will absorb the variation, he proposes to calculate only mean values of the periodic changing forces. The mean value over the rotational position of the rotors for the force in X-direction is zero, and the load resulting from the forces in Y-direction is constant for all rotational positions. He also claims the torque on the rotors to be constant. A linear pressure drop over the length of a clearance and a laminar leakage flow in the clearances is assumed. The method of Hammelberg /51;59/ was applied by Wincek /60/ to a multiphase twin screw pump claiming good results.

For the calculation of the radial forces, Geimer /54/ also splits the load into horizontal and vertical components to determine the load on the projected surfaces. This can be done for different sections. He states that the resulting force in the X-direction is higher than the force in Y-direction, changing its absolute value with the position of the rotors. The load distribution is not symmetrical. He proves his statement using a FEM calculation describing the section of a screw with 30 elements. The force in the axial direction for each rotor is calculated from the related bore diameter, with the overlap of the bores added to $rotor_I$ and subtracted for $rotor_{II}$.

It is important to note that, however using similar methods, the results of Hamelberg /51;59/ and Geimer /54/ on the radial forces are contradictory.

Hamelberg /51;59/ claims that there is no load in the X-direction, but Geimer /54/ claims a higher load in the X-direction than in Y-direction.

Ryazantsew /61/ suggests an experimental set-up to determine the forces on a double screw pump. The deflection of a screw loaded with a weight determined by theory is compared with the deflection caused by the pressure drop.

## 7.2 Theory

A comprehensive study by the author on the forces and torques on the rotors has been performed, confirming the results of Hamelberg. In addition, the distribution of the load on the bearings and its change in the course of a revolution was evaluated. However as deduced in the performance prediction section, the determination of the load on the bearing is not critical for the performance prediction of the flowmeter.

Therefore this section will only display the general logic of calculation used by the author and present a theory to prove the results obtained. This is considered especially important as methods in literature, which describe the determination of forces on the rotors, are contradictory. The proving methods described in literature are not considered appropriate for the current application. The value of an FEM analysis as proposed by Geimer /54/ is very much questionable. The reason for this is that he uses only 30 coordinates to describe a profile which is normally defined by more than 300 coordinates. This is underlined by the results of this study, which confirm the theory of Hamelberg /51;59/ and are inconsistent with Geimer /54/. The testing procedure described by Ryazantsew /61/ is not considered practicable for the current rotor design as the rotors are very much smaller and stiffer than those in the test set up of Ryazantsew /61/.

### 7.2.1 General logic

The fluid applies a load to the surface of the rotors which is, looking at the cross-section, seen as a curved line. The pressure on this surface line creates a force which is proportional to the area perpendicular to the force (Figure 37). Horizontal and vertical components are determined separately in cross-sections and integrated over the length of the rotor. The torque is calculated as the product of these forces times their mean distance to the centre of rotation. The mathematical functional relationships to describe the loads are not continuous, but change with different rotational and hence different engagement positions of the rotors. The presentations of all the mathematical functional relationships exceeds the scope of this work, but for one example, the deduction will be shown in the following.

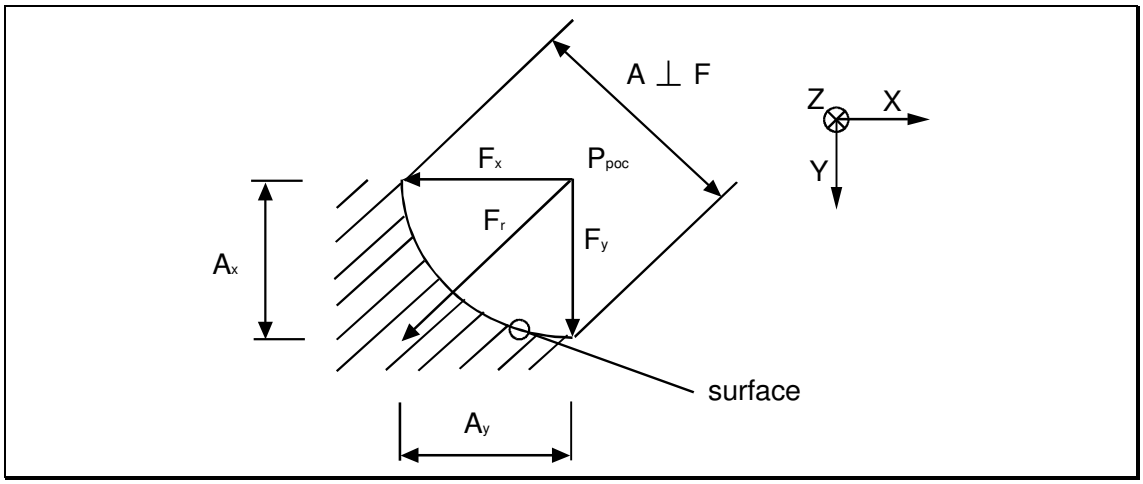


*Figure 37 Section of a curved surface; horizontal and vertical components of the hydraulic forces are determined separately*

$$F_X = p_{poc} \cdot A_X \tag{37}$$

$$F_Y = p_{poc} \cdot A_Y \tag{38}$$

And hence the total radial load:

$$F_r = \sqrt{F_X^2 + F_Y^2} \tag{39}$$

The radial loads and the torque are first calculated for one single displacement chamber. After that, the different chambers involved are assigned to their actual pressure. To prove the consistency of the equations all chambers have been assigned to the same pressure, hence it was expected that no force may be created.

Every $2\pi/m_I$ a new chamber starts and one ends. For this position two sealing lines are producing one completely separated chamber (Figure 38). When this chamber opens to the discharge side for a length of $2\pi/m_I$ all channels/chambers are directly connected to this side and therefore in this section no forces act on the rotors. A load is expected for the length of the sealing line separating inlet from outlet side (Figure 39). As the sealing line moves form inlet to outlet side, the constant load moves with it and creates a pulsing load on the bearings. A mean value of the load will be taken for the performance prediction model of the flowmeter.

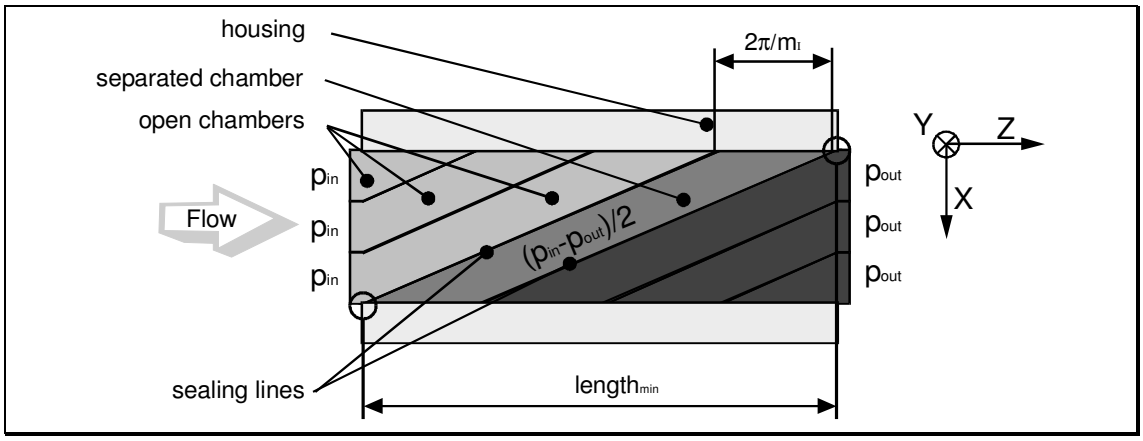


*Figure 38 Scheme for the angular position, where the rotors form a chamber, which is completely separated from inlet and outlet side*

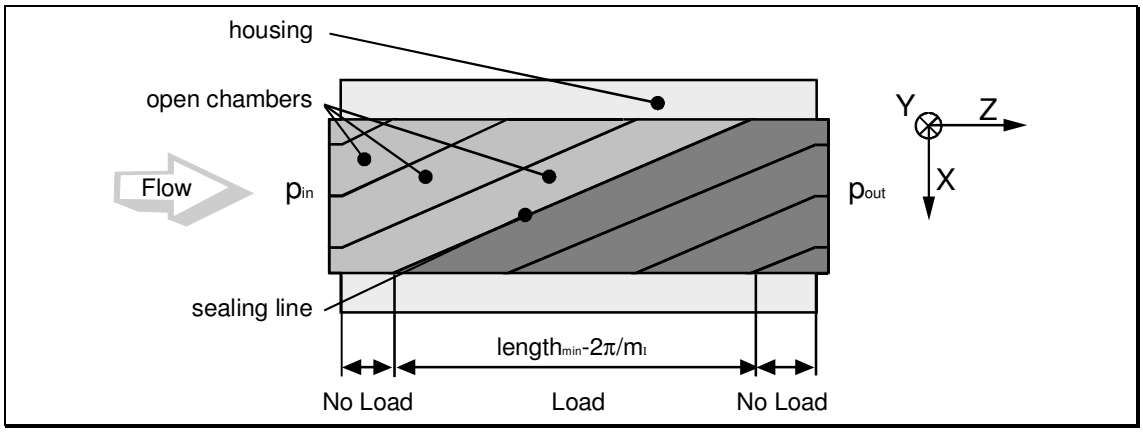


*Figure 39 Scheme for an angular position, where inlet and outlet are separated by a sealing line*

### 7.2.2 Radial load

The radial load is determined separately for horizontal and vertical components. This method is shown for one cross section. As described in the rotor geometry section, the displacement chamber is described by several significant cross sections, each representing a specified range of engagement positions. To obtain the loads for each range of positions, the projected surface is displayed as a function of the angular position $\phi$ of the rotors. With a linear pressure drop over the length of the clearance, respectively half of the surface of each clearance is assigned to the adjacent chambers (Figure 40).

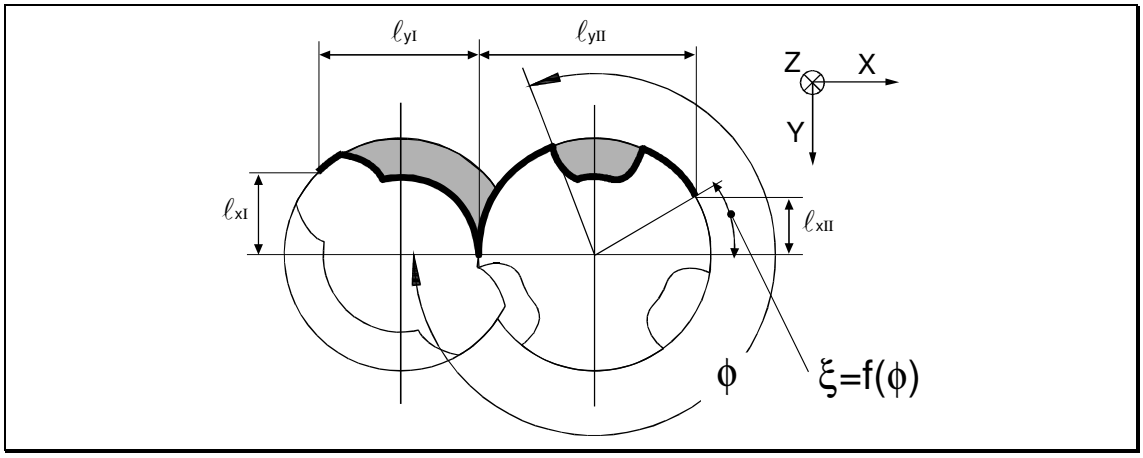


*Figure 40 Projected length in X- and Y- direction of the surface upon which fluid pressure is acting*

For the section displayed, the projected length for each direction can be related to an angle $\xi$ which describes the geometrical limits of the displacement chamber in this section. The angle $\xi$ itself is in a relationship to the rotational position $\phi$ of rotor$_{II}$.

$$\ell_{xII} = \frac{d_{oII}}{2}\sin\left(f\left(\xi\right)\right) \tag{40}$$

$$\ell_{yII} = \frac{d_{oII}}{2}\left(1+\cos\left(f\left(\xi\right)\right)\right) \tag{41}$$

with:

$\ell_{xII}$ projected length for X-direction of rotor$_{II}$

$\ell_{yII}$ projected length for Y-direction of rotor$_{II}$

$\xi$ angle describing the limits of the displacement chamber

Using the significant angles of the rotor profile as presented in the rotor geometry section, the angle $\xi$ can be calculated from the rotational position $\phi$ of rotor$_{II}$:

$$\xi = \phi - 2\beta_{II} - \sigma_{II} - \frac{\kappa_{II}}{2} \tag{42}$$

The rotational position $\phi$ of rotor$_{II}$ is related to the angle $\psi$ which can be seen as a value of the dimensionless length coordinate of the rotor:

$$\psi = \phi - \beta_{II} \tag{43}$$

Hence, the total length of the rotors $\ell_r$ is expressed by the total dimensionless length $\psi_r$ and the pitch of rotor$_{II}$:

$$\ell_r = \frac{\psi_r}{2\pi} p_{II} \tag{44}$$

The load created by the fluid pressure in one complete chamber $F_{ch}$ is related to the chamber pressure, the pitch and the integral of the projected length. The projected length values are related to the dimensionless length value of the rotors $\psi$ according to equations 42 and 43:

$$F_{ch\,x,y} = p_{poc} \frac{p_I}{2\pi} \int_{\psi=0}^{\psi=\ell_r} \ell_{x,y}(\psi) d\psi \tag{45}$$

For the total load on rotors, the pressure $p_{poc}$ for each chamber has to be assigned to either inlet or outlet pressure. The different chambers follow each other with a distance of $2\pi/m_I$. Hence the actual position is the described by $\psi$ plus/minus multiples of $2\pi/m_I$. In order to obtain the total load, the loads of all the single chambers involved can then be summarised. To simplify the equation, the inlet pressure is set to the pressure drop and the outlet pressure to zero:

$$F_{xy} = \frac{\Delta p}{\varepsilon} \frac{p_I}{2\pi} \sum_{n=-8}^{n=-1} \left( \int_{\psi=0}^{\psi=\ell_r} \ell_{xy} \left( \psi - n\left(\frac{2\pi}{m_I}\right)\right) d\psi \right) \tag{46}$$

The radial load is proportional to pressure drop, the outer diameter of rotor$_I$ and the pitch. The load divided by pressure drop is a constant value for each rotor geometry. This value is referred to as a significant load area later in the thesis. As an example the load area $f_{xII}$ of rotor$_{II}$ in X-direction is:

$$f_{xII} = \frac{F_{xII}}{\Delta p} \tag{47}$$

### 7.2.3 Torque

Using the same logic as for the loads, the torque is first calculated for a single displacement chamber and then for the complete rotor. The projected surfaces in each direction which are $\ell_{xII}$ and $\ell_{yII}$ are multiplied with the respective distances of the resulting force to the center of rotation $d_{xII}$ and $d_{yII}$ (Figure 41).

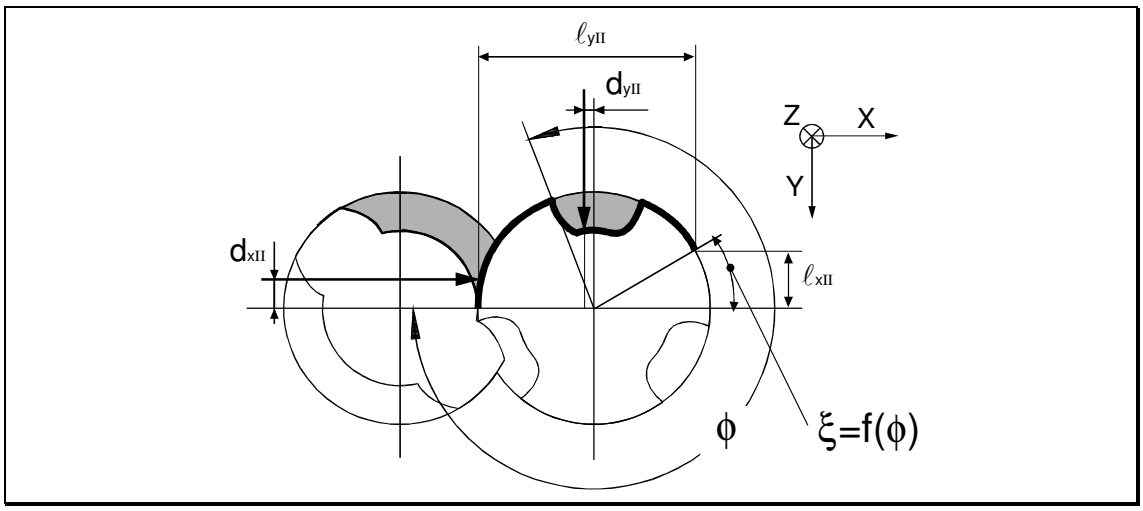


*Figure 41 Projected length values of the surface, upon which fluid pressure is acting, and the distance of the resulting forces to the center of rotation.*

The projected length values are the same as presented in equations 40 and 41. The distances to the centre of rotation are as follows:

$$d_{xII} = \frac{d_{oII}}{4}\sin\left(f\left(\xi\right)\right) \tag{48}$$

$$d_{yII} = \frac{d_{oII}}{4}\left(\cos\left(f\left(\xi\right)\right) - 1\right) \tag{49}$$

In this example the X-component is driving the rotor towards its positive direction, the Y-component towards its negative direction. The torque created by the fluid pressure in one complete chamber $T_{ch}$ is related to the chamber pressure, the pitch, and the integral of the projected length times distance to the center of rotation. The projected length values $\ell_{xII}$ and $\ell_{yII}$ and the distances $d_{xII}$ and $d_{yII}$ to the centres of rotation are related to the dimensionless length value of the rotors $\psi$ according to equations 42 and 43:

$$T_{ch} = p_{poc}\frac{p_I}{2\pi}\int_{\psi=0}^{\psi=\ell}\left[\ell_{xII}\left(\psi\right)d_{xII}\left(\psi\right) + \ell_{yII}\left(\psi\right)d_{yII}\left(\psi\right)\right]d\psi \tag{50}$$

In order to obtain the total torque on the rotors, the pressure $p_{poc}$ for each chamber has to be assigned to either inlet or outlet pressure. The different chambers follow each other with the distance of $2\pi/m_I$, and hence the actual position is the described by φ plus/minus multiples of $2\pi/m_I$. The torques of all the single chambers involved can then be summarised. Again, the inlet pressure is set to the pressure drop and the outlet pressure to zero:

$$T_{II} = \frac{\Delta p}{\varepsilon}\frac{p_I}{2\pi}\sum_{n=-8}^{n=-1}\left(\int_{\psi=0}^{\psi=\ell_r}\left[\ell_{xII}\left(\psi - n\frac{2\pi}{m_I}\right)d_{xII}\left(\psi - n\frac{2\pi}{m_I}\right) + \ell_{yII}\left(\psi - n\frac{2\pi}{m_I}\right)d_{yII}\left(\psi - n\frac{2\pi}{m_I}\right)\right]d\psi\right) \quad (51)$$

The total torque divided by the pressure drop is a constant value for each rotor geometry. This value is referred to as a significant torque volume $t_I$ for $rotor_I$, or $t_{II}$ for $rotor_{II}$, later in the thesis. As an example the load area $t_{II}$ of $rotor_{II}$ around Z-direction is:

$$t_{II} = \frac{T_{II}}{\Delta p} \quad (52)$$

In order to cross-check the results obtained, the torque on the rotors times rotational speed must equal pressure drop times the theoretical flowrate:

$$\dot{V}_{th}\Delta p = T_I\omega_I + T_{II}\omega_{II} \quad (53)$$

Using the equation for theoretical flowrate as presented in the rotor geometry section, the overall torque can be related to the flooded section of the flowmeter, pitch and pressure drop. Hence the torque can be checked against the displacement volume of the flowmeter:

$$t_I + \varepsilon\, t_{II} = A_{fl}\frac{p_I}{2\pi} \quad (54)$$

The torque is proportional to pressure drop, the square of the outer diameter of $rotor_I$ and to the pitch. However it is more convenient to calculate the overall torque related to theoretical flowrate and pressure drop as described in the performance prediction section.

### 7.2.4 Axial load

The axial load is determined for each rotor from its projected surface in axial direction. As proposed consistently by Hamelberg/51;59/ and Geimer /54/, the projected surface of $rotor_I$ is the complete circular projected area, plus the overlap of the bores times $m_I$. For $rotor_{II}$ the projected surface is the circular area less the overlap of the bores times $m_{II}$.

$$F_{aI} = \Delta p\left(A_{bI} + m_I A_{overlap}\right) \quad (55)$$

$$F_{aII} = \Delta p\left(A_{bII} - m_{II} A_{overlap}\right) \tag{56}$$

To cross-check the results, the sum of the axial forces on the two rotors must be equal to the area of the bore time the pressure drop.

$$F_{aI} + F_{aII} = A_b \Delta p \tag{57}$$

Hence:

$$\Delta p\left(A_{bI} + m_I A_{overlap}\right) + \Delta p\left(A_{bII} - m_{II} A_{overlap}\right) = A_b \Delta p \tag{58}$$

or:

$$A_{bI} + A_{bII} + A_{overlap}\left(m_I - m_{II}\right) = A_b \tag{59}$$

With the montelius condition $m_{II} - m_I = 1$ as presented in the rotor geometry section, the total area of the bore equals the sum of the two circular areas of the two rotors minus the overlap:

$$A_b = A_{bI} + A_{bII} - A_{overlap} \tag{60}$$

## 7.3 Discussion

Using the logic described above, the torque and the forces acting on the rotors can be calculated, if the pressure drop is known. To do so, the following procedure is used:

(a) An initial screw profile and pressure drop are given

(b) The different chambers of the flowmeter are related to either inlet or outlet pressure

(c) The forces and torque created by the fluid in a defined chamber are calculated separately for every chamber and direction

(d) The single forces are added to one axial and one radial force related to one rotor and the torques are added to one axial torque related to one rotor.

(e) Vary the geometry and repeat

### 7.3.1 General discussion

A 24;2/3;r profile geometry as described in the rotor geometry section was chosen and the calculation according to the logic presented was performed at a given pressure drop of 1 bar. Figure 42 shows the load distribution in Y - direction for $rotor_{II}$. The load applies only in the area of the sealing line, as proposed in section 7.2.1. The value of the forces and torques is obviously related to the variation of the geometric parameters (Figure 43 and Figure 44). The forces decrease with the ratio of diameters (Figure 43), except the axial force on $rotor_I$ which is almost constant. It is important to note that the

torque on $rotor_I$ is positive and the torque on $rotor_{II}$ negative, which means that $rotor_{II}$ is pushed in the counter direction of rotation (Figure 44). $Rotor_I$ has to convey the driving power over the profile to overcome the fluid torque and frictional torque on $rotor_{II}$. The transmission over the profile may cause additional frictional torque and additional forces on the rotors.

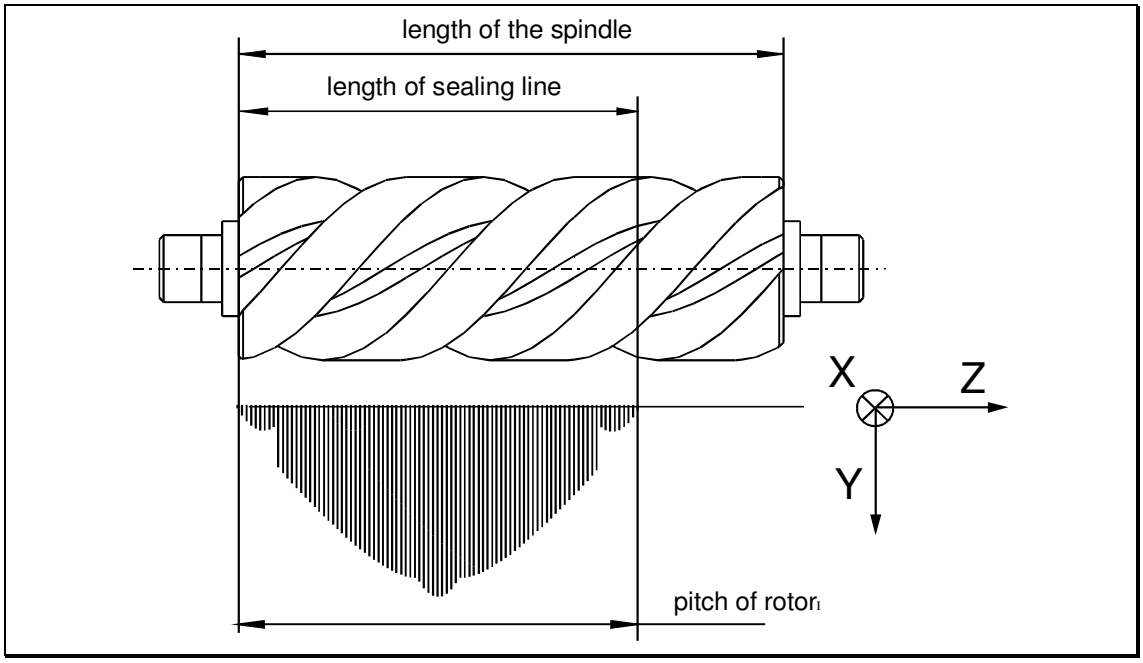


*Figure 42 Representation of the axial load on $rotor_{II}$*

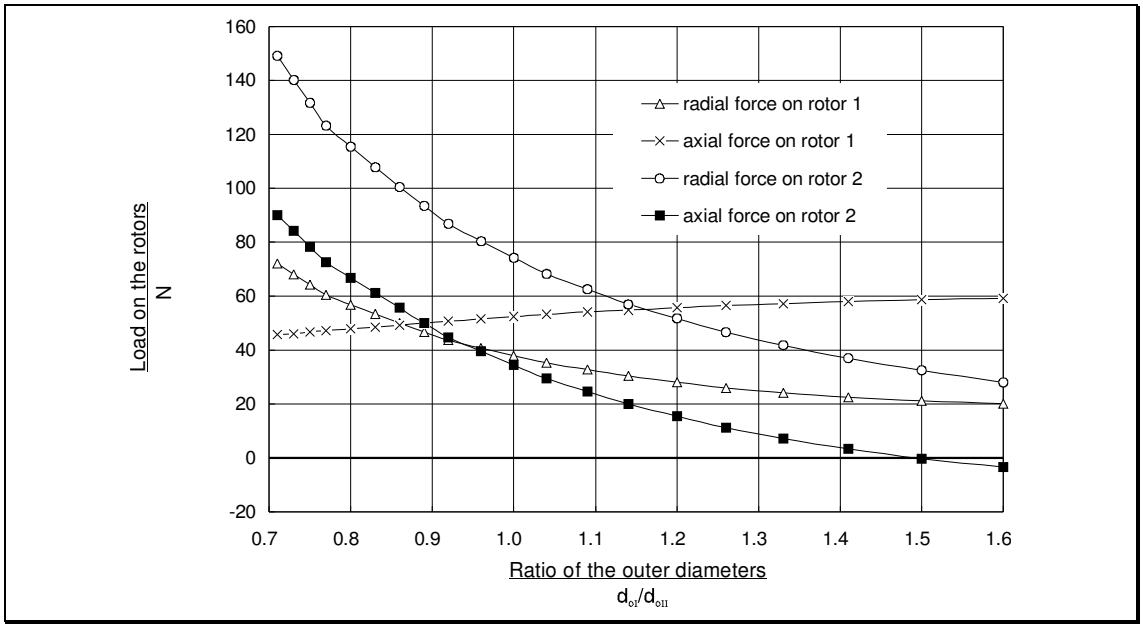


*Figure 43 The forces on the rotors of a 24;2/3 profile caused by a 1 bar pressure drop with constant angle of pitch*

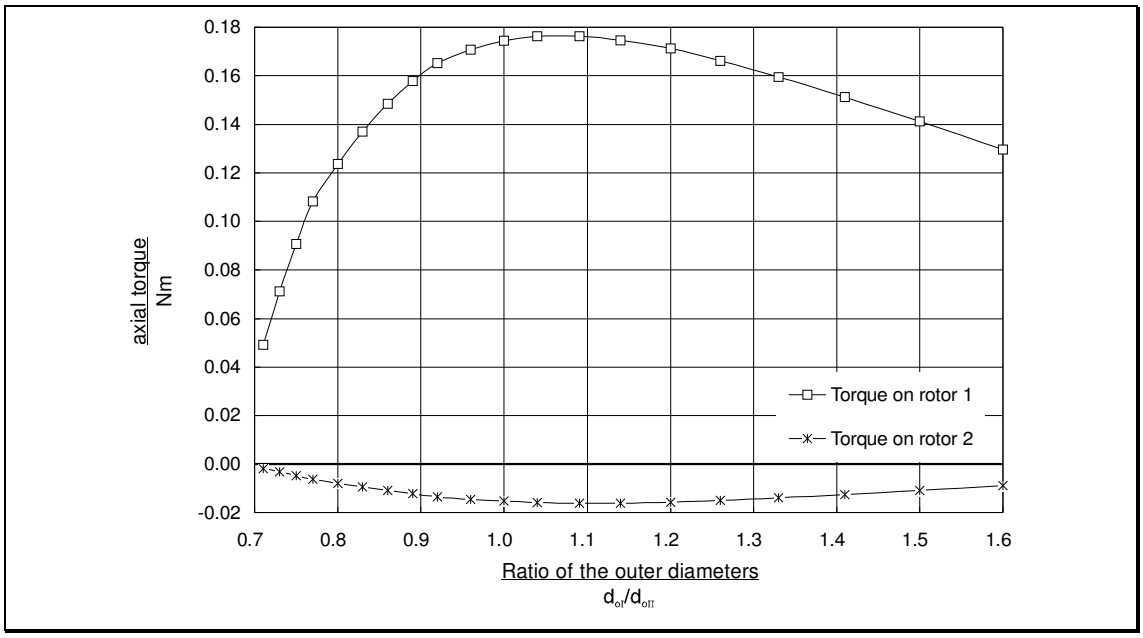


*Figure 44 The axial torques on the rotors of a 24;2/3 profile caused by a 1 bar pressure drop with constant angle of pitch*

### 7.3.2 Proof of the results

The methods to prove the validity of the model mentioned in the theory section were applied and consistent results were achieved. For a constant pressure load over all chambers, which equals a zero pressure drop, no forces or torques were created. The calculated torques acting on the rotors, compared with the theoretical power loss over the flowmeter did show a very good agreement (Figure 45). The error of fluid power against rotational power is below 2%. The results, regarding radial forces and the torque, agreed with Hamelberg /51;59/, but not with Geimer /54/. Experimental measurements on the torque and forces were not performed, because difficulties and uncertainties expected in an experimental set-up is not justified by the low priority of pressure related friction losses.

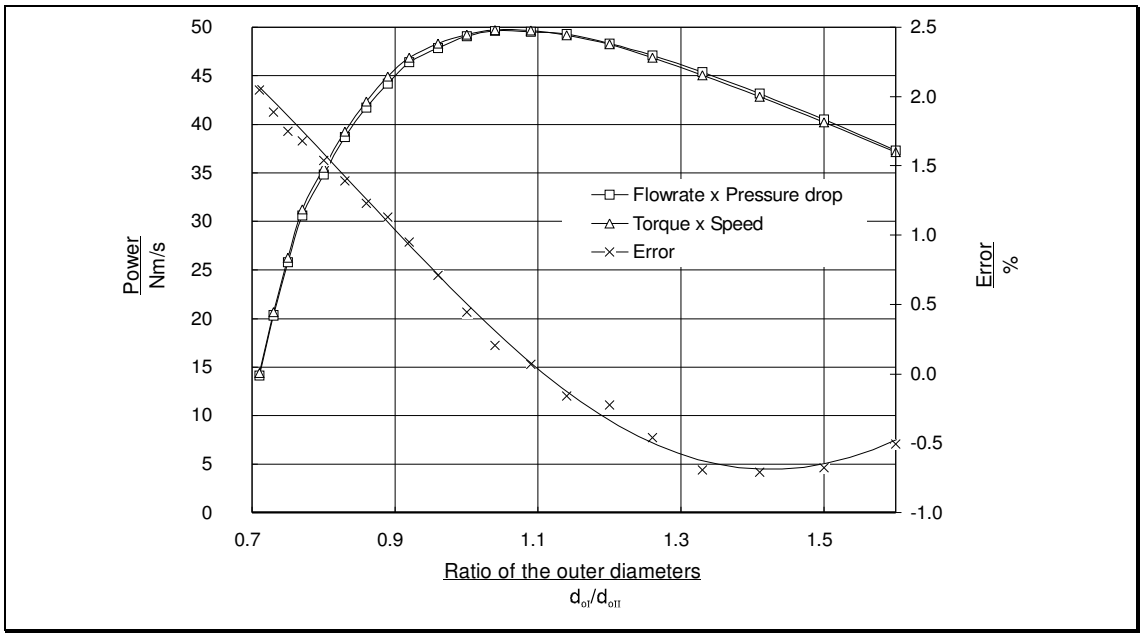


*Figure 45 The accuracy of the calculation of torques; fluid power versus rotational power with constant angle of pitch*

### 7.3.3 Load coefficients for suitable geometries

For all the selected suitable rotor geometries described in the rotor geometry section, the load areas related to the forces in the X- and Y- direction and the torque volumes have been determined (Table 5). These load values will be used to calculate the pressure related friction torque loss coefficient in the section "realisation of the model".

| Profile | Axial load rotor 1 | Axial load rotor 2 | Radial load rotor 1 | Radial load rotor 2 | Torque rotor 1 | Torque rotor 2 |
|---|---|---|---|---|---|---|
| | $f_{aI}$ | $f_{aII}$ | $f_{rI}$ | $f_{rII}$ | $t_I$ | $t_{II}$ |
| $d_{oI}$; $m_I$-$m_{II}$; ν | [mm²] | [mm²] | [mm²] | [mm²] | [mm³] | [mm³] |
| 24; 1-2; 0.92 | 510 | 412 | 156 | 377 | 1758 | -157 |
| 24; 1-2; 0.86 | 507 | 514 | 173 | 438 | 1800 | -162 |
| 24; 1-2; 0.80 | 496 | 615 | 188 | 498 | 1785 | -158 |
| 24; 2-3; 1.09 | 541 | 247 | 164 | 313 | 1763 | -161 |
| 24; 2-3; 1.00 | 520 | 342 | 189 | 368 | 1730 | -151 |
| 24; 2-3; 0.92 | 508 | 448 | 219 | 434 | 1651 | -136 |
| 24; 3-4; 1.14 | 564 | 202 | 187 | 304 | 1747 | -178 |
| 24; 3-4; 1.09 | 548 | 253 | 202 | 331 | 1715 | -168 |
| 24; 3-4; 1.00 | 519 | 358 | 233 | 389 | 1574 | -138 |
| 24; 4-5; 1.26 | 605 | 88 | 176 | 255 | 1709 | -205 |
| 24; 4-5; 1.14 | 574 | 200 | 210 | 313 | 1704 | -187 |
| 24; 4-5; 1.09 | 554 | 256 | 226 | 340 | 1638 | -169 |

*Table 5 Loads and torques for selected suitable rotor geometries*

## 7.4 Conclusion

The logic of an original method of the author is presented. With this method the loads and torques on screw rotors of a screw type flowmeter have been calculated. using the equations derived. Horizontal and vertical components are determined separately in cross-sections and integrated over the length of the rotor. The load applies only in the area of the sealing line. The value of the forces and torques is obviously related to the

variation of the geometric parameters. The torque on $rotor_I$ is positive, the torque on $rotor_{II}$ negative, which means that $rotor_{II}$ is pushed in the counter direction of rotation.

Analysed with the methods available, the equations presented have been proven to be correct. The results are inconsistent with the results presented by Geimer /54/.

In order to obtain the mechanical loss coefficient $\kappa_U$, constant load areas and torque volumes independent from pressure are presented for all suitable rotor profiles.

# 8 Bearing friction

The understanding of bearing friction torque is vital for the realisation of a mathematical model of a twin screw type PD flowmeter. This section puts focus on the theoretical investigation and experimental results of the relation between bearing friction, load and speed. The conditions for the use of the roller bearings in this application are significantly different to the conditions described in literature since the bearings are lightly loaded and flooded with a non lubricating media. Especially in the range below 500 rpm, the effect of the non-linear types of drag and leakage is of a much greater importance than the effect of influences proportional to the flow rate. As a consequence the results of numerous tests already performed by different authors under different conditions can not automatically be referred to. Hence without any experimental or theoretical values available, tests were performed to achieve the two main values: first a reliable range of the mean value of the friction torque and second its dependence or independence from load and speed.

Different theories are reviewed, which mostly refer to Palmgren /62/. He separates the total friction torque into a lubricant friction and a rolling friction torque. The use of these equations was considered not automatically applicable to the current lightly loaded and flooded bearing assembly with a friction torque below 1 Nmm. A test was performed using the retarding torque time of an accelerated disc and shaft mounted to the inner ring of a bearing. Using the experimental results, an equation was introduced to estimate the sliding frictional resistance torque. The results of the modified equations which include the sliding friction correlate better with the experimental results than the results obtained using original equations presented in literature.

## 8.1 Literature review

### 8.1.1 The influence of bearing friction on fluid pumps and motors

Bearing friction is considered an important influence on the performance of fluid pumps and motors as well as PD flowmeters. Baker /63/ and Schlösser /44/ name bearing friction as one part of frictional resistance which causes the pressure drop in the flowmeter. A comprehensive overview on the use of bearings in turbine flowmeters, is given by Baker /63/. The understanding of this application may be transformed to other types of flowmeters.

### 8.1.2 The theory of roller bearing friction

It is universally recognised that friction due to rolling of non lubricated surfaces over each other is considerably less than the dry friction encountered by sliding the identical

surfaces over each other. Notwithstanding that the motions of the contacting elements in rolling bearings are more complex than is indicated by pure rolling, rolling bearings exhibit considerably less friction than most fluid film or sleeve bearings of comparable size and load carrying ability.

Friction of any magnitude represents an power loss and causes a retarding of motion. Hence friction in a rolling bearing may be measured as a retarding torque. There are many sources of friction in rolling bearings stated by Eschmann /64/, Harris /65/, INA /66/ and Ragulskis /67/ as follows:

(a) Elastic hysteresis in rolling

(b) Sliding due to deformation of contacting elements and /or bearing geometry

(c) Spinning of rolling elements

(d) Gyroscopic pivotal motion of rolling elements

(e) Viscous friction due to lubricant action

(f) Sliding between cage and rolling elements and between cage and bearing rings

(g) Seal friction

In tests, the total friction of a bearing, which is the sum of rolling, sliding and lubricant friction, is measured as the resistance the bearing exerts against its movement. This resistance represents a torque and is generally referred to as the frictional torque $M$.

In 1957 Palmgren /62;68/ presented a set of formulae to determine the frictional resistance as the sum of rolling and lubricant friction. The theory of Palmgren which is considered as the standard theoretical literature for bearing performance is cited by Eschmann /64/, Harris /65/, and Ragulskis /67/, as well as by the bearing manufacturers catalogues INA /66/ and SKF /69/.

Ragulskis /67/ reviews in detail the theory of bearing performance and presents a comprehensive calculation of all sources of frictional resistance and the formulae of different other researchers. He comes to the conclusion that for practical purpose it is best to apply the Palmgren formula related to experimental results achieved with the actual bearing assembly.

However all formulae presented according to Palmgren /62;68/ only differ slightly from the original. All these formulae consider only the lubricant and rolling friction and not any of the other sources of frictional resistance mentioned above. Only Eschmann /64/, INA /66/ and SKF /69/ present enough information to completely calculate the retarding torque.

## 8.2 Theory

According to Eschmann /64/, INA /66/ and SKF /69/ the total friction torque consists of a lubricant friction torque $M_0$ and a rolling friction $M_1$ torque as follows:

$$M = M_0 + M_1 \tag{61}$$

The lubricant friction torque according to Eschmann /64/, INA /66/ and SKF /69/ is related to viscosity, speed and the mean bearing diameter:

$$M_0 = f_0 \times 10^{-7} \times \left(\nu_{fl} n\right)^{2/3} {d_m}^3 \text{ (Nmm)} \tag{62}$$

the following units have to be used:

unit of $\nu_{fl}$ = mm²/s
unit of $dm$ = mm
unit of $n$ = 1/min

The coefficient $f_0$ for the lubricant friction is related to the amount of fluid in the bearing. The lubrication situation closest to a flooded bearing is oil sump lubrication, and hence $f_0$ can be selected from $f_0$=1.5 to $f_0$=2 according to Eschmann /64/ and from $f_0$=2 to $f_0$=3 according to INA /66/. The maximum value for the Eschmann and INA /66/ calculation was chosen respectively.

For $\nu_{fl} n > 2000$, the theory of INA /66/ and SKF /69/ to calculate the lubricant friction torque is the same as the Eschmann /64/ theory. For $\nu_{fl} n < 2000$ the lubricant friction torque is claimed to be independent of speed:

$$M_0 = f_0 \times 160 \times 10^{-7} \times d_m^3 \text{ (Nmm) for } \nu_{fl} n < 2000 \tag{63}$$

For the rolling friction, the equations presented by the bearing manufacturers INA /66/ and SKF /69/ are similar to those introduced by Eschmann /64/ and lead to the same results. The rolling friction torque according to Eschmann /64/ is :

$$M_1 = \mu_1 f_1 P \frac{d_m}{2} \text{ (N mm)} \tag{64}$$

the following units have to be used:

unit of $P$ = N
unit of $dm$ = mm

The resulting bearing load $P$, is calculated from axial and radial load components:

$$P = \sqrt{F_r^2 + F_a^2} \tag{65}$$

with the bearing friction coefficient $\mu_1$ and the load coefficient $f_1$:

$$\mu_1 = 0.002 \times \left( \frac{P}{C_0} \right)^{1/2} \tag{66}$$

$$f_1 = (3Y - 1)\frac{F_a}{P} + \frac{0.5}{Y} - 0.5 \tag{67}$$

The value of the characteristic bearing parameter $Y$ was determined from the INA catalogue /66/ to $Y=2$.

## 8.3 Measurements

Bearing data from INA /66/ is as follows, all other parameter refer to the maximum flowrate and hence maximum pressure load of the current application.

| $d_i$ | $d_o$ | $C_0$ | $min\ F_a$ | $max\ F_a$ | $F_r$ | $n_{min}$ | $n_{max}$ |
|---|---|---|---|---|---|---|---|
| mm | mm | kN | N | N | N | rpm | rpm |
| 8 | 22 | 1.34 | 0.6867 | 3.4335 | 0.6 | 0 | 5000 |

*Table 6 Data for 608 bearing type without sealing and load*

The test rig was constructed to represent the actual flowmeter assembly, with the bearing flooded with fluid. The friction torque was determined in relation to the speed of the shaft and the load applied to the shaft. In this case the load represents the different flow rates to model the test as closely as possible to the actual device. The experimental measurements are presented as a function of speed and bearing load.

Preliminary, different methods to determine the resisting torque have been tried. One set up compared the power used by the unloaded motor, with the power needed to drive the bearing. In an other set up, the outer race was connected to a bar which itself rested on a load cell. No consistent results could be obtained. However the author noted that the friction torque to be measured was clearly below 1 Nmm. The measurement methods described above failed, because they introduced higher forces into the experimental set up, than the torque expected. Hence, the retarding time of a disk mounted to the inner race of the bearing was measured, in order to avoid any external forces or vibrations during the measurement procedure.

### 8.3.1 Theoretical background of the principle of measurement

The idea is that if the shaft in a bearing is initially spun to a definite speed, this speed then decreases until the shaft stops. The mean friction torque for deceleration between two measurement points has to be expressed as a function of the related speed difference and time interval.

$$\overline{T} = J\frac{d\omega}{dt} = 2\pi J\frac{\Delta n}{\Delta t} \tag{68}$$

### 8.3.2 The test rig and testing procedure

The test rig (Figure 46) consisted of a housing and the bearing on a vertical shaft. The discs, each representing a load of 0.69 N were assembled onto the shaft to apply a truly axial load to the bearing. The housing was flooded with Hebrosol® which is a non lubricating petrol substitute with a kinematic viscosity of 1.05 $mm^2/s$. One bearing of the type 608 was used, without sealing, from a normal manufacturing batch supplied by the manufacturer INA /66/.

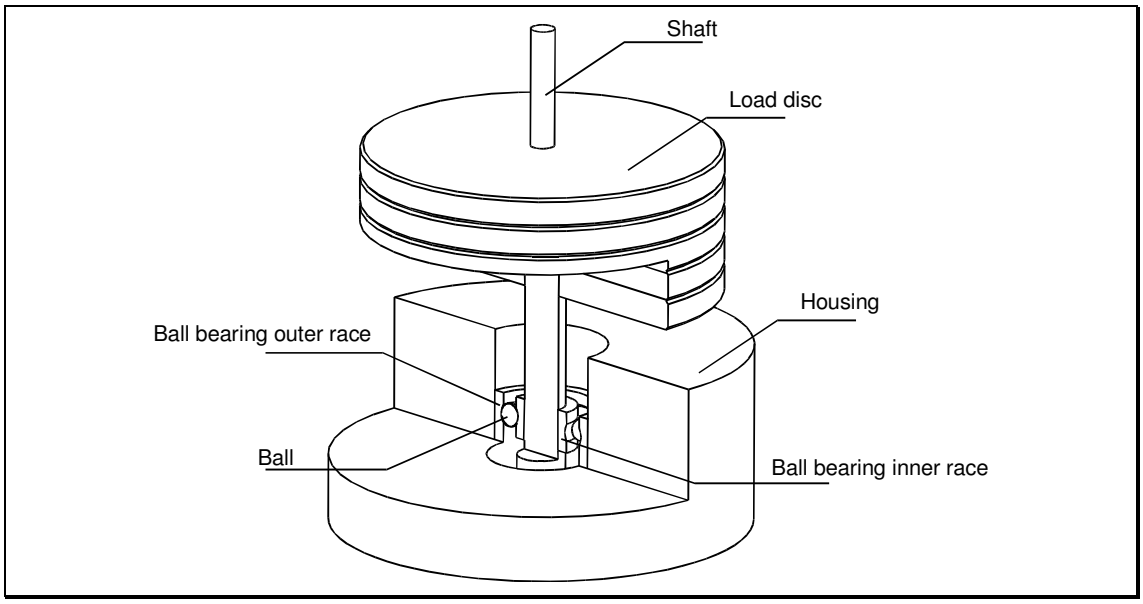


*Figure 46 Test rig using the retarding torque*

The speed of the shaft was measured using two readily available stroboscopes, one for initial time and one for the final time of the interval. The shaft was accelerated to a rotational speed of over 6000 rpm with a motor and then allowed to freely decelerate. Having reached the frequency of the first strobe, the stopwatch was started until the spinning discs had reached the frequency of the second strobe or had come to a full stop. Time and frequencies were noted. This procedure was repeated for 8 speed intervals with 10 repetitions for 5 different loads, in total 400 measurements were made. Hence

for each speed interval the mean torque was calculated from 50 measurements. The use of more sophisticated speed sensing devices was considered, but did not promise improvement for the two main disadvantages of the existing set up: an automatic interface between time and frequency measurement and the recognition of the full stop of the shaft. The friction of the discs spinning in air was found to be not relevant.

## 8.4 Results

According to the theory presented, the maximum value for the total frictional resistance was calculated as 0.35 Nmm. Using the Eschmann /64/ equations, the torque reduces with decreasing speed to almost zero, Using the INA /66/ and SKF /69/ equations the torque also reduces with decreasing speed, but then stays constant at a value of 0.2 Nmm for the range from 2000 rpm to 0 rpm (Figure 47). The frictional torque is also related to the load applied, but the variation between the unloaded to loaded cases is only 0.015 Nmm for both theories. It is important to note that this is only an approximate 10 % effective deviation for an actual 400 % increase in load.

The experimental results show that the mean value of the torque increases constantly from 0.15 Nmm with a standard deviation of 0.07 Nmm for 200 rpm to 0.42 Nmm for 5000 rpm (Figure 47) with a standard deviation of 0.035 Nmm. The maximum single value of torque measured was 0.5 Nmm. The single points of measurement show a large variation especially for the lower speeds where the range is from 0.14 Nmm to 0.25 Nmm (Figure 48). However 80 % of the measured values are within a range of ±0.1 Nmm. This range is marked in light grey in Figure 47 and Figure 48. No significant relation to the load applied could be measured.

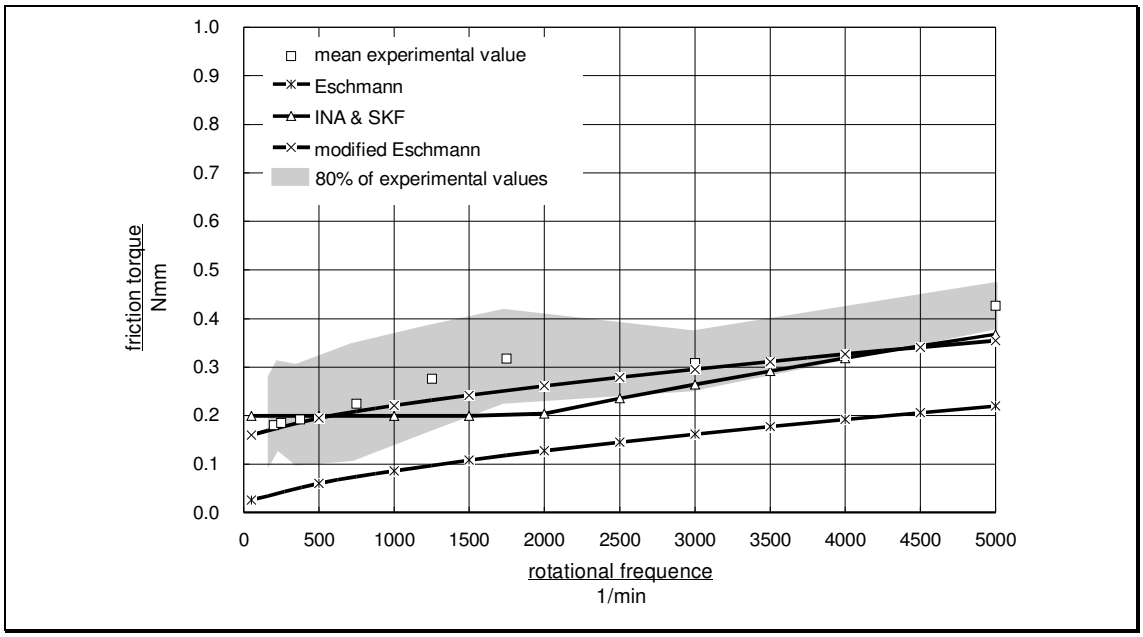


*Figure 47* *Friction torque against speed - mean values of all measurement results compared with the theory of Eschmann /64/, INA /66/ and SKF/69/ and the modified Eschmann equation*

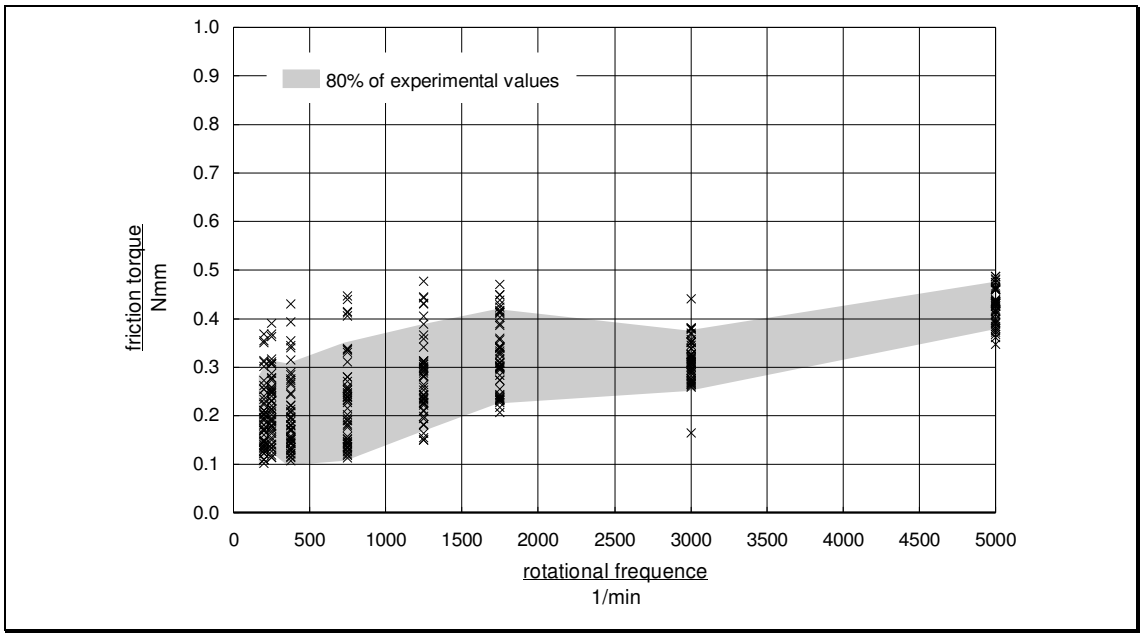


*Figure 48* *Friction torque against speed in a flooded bearing - complete measurement results; statistical 80 % limit in grey*

## 8.5 Discussion

The following observations should be noted:

(a) only one bearing was tested.

(b) only one bearing diameter was tested.

(c) the recognition of start and end point of the measurement relied on the individual judgement.

(d) The viscosity of the lubricating media was not varied

Independent of the variations in the measurements and the observation mentioned above it should be importantly noted that:

(a) The frictional torque measured is not significantly related to load.

(b) For the bearing tested, the frictional torque value for the lowest speed measured was about 0.15 Nmm ±0.07 Nmm but definitely not zero.

(c) The frictional torque increases continuously with speed from 0 to 5000 rpm.

Despite the uncommon lightly loaded bearing set up, flooded with a non lubricating media of low viscosity, the trend of the measurement can be described using the standard equations. In addition, the author proposes to include the sliding friction torque into the calculation. An estimation of the value of the constant sliding friction, which is not related to speed, load, or viscosity is extremely important for the realisation of the complete performance prediction model of the flowmeter. Considering this, the total friction torque is then consisting of lubricant friction, rolling and sliding friction:

$$M = M_0 + M_1 + M_{sl} \tag{69}$$

From the experimental results, a mean value of $M_{sl}$ for the tested bearing can be proposed to $M_{sl} \approx 0.15 \pm 0.07$ Nmm. According to literature the sliding friction torque $M_{sl}$ will be related to the mean diameter of the bearing and a friction coefficient $f_{sl}$:

$$M_{sl} = f_{sl} d_m \approx 0.15 \pm 0.07 \; Nmm \tag{70}$$

hence the coefficient $f_{sl}$ for the tested bearing can be estimated to:

$$f_{sl} \approx 0.01 \pm 0.005 \; N \tag{71}$$

The theoretical results of the Eschmann equation including the sliding friction torque $M_{sl}$ are indicated by "modified Eschmann" in Figure 47. It is expected that the comparison of friction values of different bearings of the same type may show significant higher variations than the value stated in equation (71).

## 8.6 Conclusion

The results of the measurements performed on the retarding torque time of a decelerating disc show variations, but show the same trend as that proposed by theory.

By introducing an additional sliding friction torque with the value $M_{sl} \approx 0.15 \pm 0.07$ Nmm for the tested bearing, the results correlate better with the measurement. All other theories to determine bearing friction are still valid, therefore it is expected that the equations found, are also valid for varying values of viscosity and increasing loads, though the influence of the sliding friction is then too small to be relevant. It is also expected that the value of the sliding friction torque may also vary for other bearings of the same type, however the result obtained with this bearing will be used as a starting value for the verification of the performance prediction model.

One might say the accuracy of the results obtained is rather crude. However it is important to note that the results on bearing friction of this study served to drastically narrow down the range of possible friction values in the current application, as the author did not find at all any reliable values in literature. The results of numerous tests already performed by different authors under different conditions can not automatically be referred to, and hence the author originally had to expect the friction value to be in a range between 0 Nmm and 10 Nmm.

For the screw type PD flowmeter, according to chapter 5 "General performance prediction", the constant friction torque, which is not proportional to flow rate has a significant influence on the flowmeter linearity. The introduction of a value for the independent sliding friction, which can be taken as a basis value to estimate the constant torque power loss coefficient $\kappa_C$, has hence led to a significant improvement in the validation of the flowmeter model.

# 9 Leakage and viscous friction

Slippage is the principal cause of error in displacement flowmeters. Hence if all the seals in the flowmeter were perfect, the only errors in flow measurement that these flowmeters would exhibit, would be those due to the inaccuracies of the measurement of the flowmeter displacement volume. Obviously, the seals cannot be perfect, clearances must exist for the flowmeter to operate, and these clearances allow an leakage error flow which is not registered by the rotating motion of the flowmeter. The determination of this leakage flow is the main focus of this chapter, which discusses the theoretical investigation and experimental results of the relation between the geometry of the rotors, pressure drop, rotational speed and leakage. If not explicitly mentioned, flow is considered laminar and superpositioning of velocity profiles is used. Common flow equations are applied to the current conditions and related to the screw geometry. The aim is to obtain the significant leakage loss coefficients which have been described in the performance prediction section.

Viscous friction is also very much related to the shape and size of the internal clearances and hence discussed within the scope of this report.

## 9.1 Literature review

The literature found can be divided into the general discussion of fluid friction, viscous drag and flow through annuli with an inner rotating cylinder, and in the discussion of the influence on positive displacement applications. The presentation of the literature review related to the general discussion is restricted mainly to laminar flow, as only this flow type was found to be relevant for most clearances of the current application. If not explicitly mentioned all equations are limited to:

(a) non turbulent (laminar) fluid motion in which viscous actions are strong

(b) the fluid elements are moving in straight and parallel paths

(c) Newtonian fluid to be incompressible and the process to be isothermal and steady. This implies constant density and viscosity of the fluid

(d) end conditions are neglected

### 9.1.1 Leakage flow in narrow clearances

#### *9.1.1.1 Flow in annular and triangular clearances*

Becker /70/, Obot /71/ and Tiedt /72/ have carried out a comprehensive work on flow in narrow clearances. Accordingly the laminar flowrate in an annular clearance and the

velocity in the clearance can be calculated. Obot /71/, presents results of his work on triangular clearances and proposes a theoretical description of the clearance flow identical to that of the circular tube.

For clearances with a variable height over the length, Wincek /60/ developed an equation, which can only be solved by iteration. He proved his overall calculation of static leakage for the multiphase type of screw pump to be very reliable. The flow through the clearance is determined by the breadth of the clearance and the integral of the height of the clearance over the length (Figure 67). However Geimer /54/ proposes to calculate the flow through a clearance simplified as a turbulent flow through an orifice.

#### *9.1.1.2 Flow in clearances with moving boundaries*

Yamada /73/ mentions the axial and rotating Reynolds number, which is the criterion defining laminar and turbulent flow. When the axial flow is laminar, the resistance of a flow is unaffected up to a certain rotating speed, but beyond this speed the flow resistances increases as the $Re_\omega$ increases.

Rotating Reynolds number:

$$\mathrm{Re}_\omega = \frac{uh}{\nu_{fl}} \tag{72}$$

Axial Reynolds number:

$$\mathrm{Re}_a = \frac{ch}{\nu_{fl}} \quad \mathrm{Re}_{ac} = 2300 \tag{73}$$

with:

| | |
|---|---|
| *Re* | Reynolds number |
| *c* | Velocity of the fluid flow in the clearance |
| *u* | Peripheral velocity of the inner cylinder |
| *h* | Height of clearance |
| $\nu_{fl}$ | Kinematic viscosity of the fluid |

When there is no axial flow and the speed of rotation of the inner cylinder is increased from zero, the flow in the annulus is truly laminar until a critical speed of rotation is reached, at which Taylor vortices are formed. These vortices are ring-shaped around the rotationary axis (Figure 49). Taylor analysed mathematically the critical speed of rotation, at which such vortices are formed and he confirmed them by experiment. The formation of Taylor vortices is entirely different from occurrence of a turbulent flow. When the speed of rotation of inner cylinder is increased the flow in the

annulus becomes turbulent and vortices are superimposed on the turbulent fluctuation.. Kleinert /74/ and Yamada /73/ present methods for the calculation of the critical rotational Reynolds number $R_{\omega c}$ limiting the possibility of Taylor turbulences.

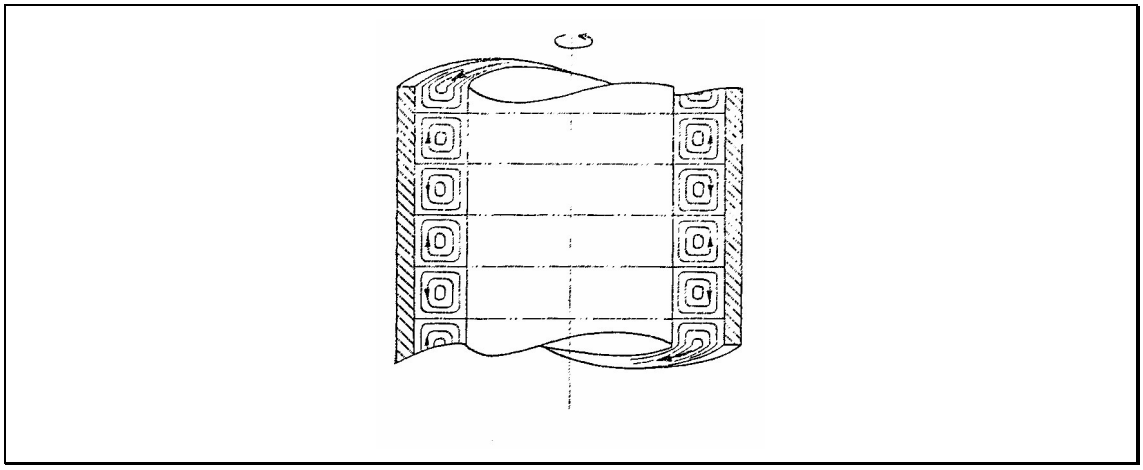

*Figure 49 Taylor vortices; Yamada /73/*

Tao /75/ and Wincek /60/ propose that the annular passage can be considered as being unwrapped. It will then form two parallel flat plates, and the flow problem will two dimensional (Figure 50). The velocity profiles can be superposed, although this will always be an estimation. Secondary flows and turbulences are not considered.

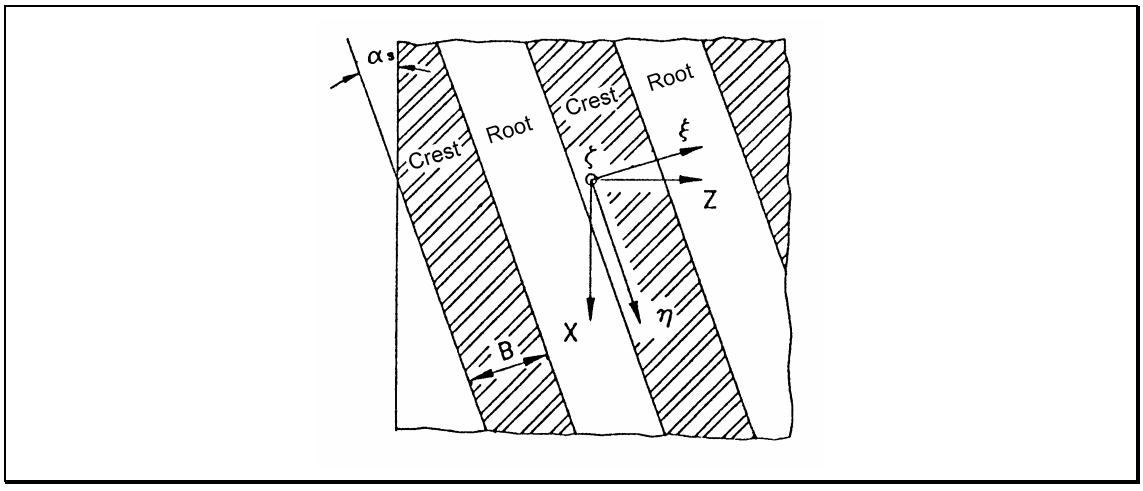


*Figure 50 Unwrapped view of a screw section; Wincek /60/*

### 9.1.2 Viscous friction and shear stress

The earliest relation between stress and rate of strain may be attributed to Newton Such shear flows are generally known as Couette flows. They can be produced by slowly shearing a thin fluid film between two large flat plates or between the surface of coaxial cylinders.

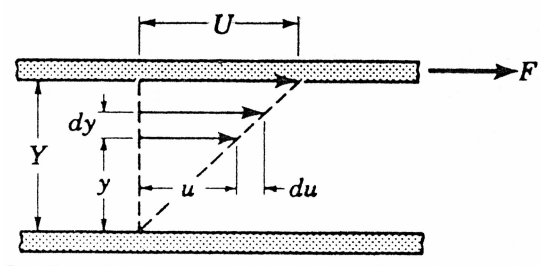


*Figure 51 Shear stress between two parallel plates moving with relative velocity Daugherty /77/*

The equation for the shear stress itself which is cited by Allen /76/, Daughtery /77/, Street /78/ and others can be considered using elementary fluid mechanics.

$$\tau = \frac{F}{A} = \eta_{fl} \frac{du}{dy} \tag{74}$$

To calculate the friction torque between the surface of coaxial cylinders, Street /78/ presents an exact calculation for the torque applied to the inner cylinder. According to Daugherty /77/, for coaxial cylinders with a constant rotational speed $\omega$, the shear stress on the inner cylinder will be larger than that on the outer because of the different radii, and thus the velocity gradient will not be constant across the gap (Figure 52). For a small height of the clearance, Street /78/ recommends using an approximation.

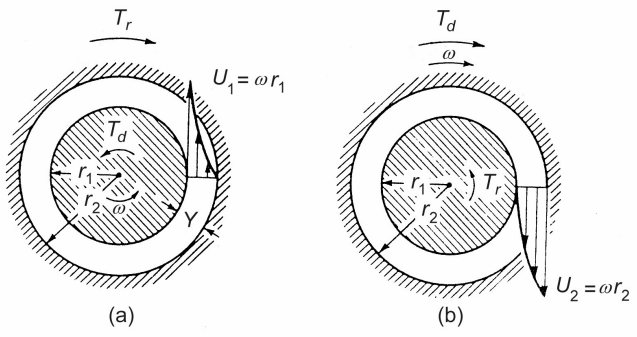


*Figure 52 Velocity profile, rotating coaxial cylinders (a) Inner cylinder rotating. (b) Outer cylinder rotating. Daugherty /77/*

### 9.1.3 Leakage and viscous friction in positive displacement applications

The influence of fluid friction and leakage in pumps and motors was first mentioned by Wilson /47;49/. The torque is proportional to the dynamic viscosity and the rotational speed. Heating of the liquid in leakage passages, due to high rates of shear, will result in a reduced viscosity and increased leakage, which is not considered in the equations above. The effective delivery of a fluid motor, Wilson /47;49/ therefore expresses as the sum of theoretical flowrate and leakage flow. The leakage flow consists of a rotational and a pressure related part. Schlösser /40;43/ presents an improved model for the pressure related leakage flow. The leakage flow can be divided into two components with the first related to the dynamic viscosity and the other related to the density. The different leakage flows are supposed to be parallel and summarised over the motor. In order to compare different sizes he introduces dimensionless factors of the volumetric losses.

In a previous work the author performed an experimental study on the leakage of twin screw pumps. Klügl /79/ discusses in his work the leakage of twin screw pumps with a 2/3 montelius profile. Experiments with this two rotor set up for a pressure gradient of 4 bar and the test fluid hebrosol have shown the following distribution of the leakage flow: circumference 2 %, root 67 %, flank 31 % and for the triangular clearance less than 0.5 %. The sealing methods used are discussed and not considered suitable for a more reliable and accurate measurement.

### 9.1.4 Rotational viscous friction and leakage in screw pumps

The clearances in a twin screw pump are first described by Hamelberg /51/. In his work he differentiates between a root and a circumference clearance. Wincek /60/ describes three different types of clearances for a 2 rotor profile of a multiphase screw pump, which are circumference, root and flank clearance. He separates those with a constant height like the annulus ring shape clearance at the circumference from those clearances with a variable height.

Geimer /54/ discusses in his work on three rotor screw pumps the results of Wincek /60/ and Hamelberg /51/. He comes to the conclusion that the flow through the circumference is insignificantly small. Hence he ignores the circumference clearance and considers the flow through root and flank clearance only. He assumes the flow in the clearance to be turbulent and does a simplified calculation as an orifice.

None of the stated authors mentions the existence of a triangular clearance. Wincek /60/, Geimer /54/ and Karassik /36/ use a linear pressure gradient $\Delta p$ for their calculations (Figure 53).

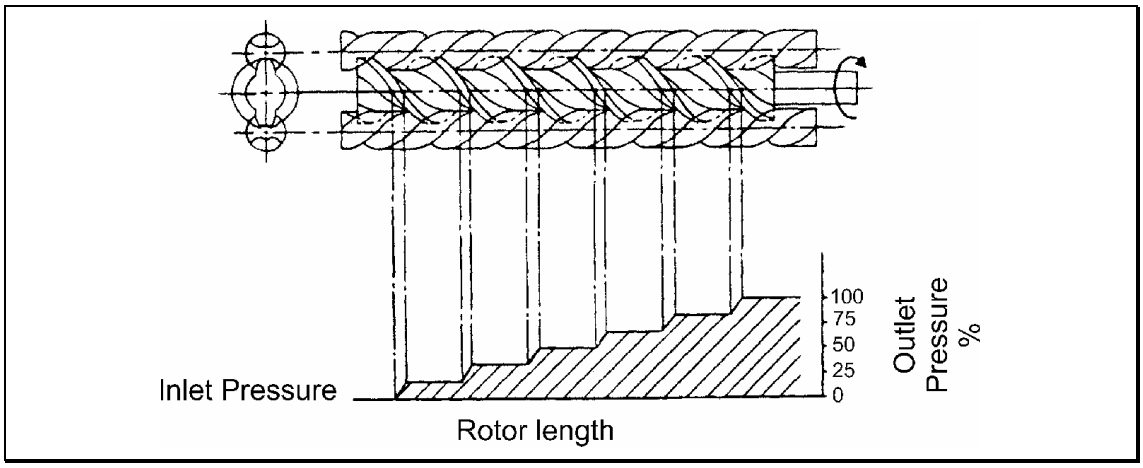


*Figure 53 Pressure gradient along a screw pump set; Karassik /36/*

Wincek /60/ has completed a comprehensive work on the rotational viscous friction and leakage flow in a 2/2 twin screw pump. For the circumference of the rotors he calculates the flow with a linear velocity profile.

## 9.2 Measurements

The intention of all experiments performed is to determine the pressure related leakage flow through the complete flowmeter, and to separate the different flows through the various clearances from each other. The ideal solution would be to seal all but one clearance and measure the remaining leakage flowrate. However, previous work of the author has shown that this can not be done effectively; Klügl /79/. If performed for circumference, flank or root clearance, the sealant will always results in a negative influence on the position of the rotors and change the measurement results significantly. Only the triangular clearance was sealed successfully.

### 9.2.1 General

Static leakage is the leakage flow through production clearances between adjacent areas which border the displacement chamber. The driving power is the pressure drop of the flowmeter, the pressure related leakage is measured with the rotors fixed in the housing, without any rotation. Viscous drag is related to the rotational speed of the flowmeter, hence the viscous drag and the resulting forces can not be measured as a stand alone value.

For the experiments a twin screw flowmeter within the normal production tolerances supplied by the manufacturer was used. The exact outer and root diameters of the rotors (Figure 54), the difference between nominal and real surface on the flanks and the diameters of the bores and the centre distance of the housing were determined by a 3D measurement machine with a tolerance of ±0.5 microns (Table 7). It is important to

remember that for laminar flow the leakage flowrate ($\dot{V}_S$) increases with $h^3$ ($h$ = height) of the clearance. A difference within the tolerance of the geometric measurement results in a calculation error of the theoretical leakage flow of up to 50 %, based on a nominal value of the height $h$ of 5 microns.

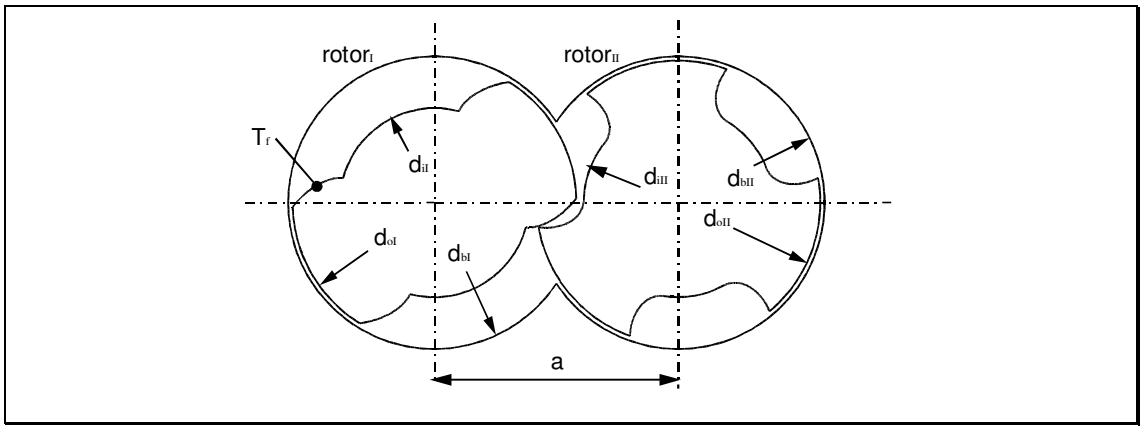


*Figure 54 Dimensions of rotors and housing*

| description | $d_{oI}$ | $d_{oII}$ | $d_{iI}$ | $d_{iII}$ | $d_{bI}$ | $d_{bII}$ | a | $T_f$ |
|---|---|---|---|---|---|---|---|---|
| | mm | mm | mm | mm | mm | mm | mm | mm |
| nominal value | 24.000 | 22.000 | 13.800 | 11.800 | 24.000 | 22.000 | 17.900 | 0.000 |
| upper margin | -0.029 | -0.029 | -0.004 | -0.004 | +0.0125 | +0.0125 | +0.015 | 0.000 |
| lower margin | -0.039 | -0.039 | -0.014 | -0.014 | -0.0075 | -0.0075 | 0.000 | -0.010 |
| mean value | 23.966 | 21.966 | 13.791 | 11.791 | 24.0025 | 22.0025 | 17.907 | -0.005 |
| measured value | 23.9659 | 21.9703 | 13.792 | 11.792 | 24.005 | 21.9992 | 17.9015 | -0.007 |

*Table 7 Measured values of the rotor and housing geometry; see Figure 54*

### 9.2.2 Test rig

The rig consisted of a constant level fluid supply a throttle valve, a weighing unit and the flowmeter which had blocked spindles (Figure 55). Two pressure gauges measured the pressure directly before and after the spindles. $Rotor_I$ was blocked by the friction of a plastic block clamped between the end of the spindle and the axial cover, to introduce no radial force or displacement into the measurement set-up (Figure 55). $Rotor_{II}$ was blocked by its engagement with $rotor_I$. The rotational position of the spindles was marked. A measurement of the axial position of the rotors in the housing was not performed; the rotors were assumed to be coaxial with the housing. As a fluid, for safety

reasons, the petrol substitute hebrosol® was used. The viscosity of hebrosol® is 1.05 N/mm² which is approximately the same as for petrol. The pressure difference could be adjusted by the throttle valve within 0.005 bar and 0.14 bar, which is the typical pressure drop in operation of the flowmeter. The procedure was as follows:

(a) The blocked flowmeter was assembled and build into the test rig.

(b) At highest pressure available the fluid was pumped through the flowmeter, to ascertain that no air was enclosed.

(c) The flowmeter was connected to the constant level tank.

(d) The desired pressure drop was adjusted with the throttle valve.

(e) The fluid was allowed to flow through the flowmeter for one minute at the adjusted pressure drop to ascertain an equilibrium.

(f) A measuring beaker was placed in the fluid flow and the stopwatch was started.

(g) After approximately one litre of the fluid had passed the flowmeter, the valve was shut and the time was noted. For a pressure drop of 0.02 bar and lower, the time interval for one measurement was as long two hours, for the highest pressure drop of 0.14 bar the time interval was about 3 minutes.

(h) The fluid, which had passed the flowmeter, was weighed and the weight was noted. The volume of the fluid was calculated from weight and density.

(i) The procedure was repeated for another pressure drop at (d).

This measurement procedure was done with one set of spindles for different angular positions. For three positions (A1, A2, A3) detailed results were obtained over the whole pressure range. For all positions no complete displacement chamber could be formed by the rotors, but inlet and outlet side were separated by a sealing line. All position were expected to show the same leakage flowrate. The position with the complete displacement chamber was omitted, because its occurrence during the course of rotation is neglectible small. In total 120 measurements were made.

In addition for two positions the same measurement was performed with a sealed triangular clearance in (T1, T2). Again the positions were chosen, so that inlet and outlet side were only separated by a sealing line. The triangular clearance was sealed by a 0.3 mm diameter wire which was fed through both of the triangular clearances. The 0.3 mm was the largest wire diameter, for which the set-up could be assembled and disassembled without any forces applied. The 0.3 mm diameter wire was removed undamaged. The existence of the clearance is hereby proved, and as no larger diameter wire could be applied, the clearance can be considered almost sealed.

Any side forces caused by sealing the triangular clearance in a different way would in turn, have caused the annular gap to be altered which would clearly have been undesirable. Hence circumference, flank and root clearances could not be sealed without any applying forces.

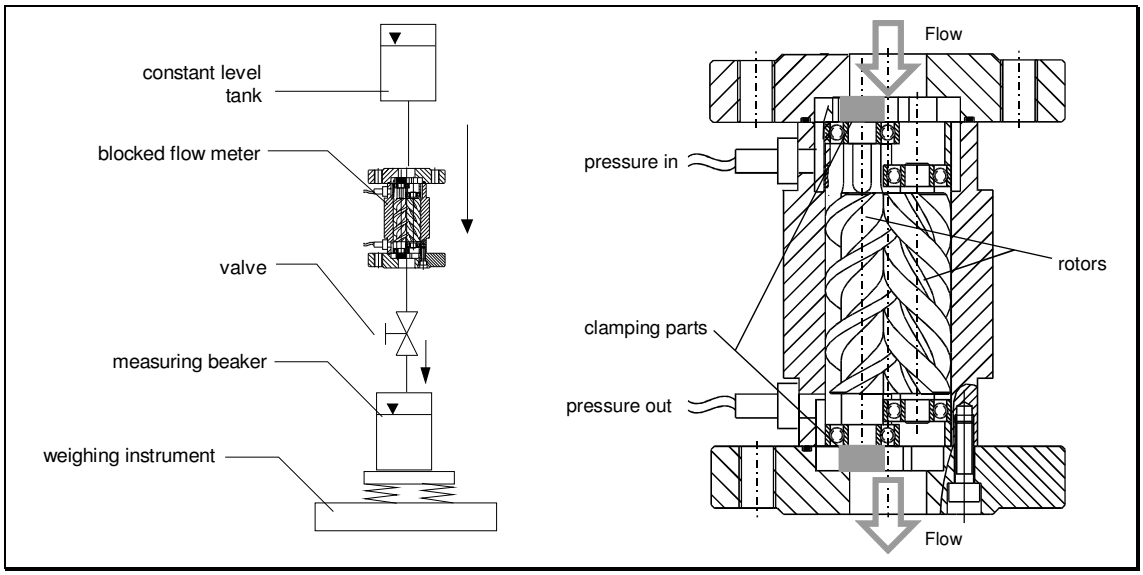


*Figure 55 Static leakage test-rig and section through the blocked flowmeter*

### 9.2.3 Interpretation of test results

The leakage flow is related to pressure and increases almost linearly with the pressure difference over the flowmeter (Figure 56). The repeatability of the measurement in any selected test position was excellent, but no significant relationship between the rotational position of the rotors and the leakage flowrate could be noted. The positions A1, A2, A3 and T1, T2 were actually selected in order to measure comparable leakage flowrates, however the results for those angular positions differed by ±30 %. The overall flowrates for positions T1 and T2 with a sealed triangular clearance were not significantly smaller than the flowrate for the unsealed positions A1, A2 and A3 (Figure 56). In order to obtained a more detailed information on how the total leakage flowrate is distributed on the different clearances, the total flowrate was analysed by dividing it into laminar and turbulent flow components. Therefore, the theory of Wincek /60/ and Schlösser /40;43/, as already proposed in the performance prediction section, was used to form an equation for the total leakage flowrate as the sum of laminar and turbulent flow.

$$\dot{V}_S = \kappa_{lam} \frac{\Delta p}{\eta_{fl}} + \kappa_{tur} \sqrt{\frac{\Delta p}{\rho_{fl}}} \qquad (75)$$

The experimental results can then be described by a levelling regression curve with a significant pair of parameters $\kappa_{lam}$ and $\kappa_{tur}$ (Figure 56). The mean value of the deviations of the measured points to the levelling curve was below 3%. The good correlation of the curve to the measured points is especially obvious in the low pressure range (Figure 57). Hence, using equation (75) is considered an adequate method of separating the different flow components, which can now be plotted and evaluated separately from each other. It shows that the turbulent proportion is very repeatable (±6 % related to total flow rate) for the unsealed positions A1, A2 and A3 (Figure 58). For a sealed triangular clearance as in positions T1 and T2 there is a significantly lower turbulent flow component, which only is 20 % of the mean value of the unsealed positions (Figure 59). Regarding the laminar flowrate, the proportions of the unsealed positions A1, A2 and A3 and the flowrates of the sealed positions T1 and T2 show a good correlation over the whole range (Figure 60).

The following points can be made:

(a) The leakage flow through a flowmeter can be separated into laminar and turbulent components.

(b) With the triangular clearance sealed, the proportion of the turbulent share is significantly smaller than without sealing.

(c) The laminar proportion is not affected by the sealing of the triangular clearance.

Hence it can be assumed that the majority of the turbulent leakage flow is caused by the triangular clearance, and that the leakage flow through the other clearances, namely circumference, root and profile clearance is laminar. This puts focus on the triangular clearance, as this clearance becomes an important influence on the flowmeter performance in the low end of the flow range where the flowmeter performs at a lower pressure drop than 0.02 bar.

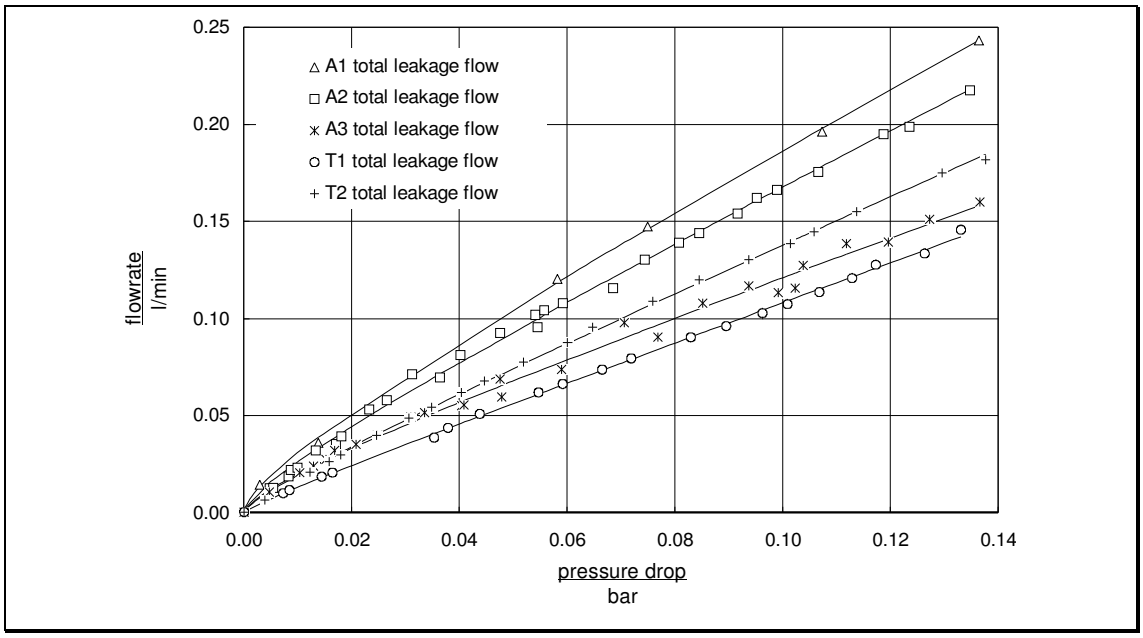


*Figure 56 Measurement of static leakage flow against pressure drop compared with* $\dot{V}_S = \Delta p \kappa_{lam} + \sqrt{\Delta p} \kappa_{tur}$ *equation*

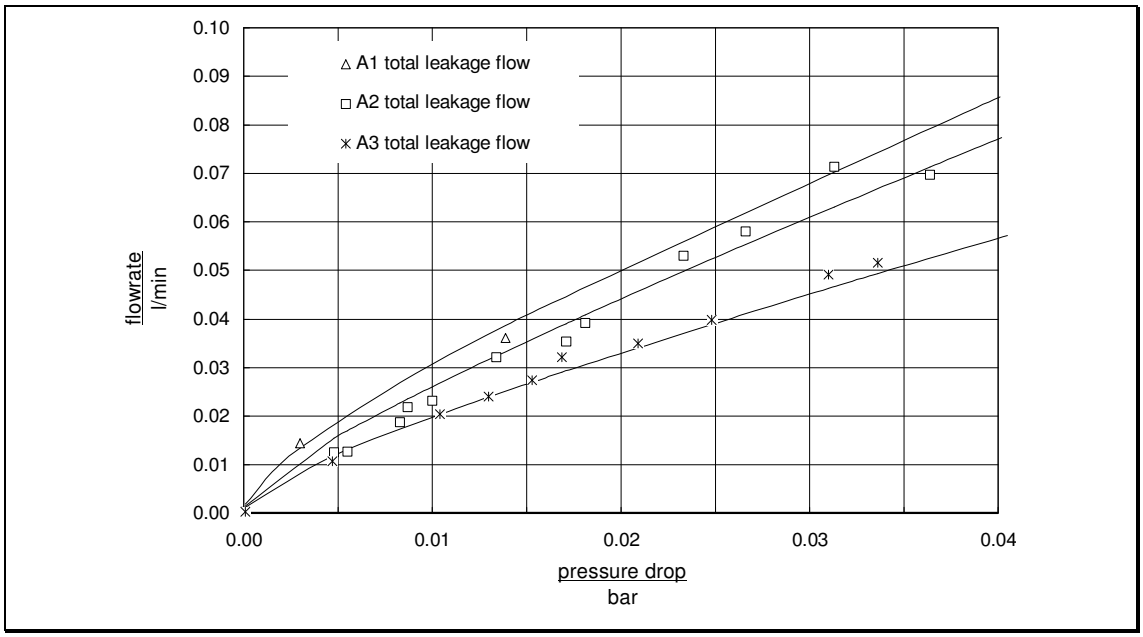


*Figure 57 Enlarged plot of Figure 56 for stated flowrate and pressure drop ranges*

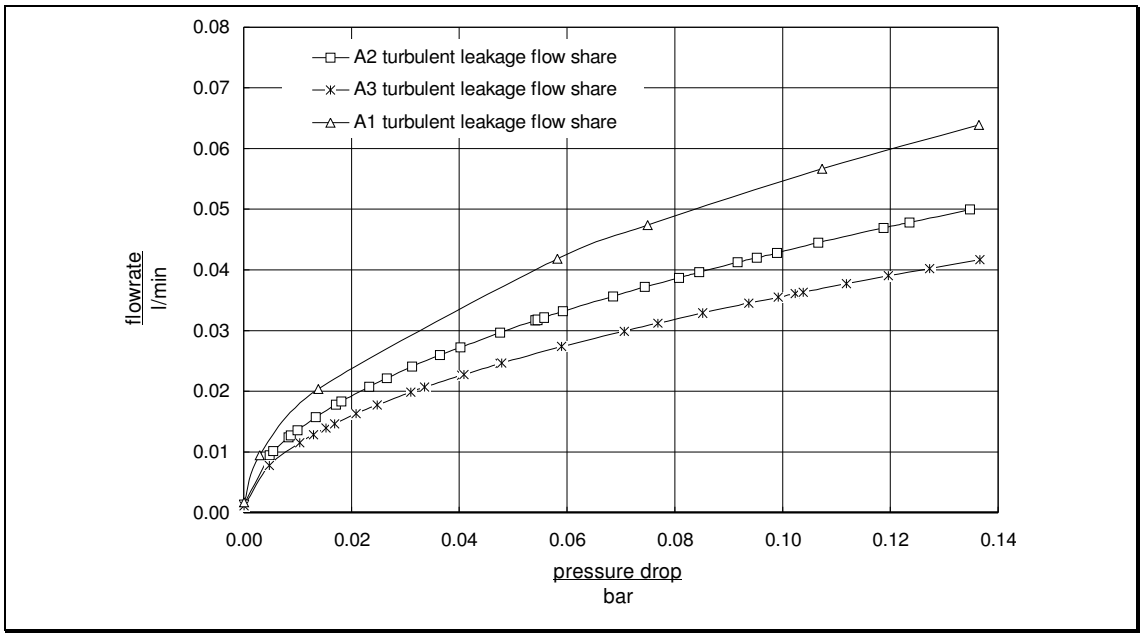


*Figure 58 Measurement of static leakage flow against pressure drop - turbulent proportion using equation (75)*

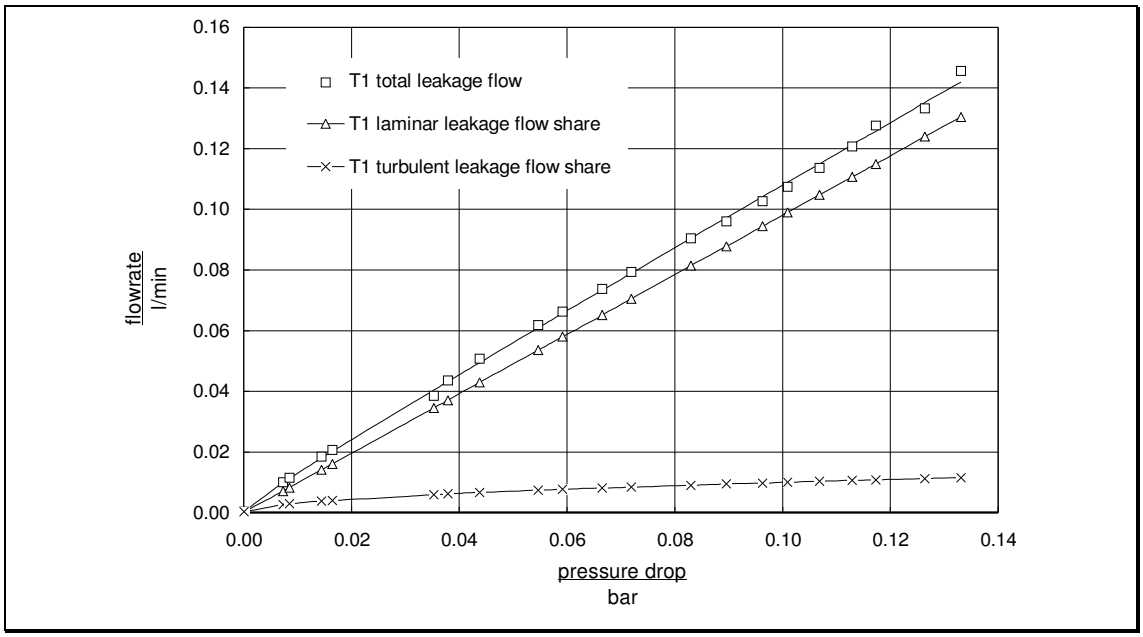


*Figure 59 Measurement of static leakage flow against pressure drop with a sealed triangular clearance- laminar and turbulent proportion using equation (75)*

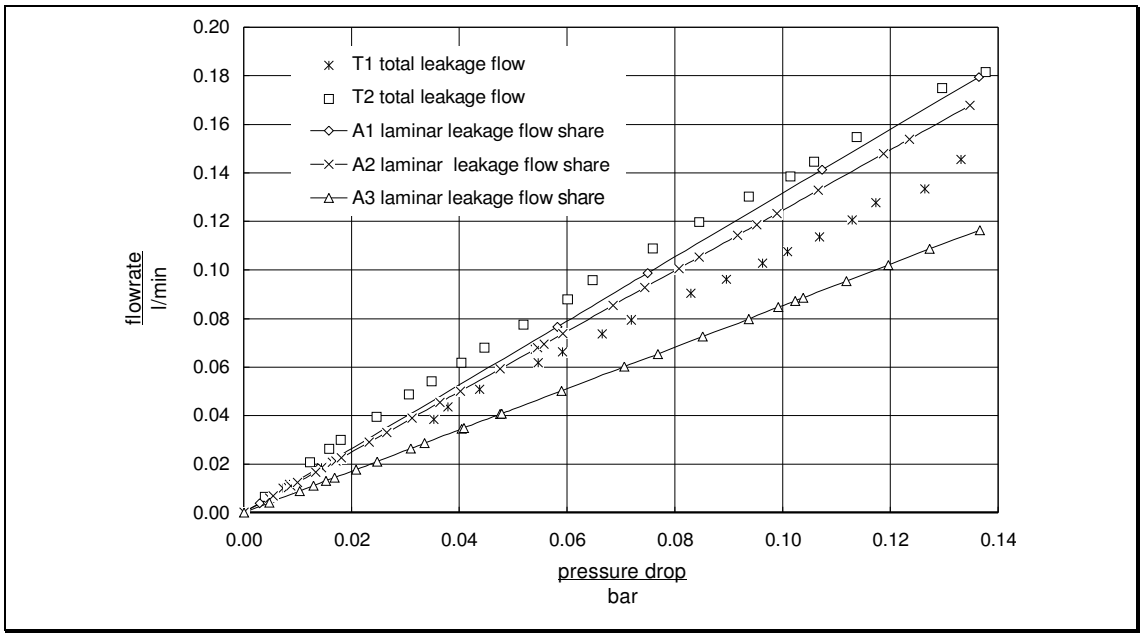


*Figure 60 Measurement of static leakage flow against pressure drop with a sealed triangular clearance - comparison with laminar component of overall leakage flow*

## 9.3 Theory

### 9.3.1 General

The work on leakage found in literature to date does not satisfactorily explain the experimental results, especially the large influence of the triangular clearance. A closer look at the theory of fluid flow in clearances was done and the geometry of the clearances has been described. Each type of clearance will be explained together with a general solution for the leakage flows related to pressure and rotational speed, as well as the viscous friction. Methods of Wincek /60/ and Schlösser /40;43/ in combination with the conventional flow theories are used.

There are three types of clearances to discuss separately.

(a) The flow and viscous friction in an annular ring shape clearance is sufficiently discussed in literature and an exact calculation can be obtained using the parametric equations stated later in this chapter.

(b) For the flow through and viscous friction in a clearance with a varying height, the author will present an analytical equation to compare with the numerical solution presented by Wincek /60/.

(c) The flow through the triangular clearance which is bordered by curved surfaces but in addition has a high height to width ratio. This results in a considerable carnot pressure loss.

#### *9.3.1.1 Description of the use of parameters*

According to Geimer /54/ and clearances of the twin rotor pump described by Wincek /60/ and Hamelberg /51/ are different to those of the cycloid twin or triple rotor design. The author, who in agreement with Wincek /60/ and Hamelberg /51/, proposes to look at a section normal to the axis to discuss the clearances, disagrees with Geimer /54/ who describes the clearances by analysing the unwrapped view of the surface of the screw.

Looking at the cross section the $m_I$ grooves in $rotor_I$ and the $m_{II}$ grooves in $rotor_{II}$ can be seen (Figure 61). For unengaged rotors the fluid could actually flow unhindered from the inlet to the outlet side of the flowmeter. The two rotors, once mated, provide a total separation with different parts of the rotors engaged with each other. As a consequence every part of the profile has to be sealed by a part of the mating rotor or the housing.

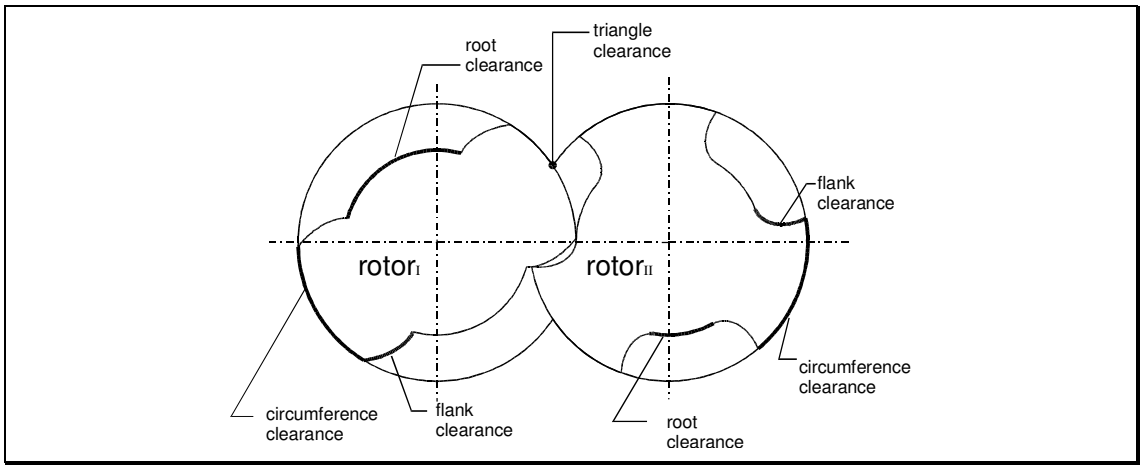


*Figure 61 Cross section through the rotors indicating the various clearances*

#### *9.3.1.2 Displacement chamber*

The PD flowmeter operates by the successive mechanical division of the metered fluid into separate pockets. For the twin screw flowmeter, the inter-meshing, helically fluted rotors trap the discrete volumes of fluid against the measuring chamber wall (Figure 62). The measuring chamber itself is of a complex three-dimensional shape.

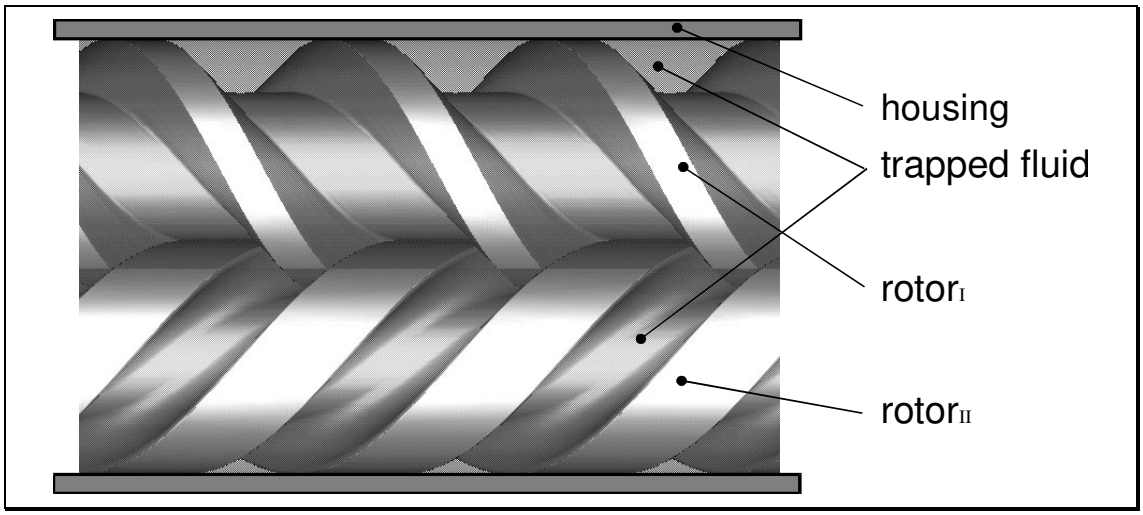


*Figure 62 3 dimensional model of a set of rotors with the trapped fluid*

According to the multi-start design of the rotors, the clearances do not only connect adjacent chambers. The root and flank clearances of rotor$_I$ actually skip one pocket, the root and flank clearances of rotor$_{II}$ two pockets. Therefore, discussing a pair of rotors with infinite length, the pressure drop at these clearances can double or triple the pressure drop between two adjacent chambers (Table 1).

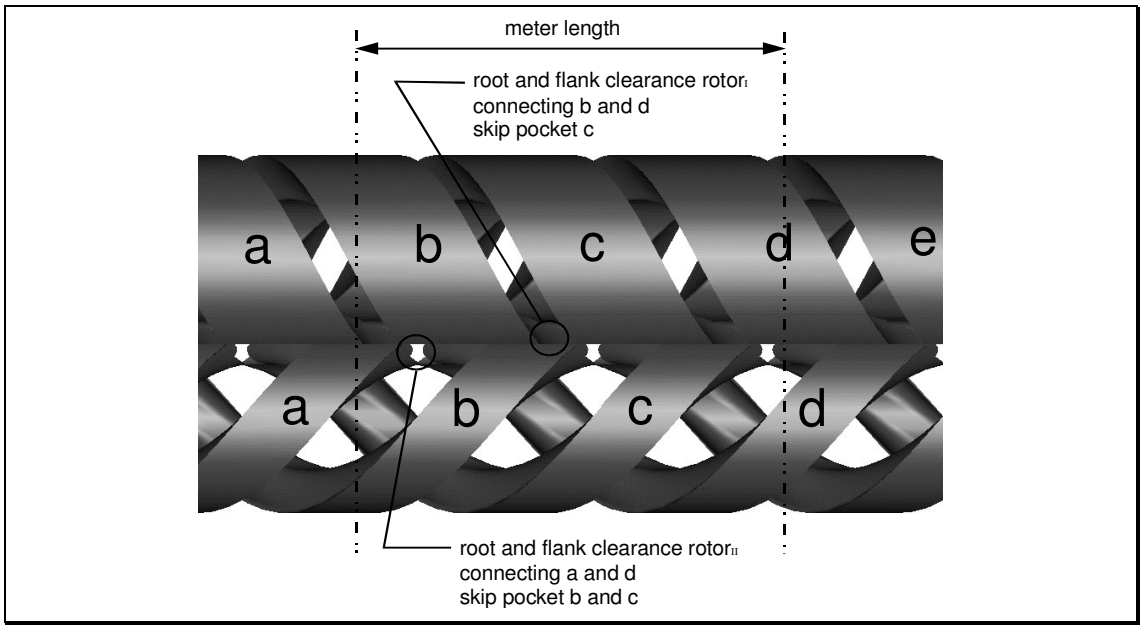


*Figure 63 3 dimensional model of the pockets of rotors with infinite length - the clearances skip adjacent pockets*

| Name | First border | Second border | Δp | Quantity |
|---|---|---|---|---|
| circumf clearance $rotor_I$ | OD of $rotor_I$ | bore in housing $rotor_I$ | 1 | 1 |
| circumf clearance $rotor_{II}$ | OD of $rotor_{II}$ | bore in housing $rotor_{II}$ | 1 | 1 |
| root clearance $rotor_I$ | root of $rotor_I$ | OD of $rotor_{II}$ | $m_I$ (2) | $m_I$ (2) |
| root clearance $rotor_{II}$ | root of $rotor_{II}$ | OD of $rotor_I$ | $m_{II}$ (3) | $m_{II}$ (3) |
| flank clearance $rotor_I$ | flank of $rotor_I$ | chamfer diameter of $rotor_{II}$ | $m_I$ (2) | $2\times m_I$ (4) |
| flank clearance $rotor_{II}$ | flank of $rotor_{II}$ | chamfer diameter of $rotor_I$ | $m_{II}$ (3) | $2\times m_{II}$ (6) |
| triangular clearance | OD of $rotor_I$ and $rotor_{II}$ | bore in the housing | 1 | 2 |

*Table 8 Listing of the different clearances, values in brackets represent the design with 2 starts on $rotor_I$; 3 starts on $rotor_{II}$*

However, the screw flowmeters used by the manufacturer Leistritz are produced to the minimum length possible as described in the rotor geometry section. The inlet and outlet side of the flowmeter are only separated by a sealing line and no complete displacement chamber, which is sealed from both sides, can be formed. Hence the volume in the flowmeter is either related to the inlet or outlet pressure and the pressure difference over all clearances is always Δp, the pressure drop between inlet and outlet side.

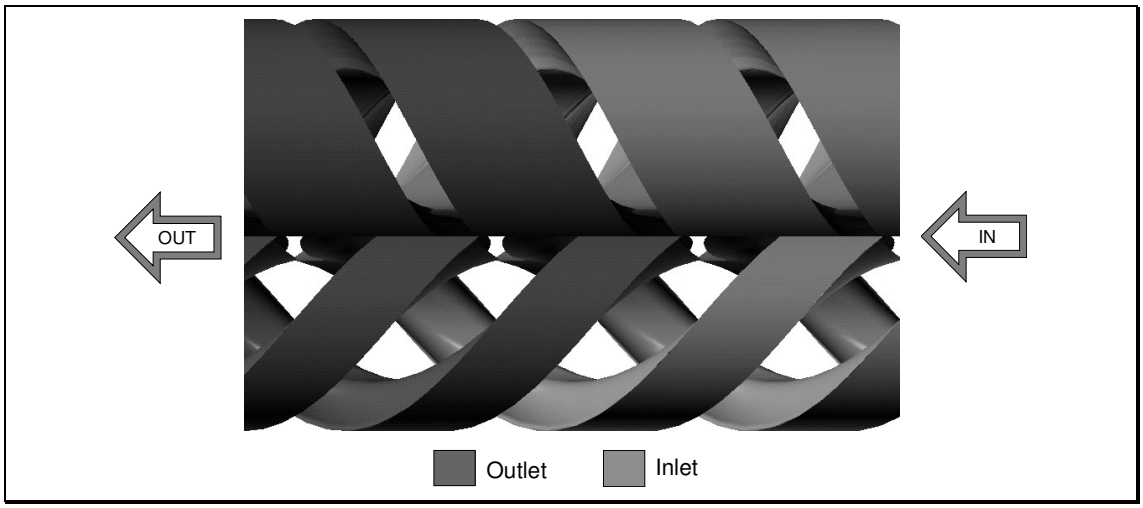


*Figure 64 3 dimensional model of the fluid connections from the inlet to the outlet side of the flowmeter*

#### *9.3.1.3 Restrictions and parameters*

Based on the flow calculation discussed in literature the method to determine the leakage flow through and friction in every clearance is described in the following. This will be done together with a detailed description of each clearance itself. This method takes into account a parametric design of the rotors, different clearances and a variable height over the length. To ascertain laminar flow the rotating and axial Reynolds number in equations (72) and (73) in section 9.1.1.2 "Flow in clearances with moving boundaries" both have to be below the critical value as described by Yamada /73/ or Kleinert /74/. A planar clearance is described by its height, length and breadth, whereas a clearance bordered by curved surfaces is described by its height, length and breadth and the curve of the surface (Figure 65). If not explicitly mentioned all equations are limited to following conditions:

(a) non turbulent (laminar) fluid motion in which viscous actions are strong

(b) the fluid elements are moving in straight and parallel paths

(c) Newtonian fluid to be incompressible and the process to be isothermal and steady. This implies constant density and viscosity of the fluid

(d) end conditions are neglected

(e) annular clearances are considered flat unwrapped

(f) different flow components are allowed to be superimposed

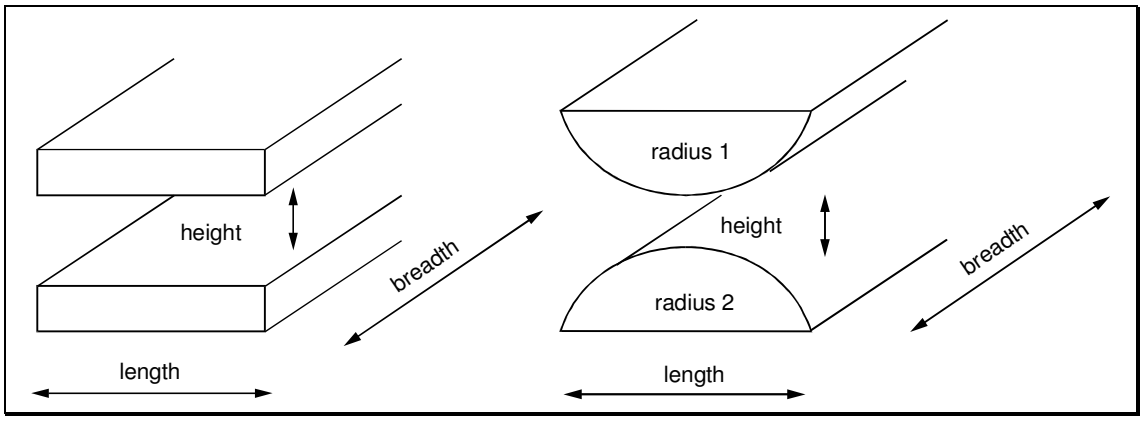


*Figure 65 The description of the variables of the clearances - length; height; breadth*

The dimensions of the clearances are related to the dimensions of the screw profile of the rotors (Figure 66). A more detailed description of the relation of the parameters to each other can be found in the rotor geometry section.

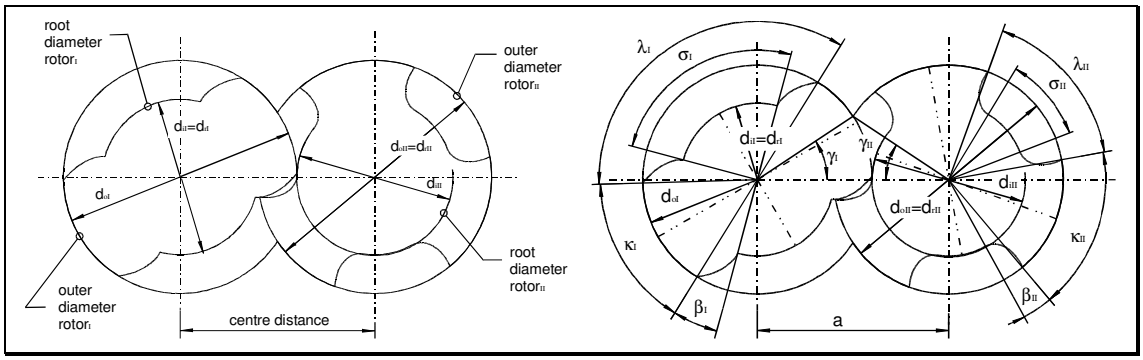


*Figure 66 Parameters of the screw profile*

#### *9.3.1.4 Approximation of a clearance with variable height*

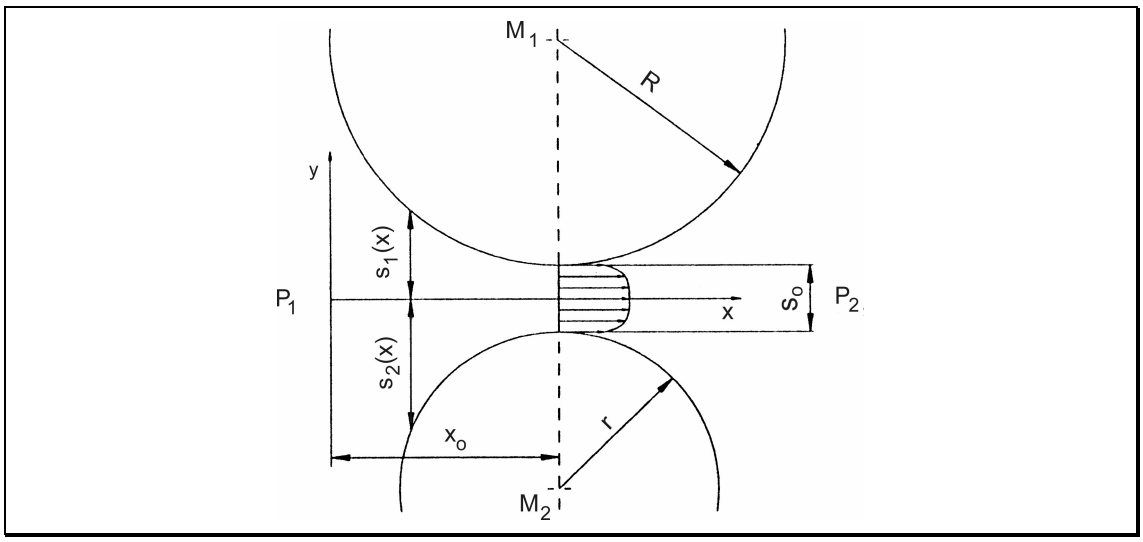


*Figure 67 Scheme of the radial clearance in a screw pump; Wincek /60/*

For laminar leakage flow Wincek /60/ describes the flow through this clearance with curved borders to:

$$\dot{V}_{SR} = \frac{\Delta p b_R}{12\eta_{fl} \int_{-x_0}^{+x_0} \frac{1}{h_R(x)^3} dx} \tag{76}$$

with the approximation of the radius of curvature of a parabola instead of the circle the clearance height can be described in relation to the two bordering radii. The influence of the limits of the integral $x_0$ decreases with the increase of the integral length. In order to solve the integral a substitution length for the clearance can be introduced. The flow through a variable height clearance then can then be approximated to:

$$\dot{V}_{SR} = \frac{\Delta p b h^{5/2}}{14{,}4\eta_{fl}} \sqrt{\left(\frac{1}{r_1} + \frac{1}{r_2}\right)} \tag{77}$$

The detailed description can be found in Appendix F "Approximation of a clearance with variable height"

### 9.3.2 Circumference clearance

The outer diameter of each rotor and the housing form the circumference clearance which is an interrupted annular ring. There is one clearance per rotor and the extension is related to the head-angle, the pitch angle and the centre angle.

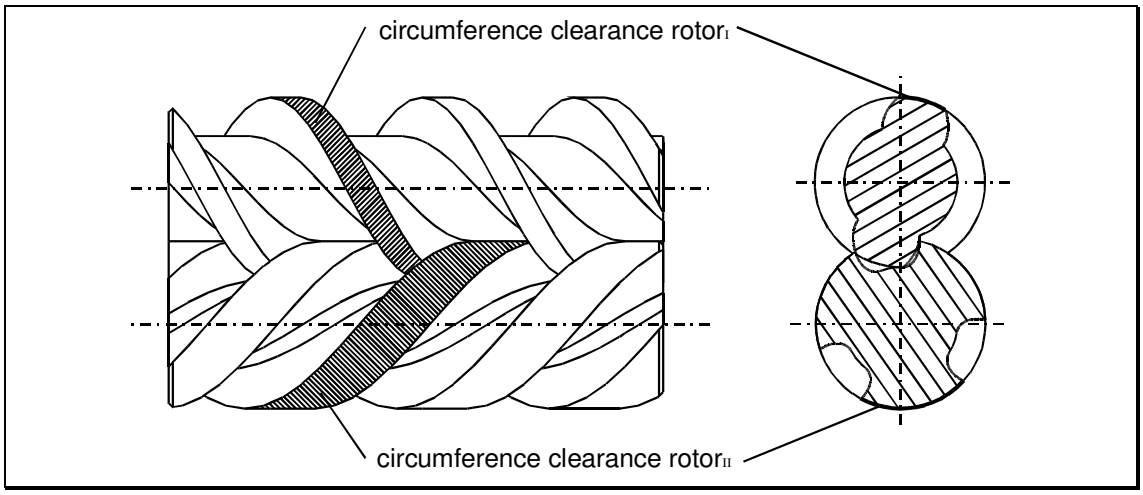


*Figure 68 The circumference clearance*

### *9.3.2.1 Leakage*

The dimensions for the clearance are:

$$\ell_C = d_o \frac{\kappa \sin\phi_P}{2} = d_o \frac{\kappa}{2} \frac{\tan\phi_P}{\sqrt{1+\tan^2\phi_P}} \tag{78}$$

$$b_C = d_o \frac{\pi - \gamma}{\cos\phi_P} = d_o (\pi - \gamma)\sqrt{1+\tan^2\phi_P} \tag{79}$$

$$h_C = \frac{1}{2}\left[\left(d_b + T_b\right) - \left(d_o + T_o\right)\right] = \frac{1}{2}\left(T_b - T_o\right) \tag{80}$$

$T_b$ and $T_o$ are the deviations from the nominal diameters and take into account the production clearances. To relate the values to either $rotor_I$ or $rotor_{II}$, the angles in the equations above have to be related to this rotor as well.

According to Becker /70/, Obot /71/ and Tiedt /72/ the velocity of the leakage flow for laminar flow conditions can described as:

$$c_{SC} = \frac{\Delta p h_C^2}{12 \rho_{fl} \nu_{fl} \ell_C} \tag{81}$$

and hence the leakage flowrate:

$$\dot{V}_{SC} = c_{SC} h_C b_C \tag{82}$$

The leakage flow can be calculated separately for each of the both rotors and described as a combined value related to the outer diameter of $rotor_I$ and a constant coefficient $K_{SC}$ not related to size and fluid properties.

$$\dot{V}_{SC} = \Delta p \frac{1}{\eta_{fl}} K_{SC} \tag{83}$$

It is important to note that the leakage flowrate $\dot{V}_{SC}$ is not related to the dimensions of the rotors, but only to the manufacturing tolerances.

#### *9.3.2.2 Rotational leakage*

The absolute surface speed of the rotors at the outer diameter is:

$$u_C = \frac{d_o}{2}\omega \tag{84}$$

The breadth $b_{\bar{C}}$ of the clearance parallel to the axis of rotation is:

$$b_{\bar{C}} = d_o \tan\phi\left(\pi - \gamma\right) \tag{85}$$

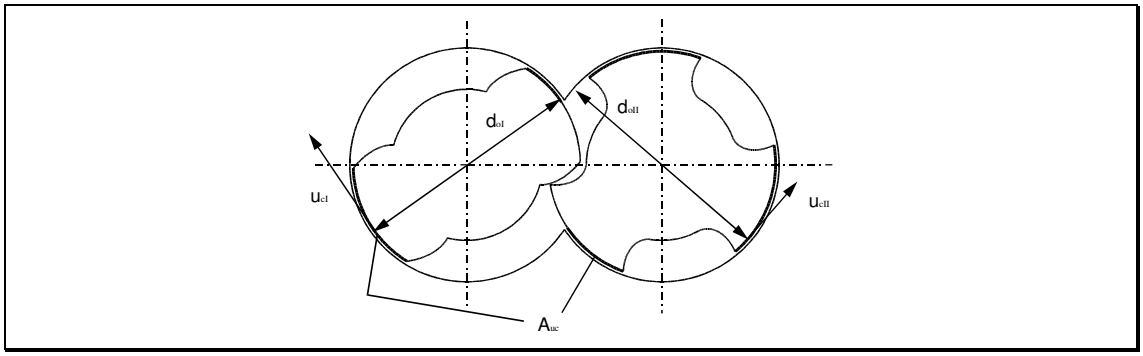


*Figure 69 The velocity vectors in the circumference clearances due to rotation*

According to Street /78/ the rotational leakage flow through the circumference clearance is related to the mean velocity in the clearance, which is equal to half the absolute surface speed of the rotor:

$$\dot{V}_{DC} = u_{Cm} h_C b_C = \frac{u_C}{2} h_C b_C \tag{86}$$

The leakage flow can now be described as a combined value related to the outer diameter of rotor$_I$ and a constant coefficient $K_{DC}$ not related to size and fluid properties:

$$\dot{V}_{DC} = d_o^2 \omega_I K_{DC} \tag{87}$$

with the coefficient $K_{DC}$ which is not directly related to the dimensions of the rotors, but only to the manufacturing tolerances.

#### *9.3.2.3 Friction*

The area exposed to fluid friction is the area of the rotors in close contact with the housing. The area is related to the minimum length of the flowmeter and the head angles. The friction torque can then be determined according to Street /78/:

$$T_{DC} = A_{DC} \eta_{fl} \frac{d_o^2}{4 h_C} \omega \tag{88}$$

with:

$$A_{DC} = \kappa m l \left( \frac{\pi - \gamma}{\pi} \right) \frac{d_o}{2} \tag{89}$$

and the length of the flowmeter which is equal to the contact length:

$$l = \frac{p_{II}}{2\pi} \left( 2\pi + \gamma_{II} - \beta_{II} \right) \tag{90}$$

The torque can be calculated separately for each of the both rotors and described as a combined torque related to the outer diameter of $rotor_I$ and a constant coefficient not related to size and fluid properties:

$$T_{DC} = d_o^4 \eta_{fl} \omega_I K_{UC} \tag{91}$$

For root and flank clearance, the rotors are rolling on each other for most of the contact line. Friction within the two rotors is small compared with viscous friction on the circumference, as shown by Wong /80/.

### 9.3.3 Root clearance

The root clearance of $rotor_I$ is bordered by the root of $rotor_I$ and the circumference of $rotor_{II}$. The root clearance of $rotor_{II}$ is bordered by the root of $rotor_{II}$ and the circumference of $rotor_I$ (Figure 70). This can be also seen in the 3 dimensional sections of the measuring chamber (Figure 71). The clearance occurs for $rotor_I$ $m_I$ times (twice), for $rotor_{II}$ $m_{II}$ times (three times).

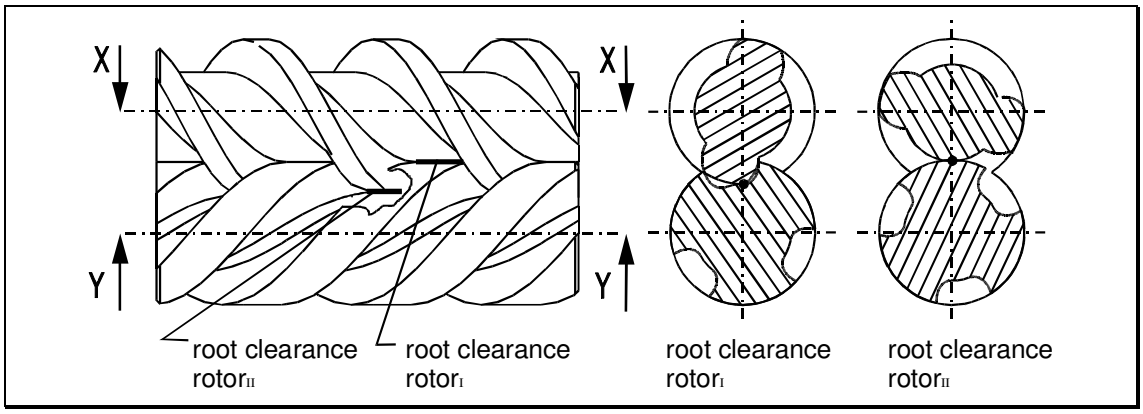


*Figure 70 The root clearance - axial sections*

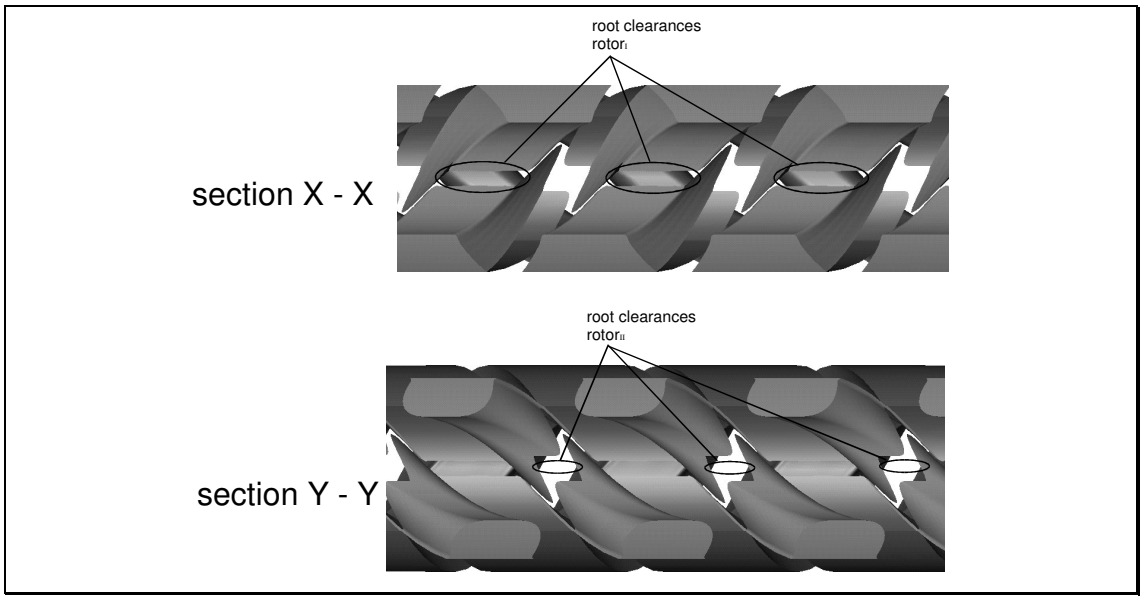


*Figure 71 Sections through the fluid in the chamber - the root clearances (see Figure 70 for positions of sections)*

### *9.3.3.1 Leakage*

The dimensions of the clearance of rotor$_I$ are:

$$b_{RI} = \kappa_{II}\frac{P_{II}}{2\pi} = d_{oI}\frac{\kappa_{II}}{2\varepsilon}\tan\phi_{PI} \tag{92}$$

$$h_{RI} = \left(a + T_a\right) - \frac{1}{2}\left[\left(d_{oII} + T_{oII}\right) + \left(d_{iI} + T_{iI}\right)\right] = T_a - \frac{1}{2}\left(T_{oII} + T_{iI}\right) \tag{93}$$

$$r_{I1} = \frac{1}{2}d_{iI} = d_{oI}\frac{\varepsilon}{2r} \tag{94}$$

$$r_{I2} = \frac{1}{2}d_{oII} = d_{oI}\frac{1}{2r} \tag{95}$$

The dimensions of the clearance of rotor$_{II}$ are:

$$b_{RII} = \kappa_{I}\frac{P_{I}}{2\pi} = d_{oI}\frac{\kappa_{I}}{2}\tan\phi_{PI} \tag{96}$$

$$h_{RII} = \left(a + T_a\right) - \frac{1}{2}\left[\left(d_{oI} + T_{oI}\right) + \left(d_{iII} + T_{iII}\right)\right] = T_a - \frac{1}{2}\left(T_{oI} + T_{iII}\right) \tag{97}$$

$$r_{II1} = \frac{1}{2}d_{iII} = d_{oI}\frac{1}{2}\left(\frac{1+\varepsilon}{r} - 1\right) \tag{98}$$

$$r_{I2} = d_{oI}\frac{1}{2} \tag{99}$$

$T_i$ and $T_o$ and $T_a$ are the deviations from the nominal values of inner and outer diameter and the center distance.

The total leakage flow through the root clearance can then be described using the geometry coefficient $K_{SR}$.

$$\dot{V}_{SR} = \Delta p \frac{\sqrt{d_{oI}}}{\eta_{fl}} K_{SR} \tag{100}$$

### *9.3.3.2 Rotational leakage*

The absolute surface speed of the rotors at a defined radius value is:

$$u = \frac{d}{2}\omega \tag{101}$$

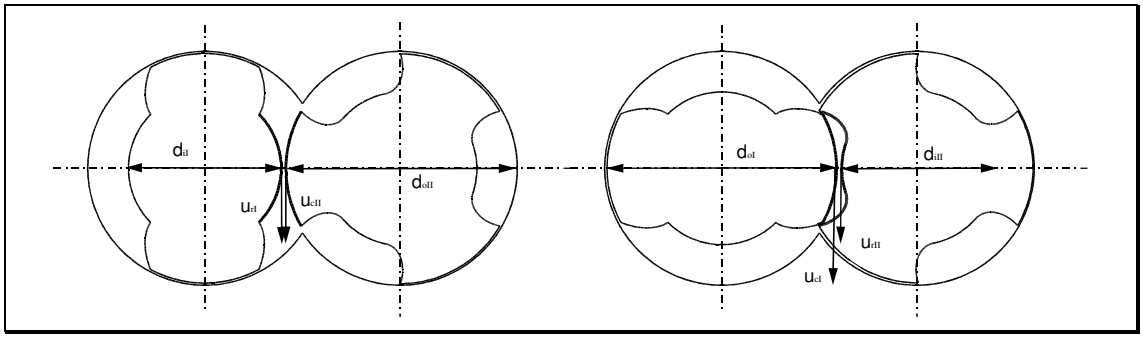


*Figure 72 The velocity vectors in the root clearance*

The mean value for the fluid velocity in the clearance is calculated in relation to the two relevant surface speeds.

The velocity for $rotor_I$ at its root is:

$$u_{rI} = d_{oI}\omega_I \frac{\varepsilon}{2r} \tag{102}$$

The velocity for $rotor_{II}$ at its root is:

$$u_{rII} = d_{oI}\omega_I \varepsilon\left(\frac{1+\varepsilon}{r} - 1\right) \tag{103}$$

The leakage flow itself in the clearance is related to the mean velocity in the clearance which is related to the relevant root and circumference clearance.

$$\dot{V}_{DR} = u_{Rm} h_R b_R = \frac{u_R + u_C}{2} h_R b_R \tag{104}$$

The rotational leakage flow can now be described as a combined value related to the outer diameter of rotor$_I$ and a constant coefficient $K_{DR}$ which is not related to size and fluid properties:

$$\dot{V}_{DR} = d_{oI}^2 \omega_I K_{DR} \qquad (105)$$

The coefficient $K_{DR}$ is not directly related to the dimensions of the rotors, but only to the geometry and the manufacturing tolerances.

### 9.3.4 Flank clearance

The flank clearance is bordered for rotor$_I$ by the flank profile of rotor$_I$ and the edge of the ridge of the circumference of rotor$_{II}$ or for rotor$_{II}$ by the flank profile of rotor$_{II}$ and the edge of the ridge of the circumference of rotor$_I$ (Figure 73). The clearance occurs for rotor$_I$ four times ($2\times m_I$), for rotor$_{II}$ six times ($2\times m_{II}$). The equations given for rotor$_I$ can be used respectively for rotor$_{II}$ . Like the root clearance the flank clearance has a varying height over the length of the clearance and hence the same equations as above will be used for the fluid flow determination.

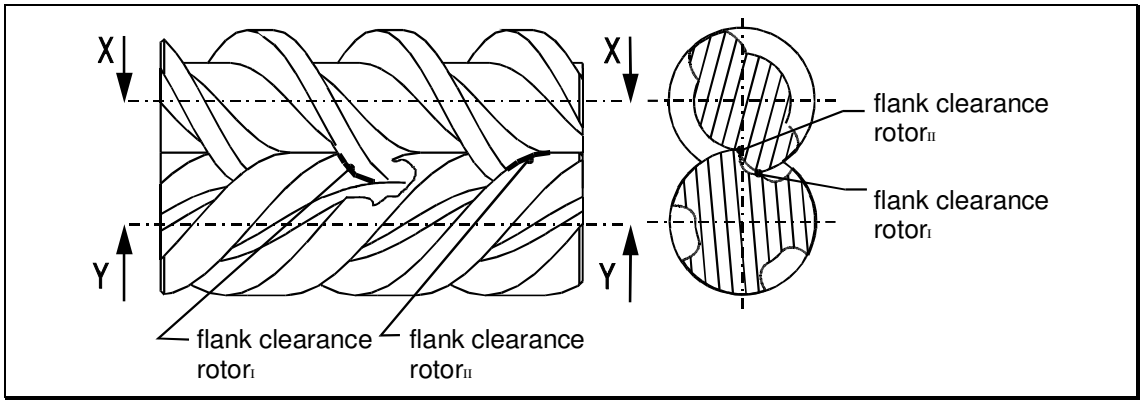


*Figure 73 The flank clearance*

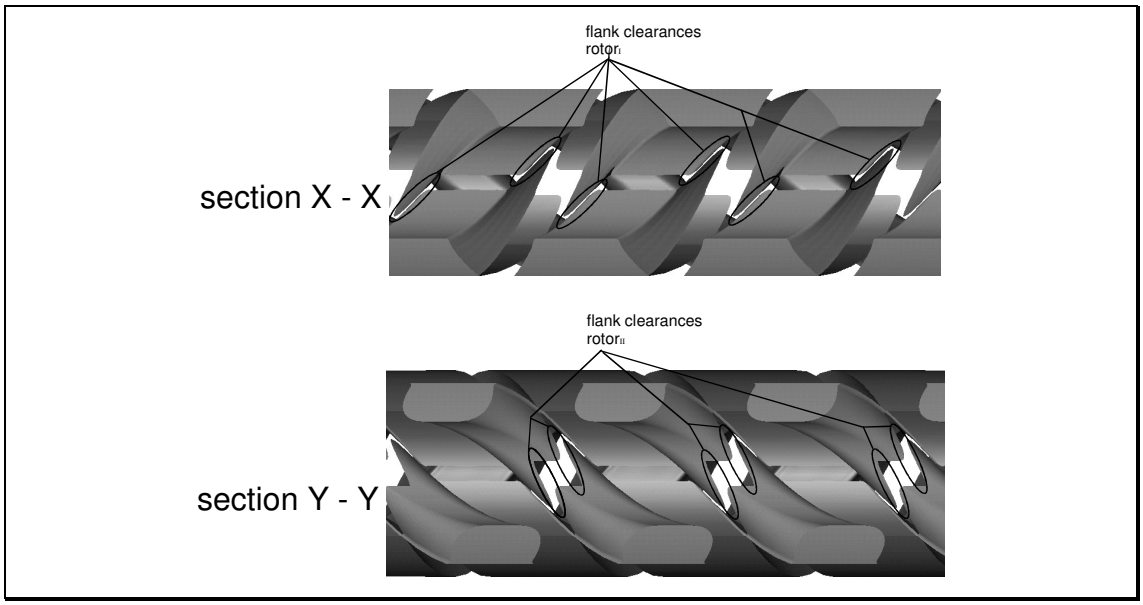


*Figure 74 Sections through the fluid in the chamber - the flank clearances (see Figure 73 for positions of sections)*

#### *9.3.4.1 Leakage*

The breadth dimensions of the clearance are:

$$b_{FI} = \gamma_{II} \frac{P_{II}}{2\pi} = d_{oI} \frac{\gamma_{II} \tan \phi_{PI}}{2\nu} \tag{106}$$

$$b_{FII} = \gamma_{I} \frac{P_{I}}{2\pi} = d_{oI} \frac{\gamma_{I} \tan \phi_{PI}}{2} \tag{107}$$

In order to calculate the minimum height of the clearance it has to be considered that $rotor_{II}$ is driven by $rotor_{I}$. Hence one flank of the profile is engaged and transmits the power (driven flank) and the other flank of the profile is idling (idling flank). If all dimensions would be at their nominal value there would be no clearances and both flanks of the profile would be in contact with their counterpart of the other rotor. With the flank profile being smaller than the nominal profile, the clearances at driven and idling flank of the profile will not be the same, but differ according to the engagement situation. The height of the clearance at the driven flank is assumed to approaches to zero, to allow the power to be transmitted. The height value of the clearance of the idling flank was determined by a computer aided design simulation. Therefore the two rotors were drawn in different rotational engagement positions using a variation of the flank tolerances. Hereby the rotors were positioned in order to obtain a zero clearance on the driven flank.

Then the height of clearance at the idling flank was measured and a mean value calculated. The following values are considered sufficient approximations:

| | | |
|---|---|---|
| $rotor_I$ driven flank | $h_{FdI} = 0.5\ T_f$ | |
| $rotor_I$ idling flank | $h_{FtI} = 4.0\ T_f$ | |
| $rotor_{II}$ driven flank | $h_{FdII} = 0.5\ T_f$ | |
| $rotor_{II}$ idling flank | $h_{FtII} = 3.0\ T_f + 0.5\ T_a$ | (108) |
| radii for $rotor_I$: | $r_1 = 3d_{ch}$ and $r_2 = \infty$ | |
| radii for $rotor_{II}$: | $r_1 = 3d_{ch}$ and $r_2 = \infty$ | (109) |

The total leakage flow through the flank clearance can then be described using the geometry coefficient $K_{SF}$.

$$\dot{V}_{SF} = \Delta p \frac{d_{oI}}{\eta_{fl}} K_{SF} \tag{110}$$

### *9.3.4.2 Rotational leakage*

The absolute surface speed of the rotors at a defined radius value calculates to:

$$u = \frac{d}{2}\omega \tag{111}$$

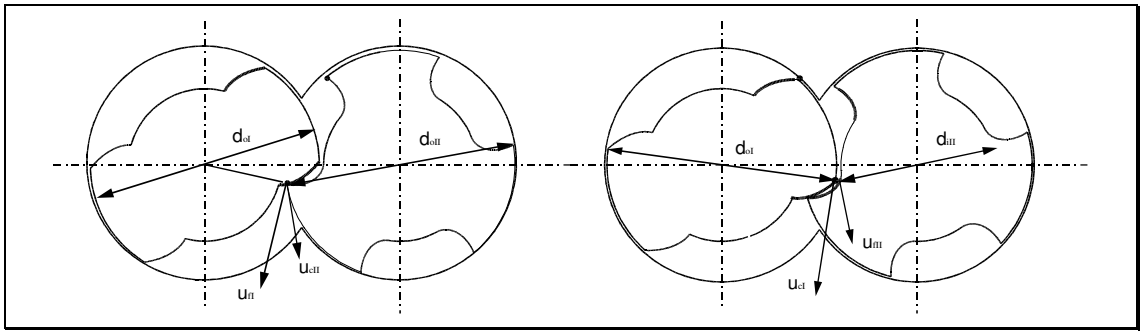


*Figure 75 The velocity vectors in the flank clearance*

The mean value for the fluid velocity in the clearance is related to the two relevant surface speeds. The mean velocity for the flank clearance of $rotor_I$ is:

$$u_{fI} = d_{oI} \frac{1}{4} \omega_I \left(1 + \frac{\varepsilon}{r}\right) \tag{112}$$

The velocity for the flank clearance of $rotor_{II}$ is:

$$u_{fII} = d_{oI} \frac{1}{4} \omega_I \varepsilon \left(\frac{2+\varepsilon}{r} - 1\right) \tag{113}$$

The leakage flow itself is related to the mean velocity in the clearance which is related to the relevant flank and circumference clearance.

$$\dot{V}_{DF} = u_F h_F b_F = \frac{u_F + u_C}{2} h_F b_F \qquad (114)$$

The rotational leakage flow can be calculated separately for each of the both rotors and described as a combined value related to the outer diameter of rotor$_I$ and a constant coefficient $K_{DF}$, not related to size and fluid properties:

$$\dot{V}_{DF} = d_{oI}^2 \omega_I K_{DF} \qquad (115)$$

with the coefficient $K_{DF}$, which is not directly related to the dimensions of the rotors, but only to the manufacturing tolerances.

### 9.3.5 Triangular clearance

The triangular clearance is bordered by the chamfer diameter of outer diameter and the housing (Figure 76). Enlarging the clearance the triangular gap can be seen formed by the two rotors and the housing (Figure 77). The different lines represent different normal cross sections normal to the axis of the flowmeter. The clearance occurs twice. It exceeds the scope of this report to analytically describe the exact shape, hence approximations related to the radius and the pitch angle are used.

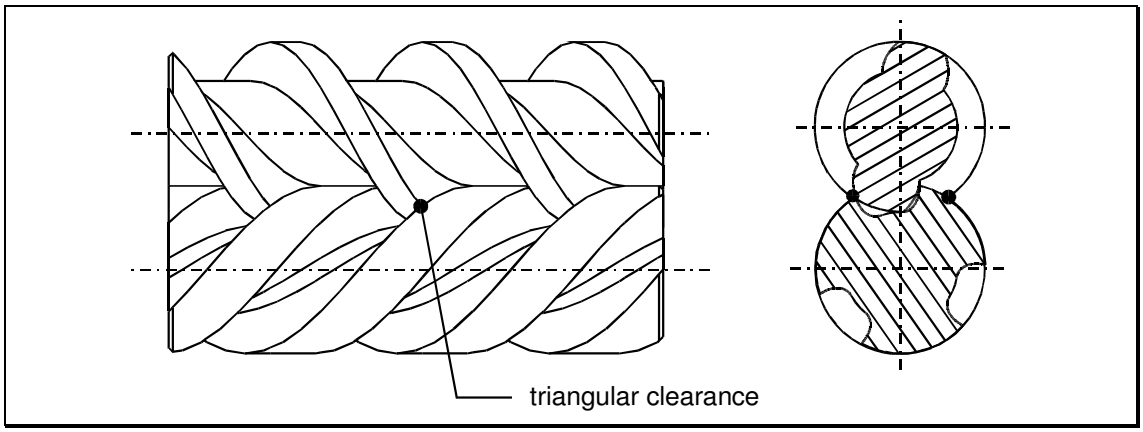


*Figure 76 The position of triangular clearance*

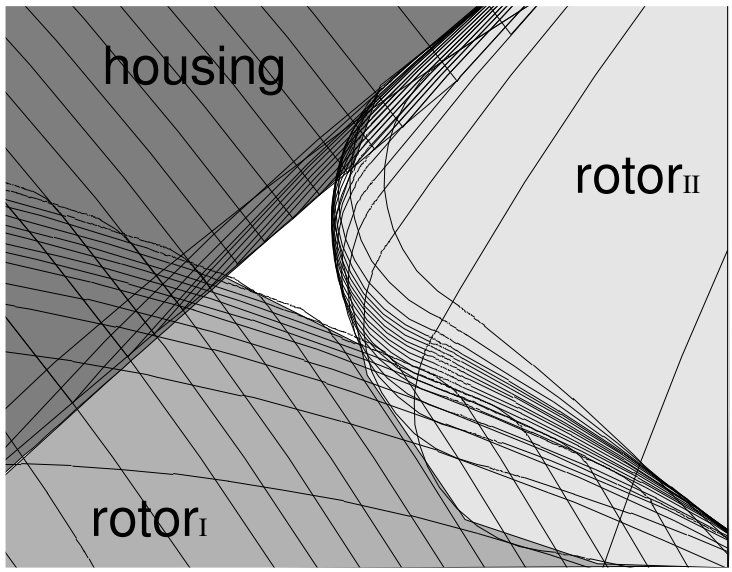


*Figure 77 Enlargement of the triangular clearance - sections normal to the axis*

Area of the clearance: $$A_T = \frac{1}{8} d_{ch}^2 \sin\phi_{PII} = \frac{1}{8} d_{ch}^2 \frac{\tan\phi_{PI}}{\sqrt{1+\tan^2\phi_{PII}}} \pm 15\% \quad (116)$$

Length of the clearance: $$\ell_T = \frac{d_{ch}}{2} \tan\phi_{PI} \pm 100\% \quad (117)$$

hydraulic diameter: $$d_H = d_{ch} \frac{\pi}{4} \sin\phi_{PII} = d_{ch} \frac{\pi}{4} \frac{\tan\phi_{PII}}{\sqrt{1+\tan^2\phi_{PII}}} \pm 15\% \quad (118)$$

The results of the measurement have shown that the leakage flow is proportional to the root of the pressure drop, but decreases with viscosity. Hence the pressure drop is according to the law of Bernoulli related to impact and frictional losses.

$$\Delta p = \frac{\rho_{fl}}{2} c^2 + \frac{\rho_{fl}}{2} c^2 \frac{l\lambda}{d_H} \quad (119)$$

for laminar flow with:

$$\lambda = \frac{64}{\mathrm{Re}} = \frac{64\nu_{fl}}{c_T d_H} \quad (120)$$

the velocity of the flow through the clearance calculates to

$$c_T = -\frac{64\nu_{fl}\ell_T}{2d_H^2} + \sqrt{\left(\frac{64\nu_{fl}\ell_T}{2d_H^2}\right)^2 + \frac{2}{\rho}\Delta p} \quad (121)$$

for turbulent flow the velocity calculates by iteration to

$$c_T = \sqrt{\frac{2\Delta p}{\rho_{fl} + \frac{\ell_T \lambda}{d_H}}} \tag{122}$$

with:

$$\lambda = \frac{0.316}{\mathrm{Re}^{0.25}} = \frac{0.316}{\left(\frac{c_T d_H}{\nu_{fl}}\right)^{0.25}} \tag{123}$$

The flowrate through the triangular clearance can then be calculated to:

$$\dot{V}_{ST} = A_T c_T \tag{124}$$

### 9.3.6 Summary

The total leakage flow is related to the pressure drop consists of its flow components through circumference clearance $\dot{V}_{SC}$, root clearance $\dot{V}_{SR}$, flank clearance $\dot{V}_{SF}$ and triangular clearance $\dot{V}_{ST}$:

$$\dot{V}_S = \dot{V}_{SC} + \dot{V}_{SR} + \dot{V}_{SF} + \dot{V}_{ST} \tag{125}$$

The total rotational leakage flow consists of its flow components through circumference clearance $\dot{V}_{DC}$, root clearance $\dot{V}_{DR}$ and flank clearance $\dot{V}_{DF}$. A rotational leakage flow through the flank clearance is not calculated.

$$\dot{V}_D = \dot{V}_{DC} + \dot{V}_{DR} + \dot{V}_{DF} \tag{126}$$

The rotational viscous friction is calculated only of the friction in the circumference clearance $T_{DC}$. According to Wong /80/, the friction torque created in other clearance is small compared with the friction in the circumference clearance.

$$T_D = T_{DC}$$

## 9.4 Results and comparison with measurement

To determine theoretical leakage flowrates, which are comparable to the experimental results, the measured dimensions from the rotors and housing are used, and the deviations T to the nominal profile have been calculated (Table 9). The accuracy of this measurement with a tolerance ±0.5 microns has been taken into account calculating the flow-rate. According to this deviations, the height of the different clearances can be determined (Table 10).

| description | $T_{oI}$ | $T_{oII}$ | $T_{iI}$ | $T_{iII}$ | $T_{bI}$ | $T_{bII}$ | $T_a$ | $T_f$ |
|---|---|---|---|---|---|---|---|---|
| | mm | mm | mm | mm | mm | mm | mm | mm |
| nominal value ±0.5 | -0.0341 | -0.0297 | -0.0080 | -0.0080 | +0.0050 | -0.0008 | +0.0015 | -0.0080 |

*Table 9 Deviations from the nominal values of the tested flowmeter*

| description | $h_{cI}$ | $h_{cII}$ | $h_{rI}$ | $h_{rII}$ | $T_f$ | $d_{ch}$ |
|---|---|---|---|---|---|---|
| | mm | mm | mm | mm | mm | mm |
| upper margin | 0.258 | 0.0258 | 0.0325 | 0.0325 | 0.0000 | 0.9000 |
| lower margin | 0.0108 | 0.0108 | 0.0075 | 0.0075 | 0.0100 | 0.7000 |
| mean value | 0.0183 | 0.0183 | 0.0200 | 0.0200 | 0.0050 | 0.8000 |
| measured value | 0.0196 | 0.0145 | 0.0189 | 0.0226 | 0.0080 | 0.9000 |

*Table 10 Clearance values of the tested flowmeter*

In order to calculate all the leakage flowrates the equations presented were solved using a computer program.

### 9.4.1 Leakage

All leakage flows except the triangular clearance are truly laminar for the observed range of pressure drop and hence proportional to the differential pressure. The flow through the triangular clearance is turbulent (Figure 78). For a pressure drop of 0.14 bar representing a high flowrate, the main proportion of the leakage flows through the flank clearance. For a pressure drop of 0.02 bar flank and triangular clearance are the main sources for leakage flow. Below 0.02 bar, which equals a low flowrate, the flow through the triangular clearance is dominant. At 0.005 bar the proportion of the triangular clearance relative to the total has reached 55 % (Figure 78 and Figure 79).

A calculation was also performed using the limits of the manufacturing tolerances. It shows that the variation of the laminar proportion is bigger than the variation in the triangular proportion. This is in accordance with the measurement results, where also the variation in the laminar proportion was bigger than the variation in the turbulent proportion. Even if all laminar clearances are set their upper limit, the flow through the triangular clearance is still dominant for a pressure drop below 0.02 bar, and hence dominant for low flowrates.

Both theory and measurement show a laminar flow through circumference, root and flank clearance and a turbulent flow through the triangular clearance. The influence of turbulent flow through the triangular clearance increases with a decreasing pressure drop. Especially in the critical range of the flowmeter with low flowrates and a small pressure drop below 0.005 bar. Comparing experimental and theoretical results the following should be kept in mind:

(a) it was not possible to measure the dimensions of the rotors accurately. The influence of the tolerance inaccuracy of ±0.5 microns, based on a 20 micron nominal value of the clearance, results in an inaccuracy of ±15% in the theoretical leakage flowrate (Figure 80).

(b) The position of the rotors in the housing could not be fixed, nor measured, The rotors are assumed to be in the middle of each bore, hence additional inaccuracy is added to the leakage flow calculation.

(c) inaccuracies in the flowrate measurement and pressure drop measurement have to be considered as well as inaccuracies in the theoretical shape of the flank and root clearance.

An exact comparison of the quantity of flow is almost impossible. For the total leakage the results of theory show a good correlation for the discussed range(Figure 80). The correlation for the turbulent proportion is even better, as the theoretical values are within the range of the experimental values (Figure 81). It is important to state that the proportion of the turbulent leakage flow share to the leakage flow is substantial to the overall performance prediction model. The validation of all equations was only performed using the test fluid hebrosol. Leakage tests with other fluids have to be performed to prove the model for a variety of fluid properties.

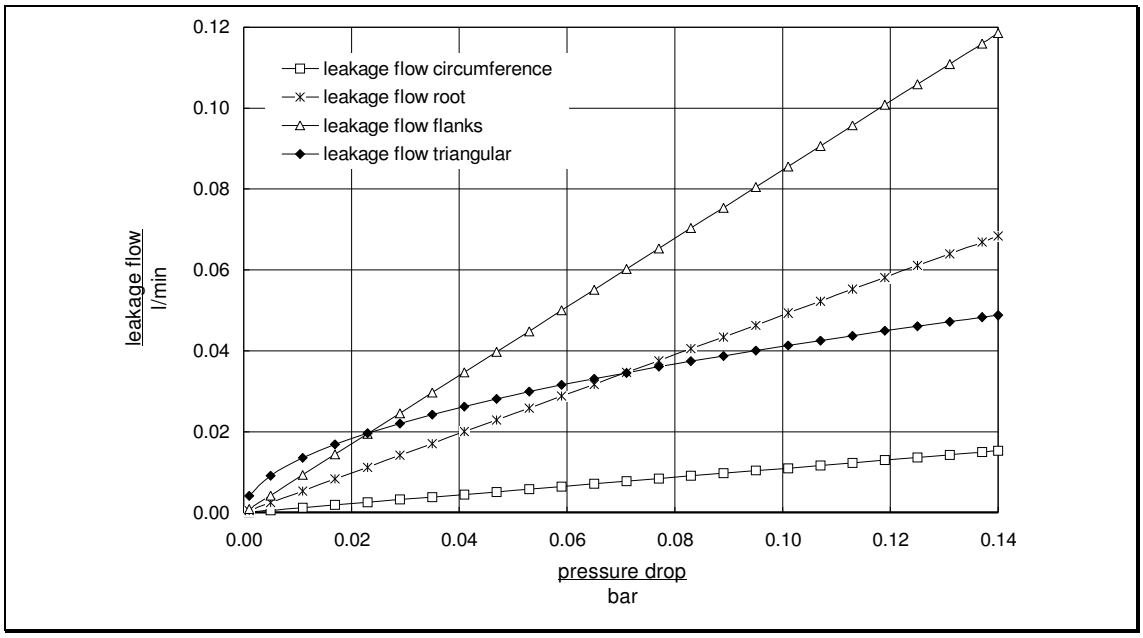


*Figure 78 Calculated static leakage flowrates through the various clearances*

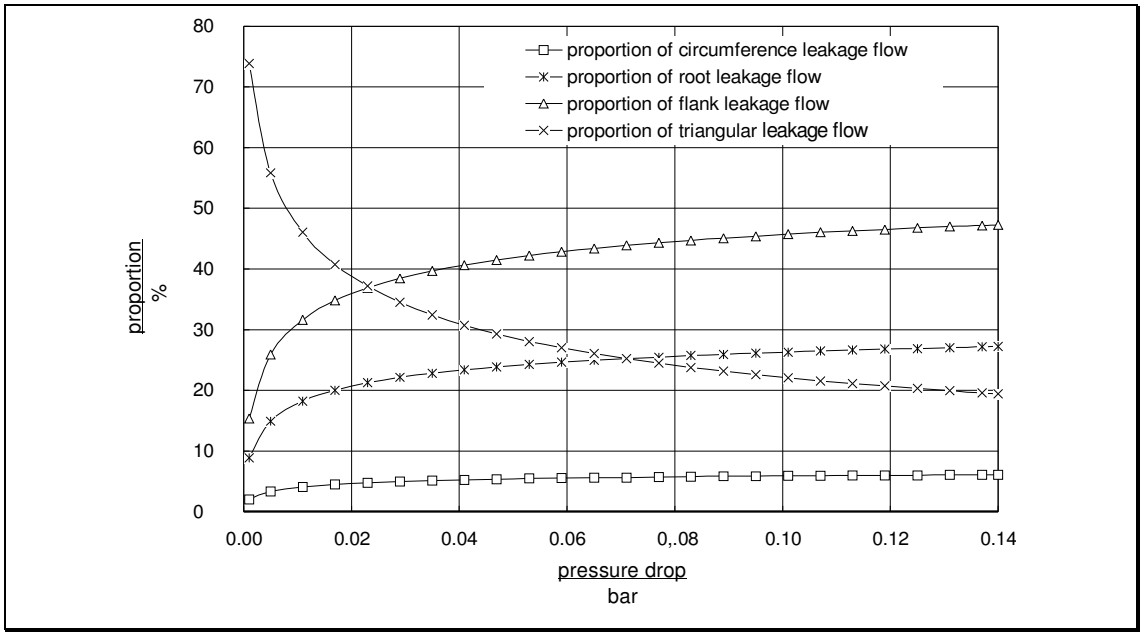


*Figure 79 The proportion of calculated static leakage flowrates through different clearances.*

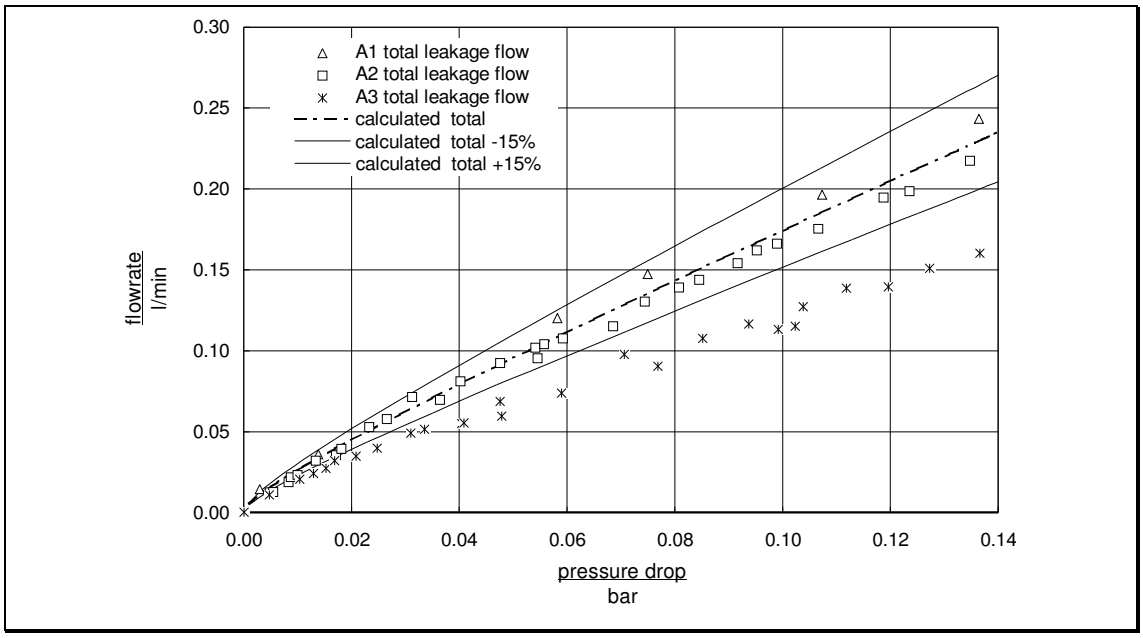


*Figure 80 Experimental and theoretical results of total static leakage flow against pressure drop*

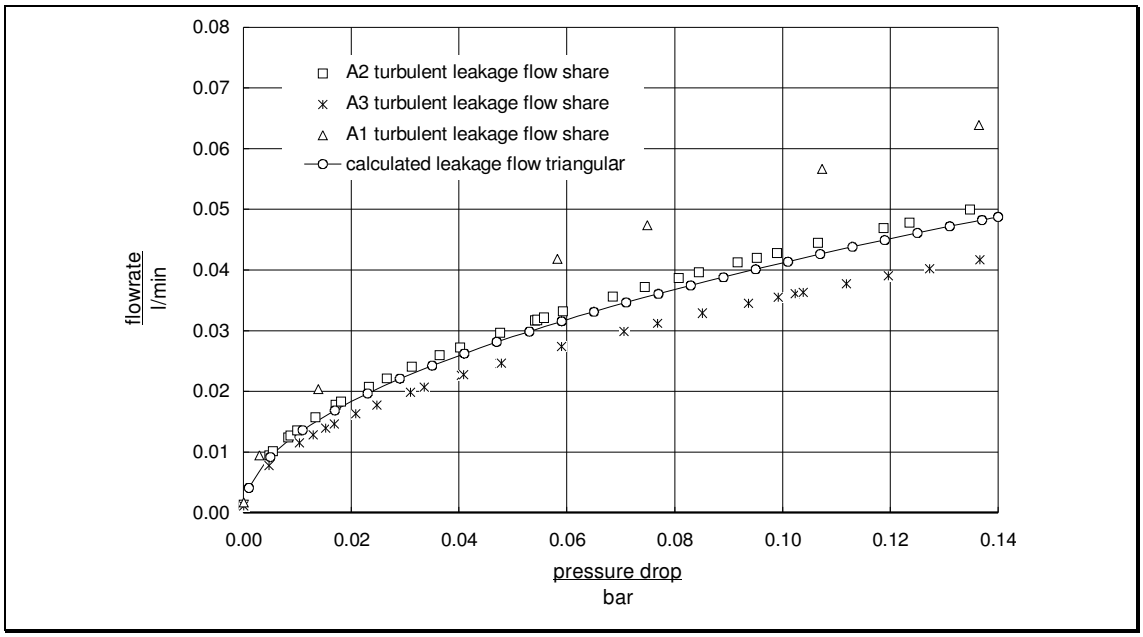


*Figure 81 Experimental and theoretical results of static leakage flow through the triangular clearance against pressure drop*

### 9.4.2 Rotational leakage and viscous friction

In order to calculate all the rotational leakage flowrates, volume and the viscous friction loss coefficients, the equation presented were solved using a computer program. For the different geometries they both vary over 100 %, but the effect of this on the total

performance of the flowmeter can not be determined without the complete model. Therefore, and because the lack of an experimental comparison, no detailed results are presented.

## 9.5 Conclusion

Leakage flow in a flowmeter is divided into four main clearances. They are located at the circumference, the flanks and the root of the rotors. In addition a triangular clearance bordered by flank and circumference of both rotors was detected. A way to determine the geometry of these clearances is presented as well as the application of flow and viscous friction theories for fluid flow in narrow planar, annular ring shape and triangular clearances to the special clearance geometries.

For the pressure related leakage, the theory proved to be a reliable approximation of the real flowrate. Both, theory and measurement show good correlation. Leakage flow is laminar, except the flow through the triangular clearance, which is turbulent. Hence the proportion of the turbulent flow increases with decreasing pressure drop for $\Delta p=0.14$ bar from 15 % to for $\Delta p=0.005$ bar over 50% of the complete leakage flowrate. It is important to point out that for a pressure drop lower than 0.02 bar, which represents a low flowrate, the flow through the triangular clearance constitutes the biggest proportion of all clearances and is therefore the most important leakage to investigate. Rotational leakage and viscous friction could not be measured.

On the rotational leakage volume and the viscous friction loss a theory is presented and loss coefficient can be calculated. However no comparison to experimental results is possible.

# 10 Summary of model restrictions

Restrictions, limitations and simplifications have been applied while discussing the separate theories occurring in the prediction model, including the fluid properties and the loss coefficients. Parts of the model are almost common knowledge, while others are more or less estimations. Not all theories presented by the author have been proven by experiments, because for some parts of the model it was impossible or out of the range of the available budget. Each of the separate problems represents one specialised field of science and the theoretical and experimental work on each of these fields could have been very much extended. It is obvious that the scope of this thesis is limited and with it the complexity and depth of all related problems. On the other hand some restriction are applied, simply to improve the traceability of parameters and relations. Previous modelling attempts of the author have shown that a more complex prediction model makes it increasingly difficult to evaluate the model itself and understand the influence and interaction of the single different parameters. However, in order to judge the prediction model and evaluate its limits of usage, the knowledge of all restrictions is extremely important. Therefore all simplifications and restrictions, which have been applied to the model, are summarised in the following:

## 10.1 Limitations in fluid properties evaluation

In the current work no temperature and or pressure compensation is applied, the change in fluid condition, especially compressibility effects according to the 50 kPa maximum pressure drop are neglected and influences of chemical properties are not taken into account. Effects of lubricity and surface tension will not be discussed. Density and viscosity values, which have not been found in any literature had to be approximated. Within the defined range of application and accuracy, no effect of these limitations is expected.

## 10.2 Limitations in experimental meter performance tests

The experimental restrictions which, on the one hand are the reason for the current work, limit on the other hand the amount of reliable performance data which can be used to compare experimental with the prediction model results. The limitations which have been listed in detail in chapter 4 "Performance of the Leistritz flowmeter" in section 4.1.4 "Limitations" are mainly the lack of clearance variations, design variations, fluid variations and turndown variations. As discussed in section 4.1.2 "Design variation tests", variations of clearance dimensions are difficult to realise as they always result in a change of the complete rotor and bearing assembly, which itself is influencing the flowmeter performance significantly. Hence the clearance influence can not be

measured as a stand alone value. Major design changes of the flowmeter could not be realised within the available budget, especially because all components needed to be machined to a very high and uniform degree of accuracy to achieve comparable results. Only some tests have been performed with a higher viscosity fluid (lubricating cutting oil with kinematic viscosity $\nu \approx 10$ mm/s²). No tests have been performed with Shellsol, petrol, diesel oil or water. The only tested turndown range was from 2-50 l/min. No flowrates above 50 l/min were tested. According to the limitations above, obviously no tests have been performed with any combination of the variations listed above. This would include for example a combination of higher viscosity and higher clearances.

The lack of performance data is a big disadvantage of the verification of the model, as the performance prediction model can only be proved and optimised for very few operating points. However it has to be kept in mind that the extrapolation beyond known limits was one of the aims of this study. Hence, for the performance prediction of flowmeters, which have not yet been produced, a larger degree of inaccuracy has to be taken into account.

## 10.3 Limitations in evaluation of the rotor geometry

In the real application the rotor profile is used for various reasons with a chamfer diameter at the edge of $rotor_{II}$ as discussed in chapter 6 "Rotor geometry". However, throughout this thesis all deliberations are related to the theoretical cycloid montelius profile, without relating to this chamfer. In the model theory, the chamfer diameter was only used in order to determine the size of the triangular clearance. The exact influence of this simplification is not known, but it is very much expected that all other influences of the chamfer are small compared to the influence of the chamfer on the size of the triangular clearance. Additionally, rolling diameters different to the outer diameter of $rotor_I$ or inner diameter of $rotor_{II}$ are not discussed within the scope of this thesis, although some influence on the performance may be expected.

All rotors were assumed to fulfil the condition "displacement chamber to be as short as possible", which means that as a result the head angle $\kappa$ can not be varied freely. A change of the head angle to a value which is different to that required for the minimum length condition certainly has an influence on all losses and leakage flows related to the circumference clearance. The degree of influence is not known and omitted in this thesis.

Rotors with a longer length than the required minimum length are not discussed and not included in the theory section. Rotors of this type would exhibit a different sealing situation, because then an extended range of rotational positions does occur, where the

rotors form a completely separated chamber. However this range of positions was omitted within this thesis, because of its complex clearance and pressure drop situation.

## 10.4 Limitations in the determination hydraulic forces on the rotors

The forces and torques are determined related to the theoretical profile. No method is known to check the results of the calculation experimentally. A theoretical method was used to cross check the results against each other and hence the results are considered reasonably reliable. Especially the most important value, which is the overall driving torque, can be determined from displacement volume, speed and pressure drop, without any detailed knowledge of its creating forces and torques.

According to the chapter 5 "General performance prediction", it can be claimed that the influence of the hydraulic forces and torques is relatively small. Accordingly also the influence of any error in its calculation is even smaller

## 10.5 Limitations in the evaluation of bearing friction

The bearing friction separates into speed dependent lubricant friction torque, the load dependent rolling friction torque and the sliding friction torque. The theories presented in literature are well known and generally confirmed by the experimental results of the author. However, as already stated in chapter 8 "Bearing friction" the following observations and restriction during the experiment should be noted:

(a) only one bearing was tested.

(b) the recognition of start and end point of the measurement relied on the individual judgement.

(c) the viscosity of the lubricating media was not varied

The speed dependent lubricant friction torque can be determined according to the common evaluated theories and its value was confirmed by measurements performed by the author. The load dependent rolling friction torque is small compared to the speed dependent lubricant friction torque which is only approximately 1 % according to theory. In the experiments performed, its existence has not been approved for the current load situation.

The following has to considered for the evaluation of the model:

(a) According to the minor priority of the load depended losses as stated in chapter 5 "General performance prediction", a simplified calculation was used for the load dependent rolling friction torque in order to obtain a linear relation to the

pressure drop. Calculations using these different equation have not shown any different results.

(b) According to the limited testing, it is expected that the sliding friction torque of other bearings can vary significantly from the torque, measured in the tests carried out by the author.

## 10.6 Limitations in the calculation of viscous fluid friction

Only the viscous friction torque in the circumference clearance between rotors and housing is considered. The influence of other clearances was found to be negligible small for normal operating conditions, as stated in chapter 9 "Leakage and viscous friction". As a consequence, for a large circumference clearance and tight flank and root clearances, the model is then expected to be less accurate.

## 10.7 Limitations in the calculation of pressure related slip

Simplifications in the flow model have been applied to root, flank and triangular clearance. However the theoretical results showed a good correlation with experiment. Especially the amount of turbulent leakage flow could be determined within an accuracy of ±15%. For the test fluid Hebrosol and other fluids with a similar viscosity, the turbulent leakage flow is directly related to the area of the clearance. For fluids with a higher viscosity, the leakage flow will be related also to viscosity and not only to the clearance area. This theory has not been proven experimentally and is considered a weak point as according to chapter 5 "General performance prediction", the flow pattern through this clearance has a high influence on the performance of the flowmeter.

## 10.8 Limitations in the calculation rotational slip

Because of its the minor influence on the flowmeter performance, as stated in chapter 5 "General performance prediction", it is considered that the rotational leakage flow as described in chapter 9 "Leakage and viscous friction", can be calculated with sufficient accuracy.

# 11 Determination of coefficients

8 different loss coefficients have been introduced in chapter 5 "General performance prediction". According to the investigations performed throughout this work, these 8 loss coefficients were determined theoretically. However, the previous chapters and the 8 loss coefficients can not be directly related to each other.

Additionally it is important to note that all coefficients are related to the speed of $rotor_I$ and all power losses occurring for $rotor_{II}$ have to be transferred to $rotor_I$ via the profile engagement. Hence every coefficient is also related to the power transfer losses in the profile engagement.

## 11.1 Influence of rotor engagement

The overall driving force to overcome the frictional resistance is the hydraulic torque on the rotors. The hydraulic torque is not driving both rotors with the same power respectively, but is only driving $rotor_I$. Therefore all the frictional resistance $P_P$ in $rotor_{II}$ has to be transmitted over the rotor profile engagement from $rotor_I$ to $rotor_{II}$ (see chapter 7 "Hydraulic forces and torques on the rotors" and more detailed section 7.3.1 "General"). The transmission over the profile causes additional frictional losses, which can be related to their different sources and therefore separately assigned to the single loss coefficients. The loss in the profile $P_{P\_loss}$ is calculated according to Matek /82/ who presented an equation for the loss calculation in helical gears. Also according to Matek /82/ the value for the friction coefficient $\mu$ was selected as 0.1 ,accordingly:

$$P_{P\_loss} = \frac{P_P \mu}{\tan \phi_{PII}} \tag{127}$$

with:

$P_{P\_loss}$ Loss in the profile
$P_P$ Power to be transmitted in the profile
$\mu$ Friction coefficient
$\phi_{PII}$ Helix angle of $rotor_{II}$

An increase in bearing load according to the axial forces caused by the helical engagement is below 1 % and hence not considered for the theoretical determination of the coefficients.

## 11.2 Viscous friction power loss coefficient $\kappa_D$

The viscous friction coefficient $\kappa_D$ is related to the viscous friction in the circumference clearance between rotors and housing. As shown by Wong /80/, other clearances have very little influence on the viscous friction loss, which is only about 2

% of the total value (see chapter 9 "Leakage and viscous friction" and more detailed section 9.3.2.3). The total viscous friction power loss $P_D$ consists of losses $P_{DI}$ in rotor$_I$, losses $P_{DII}$ in rotor$_{II}$ and the losses $P_{DPL}$ in which can be related to the transfer of power to compensate the viscous losses in rotor$_{II}$:

$$P_D = P_{DI} + P_{DII} + P_{DPL} \tag{128}$$

The power losses in rotor$_I$ and rotor$_{II}$ are related to viscosity and the viscous friction coefficients $K_{UCI}$ and $K_{UCII}$ as described in Appendix G "Leakage and viscous friction constant coefficients":

$$P_{DI} = d_o^4 \eta_{fl} \omega_I^2 K_{UCI} \tag{129}$$

$$P_{DII} = d_o^4 \eta_{fl} \omega_I^2 K_{UCII} \varepsilon \tag{130}$$

Hence using equation (127) the power losses in the profile engagement can be determined:

$$P_{DPL} = d_o^4 \frac{\eta_{fl} \omega_I^2 K_{UCII} \varepsilon \mu}{\tan \phi_{PII}} \tag{131}$$

Summarising the single losses according to equation (128), the power loss related to the viscous friction can be expressed in relation to the loss coefficients $K_{UC}$ and $K_{UCII}$. $K_{UC}$ is representing the viscous friction losses in the circumference clearance without considering the profile losses; $K_{UCII}$ represents the viscous friction losses of rotor$_{II}$:

$$P_D = d_o^4 \eta_{fl} \omega_I^2 \left( K_{UC} + \frac{K_{UCII} \mu}{\tan \phi_{PII}} \right) \tag{132}$$

Hence the viscous friction loss coefficient $\kappa_D$ as introduced in the performance prediction logic can be calculated to:

$$\kappa_D = d_o^4 \left( K_{UC} + \frac{K_{UCII} \mu}{\tan \phi_{PII}} \right) \tag{133}$$

## 11.3 Mechanical friction power loss coefficient $\kappa_U$

According to the performance prediction logic described in chapter 5 "General performance prediction", the mechanical friction power loss coefficient $\kappa_U$ is related to the pressure load. The pressure load creates forces on the rotors which then cause resisting forces in the bearings. Hence the main proportions of the mechanical friction power loss consist of the load dependent friction torque in the bearing $M_1$ as described in chapter 8 "Bearing friction", and the friction in the engagement of the two rotors

according to the power transfer of the mechanical friction in rotor$_{II}$ according to section 11.1 "Influence of rotor engagement".

The load on the bearings itself is a combined load consisting of:

(a) the fluid load.

(b) the reactive forces created by the power transfer in the profile.

(c) the weight load of the spindles.

However, the weight load of the spindles in not a pressure related load and will therefore be considered in section 11.4 "Constant torque power loss coefficient". The other forces can be summarised to one axial and one radial load on each rotor. The mechanical friction power loss $P_U$ consists of losses $P_{UI}$ in rotor$_I$ , losses $P_{UII}$ in rotor$_{II}$ and the proportion of losses $P_{UPL}$ in the engagement of the rotors, according to the transfer of power to compensate the mechanical losses in rotor$_{II}$.

$$P_U = P_{UI} + P_{UII} + P_{UPL} \tag{134}$$

According to the chapter 8 "Bearing friction", the load dependent bearing friction torque $M_I$ is related to the mean bearing diameter $d_m$ and the basic static bearing load rating $C_0$ and the load. All components, which are independent from load, can be summarised to a bearing coefficient $C_B$. The load dependent friction torque $M_I$ is then related to the axial bearing load and the bearing coefficient $C_B$.

$$M_I = C_B F_a \tag{135}$$

$$C_B \approx 0.003 \frac{d_m}{C_0} \tag{136}$$

Using this load related bearing coefficient, the mechanical friction loss $P_U$ can then be expressed related to the load areas $f_{aI}$ and $f_{aII}$ and the torque volumes $t_I$ and $t_{II}$ as presented in chapter 7 "Hydraulic forces and torques on the rotors":

$$P_U = \omega_I \Delta p \left\{ C_{BI} \left[ f_{aI} - \frac{\left(K_{dpII} - t_{II}\varepsilon\right)\tan\phi_{PII}}{d_{oII}} \right] + \varepsilon K_{dpII} + \frac{\mu_P \varepsilon \left(K_{dpII} - t_{II}\varepsilon\right)}{\tan\phi_{PII}} \right\} \tag{137}$$

Hereby $K_{dp}$ is the pressure related loss coefficient of rotor$_{II}$:

$$K_{dpII} = \left( f_{aII} - \frac{t_{II}\varepsilon\tan\phi_{PII}}{d_{oII}} \right) \Bigg/ \left( \frac{1}{C_{BII}} - \frac{\tan\phi_{PII}}{d_{oII}} \right) \tag{138}$$

Hence the mechanical friction loss coefficient $\kappa_U$ as introduced in the performance prediction logic can be calculated to:

$$\kappa_U = C_{BI}\left[ f_{aI} - \frac{\left(K_{dpII} - t_{II}\varepsilon\right)\tan\phi_{PII}}{d_{oII}} \right] + \varepsilon K_{dpII} + \frac{\mu_P \varepsilon\left(K_{dpII} - t_{II}\varepsilon\right)}{\tan\phi_{PII}} \qquad (139)$$

## 11.4 Constant torque power loss coefficient $\kappa_C$

The constant torque coefficient $\kappa_C$ is mainly related to the sliding friction torque $M_{sl}$ in the bearings as presented in the chapter 8 "Bearing friction". For each bearing, the sliding friction is related to the sliding friction coefficient $f_{sl}$ and the mean bearing diameter. The constant torque power loss $P_C$ consists of losses $P_{CI}$ in rotor$_{\mathrm{I}}$, losses $P_{CII}$ in rotor$_{\mathrm{II}}$ and the losses $P_{CLP}$ related to the transfer of power in the profile engagement to compensate for the constant torque losses in rotor$_{\mathrm{II}}$.

$$P_C = P_{CI} + P_{CII} + P_{CPL} \qquad (140)$$

The constant loss coefficient $\kappa_C$, as presented in the performance prediction logic is then related to the significant rotor geometry parameters $\varepsilon$ and $r$, the sliding friction coefficient $f_{sl}$ and the outer diameter $d_{oI}$ of rotor$_{\mathrm{I}}$:

$$\kappa_C = 2 f_{sl} \frac{d_{oI}}{r}\left[ (r+\varepsilon) + (2+\varepsilon-r)\left(1 + \frac{\mu}{\tan\phi_{PII}}\right) \right] \qquad (141)$$

It is assumed that constant friction is also present in the engagement of the rotors itself, but it was not possible to determine the related friction value. The load dependent bearing friction caused by the weight of the spindles is also a constant torque loss. However this loss is considered negligible, because its value contributes only 0.1 % to the total constant friction torque; see chapter 8 "Bearing friction" for the calculation of the load dependent bearing friction torque. This is confirmed by the experimental results of chapter 4 "Performance of the Leistritz flowmeter", where different assembly positions of the flowmeter did not show any alteration in the plot of error against flowrate.

## 11.5 Impulse power loss coefficient $\kappa_T$

According to the operation principle of positive displacement using helical rotors, theoretically the fluid is not accelerated in the flowmeter. (see principle of displacement in section 3.3.1 "Operating principle" for screw flowmeters and in section 3.6 "Screw pumps" for screw pumps in general) The rotors transport the fluid in a true axial movement. This is confirmed by measurements made by the author and by Gerrard /29/ (Figure 4). In this figure all plots of error against flowrate do not show any increased leakage at the high end of the displayed range. This is confirmed by the experimental results of the author. (see Figure 16, Figure 18, Figure 19 and Figure 20 in chapter 4

"Performance of the Leistritz flowmeter") According to chapter 5 "General performance prediction", this plot pattern of horizontal convergence for the high end of the flow range can only be explained by the non-existence, or a relatively low value, of the impulse power loss. For the current model, the value of the impulse power loss coefficient $\kappa_T$, as introduced in the performance prediction logic is therefore set to zero.

$$\kappa_T = 0 \tag{142}$$

## 11.6 Ball bearing viscous friction power loss coefficient $\kappa_B$

The ball bearing viscous friction power loss coefficient $\kappa_B$ is related to the lubricant friction torque $M_0$ in a ball bearing which is discussed in chapter 8 "Bearing friction". For each of the two rotors the loss in the two bearings and the friction loss in the transmission of the profile have to be taken into account. The ball bearing loss coefficient $\kappa_B$ can then be calculated related to the basic geometry parameters of the flowmeter:

$$\kappa_B = 1.525 \times 10^{-6} \frac{d_{oI}^3}{r^3} \left[ (r+\varepsilon)^3 + (2+\varepsilon-r)^3 \left( 1 + \frac{\mu}{\tan \phi_{PII}} \right) \right] \tag{143}$$

## 11.7 Slip coefficients $\kappa_{lam}$, $\kappa_{tur}$ and $\kappa_{rot}$

The leakage coefficients are firstly the laminar or viscosity related loss coefficient $\kappa_{lam}$, secondly the turbulent or density related leakage flow coefficient $\kappa_{tur}$ and thirdly the rotational leakage volume coefficient $\kappa_{rot}$. As described in chapter 9 "Leakage and viscous friction", the laminar leakage flow coefficient is the sum of all the single leakage flow coefficients of the different clearances. These are $K_{SC}$ for the circumference clearance, $K_{SR}$ for the root clearance and $K_{SF}$ for the flank clearance. For the triangular clearance leakage flow was separated in order to obtain a laminar $K_{T\_lam}$ and a turbulent $K_{T\_tur}$ flow component. This was done using the same method as for the experimental results of the static leakage flow measurements in section 9.2.3 "Interpretation of test results". Hence the laminar leakage loss coefficient $\kappa_{lam}$ for the viscosity related leakage can be calculated as:

$$\kappa_{lam} = K_{SC} + K_{SR} + K_{SF} + K_{T\_lam} \tag{144}$$

The turbulent leakage loss coefficient $\kappa_{tur}$ is hence solely related to the turbulent proportion of the flow through the triangular clearance:

$$\kappa_{tur} = K_{T\_tur} \tag{145}$$

The rotational leakage coefficient $\kappa_{rot}$ is the sum of all the single rotational leakage volumes of the different clearances as presented chapter 9 "Leakage and viscous

friction". These are $V_{DC}$ for the circumference clearance, $V_{DR}$ for the root clearance and $V_{DF}$ for the flank clearance. Hence rotational leakage coefficient $\kappa_{rot}$ can be calculated in as:

$$\kappa_{rot} = V_{DC} + V_{DR} + V_{DF} \tag{146}$$

# 12 Verification

The loss coefficients are calculated using the dimension and clearance values of the reference flow meter, and the equations presented in chapter 11. The values of the loss coefficients are then used for the calculation of the error against flowrate according to the equations presented in chapter 5. In order to verify the model, the theoretical results of the performance prediction model are then compared with the experimental plot of error against flowrate obtained using the reference meter. For the theoretical prediction plots, the loss coefficients were calculated using the reference flowmeter design for minimum and maximum clearances. Then the theoretical flowmeter performance for an operating range from 2 l/min to 50 l/min was determined.

## 12.1 Comparison of theoretical with experimental performance

The error of the reference flowmeter was found to be much smaller than predicted by the model (Figure 82). However, the pressure drop of both theory and measurement did show a good correlation (Figure 83). It is important to note that the deviation is not caused by a deficient general theoretical model as described in chapter 5 "General performance prediction", but a probably insufficient determination of some of the loss coefficients. Hence the following conclusions may be drawn: All coefficients which influence the pressure drop of the flowmeter can be assumed to be determined sufficiently. These are according to section 5.3.3 "Influences of the loss coefficients on pressure drop" in chapter 5:

(a) the viscous friction coefficient $\kappa_D$

(b) the pressure related friction coefficient $\kappa_U$

(c) the bearing friction coefficient $\kappa_B$

(d) the impulse coefficient $\kappa_T$

The size of the clearances has a significant influence on the performance of the flowmeter (Figure 82). Wider clearances decrease the performance, narrower clearances increase the performance. However, arithmetical mean clearances were used in the calculations relating to the reference, and hence the influence of the clearances is not regarded responsible for the deviation from the model to the measurement results. There are two remaining coefficients, which may have been determined inaccurately, and hence may be varied to improve the results. These are:

(a) the constant friction coefficient $\kappa_C$

(b) the turbulent leakage coefficient $\kappa_{lur}$

As already mentioned in section 5.4 "Conclusion" of chapter 5 "General performance prediction" these two coefficients have the main influence on the flowmeter performance. Additionally, the determination of the true value of both of these two coefficients within the required accuracy is extremely difficult. According to chapter 9 "Leakage and viscous friction" section 9.3.5 "Triangular clearance", the turbulent leakage coefficient $\kappa_T$ can be calculated to an accuracy of ±15%. According to chapter 8 "Bearing friction" section 8.5 "Discussion", the constant friction coefficient was determined to an accuracy of ±50% for the tested bearing. Additionally this value is expected to vary for a range of bearings as only one single bearing was tested. For the reference meter, which is taken for comparison, only bearings with an exceptional low friction have been used. Hence it is realistic that especially the sliding friction value may corrected to a fraction of its original value.

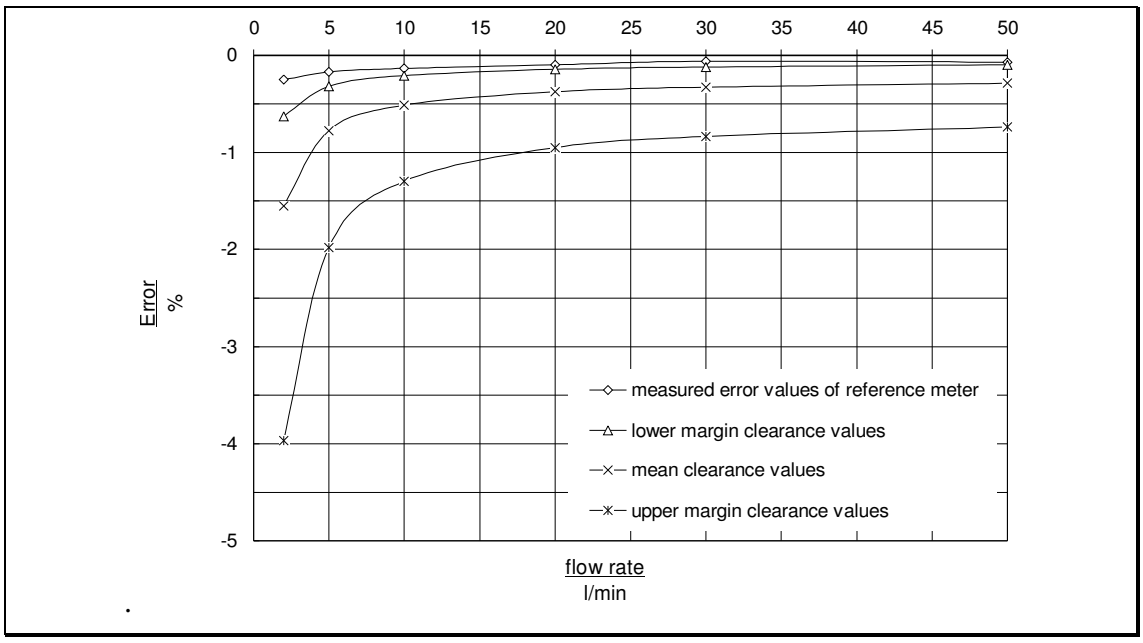


*Figure 82* *Calibration curve comparison of performance prediction model to the reference flowmeter using original loss coefficients and varying clearance values.*

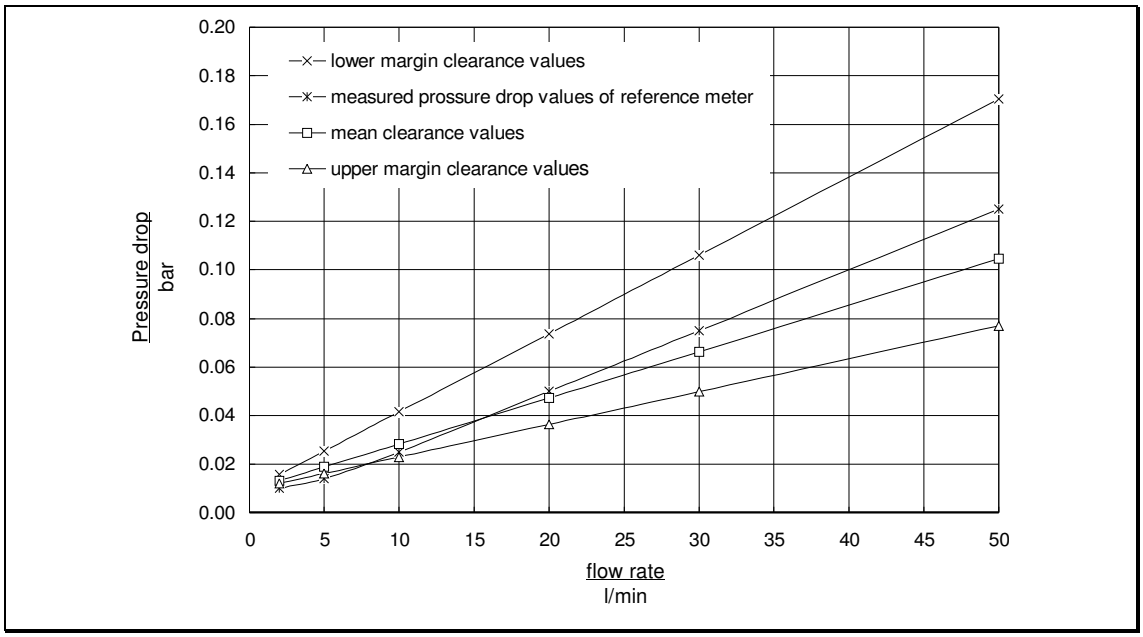


*Figure 83 Pressure drop comparison of performance prediction model to the reference flowmeter curve using original loss coefficients and varying clearance values.*

## 12.2 Proposal for an improved model

The two remaining coefficients which might have been determined inaccurate, the constant friction coefficient $\kappa_C$, and the turbulent leakage coefficient $\kappa_{tur}$, have been varied within their possible minimum and maximum limits. Realistic limits are:

(a) for the turbulent leakage coefficient $\kappa_{tur}$ a variation from 95% to 115%

(b) for the constant friction coefficient $\kappa_C$ a variation from 5% to 150%

In order to improve the results of the model, both coefficient had to be decreased. However, a decrease of the turbulent leakage flow coefficient of 15 % did not improve the result of the performance model significantly. Hence the author proposes that the sliding friction in the reference flowmeter is much lower. A sliding friction value 20% of the original value already shows a much better correlation (Figure 85), but the author proposes that a friction values which is as low as only 5 % of the original value may be used. Using this lower sliding friction, both calibration curves then show a good correlation (Figure 84).

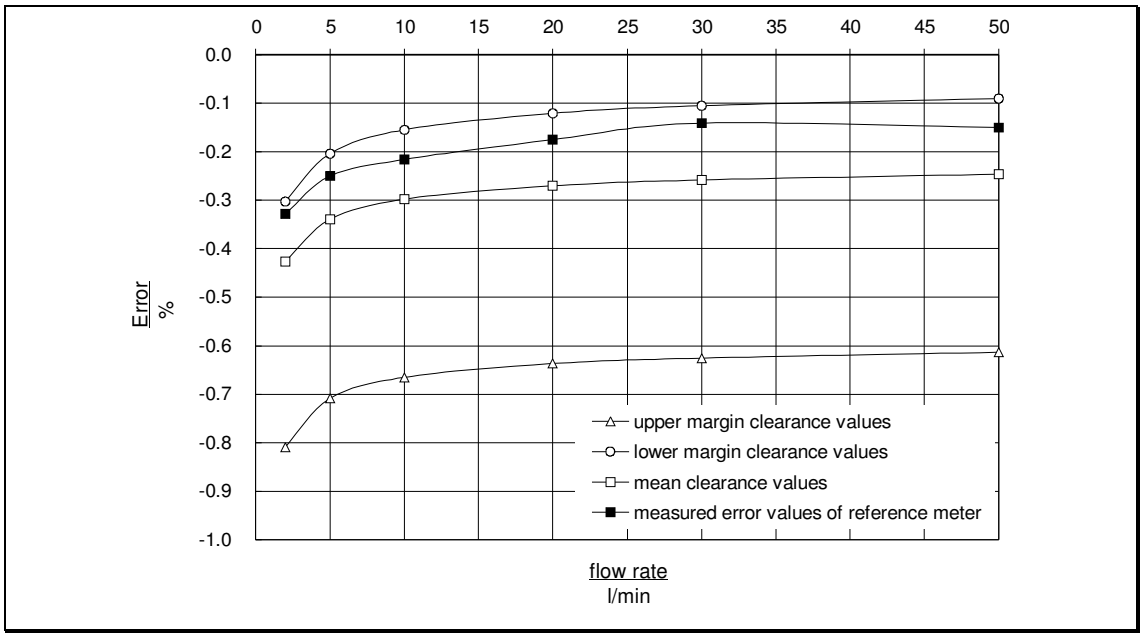


*Figure 84 Calibration curve comparison of the performance prediction model to the reference flowmeter curve using a low constant loss coefficient (5 % of original value) and varying clearance values.*

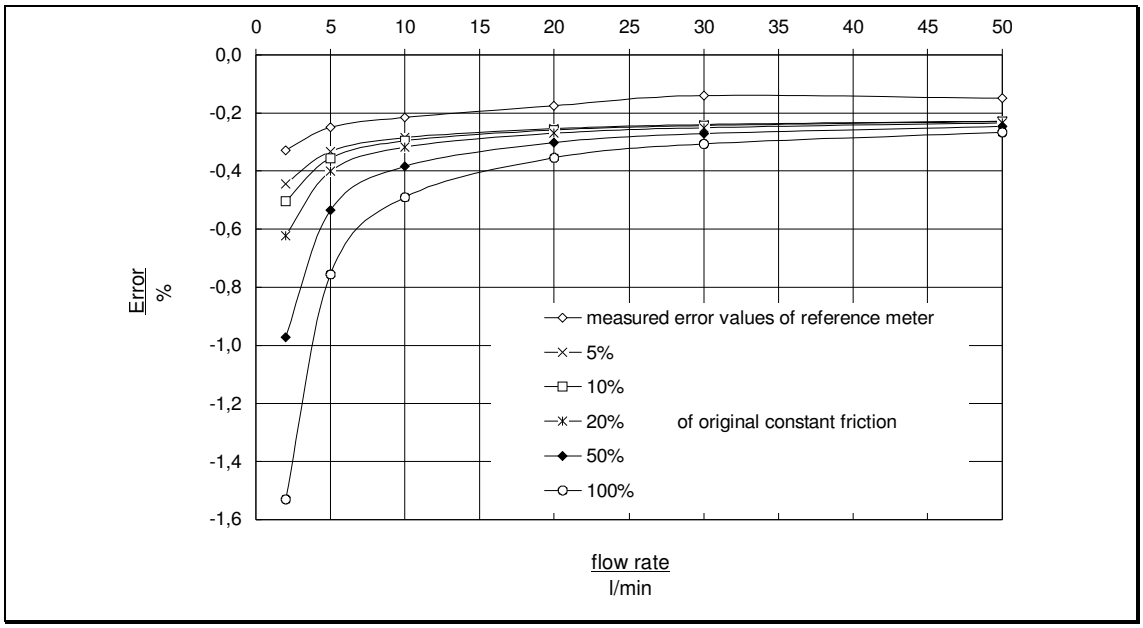


*Figure 85 Calibration curve comparison of the performance prediction model to the reference flowmeter curve using varying constant loss coefficients*

# 13 Theoretical performance discussion

The general performance of the flowmeter regarding the influence of the different coefficients has already been discussed in detail in chapter 5 "General performance prediction". This general performance behaviour will not change in the following detailed discussion and the conclusions of chapter 5 will not be repeated here. Optimum performance is considered to be achieved if the plot of error shows a minimum overall deviation from linearity. Three main questions remain to be discussed:

(a) How does the current 24;2-3;1.09 design perform for varying friction, clearance and fluid parameters?

(b) Does the size of the flowmeter affect its performance?

(c) Does any of the alternative designs perform equal or better, using the same friction, clearance and fluid parameters?

The set of parameters which can be varied for one single design are as follows:

(a) Circumference clearance value of $rotor_I$ or $rotor_{II}$

(b) Root clearance value of $rotor_I$ or $rotor_{II}$

(c) Flank clearance value of $rotor_I$ or $rotor_{II}$

(d) Triangular clearance value

(e) Sliding friction value

(f) Fluid density

(g) Fluid viscosity

(h) Speed range of operation

## 13.1 Meter performance using varying fluid properties

In order to analyse the performance of the current 24;2-3;1.09 design the procedure described in the following was found to be most suitable.

(a) A testing fluid and a temperature was selected. Both together determine fluid viscosity and density.

(b) Each clearance parameter and the speed range of operation was varied in turn in order to obtain an optimum performance of the flowmeter.

(c) The values, for which an optimum performance was achieved were noted.

The performance model was applied to a flowmeter with mean clearances for 3 different fluids, Hebrosol, Shellsol and unleaded petrol with 3 different temperature settings (-10°C, +20°C and +50 °C). For each temperature the values of viscosity and

density were taken from Table 1 in the fluid properties in chapter 2 "Fluid properties considerations". For the three tested fluids the following observations could be made (Figure 86):

(a) The plots of error against flowrate vary for different fluids and different temperatures.

(b) No trend in the influence of increasing viscosity or density on the flowmeter error could be noted for the 3 selected test fluids.

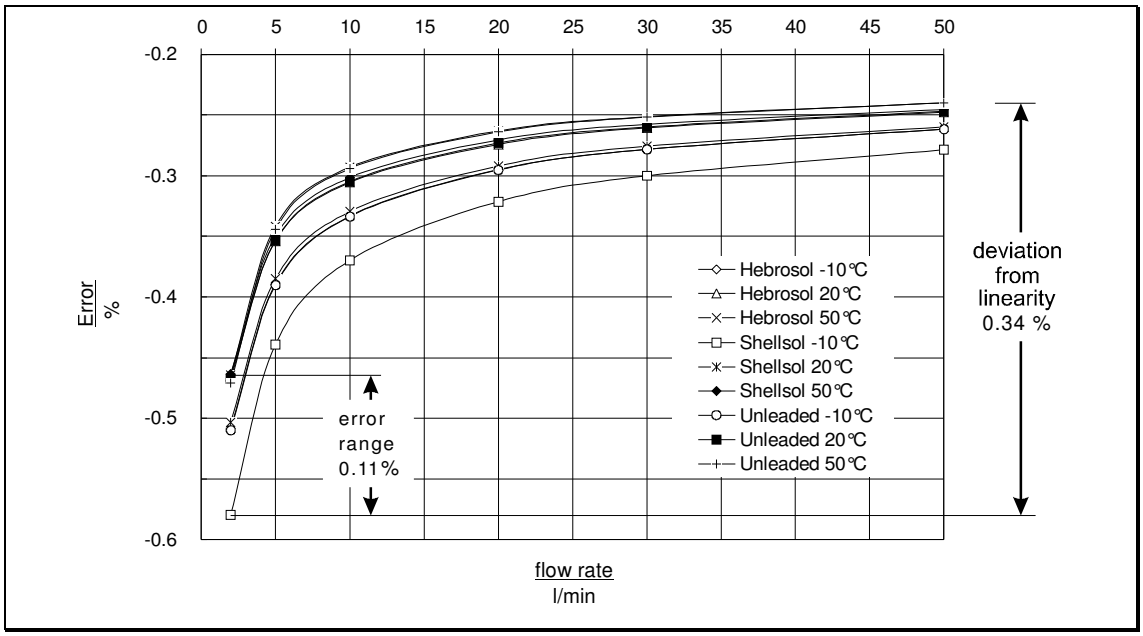


*Figure 86 Calibration curves of the performance prediction model using mean clearance values for Hebrosol, Shellsol and unleaded petrol between -10°C and +50°C. 0.15 % variation within the different fluids.*

Varying each clearance parameter for a given speed range of operation in turn, the following should be noted:

The performance of the flowmeter increases for decreasing root, flank or triangular clearances. The optimum value according to the model would be zero but for the real flowmeter the clearances have to be defined as the machining facilities allow.

For each rotor an optimum value for the circumference clearance does exist. If the clearance is increased, additional leakage will occur. If the clearance is decreased, increased fluid friction will cause a higher pressure drop and hence despite the decreased clearance an increased leakage flow. The optimum value is different for each rotor and depends on the given speed range of operation. For a given turndown, the

achievable accuracy of the flowmeter increases for higher flowrates. This involves an increasing rotor speed and an increased circumference clearance.

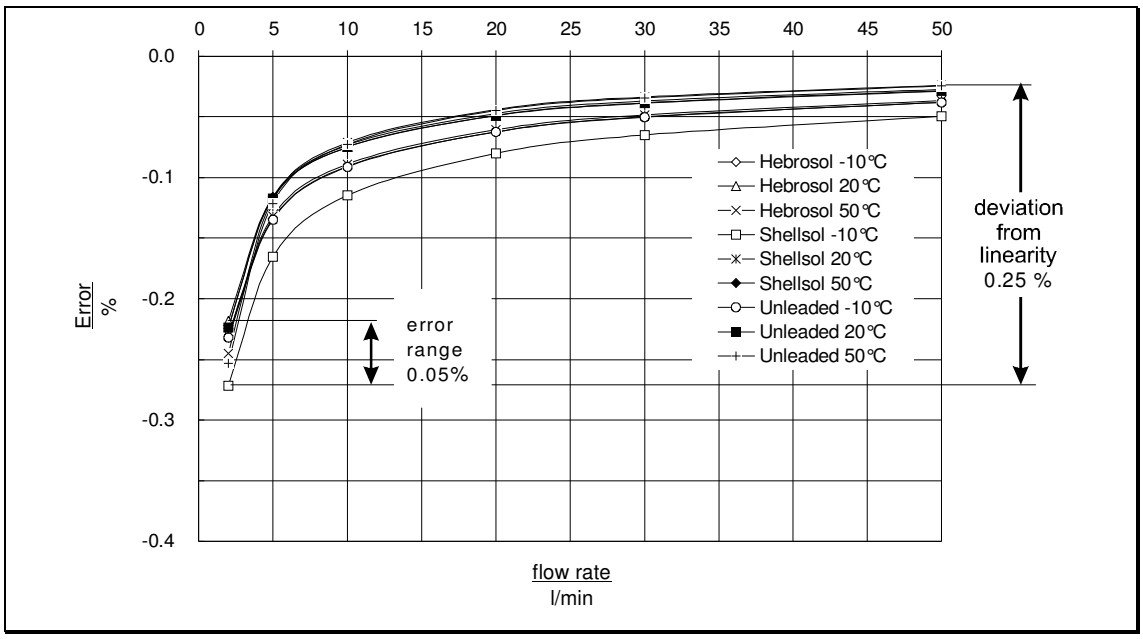


*Figure 87* *Calibration curves of the performance model using an optimised circumference clearance value for Hebrosol, Shellsol and unleaded petrol between -10°C and +50°C. 0.05 % variation within the different fluids.*

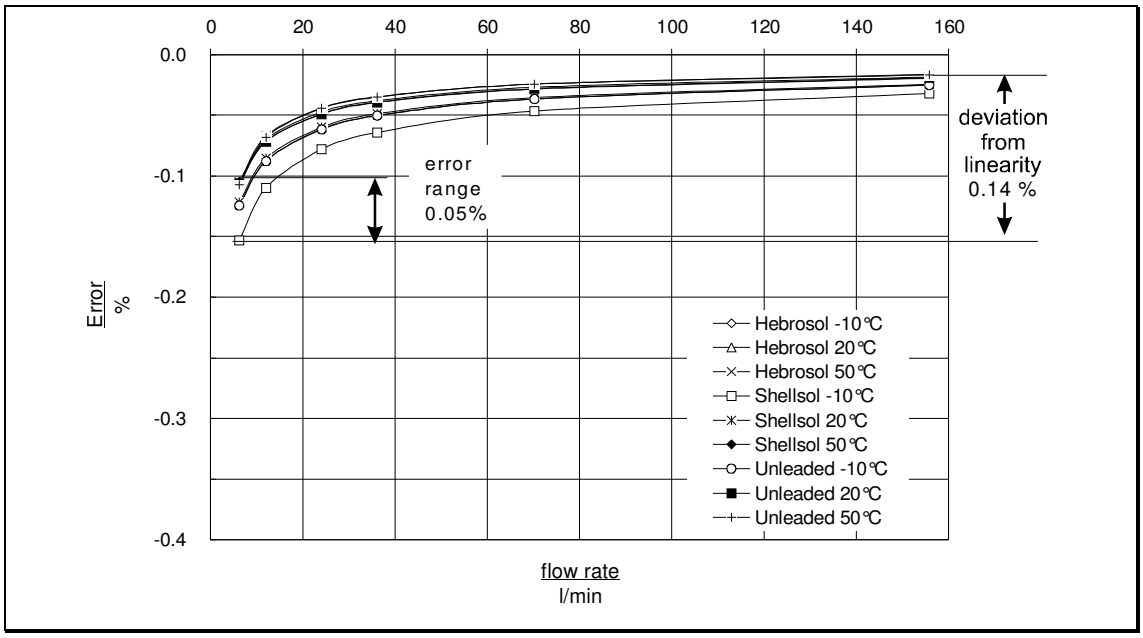


*Figure 88* *Same conditions as Figure 87, but for a meter with an increased circumference clearance, operated with an increased rotor speed. Flow range from 5 to 150 l/min*

## 13.2 Meter performance for size variations

According to the results presented above, a flowmeter of the current design performs at a higher accuracy when used for measuring higher flowrates. For a given turndown range, the flowmeter then performs with a better linearity and less sensibility to fluid changes. In order to determine the optimum size for the given application, the performance prediction model was applied to two other sizes of the flowmeter with the same design. One size with a outer diameter of $d_{oI}$ = 22 smaller than the current size, and one with a outer diameter of $d_{oI}$ = 26 larger than the current size. Hence the smaller size flowmeter showed a higher rotational speed, the larger size flowmeter showed a lower rotational speed. It is important to note that the triangular, root and flank clearances were kept constant for all sizes. For all three flowmeters the plot of error against flowrate was calculated for a flowrange of 2 l/min to 50 l/min (Figure 89) and a flowrange from 5 l/min to 125 l/min (Figure 90).

As a result, the linearity of the larger flowmeter with $d_{oI}$ = 26 was better than the linearity of the smaller flowmeter with $d_{oI}$ = 22 (Figure 89 and Figure 90). Additionally the linearity for the range of the higher flowrates (Figure 90) was better than the linearity for ranges of the lower flowrates (Figure 89).

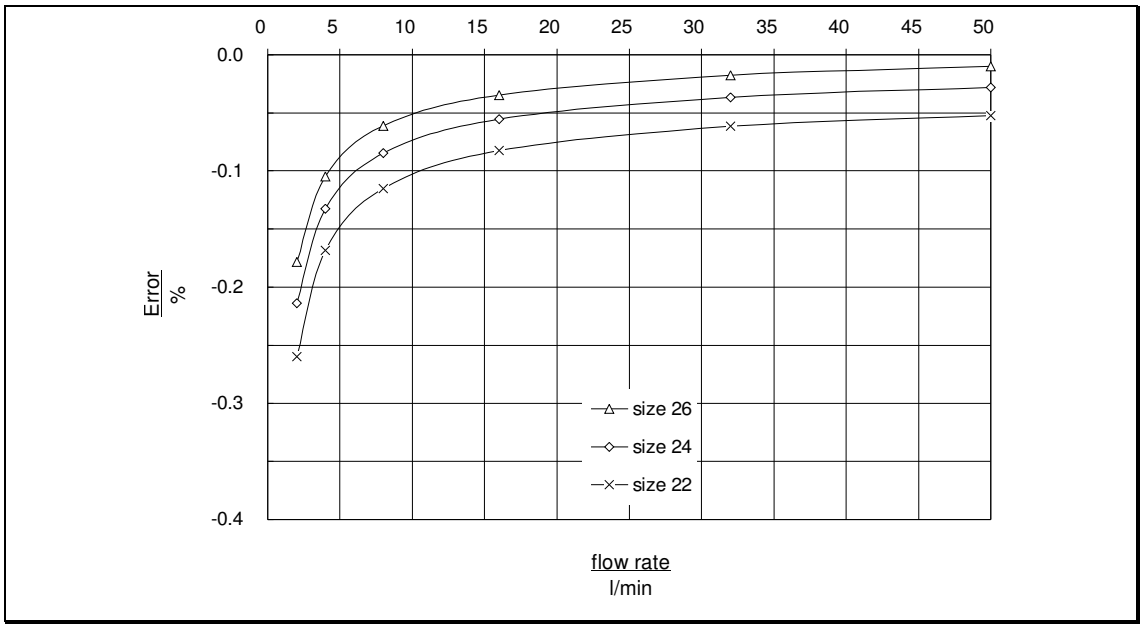


*Figure 89* *Calibration curves from the performance prediction model; comparison of three different sizes of the same flowmeter design for a flowrange from 2l/min to 50 l/min*

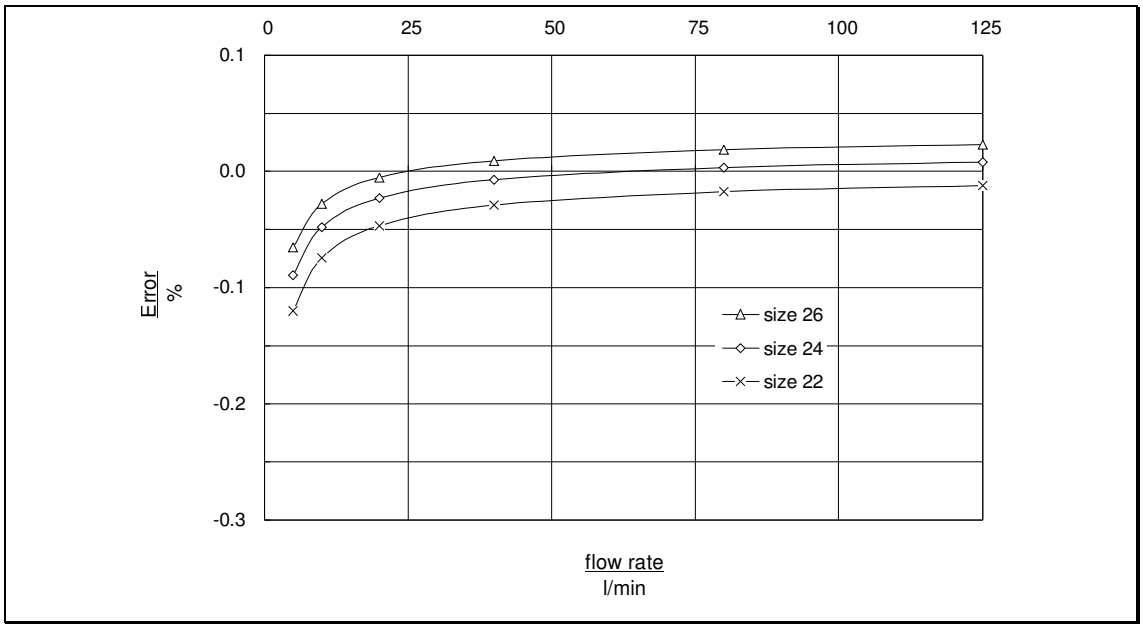


*Figure 90* *Calibration curves from the performance prediction model; comparison of three different sizes of the same flowmeter design for a flowrange from 5l/min to 125 l/min*

## 13.3 Meter performance for design variations

In order to compare different rotor designs variations, two main methods for comparison are available. Profiles with the same outer diameters of $rotor_I$ are easy to define (Table 4 "Suitable rotor geometries for a flowmeter" in chapter 6 "Rotor geometry"). However, because of the varying outer diameters of $rotor_{II}$, these profiles according to the results of section 13.2, can not be considered absolutely comparable to each other. Profiles with the same flooded cross section are more comparable to each other. This profiles can be calculated from the set of profiles in Table 4 in chapter 6 "Rotor geometry" by scaling the outer diameter of $rotor_I$ to achieve a constant flooded section for each profile. However the restrictions, as listed in chapter 6 "Rotor geometry" in section 6.4 "Selection of suitable flowmeter geometries", have to be considered.

The following procedure was first applied to a set of profiles with the same outer diameter of $rotor_I$ $d_{oI}$ = 24 mm. This is corresponding to the list of possible design variations as shown in Table 4 in chapter 6 "Rotor geometry":

(a) The range of the flowmeter was limited from 2l/min to 50 l/min

(b) The maximum pressure drop was limited to 0.15 bar

(c) Clearances for root, flank and triangular clearance were set to their mean values.

(d) The fluid parameters were set to hebrosol at 20°C, which represents the calibration fluid.

(e) The size of the circumference clearance was optimised in order to obtain a minimum deviation from linearity. This is obtained, when the difference between error value for 2 l/min and for 50 l/min is as small as possible.

(f) This circumference clearance determined is then considered to represents an optimum configuration for the requirements of flow range and fluid.

(g) The plot of error against flowrate is determined for the three relevant fluids as mentioned above. These are Hebrosol, Shellsol, and unleaded petrol.

(h) For these 3 fluids the maximum deviation from the original error value was noted.

In accordance with section 13.2 profiles with a larger flooded cross section showed a better linearity than the other profiles. This can be seen when the current 24;2-3;1.09 flowmeter design (Figure 91), which represents the upper limit of performance is compared with a 14;3-4:1.00 design (Figure 92), which represents the lower limit of performance. The second design exhibits a 60 % increased deviation from linearity.

However, as discussed above section 13.2 the performance of the flowmeters is considered to be directly related to the flooded cross section of the flowmeter. If the two flowmeters are scaled to the same value of flooded cross section, for example 262 mm², the difference in deviation from linearity is only 40 % (Figure 93).

The best alternative for the current design would be a 28;2-3;1.00 design (Figure 94). This design shows the same theoretical performance than the current 24;2-3;1.09 flowmeter design.

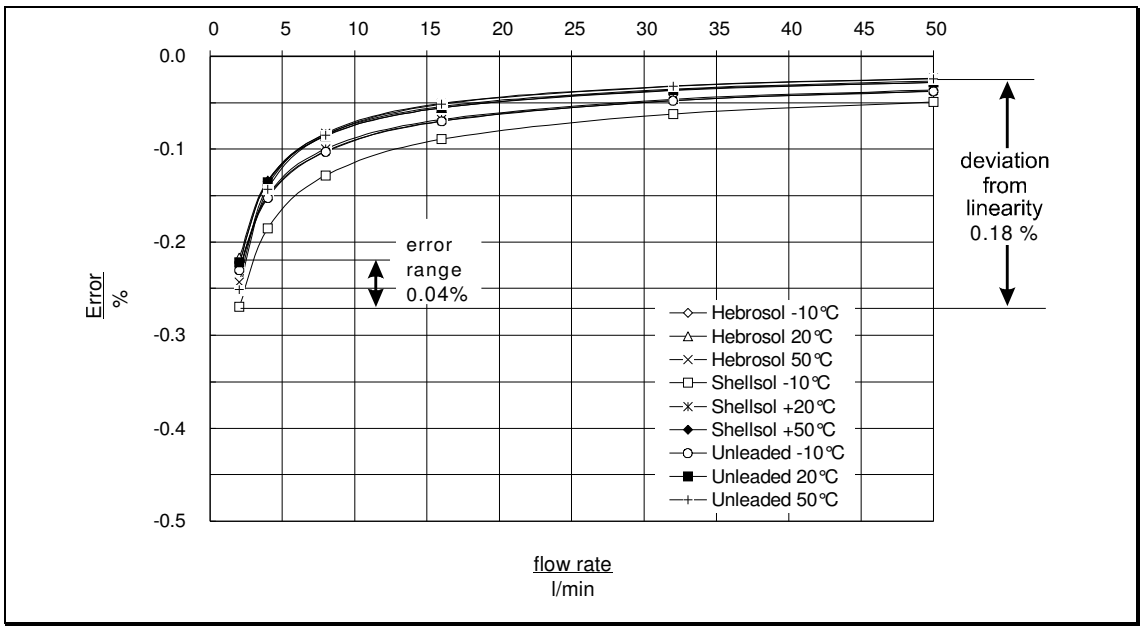


*Figure 91 Calibration curves from the performance prediction model for a 24;2-3;1.09 flowmeter with a 262 mm² flooded cross section;*

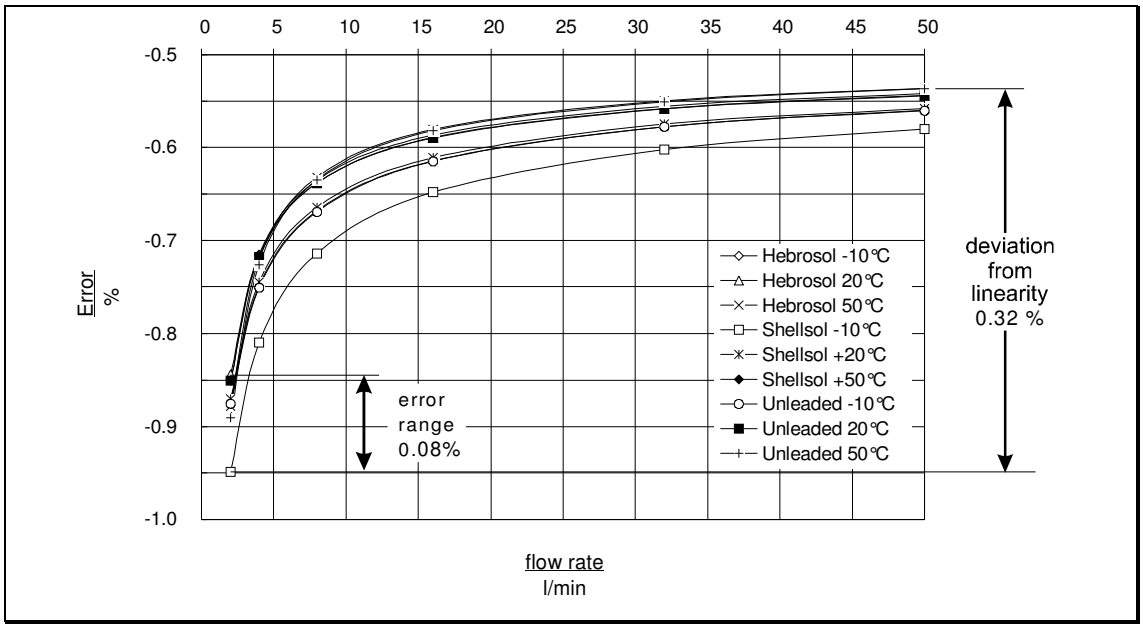


*Figure 92* *Calibration curves from the performance prediction model for a 24;3-4;1.00 flowmeter with a 188 mm² flooded cross section; compare linearity with Figure 91*

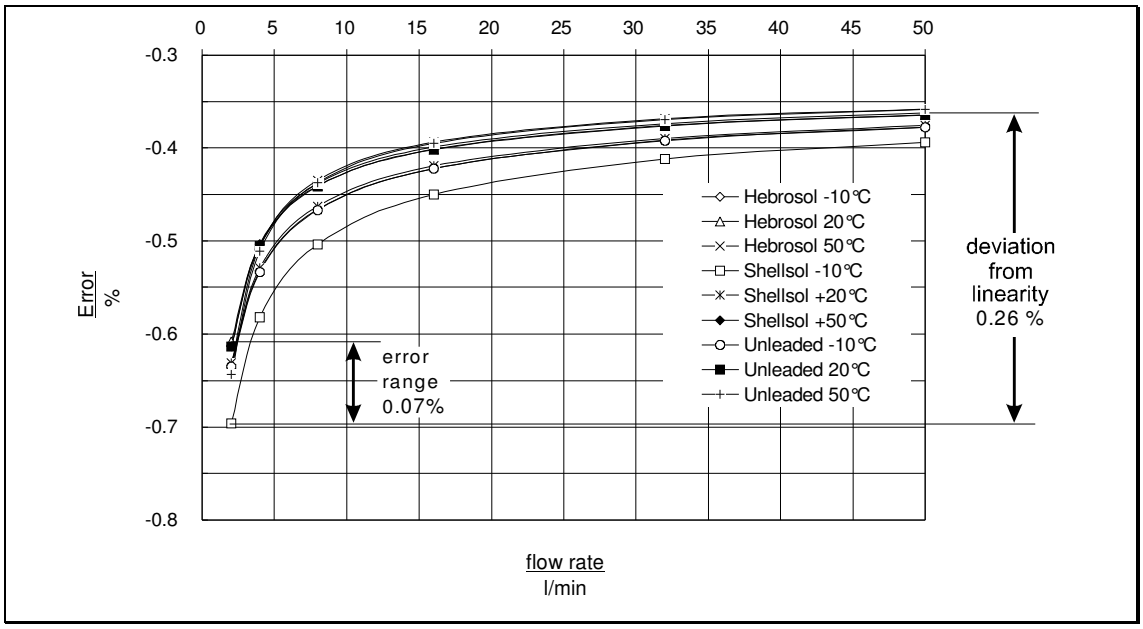


*Figure 93* *Calibration curves from the performance prediction model for a 28.44;3-4;1.00 flowmeter with a 262 mm² flooded cross section; compare linearity with Figure 91 and Figure 92*

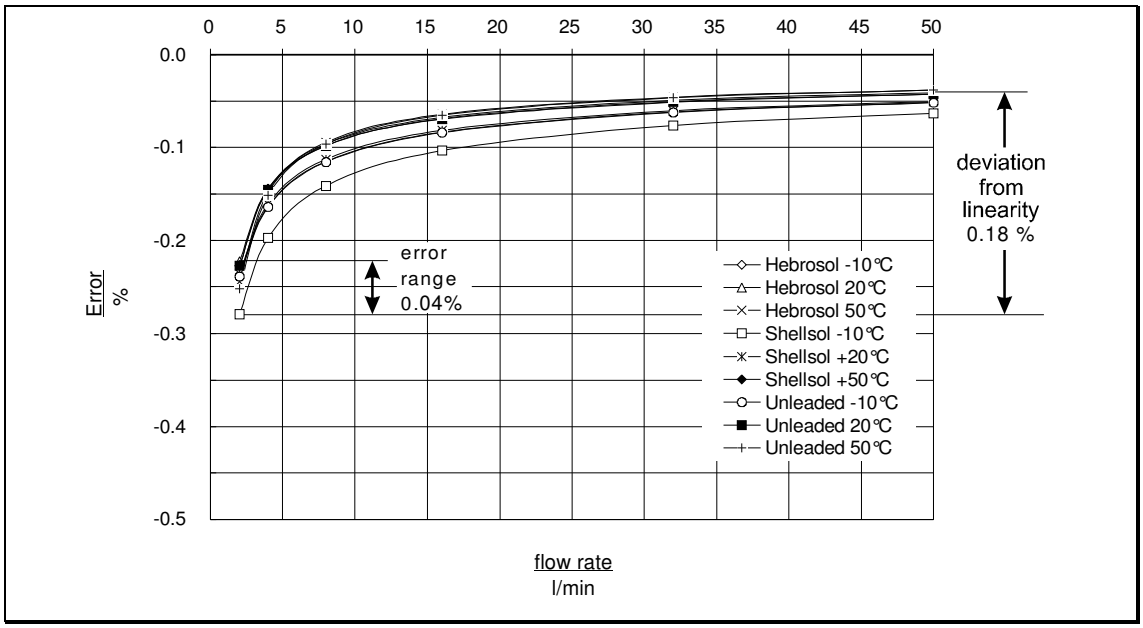


*Figure 94* *Calibration curves from the performance prediction model for a 28;2-3;1.00 flowmeter with a 330 mm² flooded cross section; compare linearity with Figure 91*

# 14 Conclusions

A general model describing a positive displacement flowmeter performance has been developed in this thesis. This model, as described below, is the original work of the author and is the result of a thorough study of the different ideas of flowmeter modelling. One main idea which the author regards as being original is the direct relation of the power loss in the fluid to the internal losses in the flowmeter. This means that the calculation of the torque on the rotor by the fluid pressure is not necessary and the error of a flowmeter can be calculated directly as a mathematical function of the given operating speed. The logic is that a flowmeter performs at a defined pressure loss for a given speed. This pressure loss times flowrate is then energy balanced against all internal losses. Pressure loss and speed are the causes of leakage. Rotational speed times the theoretical swept volume, describe the theoretical flowrate. This flowrate, when combined with the leakage flow can be used to calculate the effective or true flowrate. The performance of a positive displacement flowmeter is related to 8 coefficients describing the influence of the design of a meter on laminar slip $\kappa_{lam}$, turbulent slip $\kappa_{tur}$, rotational slip $\kappa_{rot}$, viscous friction losses $\kappa_D$, mechanical friction losses $\kappa_U$, constant torque losses $\kappa_C$, impulse losses $\kappa_T$ and ball bearing viscous friction losses $\kappa_B$, respectively. It was found that only 4 out of these 8 loss coefficients can be claimed reasons for deviation from linearity. These are the turbulent slip coefficient $\kappa_{tur}$, the constant torque loss coefficient $\kappa_C$, the impulse power loss coefficient $\kappa_T$ and the ball bearing viscous friction power loss coefficient $\kappa_B$. With those reasons for deviations absent, the plot of error over flowrate is linear and the systematic error against flowrate is constant. For a helical rotor flowmeter only 2 out of these 4 coefficients are the main reason for meter inaccuracy. These are the turbulent slip coefficient $\kappa_{tur}$ representing the amount of slip, having a turbulent flow pattern, and the constant torque power loss coefficient $\kappa_C$ representing the amount of constant friction in the flow meter which is not related to speed or load. When presenting the results from theoretical methods and experiments in order to determine slip, friction and forces in the flowmeter, the following points can be made:

(a) The profile of the helical rotors can be defined, apart from size, by three main parameters namely the ratio $r$ of the number of starts, the ratio $\varepsilon$ of the outer diameters of the two rotors and the angle of the pitch of the thread $\phi_P$. From a practical standpoint only certain values of these parameter can be used in flow meter design and only 12 different design variations are possible.

(b) A comprehensive original method is presented to calculate the loads and torques on the rotors of a helical rotor meter, where horizontal and vertical components

are determined separately in cross-sections and integrated over the length of the rotor. In addition, the distribution of the load on the bearings and its change over a revolution was evaluated. However, the determination of the load on the bearing is not critical for the performance prediction of the flowmeter and the equations presented in Appendix E may can also be used for screw pump applications. It was found that the loads on the rotors apply only in the area of the sealing line. The value of the forces and torques is related to the main geometric parameters r, $\varepsilon$ and $\phi_P$. The torque on $\text{rotor}_\text{I}$ is positive, the torque on $\text{rotor}_\text{II}$ negative. This means that the forces drive $\text{rotor}_\text{II}$ in the opposite direction to that of its rotation; hence it has to be driven by $\text{rotor}_\text{I}$. A theory to prove the validity of the method was applied and consistent confirming results were achieved. This means that for a constant pressure load over all chambers, which equals a zero pressure drop, no forces or torques were created. The calculated torques acting on the rotors, compared to the theoretic power loss over the flowmeter showed a very good agreement. The error of fluid power against rotational power is below 2%.

(c) In order to obtain a bearing friction value, measurements performed on the retarding torque time of a decelerating disc show variations, but the same trend as that proposed by theory. By introducing an additional sliding friction torque with the value $M_{sl} \approx 0.15 \pm 0.07$ Nmm for the tested bearing, the results correlate better with the measurement. It is important to note that these results served to drastically narrow down the range of possible friction values in the current application, as the author did not find any reliable values in literature.

(d) Leakage flow in a flowmeter occurs in four main clearances, which are respectively located at the circumference, the flanks and the root of the rotors. In addition, a triangular clearance bordered by flank and circumference of both rotors was detected. A method to determine the geometry of these clearances is presented as well as the application of flow and viscous friction theories for fluid flow in narrow planar, annular ring shape and triangular clearances to the clearance geometries. For the pressure related leakage, the theory proved to be a reliable approximation of the real flowrate. Theory and measurement show good correlation. Leakage flow is laminar, except the flow through the triangular clearance which is turbulent. The proportion of the turbulent flow increases with decreasing pressure drop. The turbulent share varies from 15 % for $\Delta p=0.14$ bar to over 50% for $\Delta p=0.005$ bar. It is important to point out that for a pressure drop lower than 0.02 bar, which represents a low flowrate, the flow through the

triangular clearance constitutes the biggest proportion of all clearances and is therefore the most important leakage. Rotational leakage and viscous friction could not be measured. Regarding the rotational leakage volume and the viscous friction loss, a theory is presented and the loss coefficients can be calculated. However no comparison to experimental results is possible.

Finally equations were presented to theoretically calculate the values of the 8 different loss coefficients from slip, friction and forces in a screw type flowmeter. The theoretical results of the performance model were compared to the experimental performance of the reference flowmeter. It was found that the sliding friction needed to be decreased to 5% of its original value in order to correlate the theoretical plot of error better with the measurement results. The performance prediction model using this lower sliding friction was applied to a screw flowmeter of the Leistritz type in different sizes and to other suitable rotor geometries. It was found that:

(a) Comparing the 12 possible design variations, their theoretical performance is worse or equal than the performance of the current 4;2-3;1.09 design of the Leistritz flowmeter.

(b) The worst design alternative, a 24;3-4;1.00 flowmeter design, shows a 60% decrease in linearity.

(c) The best alternative for the current design would be a 28;2-3;1.00 design. This design shows the same theoretical performance than the current 24;2-3;1.09 flowmeter design.

(d) An optimal circumference clearance value can be determined for each different fluid property and flowrate requirement.

(e) For a given range of flowrates, smaller sizes perform worse than larger sizes. This is independent of the design of the meter.

(f) For a given design, size and turndown range, the flowmeter performs better for higher flowrates.

# 15 Recommendations for future work

Two main fields of work are recommended. First an improved validation of the model using loss coefficients which are determined with a higher degree of accuracy and second, the determination of an ideal meter, including the manufacturing possibilities.

In order to increase the accuracy of comparison of theory with measurement, the ideal situation would be as follows: Determine the plot of accuracy of a selected meter and then separately determine all leakage and friction losses, the dimension of the rotors and the radial position of the rotor in the housing. The bearing fiction should be determined in the actual flow meter assembly, as the fits between outer ring of the bearing and housing or inner ring and the rotor shaft have an enormous influence on the bearing friction. Single parameters or losses should then be varied, without influencing any other parameters. This should be performed using different fluid parameters, different clearance dimensions and different bearing friction values. An experimental set up which would allow a separated, controlled and monitored variation of single loss coefficients would significantly increase the value of experimental results. However, besides the variation of the fluid parameters, a separated variation of all other parameters is considered extremely difficult to realise.

The performance model can be applied to additional meter design variations which had been omitted in the current study. These are design modifications using a variation in the pitch of the rotors or a variation in the head angle of the rotor profile. In order to comprehensively discuss all design variations, manufacturing restrictions related to different rotor designs and influencing the size of the triangular and other clearances, needs to be considered.

Additionally, experiments with carbide journal bearings, as used in turbine flowmeters should be performed, in order to find low friction bearing alternatives.

*[End of main section]*

# References

/1/ BS 7405: 1991; Guide to selection and application of flowmeters for the measurement of fluid flow in closed conduits; British Standard, p 58, p171, 1991

/2/ Adler, U. A.; Automotive Handbook.; VDI Verlag GmbH, 3rd Edition, pp 226-233, 1993

/3/ Dubbel; Taschenbuch für den Maschinenbau [Handbook for mechanical engineering] (in German); edrs. Beitz, W. Küttner, K.-H.; *Springer Verlag*, 16th edition, L6 Figure 4; Appendix E3 Figure44; Appendix D12 Table2, 1987

/4/ Menke, D.; Comparison of the procedures used to calculate the density of petroleum products; *Int Conf on the Metering of Petroleum and its Products,* 7-8 March, London, OYEZ, 1985

/5/ Eade, Robert.; Getting the most from flowmeters; *Eng Syst (Business News Publishing Co., Troy, MI, USA*, vol 13, No 2, pp 6-7, 1996

/6/ Franklin, B.; Flowmeters; *Control and Instrumentation*, Vol 22, No 11, pp 29-35, 1991

/7/ Furness, R.; FLOWMETERING - evolution or revolution; *Control and Instrumentation*, pp S15-S18, September 1994

/8/ Gerrard, D. R.; Flow measurement - of the utilities; *Control and Instrumentation*, Vol 26, No 2, pp 27-30, 1994

/9/ Gerrard, D. R.; Very low flows in sharp focus; *Control and Instrumentation*, vol 24, No 02, pp 37-38, 1992

/10/ Hendrix, A. P.; Positive displacement liquid meters; *INTECH*, Vol 29, pp 47-49, 1982

/11/ Hendrix, A. R.; Positive displacement flowmeters & their uses in peak plant operation, Instrumentation in the Power Industry; *Emerson Electr. Co., ISA Power Instrumentation Symp., Phoenix, USA: May 24-26 1982, Research Triangle Park, USA., Instrum. Soc. Am.*, vol 25, Proc. 25th, session 1, pp 13-16; 1982

/12/ Kinghorn, F. C.; Challenging areas in flow measurement; *Measurement + Control*, Vol 21, pp 229-235, Oct 1988

/13/ Medlock, R. S.; The techniques of flow measurement; *Brown Boveri Ltd., Meas. & Control,* vol 15, No 12, pp 458-463, Dec. 1982

/14/ Stevens, N.; Technology overview over flow; *Control Instrum*, vol 28, No 2, pp 35-36, 1996

/15/ Lomas, D. J.; Selecting the right flowmeter part 1; *Instrument technology*, Vol 24, part 6, pp 55-62, 1977

/16/ Mannion, J. R.; Casedy, G. A.; Fluid flow meter selection; *Flow Inc., Nalco Chem. Co., Heat Piping Air Cond.,* vol 54, No.5, pp 81-88, 1982

/17/ Reeve, A.; Can you select the right flowmeter; *Control and Instrumentation*, Vol 21, No 2, pp 43-45, 1989

/18/ Reeve, A.; Successful selection facts for flowmeters; *Control and Instrumentation*, Vol 23, No 2, pp 33-34, 1991

/19/ Cheremisinoff, N. P.; Marcel Dekker Inc.; Applied fluid flow measurement: fundamental and technology; *New York, USA., Marcel Dekker Inc., Engng. Measurement & Instrumentation /1,* p 212, 1979

/20/ Furness, R.; Fluid flow measurement; Edr. Flanagan T. P.; *Longman UK*, 1989

/21/ Dowden, R. R.; Fluid flow Measurement - A Bibliograhy; *British Hydromechanics Res. Assoc.*, Cranfield, Bedford, England, 1971

/22/ FLUIDEX; Fluid flow abstracts Database University of Cranfield, regularly updated

/23/ Baker, R. C.; Morris M. V.; Positive-displacement meters for liquids; *Transactions of the Institute of Measurement and Control*, vol 7, pp 209-20, 1985

/24/ Baker, R. C.; An Introductory Guide to Flow Measurement; *Mechanical Engineering Publications Ltd. London*, pp 3-90, 1989

/25/ Hayward T. J.; Flowmeters - a basic guide and source book for users; *Macmillan, London* , 1979

/26/ Spitzer, D. W.; *Industrial Flow Measurement*, Instrument Soc of America, 1984

/27/ Benard, C. J.; Morden, U. K.; Handbook of Fluid Flowmetering, section 4: classification and selection; *Trade & Tech. Press Ltd*., 1st edition, pp 179-196, 1988

/28/ Konopka, John; PD. Meters for liquid Measurement; *Brooks Instrument*, 1991

/29/ Gerrard, D.; Measure viscous flow over 150:1 turndown by PD meter techniques; *cont and Instrum.*, vol 11, No 4, pp 39-41, 1979

/30/ N. N.; Brooks Instrument BiRotor™ Meters; *Brooks Instrument Division*, 1994

/31/ Considine, D. M.; Considine, G. D.; Process Instruments and Controls Handbook; *McGraw-Hill Book Company*, 3rd Edition 1985, pp 4.76-4.80

/32/ Kral; Screw Volumeter OM; *Kataloque;* Kral Austria, 1992

/33/ Litre Meter; Helical Screw Flowmeters; *Litre Meter Limited, Aylesbury*, 1994

/34/ Leistritz AG; Information: Schraubenvolumeter LSV.[Information: screw flowmeter](in German); 1994

/35/ Conrad, F.; Trostman, E.; A servo controlled volume rate flowmeter; *Int. Conf. on Advances in Flow Measurement Techniques, Denmark Tech. Univ., Lyngby BHRA Fluid Engng. Warwick, UK, Sep. 9-11, 1981, Cranfield*, No H3 ,pp 223-239, 1981

/36/ Karassik, I. J.; Krutzsch, W. C.; Fraser, W. H.; Messina, J. P. (edrs.); PUMP HANDBOOK;. *McGRAW- Hill Book Company*, 2nd edition, pp 3.57-3.79, 1985

/37/ Leistritz; Screw pumps; Leistritz AG Germany, DS Nr. 1.2-10e4.92/5'; 1992

/38/ Mankin, P. A.; Measurement of liquid flow by positive displacement meters; *Southern California Meter Association, Instruments & Automation*, pp 453-457, 1955

/39/ Bavendiek, R.; Neue Methode zur Bestimmung der Verluste (Wirkungsgrade) an hydrostatischen Maschinen [New method for determining the losses of hydrostatic machines](in German); *Ölhydraulik und pneumatik*, vol 31, part 11, pp 861-866, 1987

/40/ Schlösser, W. M. J.; Ein mathematisches Modell für Verdrängerpumpen und Motoren [A mathematical model for displacement-type pumps and motors] (in German) ; *Ölhydraulik und pneumatik*, vol 5, Nr. 4, pp 122-130, 1961, A mathematical model for displacement pumps and motors; *Hydraulic Power Transmission*, Nr. 4, pp 252-257, Nr. 5, pp 324-328, 1961

/41/ Schlösser, W. M. J.; Eine Maßstabstheorie zur Vorhersage des Verhaltens von Mitgliedern einer Familie hydraulischer Verdrängermaschinen [A Scale Theory for the Prediction of the Behavior of Members of a Family of hydraulic Displacement-type Machines] (in German) ; *Ölhydraulik und pneumatik*, vol 14, Nr. 1, pp 1-5, 1970

/42/ Schlösser, W. M. J.; Hilbrands J. W.; Das theoretische Hubvolumen von Verdrängerpumpen [Theoretical Swept Volume of Displacement Pumps] (in German); *Ölhydraulik und pneumatik,* vol 7, Nr. 4, pp 133-138, 1963; Theoretical Swept Volume of Displacement Pumps; *Hydraulik Power Transmission*, vol 9, Nr. 97, 1963

/43/ Schlösser, W. M. J.; Hilbrands J. W.; Der Volumetrische Wirkungsgrad von Verdrängerpumpen [The Volumetric Efficiency of Displacement Pumps] (in German); *Ölhydraulik und pneumatik*, vol 7, Nr. 12, pp 415-420, 1963

/44/ Schlösser, W. M. J.; Hilbrands J. W.; Über den hydraulisch-mechanischen Wirkungsgrad von Verdrängerpumpen [The Hydraulic-mechanical Degree of Efficiency of Positive Displacement Pumps] (in German) ; *Ölhydraulik und pneumatik*, vol 9, Nr. 9, pp 333-338, 1965

/45/ Wilson, W. E.; Hydraulic Pumps and Motors; *Machine Design*, p 133, JAN. 1949

/46/ Wilson, W. E.; Method of evaluating test data aids design of rotary pumps; *Product engineering*, vol 16; p 653, 1945

/47/ Wilson, W. E.; Performance criteria for positive displacement pumps and fluid motors; *Transactions of ASME*, p 115, FEB. 1949

/48/ Wilson, W. E.; Positive Displacement Pumps and Fluid Motors; *Publishing Corp. New York*, p 371, 1950

/49/ Wilson, W. E.; Rotary Pump Theory ; *Transactions of ASME*, p 371, MAY 1946

/50/ Ryazantsev, V. M.; New profiles for the threads on triple screw pumps; *Soviet Engineering Research*, vol 6, No 8, pp 6-7, 1986

/51/ Hamelberg, F. W.; Investigation on Pumps - Rotor profiles, rotor forces and powers of screw pumps; (in German); *VDI-Forschungsheft no 527*, pp 5-7 and 10-11, 1968

/52/ Kalishevskii, V. L.; Investigation of the characteristics of a double-screw pump with sealed coupling (in Russian); *Khim. Neft. Mashinostr.*, No 2, pp 14-16, 1977

/53/ Ryazantsev, V. M.; Improved Profiles of rotors in triple-screw pumps; *Chem and Pet eng*, vol 17, part 5-6, pp 292-295, 1982

/54/ Geimer, H.; Meßtechnische Untersuchungen und Erstellung von Berechnungsgrundlagen zur Ermittlung der Einsatzgrenze dreispindeliger Schraubenpumpen [An experimental examination and presentation of a calculation basis in order to determine the operation limits of triple rotor screw pumps](in German); *Dissertation TH Achen Germany*, Feb.1995

/55/ Ryazantsev, V. M.; Profile of single-cut screws of double-screw pumps; *Chem. and Pet. Engng.*, vol 16, Part 5-6, pp 322-24, 1981

/56/ Ryazantsev, V. M.; Screws for large capacity twin-screw pumps; *Chem Pet Eng.*, vol 25, Part 5-6, pp 250-252, 1990

/57/ Bartsch, H.; Taschenbuch mathematischer Formeln [Handbook of mathematic equations] (in German)*; Verlag Harri Deutsch* 12th edition; pp 201-206, 1988

/58/ Dubbel; Taschenbuch für den Maschinenbau [Handbook for mechanical engineering] (in German); edrs. Beitz, W. Küttner, K.-H.; *Springer Verlag*, 16th edition, pp A68-A69; 1987

/59/ Hamelberg, F. W.; Läuferkräfte bei Schraubenpumpen [Rotor forces of screw pumps] (in German); *Dissertation Technische Hochschule Hannover*, 1966

/60/ Wincek, M.; Zur Berechnung des Förderverhaltens von Schraubenspindelpumpen bei der Förderung von Flüssigkeits-Gas-Gemischen [The calculation of the performance characteristic of screw pumps for multiphase applications] (in German); *PhD - thesis Friedrich Alexander University Erlangen* ; 1991

/61/ Ryazantsew, V. M.; Vodovenkov, V. A.; Pisarev, V. A.; Determining the forces acting on the screws of a double -screw pump; *Chem. and Pet. Engng.*, vol 14, Part 3-4, pp 222-225, 1978

/62/ Palmgren, A.; Neuere Untersuchungen über Energieverluste in Wälzlagern [Newer investigations on the energy losses in roller bearings](in German); *VDI-Berichte*, vol 20, pp 117-121, 1957

/63/ Baker, R. C.; Turbine and related flowmeters; *Flow Meas. Instr.*, vol 2, pp 147-161, 1991

/64/ Eschmann, Hasbargen, Weigand; Ball and Roller Bearings ; *R. Oldenburg Verlag 2nd edition*, pp 201-213, 1985

/65/ Harris, T. A.; Rolling Bearing Analysis ; *John Wiley & Sons, Inc.*, 1966

/66/ INA/Schaeffler; Maßkatalog 511; Kugellager Gehäuse-Einheiten; [Dimensions catalogue ball bearings and housing units](in German),INA-*Schaeffler Wälzlager OHG*, pp 18-19, 1991

/67/ Ragulskis, K.; Yurkauskas, A.; Vibrations of bearings; *Hemisphere Publishing Corporation*, pp 12-24, 1985

/68/ Palmgren, A.; Snare, B.; Influence of load and motion on the lubrication and wear of rolling bearings; *Proceedings of the conference on lubrication and wear - Institution of Mechanical Engineers*, paper 52, pp 454-458, Oct.1957

/69/ SKF; Hauptkatalog [main Catalogue](in German) ; Katalog 4000/I T, pp 56-63 1989

/70/ Becker, E.; Strömungsvorgänge in ringförmigen Spalten[Flow proceedings in annular shaped clearances](in German); *VDI-Berichte*, vol 51, pp 1133-1141, 1907

/71/ Obot, N. T.; Determination of Incompressible Flow Friction in Smooth Circular and Noncircular Passages: A generalized Approach Including Validation of the Nearly Century old Hydraulic Diameter Concept*; ASME Journal of Fluids engineering*, vol 110, pp 431-440, 1988

/72/ Tiedt, W.; Berechnung des laminaren und turbulenten Reibungswiderstandes konzentrischer und exzentrischer Ringspalte [Calculation of laminar and turbulent frictional resistance in concentric and eccentric annular clearances] (in German); *TH Darmstadt Technischer Bericht no. 4*, pp 79-89, 1968

/73/ Yamada, Y.; Resistance of a flow through an annulus with an inner rotating cylinder; *Bulletin of JSME*, vol 5, No 18, pp 302-310, 1962

/74/ Kleinert, H.-J.; Axiale Ringspaltströmung bei Rotation des Innenzylinders[Axial flow through narrow annular clearances with an inner rotating cylinder] (in German); *Wiss. Z. Techn. Universität. Dresden.*, vol 21, No 6, pp 1069-1076, 1972

/75/ Tao, L. N.; Donovan, W. F.; Through-flow in concentric and eccentric annuli of fine clearance with and without relative motion of the boundaries; *Trans. ASME*, vol 77, No 8, pp 1291-1301, 1955

/76/ Allen, T.; Ditsworth, R. L.; Fluid mechanics; *McGraw-Hill*, pp 110-111, 1972

/77/ Daugherty, R. L.; Franzini, J. B.; Fluid mechanics with engineering applications; *MCGraw-Hill*, 7th edition, No 11, pp 10-15, 1981

/78/ Street, R. L.; Watters, G. Z.; Elementary fluid mechanics; *John Wiley & Sons*, 7th edition, pp 25-22, 1993

/79/ Klügl, V. B.; Statische Leckage von Schraubenspindelpumpen [static leakage of screw pumps](in German); *Diplomarbeit Georg-Simon-Ohm-Fachhochschule Nürnberg*, 1993

/80/ Wong, W. M.; Estimation of fluid friction torque in a screw type positive displacement flowmeter, Final Year Project, B. Eng. (Hons) Degree in Mechanical

Engineering 1994/95, *Department of Mechanical and Manufacturing Engineering*, 1994/1995

/81/ Backé, W.; Grundlagen der Ölhydraulik [Fundamentals of hydraulics] (in German); TH Aachen, 7th edition 1988

/82/ Matek, W.; Muhs D. Wittel H.; Roloff/Matek Maschinenelemente [Machine parts] (in German), *Friedr. Vieweg & Sohn Braunschweig Wiesbaden*, 1987

*[End of reference section]*

# Appendix A - Units of viscosity

| dynamic viscosity $\eta_{fl}$ | |
|---|---|
| 1 Pa s | 1 Ns/m² |
| 1 mPa s | $10^{-3}$ Ns/m² |
| 1 P (Poise) | 1 g/cms = 0.1 Ns/m² |
| 1 cP (centiPoise) | $10^{-3}$ Ns/m² |

| kinematic viscosity $\nu_{fl}$ | |
|---|---|
| 1 m²/s | |
| 1 mm²/s | $10^{-6}$ m²/s |
| 1 St (Stokes) | 1cm²/s = $10^{-4}$ m²/s |
| 1 cSt (centiStokes) | $10^{-6}$ m²/s |

*Table 11 Units of viscosities; Backé /81/*

# Appendix B - Description of cycloids with theoretical profile

Both profiles of rotor$_I$ and rotor$_{II}$ are described by epicycloids. A point connected with a circle which rolls on the outside of another circle describes a cycloid. Three different types of cycloids are described by Bartsch /57/ and Dubbel /58/ as follows:

(a) A normal cycloid will be described, if the point selected is on the outer diameter of the rolling circle.

(b) An extended cycloid will be described, if the point is outside of the radius of the rolling circle.

(c) A short cycloid will be described, if the point is inside the radius of the rolling circle.

## The theoretical cycloid of rotor$_I$

Rolling diameter $d_{rI}$ of rotor$_I$ is the root diameter $d_{iI}$, the rolling diameter $d_{rII}$ of rotor$_{II}$ is the outer diameter $d_{oII}$ of rotor$_{II}$. The rolling diameter of rotor$_{II}$ rolls on the rolling diameter of rotor$_I$ and a point on the rolling diameter of rotor$_{II}$, which equals the outside diameter of rotor$_{II}$ describes a normal cycloid (a).

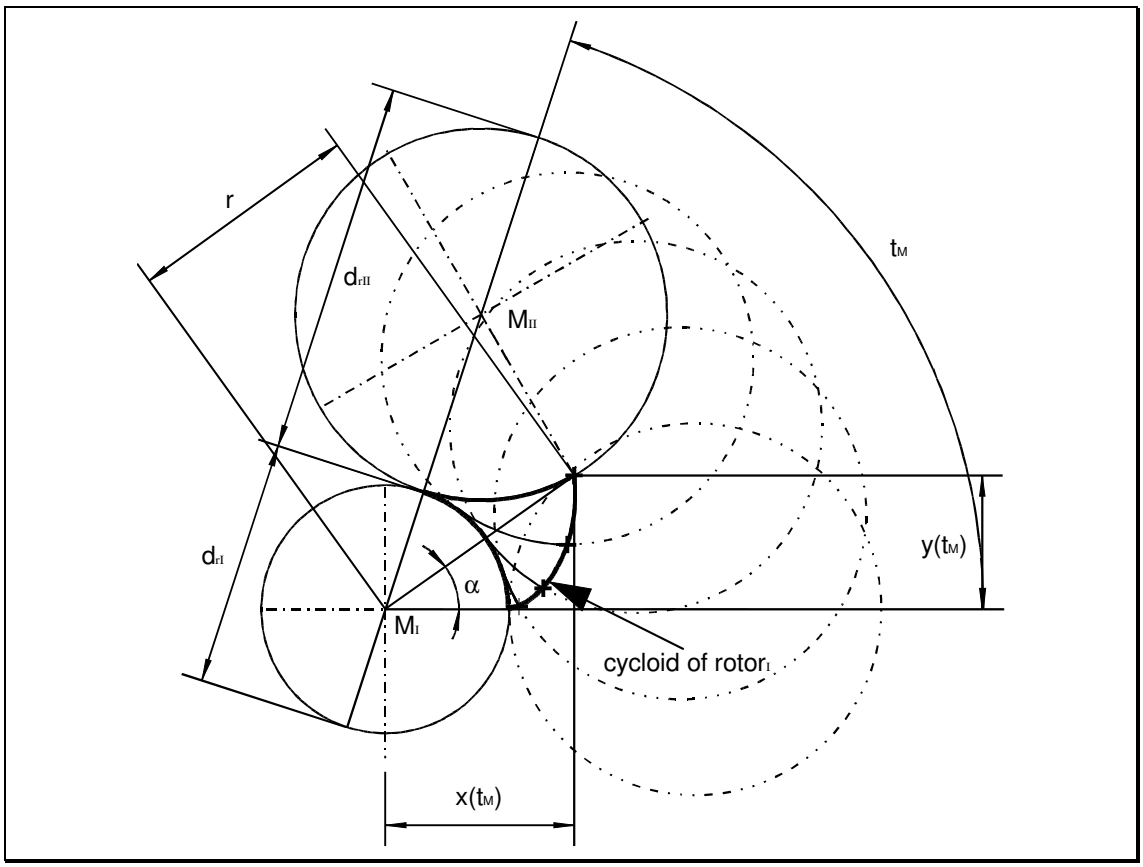


*Figure 95 Theoretical cycloid of rotor$_I$*

The cycloid can be described in two different types of mathematical equations. This is firstly the parameter form with the rolling angle $t_M$, the x-coordinate $x$ and the y-coordinate $y$ and secondly the polar coordinates with the radius coordinate $r$ and the angular coordinate $\alpha$. For the parameter form both coordinates $x$ and $y$ are described as a mathematical function of the rolling angle $t_M$:

$$x(t_M) = a\cos\left(\frac{d_{rII}}{d_{rI}}t_M\right) - \frac{d_{oII}}{2}\cos\left(\frac{2a}{d_{rI}}t_M\right) = \frac{d_{oII}}{2}\left[(1+\varepsilon)\cos\left(\frac{1}{\varepsilon}t_M\right) - \cos\left(\left(\frac{1}{\varepsilon}+1\right)t_M\right)\right]$$

$$y(t_M) = a\sin\left(\frac{d_{rII}}{d_{rI}}t_M\right) - \frac{d_{oII}}{2}\sin\left(\frac{2a}{d_{rI}}t_M\right) = \frac{d_{oII}}{2}\left[(1+\varepsilon)\sin\left(\frac{1}{\varepsilon}t_M\right) - \sin\left(\left(\frac{1}{\varepsilon}+1\right)t_M\right)\right]$$

If the cycloid is described by polar coordinates, the angular coordinate $\alpha$ can be directly related to the radius coordinate $r$. Inversely a direct mathematical relation of the radius coordinate to the angular coordinate is not possible:

$$\alpha(r_I) = \frac{1}{\varepsilon}\arccos\left(\frac{4a^2 + d_{oII}^2 - 4r_I^2}{4ad_{oII}}\right) - \arccos\left(\frac{4a^2 - d_{oII}^2 + 4r_I^2}{4a2r_I}\right)$$

## The theoretical cycloid of rotor$_{II}$

Rolling diameter $d_{rI}$ of rotor$_I$ is the root diameter $d_{iI}$ , the rolling diameter $d_{rII}$ of rotor$_{II}$ is its outside diameter $d_{oII}$. The rolling diameter of rotor$_I$ rolls on the rolling diameter of rotor$_{II}$ and a point on the rolling diameter of rotor$_{II}$ which equals the outside diameter of rotor$_I$ describes an extended cycloid (b).

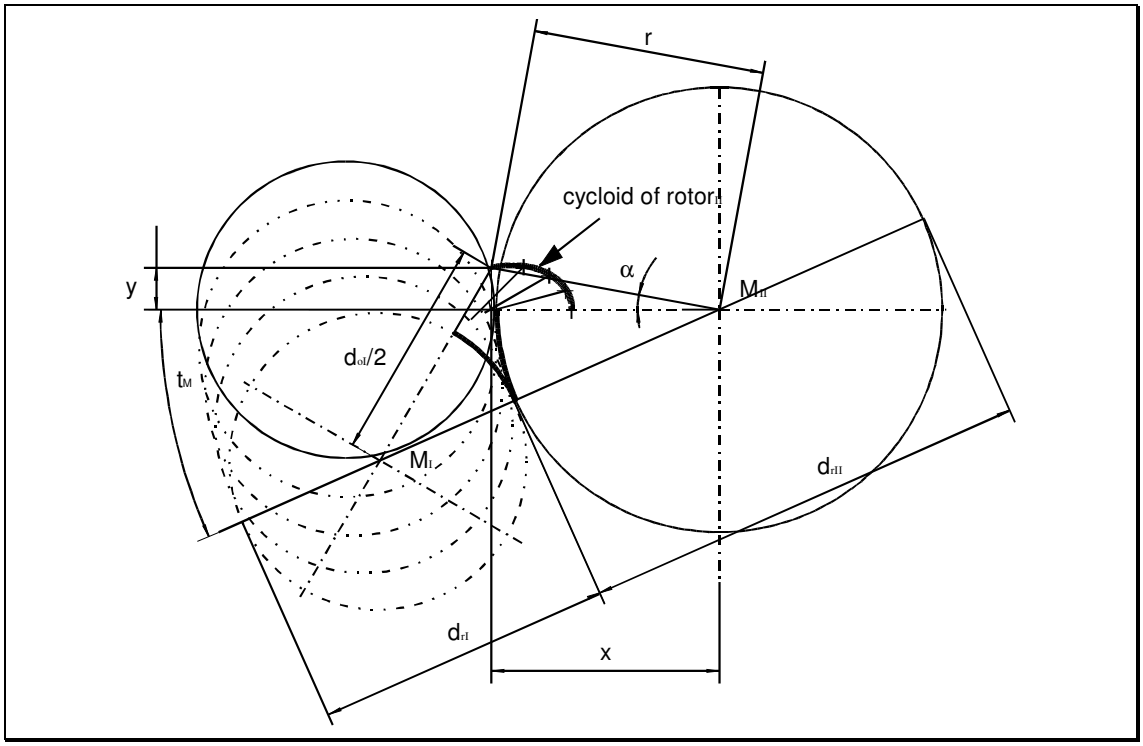


*Figure 96 Theoretical cycloid of rotor$_{II}$*

Again the cycloid can be described using either parameter form or polar coordinates. The parameter form is as follows:

$$x(t_M) = a\cos\left(\frac{d_{rII}}{d_{rI}}t_M\right) - \frac{d_{oI}}{2}\cos\left(\frac{2a}{d_{rI}}t_M\right) = \frac{d_{oII}}{2}\left[(1+\varepsilon)\cos\left(\frac{1}{\varepsilon}t_M\right) - \varepsilon\cos\left(\left(\frac{1}{\varepsilon}+1\right)t_M\right)\right]$$

$$y(t_M) = a\sin\left(\frac{d_{rII}}{d_{rI}}t_M\right) - \frac{d_{oI}}{2}\sin\left(\frac{2a}{d_{rI}}t_M\right) = \frac{d_{oII}}{2}\left[(1+\varepsilon)\sin\left(\frac{1}{\varepsilon}t_M\right) - \varepsilon\sin\left(\left(\frac{1}{\varepsilon}+1\right)t_M\right)\right]$$

For the polar coordinates, the angular coordinate can be directly related to the radius coordinate. Inversely a direct mathematical relation of the radius coordinate to the angular coordinate is not possible :

$$\alpha(r_{II}) = \arccos\left(\frac{4a^2 + 4r_{II}^2 - d_{oI}^2}{4a2r_{II}}\right) - \nu\arccos\left(\frac{4a^2 + d_{oI}^2 - 4r_{II}^2}{4ad_{oI}}\right)$$

# Appendix C - Description of cycloids with a corrected profile

In order to describe the corrected profile, the same mathematical equations as for the theoretical profile are used. However, due to manufacturing reasons as described by Ryazantsev /53/ the sharp edge at the root of the cycloid has to be avoided. In order to do this, the third method described by Ryazantsev /53/ is applied. (See also section 6.1.1 "Montelius screw profiles" page 41) The rotor$_{II}$ chamfer is formed by the arc of a circle while the profile of the driven rotor is an equidistant simple epicycloid described by the centre of this circle.

Because of the chamfer radius, the rolling diameter is not restricted to the outer diameter of rotor$_{II}$ respectively the root diameter of rotor$_{I}$. The rolling diameter of rotor$_{II}$ can be up to $0.9d_{ch}$ smaller than the actual outer diameter.

## The corrected cycloid of rotor$_{I}$

The rolling diameter $d_{rII}$ of rotor$_{II}$ rolls on rolling diameter $d_{rI}$ of rotor$_{I}$ and a circle with the radius $d_{rII}$ - $d_{ch}$ describes the cycloid of the centre of the chamfer circle. An equidistant then describes the profile of rotor$_{I}$.

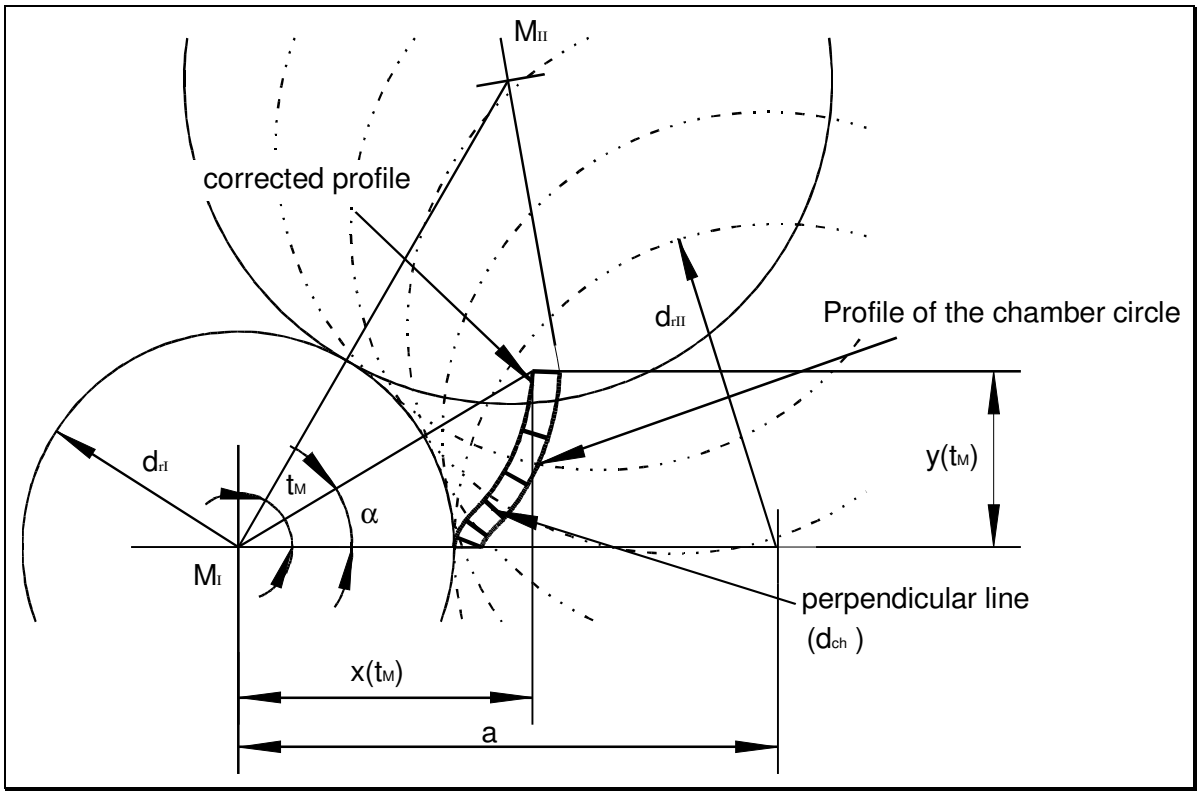


*Figure 97 Corrected cycloid of rotor$_{I}$*

The equations for the coordinates of the corrected profile can only be presented in the parameter form. *f* is the factor of the offset of the rolling diameters with the maximum value 0.9.

$$x(t_M) = (d_{oII} - fd_{ch})\frac{1+\varepsilon}{2}\cos\left(\frac{1}{\varepsilon}t_M\right) - \left(\frac{d_{oII}}{2} - \frac{d_{ch}}{2}\right)\cos\left(\left(\frac{1}{\varepsilon}+1\right)t_M\right) - \frac{d_{ch}}{2}\cos\alpha_n$$

$$y(t_M) = (d_{oII} - fd_{ch})\frac{1+\varepsilon}{2}\sin\left(\frac{1}{\varepsilon}t_M\right) - \left(\frac{d_{oII}}{2} - \frac{d_{ch}}{2}\right)\sin\left(\left(\frac{1}{\varepsilon}+1\right)t_M\right) - \frac{d_{ch}}{2}\sin\alpha_n$$

with $\alpha_n = \arctan(y_n/x_n)$, which is the gradient of the perpendicular. The values of $x_n$ and $y_n$ can be calculated as follows:

$$x_n(t_M) = -(d_{oII} - fd_{ch})\frac{1+\varepsilon}{2\varepsilon}\sin\left(\frac{1}{\varepsilon}t_M\right) + \left(\frac{d_{oII}}{2} - \frac{d_{ch}}{2}\right)\cdot\left(\frac{1}{\varepsilon}+1\right)\sin\left(\left(\frac{1}{\varepsilon}+1\right)t_M\right)$$

$$y_n(t_M) = -(d_{oII} - fd_{ch})\frac{1+\varepsilon}{2\varepsilon}\cos\left(\frac{1}{\varepsilon}t_M\right) + \left(\frac{d_{oII}}{2} - \frac{d_{ch}}{2}\right)\cdot\left(\frac{1}{\varepsilon}+1\right)\cos\left(\left(\frac{1}{\varepsilon}+1\right)t_M\right)$$

the polar coordinates can be determined as a function of the parameter form :

$$r(t_M) = \sqrt{x^2(t_M) + y^2(t_M)}$$

$$\alpha_I(t_M) = \arctan\left(\frac{y(t_M)}{x(t_M)}\right)$$

The profile angle $\beta_{II}$ for $\alpha(d_{oI})$ can not be calculated directly. Hence it is necessary to determine $\alpha$ related to the parameter *t* for $r(t_M) = d_{oI}/2$. This has to be done by iteration for $t_{doI}$ in order to fulfil the following condition:

$$\sqrt{x^2(t_M) + y^2(t_M)} = \frac{d_{oI}}{2}$$

## The corrected cycloid of $rotor_{II}$

The corrected cycloid of $rotor_{II}$ is the identical to the theoretical cycloid except for the chamfer radius.

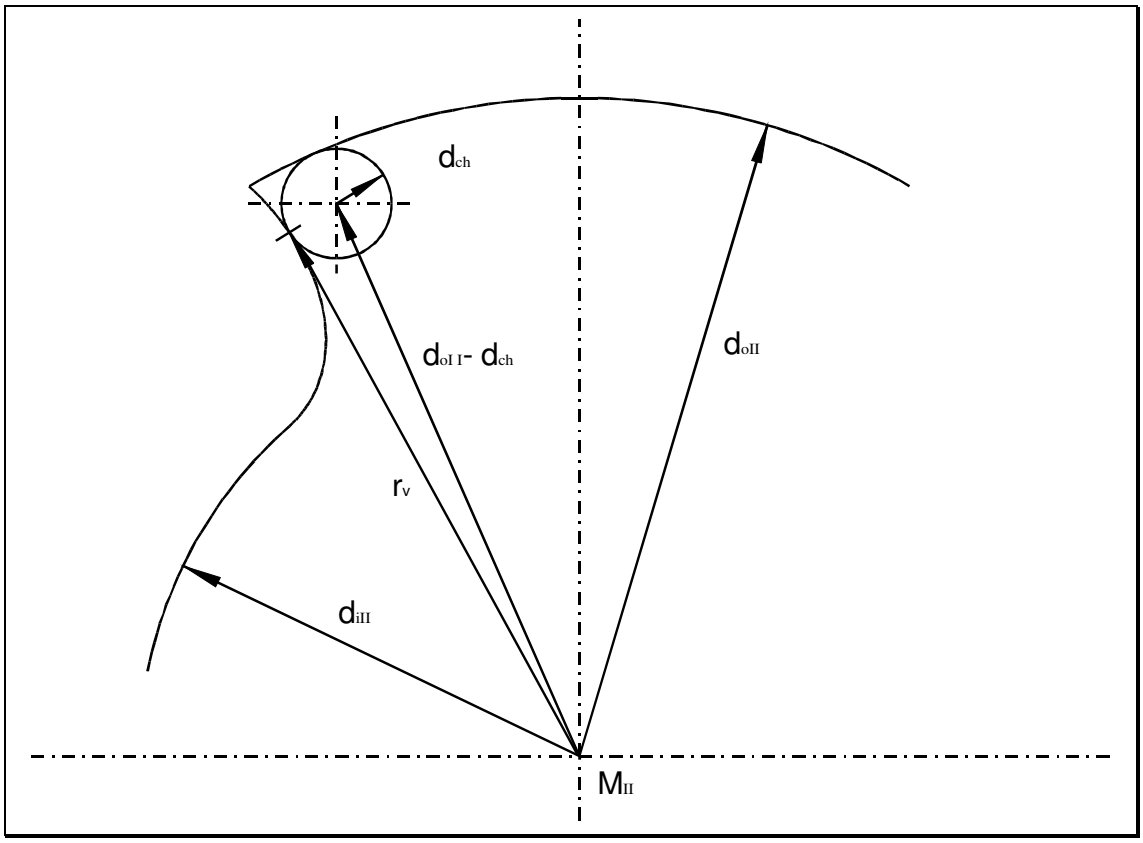


*Figure 98 Corrected cycloid of $rotor_{II}$*

For further calculations, for example the determination of the cross section, it is important to know the point of transition from cycloid to the chamfer circle. In order to determine this transition point with the radius coordinate $r_v$, the gradient of the cycloid may be compared with the gradient of the chamfer circle.

# Appendix D - Calculation of fluid area of the theoretical profile

The fluid area of the helical screw flowmeter is the area of the eight shape bore less the sectional areas of the rotors. (see section 6.5 "Theoretical flow rate" page 55). The areas of all three sections have to be determined separately.

## Calculation of the cross section of the bore

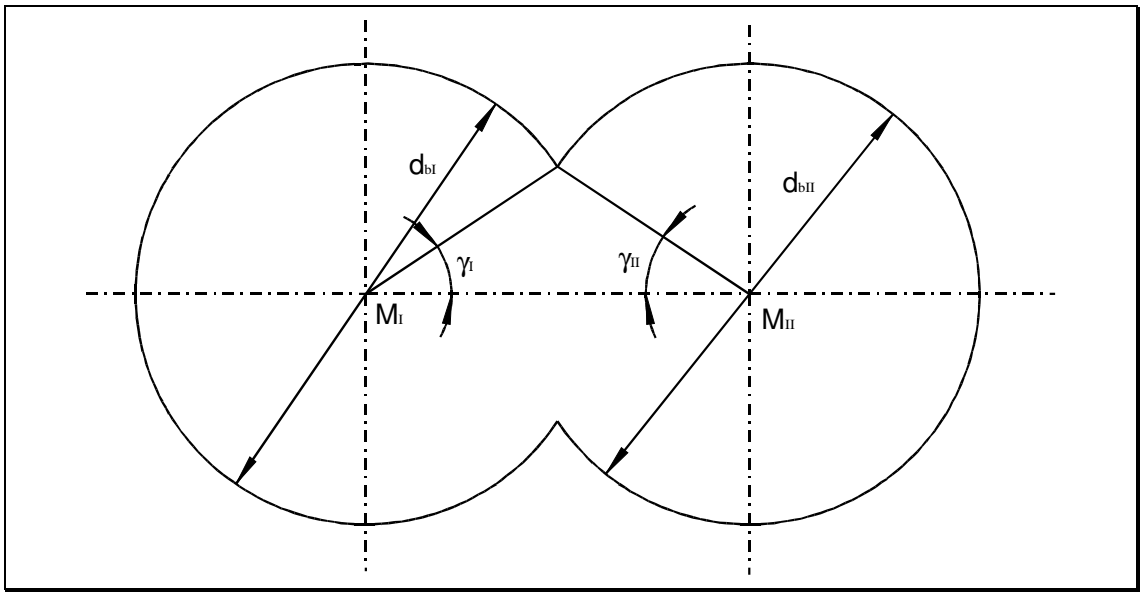


*Figure 99 Section of the bore*

The area of the cross section of the bore is related to the areas of the two single bores minus the overlapping section:

$$A_b = \frac{\pi}{4} d_{bI}^2 - \frac{1}{8} d_{bI}^2 \left(2\gamma_I - \sin\left(2\gamma_I\right)\right) + \frac{\pi}{4} d_{bII}^2 - \frac{1}{8} d_{bII}^2 \left(2\gamma_{II} - \sin\left(2\gamma_{II}\right)\right)$$

## Calculation of the cross section of rotor$_I$

In order to obtain the area of the section of rotor$_I$ the area of this rotor is separated into three single areas as shown in Figure 100. This is the inner area $A_1$, the profile section $A_2$ and the outer diameter area $A_3$.

$$A_I = A_1 + A_2 + A_3$$

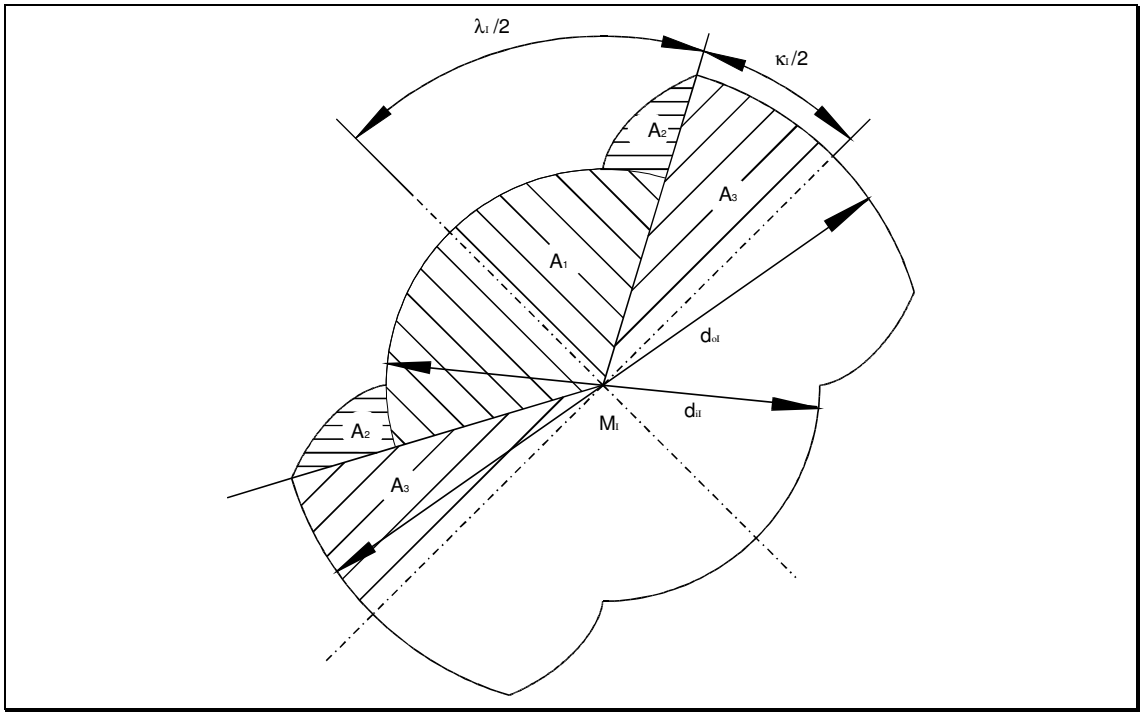


*Figure 100 Section of rotor$_I$ theoretical profile*

The inner area $A_1$ is a segment of a circle which is described by the diameter $d_{iI}$ and the centre angle $\lambda$:

$$A_1 = \frac{d_{iI}^2}{8} \cdot \lambda_I m_I$$

The profile area $A_2$ is the integral of the profile cycloid in polar coordinates from the root to the circumference.:

$$A_2 = 2m_I \int_{\frac{d_{iI}}{2}}^{\frac{d_{oI}}{2}} \left\{ r_I \times \left[ \beta_I - \frac{1}{\varepsilon} \arccos\left( \frac{4a^2 + d_{oII}^2 - 4r_I^2}{4ad_{oII}} \right) - \arccos\left( \frac{4a^2 - d_{oII}^2 + 4r_I^2}{4a2r_I} \right) \right] \right\} dr$$

The outer diameter area $A_3$ is a segment of a circle which is described by the diameter $d_{oI}$ and the centre angle $\kappa$:

$$A_3 = \frac{d_{oI}^2}{8} \kappa_I m_I$$

## Calculation of the cross section of rotor$_{II}$

The area $A_{II}$ of rotor$_{II}$ is separated into three single areas. They are shown in Figure 101. This is again the root section $A_1$, the profile section $A_2$ and the outer diameter section $A_3$.

$$A_{II} = A_1 + A_2 + A_3$$

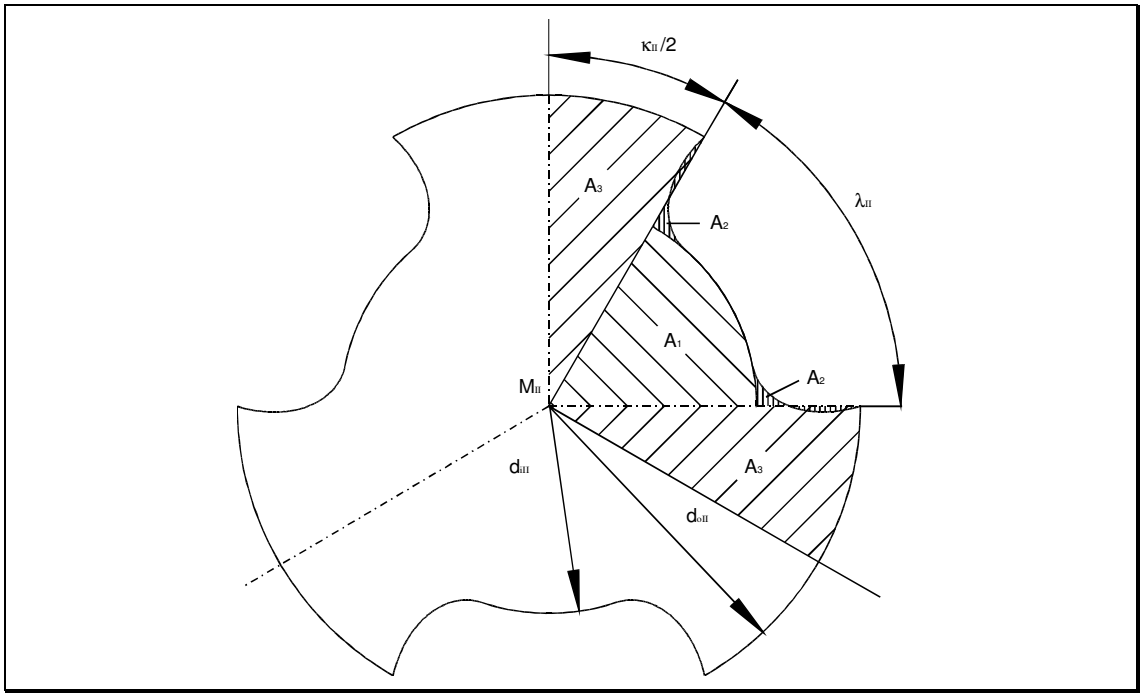


*Figure 101 Section of rotor$_{II}$ theoretical profile*

The inner area $A_1$ is a segment of a circle which is described by the diameter $d_{iII}$ and the centre angle $\lambda$:

$$A_1 = \frac{d_{iII}^2}{8}\lambda_I m_{II}$$

The profile area $A_2$ is the integral of the profile cycloid in polar coordinates from the root to the circumference.:

$$A_2 = 2m_{II}\int_{\frac{d_{iII}}{2}}^{\frac{d_{oII}}{2}}\left\{r_{II}\times\left[\beta_{II} - \arccos\left(\frac{4a^2 + 4r_{II}^2 - d_{oI}^2}{4a2r_{II}}\right) - \nu\arccos\left(\frac{4a^2 + d_{oI}^2 - 4r_{II}^2}{4ad_{oI}}\right)\right]\right\}dr_{II}$$

The outer diameter area $A_3$ is a segment of a circle which is described by the diameter $d_{oII}$ and the centre angle $\kappa$:

$$A_3 = \frac{d_{oII}^2}{8}\kappa_{II} m_{II}$$

# Appendix E - Calculation of hydraulic loads

In the following the program library of the author used to calculate the hydraulic loads is listed. All equations in this library have been deduced using the logic described in section 7.2 "Theory" of chapter 7 "Hydraulic forces and torques on the rotors". The "/*" and "*/" signs indicate the start respectively end of comments. The functions return the dimensionless value which is needed to calculate the projected length as defined in section 7.2.2 "Radial load" on page 61. The input variables are the angular length $\psi$ coordinate of the section and the profile described by the ratio $\varepsilon$ of starts and ratio $r$ of outer diameters.

The following library functions have been defined:

rotor2_fx dimensionless projected length for force in radial X-direction of $rotor_{II}$

rotor2_fy dimensionless projected length for force in radial Y-direction of $rotor_{II}$

rotor2_t dimensionless projected area for torque on $rotor_{II}$

rotor1_fx dimensionless projected length for force in radial X-direction of $rotor_{I}$

rotor1_fy dimensionless projected length for force in radial Y-direction of $rotor_{I}$

rotor1_t dimensionless projected area for torque on $rotor_{I}$

```
/********* Function dimensionless projected length for force in radial X-direction of rotorII *********/
double rotor2_fx(psi, eps, r)
double psi, eps, r;
/********* Variables *********/
/*********  only one chamber; psi = 0 is the start of the chamber *********/
/*********  daI  =    outer diameter of rotor1  *********/
/*********  daII  =   outer diameter of rotor2 *********/
/*********  eps  =     ratio of number of starts       mI/mII          *********/
/*********  r  =      ratio of outer diameters       *********/
{
double betaII, kII, mII, t, fx, a, gammaI, gammaII;
/**********    Calculation    **********/
mII = 1.0/(1.0 - eps);
a = 1.0 + eps;
gammaI = acos((pow(a,2.0) + pow(r,2.0) - 1.0)/(2.0*a*r));
gammaII = acos((pow(a,2.0) - pow(r,2.0) + 1.0)/(2.0*a));
betaII = gammaII - (eps * gammaI);
kII = ((2.0*PI)/mII) - gammaII - betaII;
t = (2.0*PI) + gammaII - betaII;
fx = 0.0;
/*********  engagement position 1     - H < psi <  - G  *********/
if (0.0<psi && psi<gammaII - betaII)
fx = r*(sin(psi/eps) - sin(gammaI - (psi/eps))) - sin(psi - gammaII);
/*********  engagement position 2     - G < psi <  - F   *********/
if (gammaII - betaII<psi && psi<gammaII)
 fx =  - sin(psi - gammaII) + sin(psi + (kII/2.0) + betaII);
/*********  engagement position 3     - F < psi <  - D   *********/
```

```
if (gammaII<psi && psi<(2.0*PI/mII) - betaII)
  fx = sin(psi + (kII/2.0) + betaII);
/*********  engagement position 4     - D < psi <  - C   *********/
if ((2.0*PI/mII) - betaII<psi && psi<(2.0*PI/mII) + gammaII - betaII)
  fx = sin(psi + (kII/2.0) + betaII) - sin(psi - (2.0*PI/mII) + betaII);
/*********  engagement position 5a    - C < psi < A    *********/
if ((2.0*PI/mII) + gammaII - betaII<psi && psi<t/2.0)
   fx = sin(psi + (kII/2.0) + betaII) - sin(psi + (kII/2.0) + betaII - (2.0*PI/mII));
/*********  engagement position 5b    A < psi < C    *********/
if (t/2.0<psi && psi<(2.0*PI)*(1.0 - (1.0/mII)))
   fx = sin(t - psi + (kII/2.0) + betaII) - sin(t - psi + (kII/2.0) + betaII - (2.0*PI/mII));
/*********  engagement position 6     C < psi < D    *********/
if ((2.0*PI)*(1.0 - (1.0/mII))<psi && psi<gammaII + (1.0 - (1.0/mII))*(2.0*PI))
  fx = sin(t - psi + (kII/2.0) + betaII) - sin(t - psi + betaII - (2.0*PI/mII));
/*********  engagement position 7     D < psi < F    *********/
if (gammaII + (1.0 - (1.0/mII))*(2.0*PI)<psi && psi<(2.0*PI) - betaII)
  fx = sin(t - psi + (kII/2.0) + betaII);
/*********  engagement position 8     F < psi < G   *********/
if ((2.0*PI) - betaII<psi && psi<(2.0*PI))
  fx =  - sin(t - psi - gammaII) + sin(t - psi + (kII/2.0) + betaII);
/*********  engagement position 9     G < psi < H    *********/
if (2.0*PI<psi && psi<(2.0*PI) + gammaII - betaII)
  fx = r*(sin((t - psi)/eps) - sin(gammaI - ((t - psi)/eps))) - sin(t - psi - gammaII);
if (eps =  = 0.5)
{
fx = 0.0;
/*********  engagement position 1     - H < psi <  - G   *********/
if (0.0<psi && psi<gammaII - betaII)
   fx = r*(sin(psi/eps) - sin(gammaI - (psi/eps))) - sin(psi - gammaII);
/*********  engagement position 2     - G < psi < A   *********/
if (gammaII - betaII<psi && psi<t/2.0)
   fx = fx + sin(psi + (kII/2.0) + betaII);
/*********  engagement position 3     - G < psi <  - F   *********/
if (gammaII - betaII<psi && psi<gammaII)
   fx = fx - sin(psi - gammaII);
/*********  engagement position 4     - D < psi <  - C   *********/
if ((2.0*PI/mII) - betaII<psi && psi<(2.0*PI/mII) + gammaII - betaII)
  fx = fx - sin(psi - (2.0*PI/mII) + betaII);
/*********  engagement position 5a    - C < psi < A    *********/
if ((2.0*PI/mII) + gammaII - betaII<psi && psi<t/2.0)
   fx = fx - sin(psi + (kII/2.0) + betaII - (2.0*PI/mII));
/*********  engagement position 5c    C < psi >  - C   *********/
/*********if ((1.0 - (1.0/mII))*(2.0*PI)<psi && psi<(2.0*PI/mII) + gammaII - betaII) *********/
*********fx = fx + 1.0;*********/
/*********  engagement position 5b    A < psi < C   *********/
if (t/2.0<psi && psi<(2.0*PI)*(1.0 - (1.0/mII)))
   fx = fx - sin(t - psi + (kII/2.0) + betaII - (2.0*PI/mII));
/*********  engagement position 6     C < psi < D C   *********/
if ((2.0*PI)*(1.0 - (1.0/mII))<psi && psi<gammaII + (1.0 - (1.0/mII))*(2.0*PI))
  fx = fx - sin(t - psi + betaII - (2.0*PI/mII));
/*********  engagement position 7     F < psi < G C   *********/
if ((2.0*PI) - betaII<psi && psi<(2.0*PI))
  fx = fx - sin(t - psi - gammaII);
/*********  engagement position 8     A < psi < G C    *********/
if (t/2.0<psi && psi<(2.0*PI))
  fx = fx + sin(t - psi + (kII/2.0) + betaII);
/*********  engagement position 9     G < psi < H   *********/
```

```
if (2.0*PI<psi && psi<(2.0*PI) + gammaII - betaII)
  fx = r*(sin((t - psi)/eps) - sin(gammaI - ((t - psi)/eps))) - sin(t - psi - gammaII);
  }
return (fx);
}

/********* Function dimensionless projected length for force in radial Y-direction of rotor_II *********/
double rotor2_fy(psi, eps, r)
double psi, eps, r;
/*********  Variables *********/
/*********  only one chamber; psi = 0 is the start of the chamber *********/
/*********  daI  =   outer diameter of rotor1  *********/
/*********  daII  =  outer diameter of rotor2 *********/
/*********  eps  =    ratio of number of starts      mI/mII         *********/
/*********  r  =     ratio of outer diameters       *********/
{
double betaII, kII, mII, t, fy, a, gammaI, gammaII;
/**********    Calculation    **********/
mII = 1.0/(1.0 - eps);
a = 1.0 + eps;
gammaI = acos((pow(a,2.0) + pow(r,2.0) - 1.0)/(2.0*a*r));
gammaII = acos((pow(a,2.0) - pow(r,2.0) + 1.0)/(2.0*a));
betaII = gammaII - (eps * gammaI);
kII = ((2.0*PI)/mII) - gammaII - betaII;
t = (2.0*PI) + gammaII - betaII;
fy = 0.0;
/*********  engagement position 1     - H < psi <  - G   *********/
if (0.0<psi && psi<gammaII - betaII)
   fy = r + a - r*(cos(psi/eps) + cos(gammaI - (psi/eps))) - cos(psi - gammaII);
/*********  engagement position 2     - G < psi <  - F   *********/
if (gammaII - betaII<psi && psi<gammaII)
   fy =  - cos(psi - gammaII) + 1.0 + cos(psi + betaII + (kII/2.0)) - 1.0;
/*********  engagement position 3     - F < psi <  - D   *********/
if (gammaII<psi && psi<(2.0*PI/mII) - betaII)
   fy = cos(psi + betaII + (kII/2.0)) - 1.0;
/*********  engagement position 4     - D < psi <  - C   *********/
if ((2.0*PI/mII) - betaII<psi && psi<(2.0*PI/mII) + gammaII - betaII)
   fy = cos(psi + betaII + (kII/2.0)) - 1.0 - cos(psi - (2.0*PI/mII) + betaII) + 1.0;
/*********  engagement position 5a    - C < psi < A    *********/
if ((2.0*PI/mII) + gammaII - betaII<psi && psi<PI + (gammaII/2.0) - (betaII/2.0))
   fy = cos(psi + betaII + (kII/2.0)) - 1.0 - cos(psi + betaII + (kII/2.0) - (2.0*PI/mII)) + 1.0;
/*********  engagement position 5b   A < psi < C     *********/
if (PI + (gammaII/2.0) - (betaII/2.0)<psi && psi<(2.0*PI)*(1.0 - (1.0/mII)))
   fy =  - (cos(t - psi + betaII + (kII/2.0)) - 1.0 - cos(t - psi + (betaII + kII/2.0) - (2.0*PI/mII)) + 1.0);
/*********  engagement position 6    C < psi < D     *********/
if ((2.0*PI)*(1.0 - (1.0/mII))<psi && psi<gammaII + (1.0 - (1.0/mII))*(2.0*PI))
   fy =  - (cos(t - psi + betaII + (kII/2.0)) - 1.0 - cos(t - psi - (2.0*PI/mII) + betaII) + 1.0);
/*********  engagement position 7    D < psi < F     *********/
if (gammaII + (1.0 - (1.0/mII))*(2.0*PI)<psi && psi<(2.0*PI) - betaII)
   fy =  - (cos(t - psi + betaII + (kII/2.0)) - 1.0);
/*********  engagement position 8    F < psi < G     *********/
if ((2.0*PI) - betaII<psi && psi<(2.0*PI))
   fy =  - ( - cos(t - psi - gammaII) + 1.0 + cos(t - psi + betaII + (kII/2.0)) - 1.0);
/*********  engagement position 9    G < psi < H     *********/
if (2.0*PI<psi && psi<(2.0*PI) + gammaII - betaII)
   fy =  - (r + a - r*(cos((t - psi)/eps) + cos(gammaI - ((t - psi)/eps))) - cos(t - psi - gammaII));
if(eps =  = 0.5)
```

```
{
fy = 0.0;
/*********  engagement position 1     - H < psi <  - G   *********/
if (0.0<psi && psi<gammaII - betaII)
   fy = r + a - r*(cos(psi/eps) + cos(gammaI - (psi/eps))) - cos(psi - gammaII);
/*********  engagement position 2     - G < psi <  - F   *********/
if (gammaII - betaII<psi && psi<gammaII)
   fy = fy - cos(psi - gammaII) + 1.0;
/*********  engagement position 3b     - G < psi <  - A   *********/
if (gammaII - betaII<psi && psi<t/2.0)
   fy = fy + cos(psi + betaII + (kII/2.0)) - 1.0;
/*********  engagement position 4     - D < psi <  - C   *********/
if ((2.0*PI/mII) - betaII<psi && psi<(2.0*PI/mII) + gammaII - betaII)
   {
   if (psi<t/2.0)
   fy = fy + ( - cos(psi - (2.0*PI/mII) + betaII) + 1.0);
   if (psi>t/2.0)
   fy = fy + ( - cos(t - psi - (2.0*PI/mII) + betaII) + 1.0);
   }
/*********  engagement position 5a    - C < psi < A    *********/
if ((2.0*PI/mII) + gammaII - betaII<psi && psi<PI + (gammaII/2.0) - (betaII/2.0))
   fy = fy - cos(psi + betaII + (kII/2.0) - (2.0*PI/mII)) + 1.0;
/*********  engagement position 5c    A < psi <  - C    *********/
if (PI + (gammaII/2.0) - (betaII/2.0)<psi && psi<(2.0*PI/mII) + gammaII - betaII)
   fy = fy - ( - cos(t - psi + betaII + kII/2.0 - (2.0*PI/mII)) + 1.0);
/*********  engagement position 5d   C < psi < A     *********/
if ((2.0*PI)*(1.0 - (1.0/mII))<psi && psi<t/2.0)
   fy = fy + ( - cos(psi + betaII + (kII/2.0) - (2.0*PI/mII)) + 1.0);
/*********  engagement position 5b   A < psi < C     *********/
if (t/2.0<psi && psi<(2.0*PI)*(1.0 - (1.0/mII)))
   fy = fy - ( - cos(t - psi + (betaII + kII/2.0) - (2.0*PI/mII)) + 1.0);
/*********  engagement position 6    C < psi < D     *********/
if ((2.0*PI)*(1.0 - (1.0/mII))<psi && psi<gammaII + (1.0 - (1.0/mII))*(2.0*PI))
   {
   if (psi>t/2.0)
   fy = fy - ( - cos(t - psi - (2.0*PI/mII) + betaII) + 1.0);
   if (psi<t/2.0)
   fy = fy - ( - cos(psi - (2.0*PI/mII) + betaII) + 1.0);
   }
/*********  engagement position 7    D < psi < F     *********/
/*********if (gammaII + (1.0 - (1.0/mII))*(2.0*PI)<psi && psi<(2.0*PI) - betaII)*********/
   /*********fy = fy + 1.0;*********/
/*********  engagement position 7b   A < psi < G     *********/
if  (t/2.0<psi && psi<(2.0*PI))
   fy = fy - (cos(t - psi + betaII + (kII/2.0)) - 1.0);
/*********  engagement position 8    F < psi < G     *********/
if ((2.0*PI) - betaII<psi && psi<(2.0*PI))
   fy = fy - ( - cos(t - psi - gammaII) + 1.0);
/*********  engagement position 9    G < psi < H     *********/
if (2.0*PI<psi && psi<(2.0*PI) + gammaII - betaII)
   fy =  - (r + a - r*(cos((t - psi)/eps) + cos(gammaI - ((t - psi)/eps))) - cos(t - psi - gammaII));
}
return (fy);
}
/********* Function dimensionless projected area for torque on rotor_II *********/
double rotor2_t(psi, eps, r)
double psi, eps, r;
```

```
/*********  Variables *********/
/*********  only one chamber; psi = 0 is the start of the chamber *********/
/*********  daI =    outer diameter of rotor1  *********/
/*********  daII =   outer diameter of rotor2 *********/
/*********  eps =     ratio of number of starts       mI/mII          *********/
/*********  r =      ratio of outer diameters       *********/
{
double gammaI, gammaII, kII, a, t, mII, betaII, mt;
/**********    Calculation     **********/
mII = 1.0/(1.0 - eps);
a = 1.0 + eps;
gammaI = acos((pow(a,2.0) + pow(r,2.0) - 1.0)/(2.0*a*r));
gammaII = acos((pow(a,2.0) - pow(r,2.0) + 1.0)/(2.0*a));
betaII = gammaII - (eps  * gammaI);
kII = ((2.0*PI)/mII) - gammaII - betaII;
t = (2.0*PI) + gammaII - betaII;
mt = 0.0;
/*********  engagement position 1     - H < psi <  - G    *********/
if (0.0<psi && psi<gammaII - betaII)
   {
mt = 0.5*pow((r * sin(psi/eps)),2.0);
mt = mt - (( - sin(psi - gammaII) - r * sin(gammaI - (psi/eps)))*0.5*( - sin(psi - gammaII) + r * sin(gammaI
- (psi/eps))));
mt = mt + r*(1.0 - cos(psi/eps))*(a - 0.5*r*(1.0 - cos(psi/eps)));
mt = mt + (a - r * cos(gammaI - (psi/eps)) - cos(gammaII - psi))*(cos(gammaII - psi) - 0.5*(a - r *
cos(gammaI - (psi/eps)) - cos(gammaII - psi)));
}
/*********  engagement position 2 to engagement position 8    - G < psi < G   *********/
if (gammaII - betaII<psi && psi<2.0*PI)
  mt = 0.0;
/*********  engagement position 9    G < psi < H     *********/
if (2.0*PI<psi && psi<(2.0*PI) + gammaII - betaII)
   {
 psi = t - psi;
mt = 0.5*pow((r * sin(psi/eps)),2.0);
 mt = mt - (( - sin(psi - gammaII) - r * sin(gammaI - (psi/eps)))*0.5*( - sin(psi - gammaII) + r *
sin(gammaI - (psi/eps))));
 mt = mt + r*(1.0 - cos(psi/eps))*(a - 0.5*r*(1.0 - cos(psi/eps)));
 mt = mt + (a - r * cos(gammaI - (psi/eps)) - cos(gammaII - psi))*(cos(gammaII - psi) - 0.5*(a - r *
cos(gammaI - (psi/eps)) - cos(gammaII - psi)));
 mt =  - mt;
 psi = t - psi;
   }
return (mt);
}
/********* Function dimensionless projected length for force in radial X-direction of rotor_I *********/
double rotor1_fx(psi, eps, r)
double psi, eps, r;
/*********  Variables *********/
/*********  only one chamber; psi = 0 is the start of the chamber *********/
/*********  daI =    outer diameter of rotor1  *********/
/*********  daII =   outer diameter of rotor2 *********/
/*********  eps =     ratio of number of starts       mI/mII          *********/
/*********  r =      ratio of outer diameters       *********/
{
double kII, fx, gammaI, gammaII, t, mI, mII, betaII, a;
/**********     Calculation     **********/
```

```
mII = 1.0/(1.0 - eps);
mI = eps/(1.0 - eps);
a = 1.0 + eps;
gammaI = acos((pow(a,2.0) + pow(r,2.0) - 1.0)/(2.0*a*r));
gammaII = acos((pow(a,2.0) - pow(r,2.0) + 1.0)/(2.0*a));
betaII = gammaII - (eps * gammaI);
kII = ((2.0*PI)/mII) - gammaII - betaII;
t = (2.0*PI) + gammaII - betaII;
fx = 0.0;
/*********  engagement position 1     - H < psi <  - G    *********/
if (0.0<psi && psi<gammaII - betaII)
   fx =  - r*(sin(psi/eps) - sin(gammaI - (psi/eps))) + sin(psi - gammaII);
/*********  engagement position 2     - G < psi <  - F    *********/
if (gammaII - betaII<psi && psi<gammaII)
   fx = sin(psi - gammaII) - r*(sin(0.5*((psi/eps) + gammaI)));
/*********  engagement position 3a    - F < psi <  - E    *********/
if (gammaII<psi && psi<2.0*(gammaII - betaII))
  fx =  - r*(sin(0.5*((psi/eps) + gammaI)));
/*********  engagement position 3b    - E < psi <  - D    *********/
if (2.0*(gammaII - betaII)<psi && psi<(2.0*PI/mII) - betaII)
  fx =  - r * sin((psi/eps) - (0.5*gammaI));
/*********  engagement position 4     - D < psi <  - C    *********/
if ((2.0*PI/mII) - betaII<psi && psi<(2.0*PI/mII) + gammaII - betaII)
  fx = sin(psi + betaII - (2.0*PI/mII)) - r * sin((psi/eps) - (0.5*gammaI));
/*********  engagement position 5c    - C < psi <  - B    *********/
if ((2.0*PI/mII) + gammaII - betaII<psi && psi<2.0*((PI/mII) + gammaII - betaII))
   fx =  - r * sin((psi/eps) - (0.5*gammaI)) + r * sin(0.5*((psi/eps) - ((2.0*PI)/mI) + gammaI));
/*********  engagement position 5d    - B < psi < A     *********/
if (2.0*((PI/mII) + gammaII - betaII)<psi && psi<PI + (gammaII/2.0) - (betaII/2.0))
   fx =  - r * sin((psi/eps) - (0.5*gammaI)) + r * sin((psi/eps) - (0.5*gammaI) - ((2.0*PI)/mI));
/*********  engagement position 5e    A < psi < B     *********/
if (PI + (gammaII/2.0) - (betaII/2.0)<psi && psi<(1.0 - (1.0/mII))*2.0*PI - gammaII + betaII)
   fx =  - r * sin(((t - psi)/eps) - (0.5*gammaI)) + r * sin(((t - psi)/eps) - (0.5*gammaI) - ((2.0*PI)/mI));
/*********  engagement position 5f    B < psi < C     *********/
if ((1.0 - (1.0/mII))*2.0*PI - gammaII + betaII<psi && psi<(1.0 - (1.0/mII))*2.0*PI)
   fx =  - r * sin(((t - psi)/eps) - (0.5*gammaI)) + r * sin(0.5*(((t - psi)/eps) - ((2.0*PI)/mI) + gammaI));
/*********  engagement position 6     C < psi < D     *********/
if ((1.0 - (1.0/mII))*2.0*PI<psi && psi<(1.0 - (1.0/mII))*2.0*PI + gammaII)
  fx =  - r * sin(((t - psi)/eps) - (0.5*gammaI)) + sin(t - psi + betaII - (2.0*PI/mII));
/*********  engagement position 7a    D < psi < E     *********/
if ((1.0 - (1.0/mII))*2.0*PI + gammaII<psi && psi<(2.0*PI) - gammaII + betaII)
  fx =  - r * sin(((t - psi)/eps) - (0.5*gammaI));
/*********  engagement position 7b    E < psi < F     *********/
if ((2.0*PI) - gammaII + betaII<psi && psi<(2.0*PI) - betaII)
  fx =  - r * sin(0.5*(((t - psi)/eps) + gammaI));
/*********  engagement position 8     F < psi < G     *********/
if ((2.0*PI) - betaII<psi && psi<2.0*PI)
  fx =  - r * sin(0.5*((t - psi)/eps + gammaI)) + sin(t - psi - gammaII);
/*********  engagement position 9     G < psi < H     *********/
if (2.0*PI<psi && psi<(2.0*PI) + gammaII - betaII)
  fx =  - r * sin(((t - psi)/eps) - sin(gammaI - ((t - psi)/eps))) + sin(t - psi - gammaII);
return (fx);
}
/********* Function dimensionless projected length for force in radial Y-direction of rotor_I *********/
double rotor1_fy(psi, eps, r)
double psi, eps, r;
/*********  Variables *********/
```

```
/*********  only one chamber; psi = 0 is the start of the chamber *********/
/*********  daI  =    outer diameter of rotor1  *********/
/*********  daII  =   outer diameter of rotor2 *********/
/*********  eps  =     ratio of number of starts       mI/mII          *********/
/*********  r  =      ratio of outer diameters       *********/
{
double kII, fy, gammaI, gammaII, t, mI, mII, betaII, a;
/**********     Calculation     **********/
mII = 1.0/(1.0 - eps);
mI = eps/(1.0 - eps);
a = 1.0 + eps;
gammaI = acos((pow(a,2.0) + pow(r,2.0) - 1.0)/(2.0*a*r));
gammaII = acos((pow(a,2.0) - pow(r,2.0) + 1.0)/(2.0*a));
betaII = gammaII - (eps * gammaI);
kII = ((2.0*PI)/mII) - gammaII - betaII;
t = (2.0*PI) + gammaII - betaII;
fy = 0.0;
/*********  engagement position 1      - H < psi <  - G     *********/
if (0.0<psi && psi<gammaII - betaII)
   fy =  - (r + a - r*(cos(psi/eps) + cos(gammaI - (psi/eps))) - cos(psi - gammaII));
/*********  engagement position 2      - G < psi <  - F     *********/
if (gammaII - betaII<psi && psi<gammaII)
   fy =  - a + cos(psi - gammaII) + (r * cos(0.5*((psi/eps) + gammaI)));
/*********  engagement position 3a     - F < psi <  - G     *********/
if (gammaII<psi && psi<2.0*(gammaII - betaII))
  fy =  - eps + (r * cos(0.5*((psi/eps) + gammaI)));
/*********  engagement position 3b     - E < psi <  - D     *********/
if (2.0*(gammaII - betaII)<psi && psi<2.0*(PI/mII) - betaII)
  fy =  - eps + (r * cos((psi/eps) - (gammaI/2.0)));
/*********  engagement position 4      - D < psi <  - C     *********/
if ((2.0*PI/mII) - betaII<psi && psi<(2.0*PI/mII) + gammaII - betaII)
   fy =  - a + (r * cos((psi/eps) - (gammaI/2.0))) + cos(psi + betaII - (2.0*PI/mII));
/*********  engagement position 5c     - C < psi <  - B     *********/
if ((2.0*PI/mII) + gammaII - betaII<psi && psi<2.0*((PI/mII) + gammaII - betaII))
   fy = r * cos((psi/eps) - (gammaI/2.0)) - (r * cos(0.5*((psi/eps) - (2.0*PI/mI) + gammaI)));
/*********  engagement position 5d     - B < psi < A      *********/
if (2.0*((PI/mII) + gammaII - betaII)<psi && psi<PI + (gammaII/2.0) - (betaII/2.0))
   fy = r * cos((psi/eps) - (gammaI/2.0)) - (r * cos((psi/eps) - (2.0*PI/mI) - (gammaI/2.0)));
/*********  engagement position 5e     A < psi < B      *********/
if (PI + (gammaII/2.0) - (betaII/2.0)<psi && psi<(1.0 - (1.0/mII))*2.0*PI - gammaII + betaII)
   fy =  - (r * cos(((t - psi)/eps) - (gammaI/2.0)) - (r * cos(((t - psi)/eps) - (2.0*PI/mI) - (gammaI/2.0))));
/*********  engagement position 5f     B < psi < C      *********/
if ((1.0 - (1.0/mII))*2.0*PI - gammaII + betaII<psi && psi<(1.0 - (1.0/mII))*2.0*PI)
  fy =  - (r * cos(((t - psi)/eps) - (gammaI/2.0)) - (r * cos(0.5*(((t - psi)/eps) - (2.0*PI/mI) + gammaI))));
/*********  engagement position 6      C < psi < D      *********/
if ((1.0 - (1.0/mII))*2.0*PI<psi && psi<(1.0 - (1.0/mII))*2.0*PI + gammaII)
  fy =  - ( - a + (r * cos(((t - psi)/eps) - (gammaI/2.0))) + cos(t - psi + betaII - (2.0*PI/mII)));
/*********  engagement position 7a     D < psi < E      *********/
if ((1.0 - (1.0/mII))*2.0*PI + gammaII<psi && psi<(2.0*PI) - gammaII + betaII)
  fy =  - ( - eps + (r * cos(((t - psi)/eps) - (gammaI/2.0))));
/*********  engagement position 7b     E < psi < F      *********/
if ((2.0*PI) - gammaII + betaII<psi && psi<(2.0*PI) - betaII)
  fy =  - ( - eps + (r * cos(0.5*(((t - psi)/eps) + gammaI))));
/*********  engagement position 8      F < psi < G      *********/
if ((2.0*PI) - betaII<psi && psi<2.0*PI)
  fy =  - ( - a + (r * cos(0.5*(((t - psi)/eps) + gammaI))) + cos(t - psi - gammaII));
/*********  engagement position 9      G < psi < H      *********/
```

```
if (2.0*PI<psi && psi<(2.0*PI) + gammaII - betaII)
   fy = (r + a - r*(cos((t - psi)/eps) + cos(gammaI - ((t - psi)/eps))) - cos(t - psi - gammaII));
return (fy);
}
/********* Function dimensionless projected area for torque on rotor_I *********/
double rotor1_t(psi, eps, r)
double psi, eps, r;
/*********  Variables *********/
/*********  only one chamber; psi = 0 is the start of the chamber *********/
/*********  daI  =    outer diameter of rotor1  *********/
/*********  daII  =   outer diameter of rotor2 *********/
/*********  eps  =     ratio of number of starts       mI/mII          *********/
/*********  r  =      ratio of outer diameters       *********/
{
double kII, mt, fx, fy, gammaI, gammaII, mII, betaII, t, a;
/**********       Calculation       **********/
mII = 1.0/(1.0 - eps);
a = 1.0 + eps;
gammaI = acos((pow(a,2.0) + pow(r,2.0) - 1.0)/(2.0*a*r));
gammaII = acos((pow(a,2.0) - pow(r,2.0) + 1.0)/(2.0*a));
betaII = gammaII - (eps * gammaI);
kII = ((2.0*PI)/mII) - gammaII - betaII;
t = (2.0*PI) + gammaII - betaII;
mt = 0.0;
/*********  engagement position 1a     - H < psi <  - F    *********/
if (0.0<psi && psi<gammaII)
   mt = 0.5*(pow(r,2.0) - 1.0 - pow(a,2.0) + (2.0*a*cos(gammaII - psi)));
/*********  engagement position 3      - F < psi <  - D    *********/
if (gammaII<psi && psi<(2.0*PI/mII - betaII))
   mt = 0.5*(pow(r,2.0) - pow(eps,2.0));
/*********  engagement position 4      - D < psi <  - C    *********/
if ((2.0*PI/mII - betaII)<psi && psi<((2.0*PI/mII) + gammaII - betaII))
   mt = 0.5*(pow(r,2.0) - 1.0 - pow(a,2.0) + (2.0*a*cos(psi - (2.0*PI/mII) + betaII)));
/*********  engagement position 6      C < psi < D     *********/
if ((2.0*PI)*(1.0 - (1.0/mII))<psi && psi<gammaII + (1.0 - (1.0/mII))*(2.0*PI))
   mt = mt - 0.5*(pow(r,2.0) - 1.0 - pow(a,2.0) + (2.0*a*cos(t - psi - (2.0*PI/mII) + betaII)));
/*********  engagement position 7      D < psi < F     *********/
if (gammaII + (1.0 - (1.0/mII))*(2.0*PI)<psi && psi <(2.0*PI) - betaII)
   mt =  - 0.5*(pow(r,2.0) - pow(eps,2.0));
/*********  engagement position 8a     F < psi < H     *********/
if ((2.0*PI) - betaII<psi && psi<(2.0*PI) + gammaII - betaII)
   mt =  - 0.5*(pow(r,2.0) - 1.0 - pow(a,2.0) + (2.0*a*cos(gammaII - t + psi)));
return (mt);
}
```

# Appendix F - Approximation of a clearance with variable height

For laminar leakage flow Wincek /60/ describes the flow through this clearance with curved borders to:

$$\dot{V}_{SR} = \frac{\Delta p b_R}{12\eta_{fl} \int_{-x_0}^{+x_0} \frac{1}{h_R(x)^3} dx}$$

with the approximation of the radius of curvature of a parabola instead of the circle the function to describe the clearance height related to the two bordering radii is:

$$h_R(x) = h_R + x^2\left(\frac{1}{r_1} + \frac{1}{r_2}\right)$$

Using

$$q = h_R\left(\frac{1}{r_1} + \frac{1}{r_2}\right)^{-1}$$

$$h_R(x) = \left(\frac{1}{r_1} + \frac{1}{r_2}\right)\left(q + x^2\right)$$

the remaining integral $\left(\frac{1}{r_1} + \frac{1}{r2}\right)^{-3} \int_{-½}^{½} \frac{1}{\left(q + x^2\right)^3} dx$ can now be solved analytically to:

$$\int_{-x_0}^{x_0} \frac{1}{\left(q + x^2\right)^3} dx = \frac{x_0}{2q\left(x_0^2 + q\right)^2} + \frac{3}{4q^{5/2}} \arctan\frac{2x_0}{\sqrt{4q}} + \frac{3x_0}{4q^2\left(x_0^2 + q\right)}$$

The influence of the limits of the integral $x_0$ decreases with the increase of the integral length. Solving the integral a substitution length for the clearance can be introduced:

$$\ell_{subst} = 1{,}2\sqrt{\left(\frac{1}{r_1} + \frac{1}{r_2}\right)^{-1}}\, h$$

The flow through a variable height clearance now can then be approximated to:

$$\dot{V}_S = \frac{\Delta p b h^3}{12\eta_{fl}\ell_{subst}} = \frac{\Delta p b h^{5/2}}{14{,}4\eta_{fl}} \sqrt{\left(\frac{1}{r_1} + \frac{1}{r_2}\right)}$$

and hence the maximum velocity in the clearance to:

$$c_S = \frac{\Delta p h^{3/2}}{10\eta_{fl}} \sqrt{\left(\frac{1}{r_1} + \frac{1}{r_2}\right)}$$

# Appendix G - Leakage and viscous friction constant coefficients

The leakage and friction value can be calculated related to a set of constant coefficients. The coefficients are calculated in accordance with section 9.3 "Theory" of chapter 9 "Leakage and viscous friction.

(a) Pressure related leakage through circumference clearance:

$$\dot{V}_{SC} = \Delta p \frac{1}{\eta_{fl}} K_{SC}$$

with:

$$K_{SC} = \frac{1}{6 \tan \phi_{PI}} \left[ h_{CI}^3 \frac{\pi - \gamma_I}{\kappa_I} \left(1 + \tan^2 \phi_{PI}\right) + h_{CII}^3 \frac{\varepsilon}{r} \frac{\left(\pi - \gamma_{II}\right)}{\kappa_{II}} \left(1 + \frac{r^2}{\varepsilon^2} \tan^2 \phi_{PI}\right) \right]$$

(b) Rotational leakage through circumference clearance:

$$\dot{V}_{DC} = d_o^2 \omega_I K_{DC}$$

with the coefficient $K_{DC}$ which is not directly related to the dimensions of the rotors, but only to the manufacturing tolerances:

$$K_{DC} = \frac{1}{8} \left[ h_{CI} \left(\pi - \gamma_I\right) \tan \phi_{PI} + \frac{1}{r} h_{CII} \left(\pi - \gamma_{II}\right) \tan \phi_{PI} \right]$$

(c) Friction torque in circumference clearance

$$T_{UC} = d_o^4 \eta_{fl} \omega_I K_{UC}$$

with:

$$K_{UC} = \tan \phi_{pI} \frac{2\pi + \gamma_{II} - \beta_{II}}{16 \nu \pi} \left( \frac{\varepsilon}{1 - \varepsilon} \right) \left[ \kappa_I \frac{\left(\pi - \gamma_I\right)}{h_{CI}} + \kappa_{II} \frac{1}{r^3} \frac{\left(\pi - \gamma_{II}\right)}{h_{CII}} \right]$$

and

$$K_{UC} = K_{UCI} + K_{UCII}$$

with:

$$K_{UCI} = \tan \phi_{pI} \frac{2\pi + \gamma_{II} - \beta_{II}}{16 \nu \pi} \left( \frac{\varepsilon}{1 - \varepsilon} \right) \left[ \kappa_I \frac{\left(\pi - \gamma_I\right)}{h_{CI}} \right]$$

$$K_{UCII} = \tan \phi_{pI} \frac{2\pi + \gamma_{II} - \beta_{II}}{16 \nu \pi} \left( \frac{\varepsilon}{1 - \varepsilon} \right) \left[ \kappa_{II} \frac{1}{r^3} \frac{\left(\pi - \gamma_{II}\right)}{h_{CII}} \right]$$

(d) Pressure related leakage through root clearance:

$$\dot{V}_{SR} = \Delta p \frac{\sqrt{d_{oI}}}{\eta_{fl}} K_{SR}$$

with the approximation for $K_{SR}$:

$$K_{SR} = \frac{\tan\phi_{PI}}{28.8}\left[ m_I \frac{\kappa_{II} h_{RI}^{5/2}}{\varepsilon}\sqrt{\left(\frac{2r}{\varepsilon}+2r\right)} + m_{II}\kappa_I h_{RII}^{5/2}\sqrt{\left(\frac{r}{(1+\varepsilon-r)}+2\right)}\right]$$

(e) Rotational leakage through root clearance:

$$\dot{V}_{DR} = d_{oI}^2 \omega_I K_{DR}$$

with:

$$K_{DR} = \frac{\tan\phi_{PI}}{4}\left[ m_I \frac{\kappa_{II} h_{RI}}{r} + m_{II}\kappa_I h_{RI}\left(\left(\frac{1+\varepsilon-r}{r}\right)\varepsilon + \frac{1}{2}\right)\right]$$

(f) Pressure related leakage flow through the flank clearance:

$$\dot{V}_{SF} = \Delta p \frac{d_{oI}}{\eta_{fl}} K_{SF}$$

with the approximation for $K_{SF}$:

$$K_{SF} = \frac{T_f^{5/2}\tan\phi_{PI}}{14.4\sqrt{d_{ch}}}\left( m_I 1.8\frac{\gamma_{II}}{\varepsilon} + m_{II} 2\gamma_I\right)$$

(g) Rotational leakage flow through the flank clearance:

$$\dot{V}_{DF} = d_{oI}^2 \omega_I K_{DF}$$

with:

$$K_{DF} = T_f \tan\phi_{PI}\left[ m_I \frac{\gamma_{II}}{3.5\varepsilon}\left(3+\frac{\varepsilon}{r}\right) + m_I \frac{\nu\gamma_I}{4}\left(\frac{6+\varepsilon-r}{r}\right)\right]$$

*[End of appendices]*